Author:
Wilson, Stacey

Title:
Modulation of the herg potassium channel function by extracellular acidosis

single channel effects and underlying basis

MODULATION OF THE HERG POTASSIUM CHANNEL FUNCTION BY EXTRACELLULAR ACIDOSIS: SINGLE CHANNEL EFFECTS AND UNDERLYING BASIS

Stacey Leigh Wilson

A dissertation submitted to the University of Bristol in accordance to the requirements of the Doctor of Philosophy in the Faculty of Biomedical Sciences

Department of Physiology, Pharmacology and Neuroscience

December 2017

Word Count: 52,824

Abstract

Human *ether-à-go-go-related gene* (hERG) potassium channels underlie the rapid delayed rectifier K^+ current (I_{Kr}) and play an important role in repolarisation of cardiac action potentials (APs). Pathological events such as cardiac ischaemia can lead to a decrease in extracellular pH (acidosis). Extracellular acidosis is known to modulate the hERG current (I_{hERG}) but the underlying mechanism(s) are not completely known. The aims of this study were: (1) to establish the effects of acidosis on macroscopic and single-channel $I_{hERG,}$ investigating both hERG1a and hERG1b isoforms; (2) to use an amino acid modifying reagent and site-directed mutagenesis to probe the molecular basis of proton modulation of I_{hERG}, focusing on the hERG1a isoform.

Whole-cell and cell-attached patch-clamp recordings were made at ambient temperature of wild-type I_{hERG} from mammalian cell lines (HEK-293 or CHO). When external pH (pH_e) was reduced from 7.4 to 6.3, macroscopic I_{hERG} amplitude and conductance decreased, activation was positively shifted, and deactivation kinetics were accelerated. Results obtained in the cell-attached configuration showed a reduction at pH_e 6.3 in single-channel I_{hERG} amplitude and conductance, decreased open- and burst-durations and increased closed-time durations. These effects at the single-channel level account for the modulation of macroscopic I_{hERG} by acidic pH_e. The first known single-channel recordings from hERG1b showed that this isoform retained sensitivity to acidic pH_e, indicating that N-terminal differences between the two isoforms are not critical for proton sensitivity.

Experiments completed with a range of extracellular pH values (4.5 – 8.0) revealed that different features of I_{hERG} have distinct pK_a values, suggesting multiple sites of proton modulation. Titratable residues located in the pore region of the hERG1a channel were mutated to determine if they were responsible for pH sensitivity. The double mutation E575Q/H578N appeared to remove the proton reduction of channel conductance, thus identifying a novel proton sensor on the hERG channel.

Abstract word count: 298 (abstract word limit: 300)

Dedication and Acknowledgements

Firstly, I would like to give my deepest thanks to my supervisors Professor Jules Hancox and Professor Neil Marrion. Your knowledge, patience, support and enthusiasm in my work has motivated me to get to where I am today. My thanks also go to the members of my panel, Dr Andrew James and Professor David Sheppard, who have patiently given me sound advice throughout my PhD. I would also like to thank Dr Christopher Dempsey for providing the homology/structural models of hERG used in this thesis.

Secondly, I thank my parents, family and friends who have supported me throughout my PhD. I will almost miss the recurring question of “how are your cells this week?”

I would like to thank the past and present members of the Hancox, Marrion and DW4 labs. You have all helped me one way or another and cannot thank you all enough. Particular thanks go to: Jane, who helped ease me into the PhD lab-life; Chunyun, who I worked alongside with and; Yi Hong, who provided me with the knowledge and ability to carry out my molecular biology work.

Finally, to Matthew. You have helped me in more ways than you know. For that, I thank you.

Author’s Declaration

I declare that the work in this dissertation was carried out in accordance with the requirements of the University's *Regulations and Code of Practice for Research Degree Programmes* and that it has not been submitted for any other academic award. Except where indicated by specific reference in the text, the work is the candidate's own work. Work done in collaboration with, or with the assistance of, others, is indicated as such. Any views expressed in the dissertation are those of the author.

SIGNED: ..... DATE:.....

List of Contents

List of Figures

List of Tables

List of Abbreviations

$[H^+]$	H^+ ion concentration
$[K^+]$	K^+ ion concentration
$[K^+]_e$	Extracellular K^+ ion concentration
Ag	Silver
ANOVA	Analysis of variance
AP	Action Potential
APD	Action Potential Duration
APD_{90}	Action Potential Duration at 90% repolarisation
AV node	Atrio-ventricular node
BPM	Beats per minute
˚C	degrees Celsius
Ca^{2+}	Calcium ion
cDNA	complementary Deoxyribonucleic Acid
CHO	Chinese Hamster Ovary
Cl^-	Chloride
CNG	Cyclic Nucleotide-Gated ion channels
CO_2	Carbon Dioxide
D	Aspartic acid residue
DEPC	Diethylpyrocarbonate
DMEM	Dulbecco's Minimum Essential Medium with Glutamax-1
DMSO	Dimethyl sulfoxide
DNA	Deoxyribonucleic acid
E	Glutamic acid residue
EAD	Early After Depolarisations
EAG	*ether-à-go-go* gene
ECG	Electrocardiogram
eGFP	enhanced Green Fluorescent Protein
EGTA	Ethylene glycol-bis(2-aminoethylether)-N,N,N',N'-tetraacetic acid
E_{Rev}	Reversal potential
F	Phenylalanine residue
FBS	Fetal bovine serum
FRET	Fluroscence resonance energy transfer
G	Glycine residue

g	gram
G_{max}	Maximal conductance
GΩ	Gigaohm
H^+	hydrogen/proton
HCl	Hydrochloric acid
HCN	Hyperpolarisation-activated Cyclic Nucleotide-gated channels
HEK	Human Embryonic Kidney
HEPES	4-(2-hydroxylethyl)-1-piperazineethanesulphonic acid
hERG	human *ether-à-go-go-related* gene
I	Isoleucine amino acid residue
I_{hERG}	hERG current
I_K	Delayed rectifier K^+ current
I_{K1}	Inward rectifier K^+ current
I_{Kr}	Rapid delayed rectifier K^+ current
I_{Ks}	Slow delayed rectifier K^+ current
I_{Na}	Inward Na^+ current
I_{Pulse}	hERG pulse current
I_{Tail}	hERG tail current
I_{to}	transient outward K^+ current
I-V relation	Current-Voltage relation
K	Lysine residue
k	Slope factor (for voltage dependent activation/inactivation relations)
K^+	Potassium
kHz	kilohertz
K_v channels	Voltage-gated potassium channels
LB	Lysogeny broth
LJP	Liquid Junction Potential
LQTS	Long QT syndrome
m	milli-
M	$mol.l^{-1}$
mM	$millimole.l^{-1}$
MES	4-Morpholineethanesulfonic acid
MI	Myocardial infarction
mRNA	Messenger Ribonucleic Acid

ms	Millisecond
mV	millivolt
N	Asparagine residue
n	nano-
Na^+	Sodium
NaOH	Sodium hydroxide
p	pico-
PAS domain	Per-Arnt-Sim domain
PBS	Phosphate Buffered Saline
PCR	Polymerase Chain Reaction
PEI	Polyethylenimine
pH	$-Log_{10}$ (H^+ concentration)
pH_e	pH of the external solution/ external pH
pKa	Acid dissociation constant on a logarithmic scale
pS	picosiemens
P/S	Penicillin/Streptomycin
Q	Glutamine residue
rpm	Revolutions per minute
SA node	Sinoatrial node
SEM	Standard Error of the Mean
SOC	Super optimal broth with catabolite repression
SQTS	Short QT Syndrome
T	Threonine residue
TdP	Torsades de Pointes
TDR	Transmural dispersion of repolarisation
τ	Time constant
τ_{Fast}	Fast time constant
τ_{Slow}	Slow time constant
µ	micro-
µl	microlitre
V	Valine residue
$V_{0.5}$	Half-maximal activation/inactivation voltage
W	Tryptophan residue
WT	Wild type

1. General Introduction

1.1 Heart structure and function

The heart is a muscular pump that provides a continuous circulation of blood through the systemic and pulmonary circulations, allowing the supply and exchange of oxygen and nutrients throughout the body. Normal heart electrophysiology is determined by the generation and propagation of action potentials coordinated with a period of relaxation and refractoriness (Nerbonne & Kass 2005).

1.1.1 The cardiac action potential and electrocardiogram

Action potentials (APs) in the heart are generated by the movement of ions across the cardiac cell membrane in response to a change in the membrane potential. Electrical activity within the heart is initiated by the sinoatrial (SA) node (Figure 1-1 – top panel), known to act as the cardiac pacemaker, and then spreads via gap junctions throughout the right and left atria. The signal reaches the atrioventricular (AV) node, in which a critical delay (~100 ms) occurs before AV node depolarisation (Nerbonne & Kass 2005). Excitation of the AV node spreads to the apex of the heart via the His-Purkinje system, allowing ventricular depolarisation.

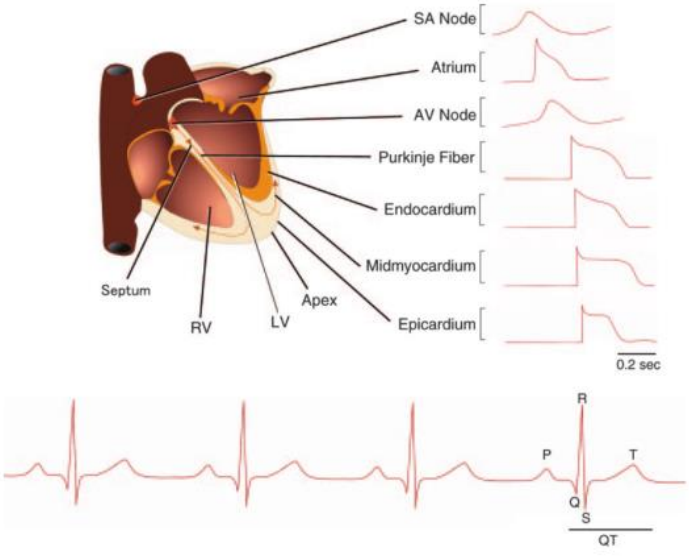

Figure 1-1 Electrical activity within the heart.

Schematic diagram (top panel) of a human heart and the action potentials generated in different regions of the heart. Bottom panel represents a surface electrocardiogram.
Image taken from Nerbonne & Kass, 2005

Surface electrocardiograms (ECGs) can detect and measure the AP phases in different regions of the heart. Atrial depolarisation gives rise to the P wave seen on an ECG, followed by ventricular depolarisation and repolarisation which correspond to the QRS complex and T wave respectively (Hurst 1998) (Figure 1-1 – bottom panel). Intervals between these waves correspond to physiological events; for example, the PR interval corresponds to the time it takes for the electrical impulse to travel from the SA node through the AV node. The ST segment is the period for which the ventricles are depolarised and the QT interval represents the period encompassing ventricular depolarisation and repolarisation.

1.1.2 Ion channels involved in the cardiac action potential

The AP waveform and duration varies in different regions of the heart (Figure 1-1 – top panel); this is caused by the differences in ion channel expression (Nerbonne & Kass 2005; Roden et al. 2002; Grant 2009).

The main cardiac sodium channel $Na_v1.5$ isoform predominately underpins the cardiac sodium current I_{Na}, which underlies the rapid upstroke (phase 0, see Figure 1-2) of the ventricular/atrial APs (Katz 1993; Nerbonne & Kass 2005; Veerman et al. 2015). Rapid voltage-dependent activation (within 1 ms) allows sodium to flow into the cells causing depolarisation (Veerman et al. 2015). The change in membrane potential that occurs in phase 0, causes the activation of the transient voltage-gated K^+ current ($I_{to,1}$) with subsequent inactivation of I_{Na} (Nerbonne & Kass 2005). The $I_{to,\,1}$ is responsible for early rapid repolarisation (phase 1, Figure 1-2), of the action potential and has a fast and slow component named $I_{to,\,f}$ and $I_{to,\,s}$ respectively (Tamargo et al. 2004; Grant 2009). $I_{to,\,f}$ is the principle subtype expressed in atrial tissue, whereas both components are expressed and contribute to phase 1 in human ventricle (Tamargo et al. 2004; Nerbonne & Kass 2005; Grant 2009). The inactivation of the Na_V channels and opening of I_{to} makes the membrane slightly more negative giving rise to the characteristic 'notch' of the AP (Nerbonne & Kass 2005; Tamargo et al. 2004).

Depolarisation of the membrane potential causes the activation of L-type calcium current ($I_{Ca,\,L}$). The influx of calcium through the L-type calcium channels is the main trigger that initiates the process of excitation-contraction coupling (Bers & Perez-Reyes 1999; Bers 2002). The duration of the plateau phase is dependent on the balance of calcium influx

and potassium efflux (Tamargo et al. 2004). As the calcium channels inactivate, the K^+ currents dominate and repolarisation begins as a result. Unlike the sodium and calcium currents, there are several distinct potassium channels responsible for the repolarisation (phase 3) of the action potential as well as the maintenance of the resting membrane potential (Nerbonne & Kass 2005). Three broad classes of repolarising K^+ currents have been formed: transient outward currents (I_{to}) which are responsible for early (phase 1) repolarisation; delayed, outwardly rectifying K^+ currents which determine the repolarisation (phase 3) and; the inward rectifier (I_{K1}) current is responsible for terminal repolarisation (Nerbonne 2016). The potassium channels that are involved in phase 3 carry the rapid delayed rectifier current (I_{Kr}), the slowly activating delayed rectifier current (I_{Ks}) and the inward rectifier current (I_{K1}) (Nerbonne & Kass 2005; Cheng & Kodama 2004; James et al. 2007; Grant 2009; Nerbonne 2016). The voltage-insensitive inward rectifying potassium

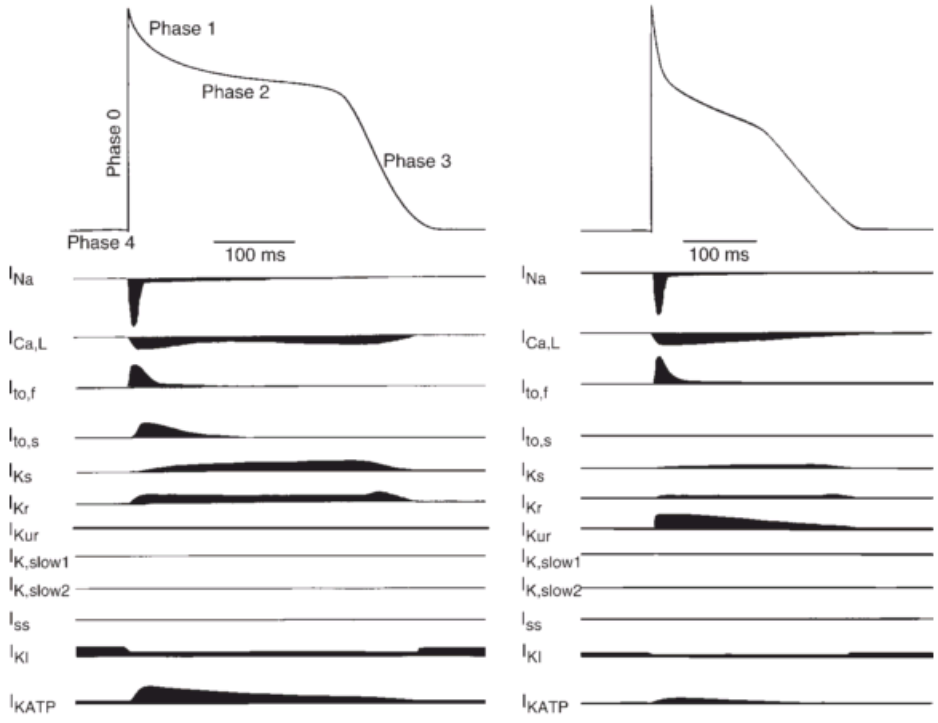

Figure 1-2 Human action potential waveforms and the underlying currents.

Schematic diagram showing currents underlying the ventricular (left panel) and atrial (right panel) action potential. Similarities are seen in the sodium and calcium currents, but varying expression levels of potassium currents result in waveforms.
Image taken from Nerbonne & Kass, 2005.

current, I_{K1}, is responsible for terminating phase 3 of repolarisation and setting the resting membrane potential (phase 4) (Tamargo et al. 2004). K_{ir} channels lack the S4 voltage sensor and so are voltage-insensitive, but the strong inward rectification is attributed to intracellular block by cations and polyamines (Nerbonne 2016; Hibino et al. 2010). Kir2.1 subunits are encoded by the KCNJ2 gene and are present in both atrial and ventricular myocytes, with higher expression seen in the ventricles to protect from pacemaker activity (Tamargo et al. 2004; Grant 2009; Nerbonne 2016). Kir2.2 (KCNJ12) and Kir2.3 (KCNJ4) subunits are present in ventricular myocytes but contribute to a lesser extent than the Kir2.1 subunit (Tamargo et al. 2004; Nerbonne 2016). It should be noted, that in atrial myocytes, the dominant repolarising potassium current is carried by a rapidly activating, non-inactivating current (I_{Kur}) that is not expressed in ventricular myocytes or Purkinje fibres (Nerbonne & Kass 2005). The I_{KATP} channel is formed by the co-assembly of four α-subunits with four regulatory SUR2A subunits (Grover & Garlid 2000; Tamargo et al. 2004; Nerbonne & Kass 2005). Cardiac K_{ATP} channels protect against stress responses, such as hypoxia or ischaemia, and is involved in action potential duration adaptation in response to a sudden increase in heart rate (Foster & Coetzee 2016).

The duration of the cardiac action potential is markedly prolonged compared with other APs in excitable tissues such as that found in the nervous system. The length of the cardiac action potential has physiological significance. Firstly, the action potential duration (APD), and more importantly the length of the AP plateau phase, allows for sufficient entry of Ca^{2+} to enter the myocyte. This influx of Ca^{2+} plays a role in the excitation-contraction coupling sequence which is followed by further calcium release from the sarcoplasmic reticulum (SR) (Bers 2002). Secondly, the delayed response of repolarisation (carried by the delayed rectifier potassium current) determines the length of phase 3 of the action potential and in turn determines the effective refractory period (ERP) (Burton & Cobbe 2001; James et al. 2007). This is highly important for normal functioning of the heart as the plateau phase and prolonged repolarisation can influence the heart's ability to prevent premature depolarisation (Sanguinetti & Tristani-Firouzi 2006; Perry et al. 2015).

As the I_{Kr} component of the delayed rectifier potassium current is the subject of this thesis, the characteristics of channels that underlie this current will be considered in further detail in the next section.

1.2 I_{Kr} and hERG

The cardiac I_K current was first characterised in the late 1960's in sheep Purkinje fibres and was thought to contain at least two separate components which were named i_{x1} and i_{x2} (Noble & Tsien 1969). The two components have since been identified as I_{Kr} (i_{x1}) and I_{Ks} (i_{x2}) and are distinguished by their kinetic and pharmacological properties (Sanguinetti & Jurkiewicz 1990; Sanguinetti et al. 1995; Sanguinetti et al. 1996). Firstly, the activation kinetics upon depolarisation are much faster for I_{Kr} compared with I_{Ks} (Figure 1-3A). Secondly, I_{Kr} and I_{Ks} show different current-voltage (I-V) relations. As seen in Figure 1-3B, the I_{Kr} component shows a region of negative slope in the I-V relation at more depolarised potentials. In contrast, I_{Ks} shows a linear relationship in the same voltage range (Figure 1-3B). The final comparison between the two components can be made in their pharmacological differences; previous work has shown that the I_{Kr} component was preferentially blocked by methanesulphonanilide-based class III antiarrhythmic drugs (Sanguinetti & Jurkiewicz 1990; Lees-Miller et al. 2000; Mitcheson, Chen & Sanguinetti

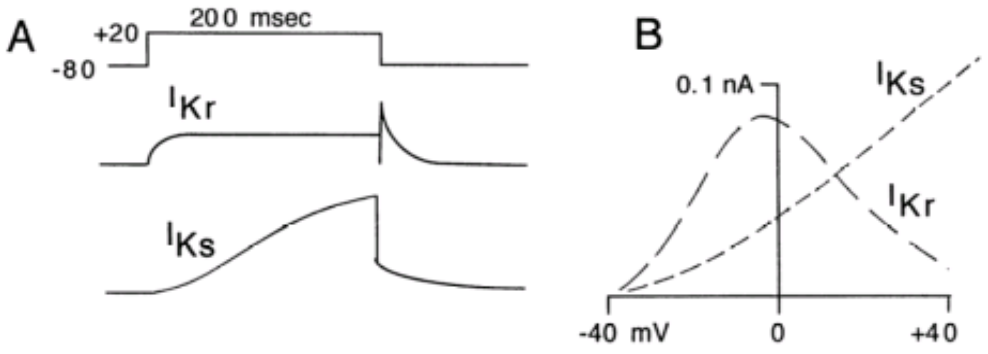

Figure 1-3 Schematic diagram showing the features of the two components that form the delayed rectifier K^+ current.

A. The two I_K components I_{Kr} and I_{Ks} and their current profile upon depolarisation to +20 mV to display activation kinetics. .

B. The current voltage relationship for both I_{Kr} and I_{Ks} in guinea pig ventricular myocytes.

Figure is from (Sanguinetti & Keating 1997)
2000).

Since the identification of the two components of I_K, subsequent work has confirmed the presence of the rapid component of delayed rectifier I_K in cells from different cardiac

regions from several species. These include: human atrial and human ventricular myocytes (Wang et al. 1994; Li et al. 1996); rabbit sinoatrial (Noma & Irisawa 1976; DiFrancesco et al. 1979), nodal (Ito & Ono 1995) and ventricle (Clay et al. 1995); guinea-pig sinoatrial (Horie et al. 1990), ventricle (Sanguinetti & Jurkiewicz 1990; Chinn 1993), and atrium (Sanguinetti & Jurkiewicz 1991); canine atrium and ventricle (Gintant 1996), frog atrium (Ojeda & Rougier 1974), and embryonic chick atrial cells (Shrier & Clay 1986).

1.2.1 hERG encodes the pore-forming subunit of I_{Kr} channels

The *human ether-à-go-go Related Gene* (*hERG*) encodes the pore forming subunit of a delayed rectifier potassium channel. *KCNH2*, alternative nomenclature of the *hERG* gene, was first cloned in the human hippocampus complementary Deoxyribonucleic Acid (cDNA) library when screened with the mouse homolog of the *Drosophilia* EAG gene (Warmke & Ganetzky 1994). It was noted that *hERG* is located on chromosome 7 in humans and shares similarities with both voltage gated potassium (VGK) channels as well as cyclic nucleotide-gated (CNG) channels (Warmke & Ganetzky 1994). With 17 genes implicated with congenital long QT syndrome (LQTS; an inherited arrhythmia that is characterised by prolonged QT interval which can lead to torsade de pointes), the important discovery of the *hERG* location shed light on the gene responsible for some clinical cases of long QT syndrome (LQT2) (El-Sherif et al. 2017). In addition to the LQT locus on chromosome 11 (Keating et al. 1991), two additional loci have been identified with LQT2 linked to markers on chromosome 3p21-24 and 7q35-36 (Jiang et al. 1994). Further work showed that *hERG* was mapped to chromosome 7q35-36 with strong expression in the heart suggesting that mutations in *hERG* are responsible for LQT2 (Curran et al. 1995). At this point the function of *hERG* was unknown, but with strong expression in the heart as well as the presence of *hERG* mutations associated with LQT, it was hypothesised to play a role in cardiac repolarisation (Curran et al. 1995). To determine its role, characterisation of hERG was perfomed by injecting the full-length hERG cRNA and expression in *Xenopus* oocytes (Sanguinetti et al. 1995; Trudeau et al. 1995). Using voltage-clamp techniques, it was observed that hERG encodes a delayed rectifier potassium channel that possesses properties like that of native I_{Kr} (Sanguinetti et al. 1995; Trudeau et al. 1995). Although it shares many similarities with I_{Kr}, it was shown that hERG channels expressed in the *Xenopus* oocytes expression system were resistant to block by methanesulphonanilide antiarrhythmic drugs such as MK-499 and E-4031 (Sanguinetti et al. 1995). At the time it was suggested that hERG interacts with a protein that possesses the receptor responsible

for methanesulphonanilide block (Sanguinetti et al. 1995). Since then, studies have confirmed that accessory subunits are not required for hERG block by methanesulphonanilides in the mammalian HEK-293 cell line (Snyders & Chaudhary 1996) and that for pharmacological studies, *Xenopus* oocytes reduce drug potency likely due to the vitelline membrane which can influence drug access and large amounts of yolk present which can absorb the drug (Witchel et al. 2003; Po et al. 1999).

The main transcript *hERG-1a* gives rise to a hERG channel protein that is 1,159 amino acids in length (Warmke & Ganetzky 1994). Four other *hERG* transcripts have been identified: *hERG-1b* is a protein that is missing the first five exons of *hERG-1a* with an alternative exon 5b (Lees-Miller et al. 1997; London et al. 1997) and completely identical to *hERG-1a* from exon 6 onwards (Vandenberg et al. 2012); *hERG-1c* or *hERG-3.1* is identical to *hERG-1a* from the end of exon 3 (Huffaker et al. 2009); a C-terminal splice variant of *hERG* contains a separate and unique stop codon sequence and is referred to as $hERG_{USO}$ (Kupershmidt et al. 1998) (see Figure 1-4).

1.2.2 hERG and interacting proteins

The current carried by homomeric hERG1a channels (I_{hERG}) differs to native I_{Kr} in terms of gating, regulation by external K^+ and single-channel conductance (Tseng 2001; Tristani-Firouzi & Sanguinetti 2003). Previous studies suggested that hERG channels could co-assemble with modulating subunits that result in the native I_{Kr}. Both KCNE1 (minK) and KCNE2 (MiRP1) β subunits have been proposed to be likely candidates and both have been shown to associate with hERG (McDonald et al. 1997; Abbott et al. 1999; Sesti et al.

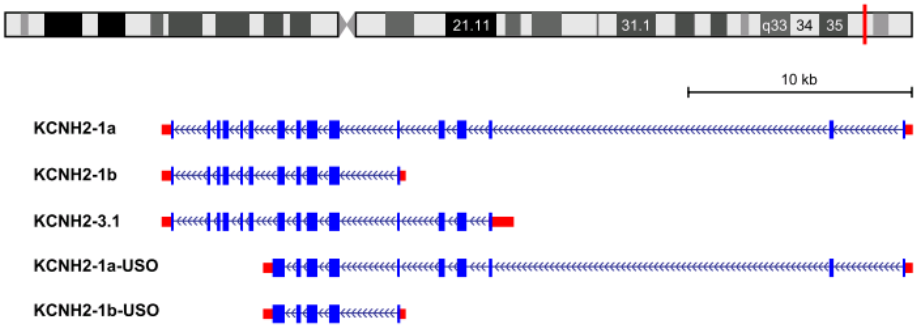

Figure 1-4 The genomic structure of *hERG*

hERG is located on chromosome 7, is transcribed in the reverse direction and has three alternative transcription start sites and two alternative stop sites.

Image taken from (Vandenberg et al. 2012)

2000; Anantharam & Abbott 2005; Du et al. 2013). However, the role of KCNE subunits and their ability to regulate hERG channel function is a topic of debate (Abbott et al. 2007). There is disagreement in the role of KCNE2 when co-expressed with hERG in heterologous expression systems. One study completed in *Xenopus* oocytes observed an approximate +10 mV shift in the voltage-dependence of activation (Abbott et al. 1999). Studies completed in Chinese Hamster Ovary (CHO) and Human Embryonic Kidney (HEK) cells have reported either a negative shift or no change in the voltage-dependence (Cui et al. 2000; Mazhari et al. 2001; Weerapura et al. 2002; Lu et al. 2003). It appears that in heterologous expression systems, hERG channels interact with MiRP1 but it has been shown that the expression levels of MiRP1 is low in atrial and ventricular tissue (Pourrier et al. 2003; Lundquist et al. 2005). As a result, it can be assumed that the interaction of hERG and MiRP1 in native tissue is unlikely.

Other interacting partners such as KCNQ1 (pore-forming subunit of I_{Ks}) and K^+ channel regulator (KCR-1) have been shown to alter the function of hERG channels. A study in which co-expression of KCNQ1 with hERG in a mammalian cell line resulted in significant acceleration in hERG channel deactivation which closely resembled I_{Kr} kinetics (Ehrlich et al. 2004). The same experiments showed that the co-expression of hERG with KCNQ1 increased the plasma membrane expression of hERG (Ehrlich et al. 2004). The KCR protein has been shown to associate with hERG and rEAG channels, and when expressed in the CHO expression system it appears to render the hERG channel less sensitive to classic hERG blockers such as dofetilide (Hoshi et al. 1998; Kupershmidt et al. 2003).

There has been increasing evidence that the native I_{Kr} is a heteromer of the hERG 1a and a splice variant of hERG1. The truncated C-terminal splice variant, $hERG_{USO}$ does not form functional homomeric channels but co-expression with hERG1a results in a hERG current with altered properties: a reduction in current amplitude, acceleration of activation and shifting the voltage-dependence of activation is observed (Kupershmidt et al. 1998). A more promising co-assembly of subunits is between the hERG1a and 1b isoforms, with increasing evidence that the two isoforms co-express (Lees-Miller et al. 1997; London et al. 1997; Larsen et al. 2008; Jones et al. 2004; Sale et al. 2008; Phartiyal et al. 2008; McPate, H Zhang, et al. 2009; Larsen & Olesen 2010; Du et al. 2011; Jones et al. 2014; Liu et al. 2016; McNally et al. 2017). Characterisation of the hERG1b isoform and the its possible physiological role in native I_{Kr} will be discussed in Chapter 4.

1.2.3 hERG channel structure

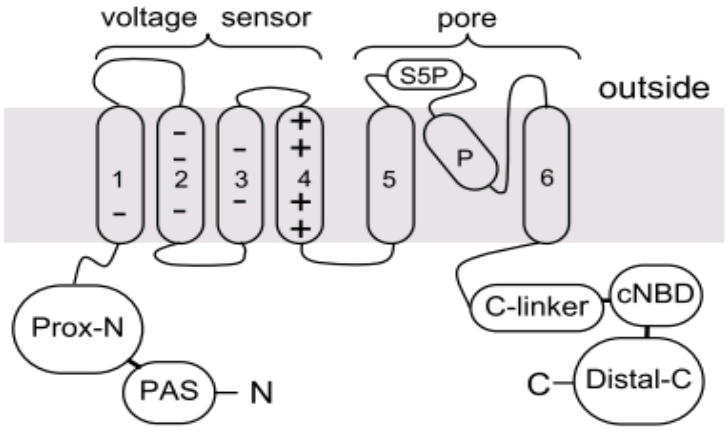

Figure 1-5 Basic structure of a hERG1a channel subunit.

The S1-S6 are transmembrane segments that are connected via linkers. The intervening pore loop between S5 and S5 contains the S5-P linker and the pore helix. Both the N- and C-termini of the protein are intracellular.
Image taken from (Perrin et al. 2008)

As previously mentioned, the main transcript *KCNH2-1a* encodes the pore-forming subunit of K_V11.1 or hERG1a channels. Each subunit consists of six transmembrane segments (S1-S6) with the voltage sensor domain (VSD) composed of S1-S4 and the S5-S6 including the intervening pore loop forming the pore domain (see Figure 1-5). The four subunits co-assemble to form a tetramer with the pore domain from each subunit lining the central ion conduction pathway (Vandenberg et al. 2012). hERG channels also contain cytoplamsic regions that contain domains important for hERG structure and function. The cytoplasmic N-terminus of hERG, and other members of the EAG family, contains a Per-Arnt-Sim (named after the proteins in which they were discovered; PAS) regulatory protein domain and appears to play a role in channel gating (Cabral et al. 1998). The C-terminus of the channel contains a cyclic nucleotide-binding domain (cNBD) which shares structural similarities with CNG channels and hyperpolarisation-activated cyclic nucleotide-modulated (HCN) channels (Warmke & Ganetzky 1994; Gustina & Trudeau 2011).

The N-terminal region of the hERG channel is approximately 390 residues with a structurally distinct region that is conserved in the eag channel family. Amino acids 1-135 encode the ‘eag’ domain and contains the PAS domain which is thought to be an important

structure for normal channel gating (Cabral et al. 1998). Using N-terminal deletion mutations, previous studies have shown that just the first 16 amino acid residues are needed for the slow deactivation kinetics (Wang et al. 1998; Wang et al. 2000) of hERG channels, whilst more extensive amino-terminal truncations mimic this phenotype (Schönherr & Heinemann 1996; Spector et al. 1996; Wang et al. 1998; Trudeau et al. 2011). Indeed, the hERG1b isoform lacks the N-terminal sequence of hERG1a and instead possesses a unique 36-amino acid N-terminal. With the absence of the 'eag' domain, hERG1b homomeric channels exhibit much faster deactivation in comparison to hERG1a channels (Lees-Miller et al. 1997; London et al. 1997).

The voltage sensing region comprises the S1-S4 domains of hERG in which opening of the channel is regulated by conformational changes in the voltage sensor (Tao et al. 2010). The presence of a positively charged lysine or arginine residue in every third position in the S4 helical domain makes it the primary voltage sensor (Sanguinetti & Tristani-Firouzi 2006). Mutagenesis studies of the S4 segment shows that substitution of any of the charges alter voltage-dependence of gating, with R531 (located in the middle of the S4 transmembrane segment) identified as the most important residue for voltage-sensing (Zhang et al. 2004; Piper et al. 2005; Subbiah et al. 2005). In the other transmembrane helices of the VSD (S1-S3), particular negatively charged acidic residues are believed to form salt bridges with certain basic residues found in the S4 (Liu et al. 2003; Zhang et al. 2005). A recent study has recently highlighted the importance of the S1 helix in hERG channels, which shows low homology with other K_v channels, in the physiological function and expression of K_v11.1 channels (Phan et al. 2017). Results showed that S1 residues contains side chains that are in close proximity to either residues in the S2 helix or the S4 helix in the same subunit and are thought to stabilise the S4 voltage sensor (Phan et al. 2017).

The pore domain is composed of an outer (S5) helix and an inner (S6) helix with an intervening pore loop. The pore itself is asymmetrical and changes in its dimensions depending on whether the channel is in the open or closed state (Sanguinetti & Tristani-Firouzi 2006). At the extracellular end of the pore lies the selectivity filter; the highly conserved T-V-G-Y-G sequence amongst potassium channels (also known as the K^+ signature sequence) is located at the carboxy-terminal end of the pore helix (Heginbotham et al. 1994; Doyle et al. 1998). In hERG channels, the threonine and tyrosine are

respectively substituted with a serine and phenylalanine but still show high selectivity for K^+ over Na^+ (p_K:p_{Na} > 1000:1) suggesting conservation of the selectivity filter structure (Sanguinetti et al. 1995; Trudeau et al. 1995; Sanguinetti & Tristani-Firouzi 2006). At the cytoplasmic end of the pore domain, the area widens to form the central cavity (Sanguinetti & Tristani-Firouzi 2006). The S6 helices line the central cavity and forms the activation gate which controls the transitions between the open and closed state (Wang et al. 2011). Crystal structure comparison of several potassium channels show that the cytoplasmic end of the S6 is tightly packed in the closed state and splayed apart in the open state which would constrict (closed state) or allow (open state) the passage of ions (Doyle et al. 1998; Jiang et al. 2002; Long 2005a). In voltage-dependent potassium channels, a conserved Pro-Val-Pro (PVP) motif causes a kink in the S6 helices that allows interactions with the S4-S5 linker (Long 2005a; Long 2005b). This provides structural and functional importance for electromechanical coupling between the voltage sensor domain and the activation gate. hERG channels, however, lack the PVP motif found in the S6 helix and a recent study has identified the location using a proline scan of the S6 helix with glutamine at position 664 defining the boundary (Thouta et al. 2014). The structure of the hERG channel in the open state has recently been resolved (Wang & MacKinnon 2017). In comparison to K_V1-K_V9, voltage sensor movements in hERG channels are transmitted in part through S4-mediated displacements of S5 (Wang & MacKinnon 2017).

The hERG C-terminus contains a C-linker region and a cyclic nucleotide-binding homology domain. As mentioned, hERG channels share structural homology of the cNBD with other channels such as CNG and HCN channels but, unlike HCN channels, hERG channels appear to be unaffected by cAMP (Sanguinetti & Tristani-Firouzi 2006). Structural resolution of the C-linker/cNBHD of an ERG channel shows that a negatively charged cavity in place of the positively charges cavity that is seen in HCN2 channels (Brelidze et al. 2013). This negatively charged β-roll cavity is expected to play a part in the prevention of regulation by cyclic nucleotides in the KCNH family; a short β9-strand that acts as a an intrinsic ligand blocks the entry of cyclic nucleotides and is conserved amongst other members of the KCNH2 channel family (Brelidze et al. 2009; Brelidze et al. 2012; Marques-Carvalho et al. 2012). Studies have shown that the cNBHD preferentially binds with the eag domain (found in the N-terminal of KCNH channels) and appears to be critical for normal channel gating (Gustina & Trudeau 2011; Gustina & Trudeau 2012; Haitin et al. 2013).

1.2.4 hERG channel gating

Like other voltage-gated potassium channels, the hERG channel can exist in three conformational states; closed, open and inactivated. The hERG channel is different from other VGK channels due to its unusual gating kinetics; the transitions between the open and closed states are markedly slower than the transition between the open and inactivated states (see Figure 1-6).

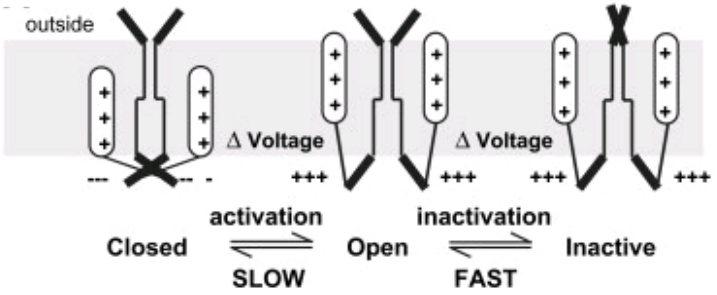

Figure 1-6 The three states of hERG channel gating.

hERG channels can exist in one of three states; closed, open or inactive. The transitions between the states are voltage-dependent with the transition between the open and inactivated state showing very fast gating kinetics compared to the unusually slow kinetics of the transition between open and closed states.
Image taken from (Perrin et al. 2008).

Due to its important role in repolarisation of cardiac action potentials, understanding the kinetics of hERG gating is of considerable importance. Experimental and simulation studies have attempted to elucidate the gating of hERG channels. A review of the available models of I_{Kr} and hERG gating that hERG is best represented by a linear Markov model that includes three closed states, one open state and one inactivated state (see Figure 1-7 (Bett et al. 2011)).

The review by Bett et al has suggested that hERG is best represented by a linear Markov model as shown in Figure 1-7, in which a minimum of three closed states are needed to reproduce the sigmoidicity of activation (Bett et al. 2011). The linear Markov model shows that hERG must proceed through the open state before entering the inactivated state (Figure 1-7).

$$C_1 \underset{\beta_1}{\overset{\alpha_1}{\rightleftharpoons}} C_2 \underset{K_b}{\overset{K_f}{\rightleftharpoons}} C_3 \underset{\beta_2}{\overset{\alpha_2}{\rightleftharpoons}} O \underset{\beta_1}{\overset{\alpha_1}{\rightleftharpoons}} I.$$

Figure 1-7 Markov model of hERG gating.

A model developed by Wang et al of hERG gating which includes three closed states (one of which is voltage-insensitive), one open state and one inactivated state (Wang et al. 1997)

Image taken from (Bett et al. 2011)

1.2.4.1 hERG current profile during a standard voltage 'step' protocol

To study characteristics features of I_{hERG}, the use of a two 'square' voltage step pulse protocol is routinely used (Trudeau et al. 1995; Sanguinetti et al. 1995). Figure 1-8 shows a representative trace of an I_{hERG} recording obtained at room temperature from HEK-293 cells stably expressing the hERG channel. With a holding potential of -80 mV an initial but brief (50 ms) depolarising pulse to -40 mV is made. A longer depolarising pulse of 2

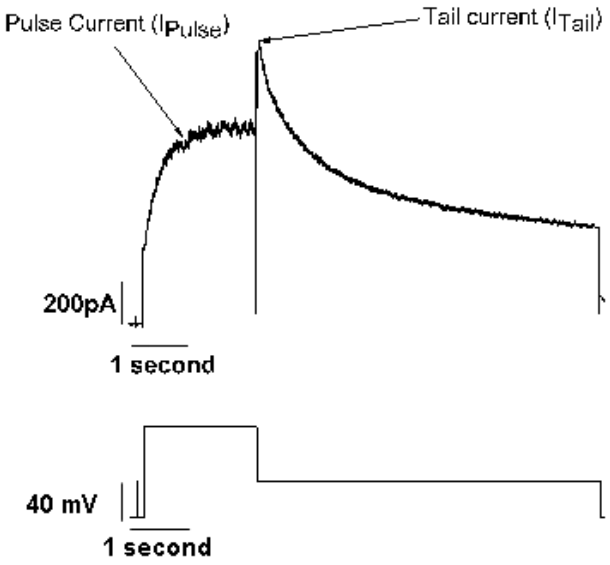

Figure 1-8 Example trace of I_{hERG} elicited by a standard voltage protocol.

Current was recorded from hERG-expressing HEK-293 cells. The first depolarisation to +20 mV (2 seconds) from a holding potential of -80 mV produces and outward current (I_{Pulse}) that levels off due to channel inactivation. The following step (6 seconds) to -40 mV evokes a larger outward current (I_{Tail}) as channels a relieved from inactivation and re-open before deactivating back to the closed state.

seconds to +20 mV causes activation of hERG channels (seen as an outward current, I_{Pulse}) which plateaus. Repolarisation to -40 mV evokes a larger outward tail current (I_{Tail}) which slowly deactivates in a bi-exponential manner. The large tail current is characteristic of I_{Kr}/I_{hERG} due to the inward rectification at positive potentials that reduces outward current (I_{Pulse}) upon depolarisation. Inactivation is rapidly removed upon repolarisation and results in the opening of the channels to then slowly deactivate.

1.2.4.2 hERG channel activation

The time-course of hERG channel activation is slow and usually requires hundreds of milliseconds to reach steady-state (Wang et al. 1997), suggesting that slow activation is a result of slow movement of the voltage sensor. Indeed because of the slow activation, direct measurement of the rate of activation is not possible due to overlapping inactivation (Liu et al. 1996). Previous work has established that depolarisation of the membrane causes the positively charged S4 helix to move toward the extracellular interface (Vandenberg et al. 2012). This movement is electromechanically connected to the activation gate that is positioned on the cytoplasmic side of the ion conduction pathway (Vandenberg et al. 2012). The physical interaction of the S4-S5 linker with the cytoplasmic end of the S6 helices is the connection between hERG channel activation and S4 movement (Tristani-Firouzi et al. 2002; Long 2005b; Van Slyke et al. 2010; Ng et al. 2012). Much research has been carried out to determine the molecular basis of the slow activation of hERG. There are two possible causes of slow activation kinetics: the voltage sensor moves slowly in response to a change in membrane potential or; the coupling of the voltage sensor movement to the opening of the activation gate (Vandenberg et al. 2004). Experiments using fluorescence resonance energy transfer (FRET) measurements showed that S4 movement undergoes both rapid and slow voltage-dependent changes with the slow movement links well with the voltage-dependence of activation (Smith & Yellen 2002). Consistent with these findings, a rapid component of activation was also observed in cut-open oocyte experiments measuring gating charge (Piper et al. 2003). This rapid component was 100 times faster than the slower component and has been suggested to be linked with the rapid voltage-dependent inactivation of hERG channels (Smith & Yellen 2002; Piper et al. 2003). A more recent study recorded voltage sensor domain currents and the rates of modification by [2-(trimethylammonium)ethyl] methanethiosulfonate chloride (MTSET) (Wang et al. 2013). Results from this study showed two charge systems, Q_1 and Q_2, with Q_2 possessing a much slower time constant

compared with Q_1 in the range of potentials where hERG channels are activated (Wang et al. 2013). It has been suggested that hERG channel activation is not controlled exclusively by the slow rearrangement of the bulk gating charge but also by cytoplasmic domain interactions that stabilise the open state (Wang et al. 2013; Goodchild et al. 2015).

1.2.4.3 hERG channel deactivation

Deactivation is the transition between the open and the closed state(s) which, in hERG channels, occurs slowly in comparison to its inactivation kinetics. Rapid recovery from inactivation as the membrane potential repolarises paired with the slow deactivation kinetics allows hERG channels to play an important role in action potential repolarisation (Trudeau et al. 1995; Cabral et al. 1998; Hancox et al. 1998; Zhou et al. 1998; Tseng 2001; Sanguinetti & Tristani-Firouzi 2006). Cytosolic domains have been shown to modulate hERG channel deactivation kinetics. A major determinant is the N-terminal PAS domain; partial or complete deletion of the PAS domain results in accelerated deactivation (Schönherr & Heinemann 1996; Spector et al. 1996; Wang et al. 1998; Trudeau et al. 2011). Acceleration in channel deactivation is also observed with point mutations within the PAS-cap domain (residues 1-25 (Muskett et al. 2011; Ng et al. 2011)) and the PAS domain (residues 26-135 (Cabral et al. 1998; Chen et al. 1999; Gustina & Trudeau 2009)). As well as the N-terminus, hERG channels contain a large C-terminus which has also been implicated to be involved in channel deactivation. Removal of the distal C-terminal tail (~ residues 873-1159) shows little effect on the rate of deactivation kinetics (Akhavan et al. 2003; Gustina & Trudeau 2011), whereas removal of the cNBH domain (~ residues 749-872) shows a phenotype similar to that seen in the deletion of the N-terminus (see Figure 1-5 for general hERG1a topology (Akhavan et al. 2003; Gustina & Trudeau 2011)). These results suggest that some form of interaction may occur between the two cytoplasmic domains to play a role in the rate of deactivation. Consistent with this, a recent study showed that specific residues form charge-charge interactions between the two domains (Ng et al. 2014). An extra transient interaction is thought to be made between the disordered region of the N-Cap domain and the C-linker to regulate slow channel deactivation (Ng et al. 2014).

The cytoplasmic S4-S5 linker is also proposed to play a role in the deactivation of hERG channels. The S4-S5 linker forms interactions with the cytoplasmic end of the S6 so is important in the electromechanical coupling of voltage sensor movement with gating of the

ion conduction pathway (Tristani-Firouzi et al. 2002; Long 2005b; Van Slyke et al. 2010; Ng et al. 2012; Perry et al. 2015). Isolation studies of this region shows that the S4-S5 linker forms and amphipathic helix suggesting that it lies parallel to the membrane (Ng et al. 2012) making it a likely candidate for interactions between cytoplasmic domains. The introduction of cysteines in the disordered N-Cap region and in the S4-S5 linker have been shown to form disulphide bonds suggesting proximity to one another (De La Peña et al. 2011). Recent mutagenesis studies have shown that tyrosine residues Y542 and Y545 located in the S4-S5 linker play a role in stabilising the open state of hERG channels (Ng et al. 2016).

1.2.4.4 Inactivation of the hERG potassium channel

Upon depolarisation, voltage-gated potassium channels transition to the activated state with most able to enter a stable non-conducting state (inactivated) via a process known as inactivation (Rasmusson et al. 1998). A majority of voltage-gated potassium channels will undergo one, or both, of two types of inactivation known as N-type and C-type (Perry et al. 2015). N-type inactivation occurs through a 'ball-and-chain' mechanism, in which residues located on the N-terminal of the channel bind to the activated channel and obstruct the intracellular mouth of the channel (Hoshi et al. 1990; Rasmusson et al. 1998). An early study dismissed the idea that hERG inactivates via this mechanism due to the observation that removal of the cytoplasmic N-terminus did not eliminate inactivation (Schönherr & Heinemann 1996; Spector et al. 1996)

C-type inactivation has been identified in *Shaker* K^+ channels when N-type inactivation has been removed (Hoshi et al. 1991). The mechanism for C-type inactivation, also known as 'collapse of the pore', involves a conformational change in the selectivity filter region that occludes the conduction of ions (Hoshi & Armstrong 2013). The inactivation observed in hERG channels closely resembles the C-type mechanism of Shaker K^+ channels but with rapid voltage-dependent gating kinetics (Smith et al. 1996). This voltage-dependent rapid inactivation allows hERG channels to be inactive during depolarised potentials of the cardiac AP which is particularly important as this limits the outward I_{hERG} during the plateau phase and delays repolarisation (Smith et al. 1996; Spector et al. 1996; Vandenberg et al. 2004). The recovery from inactivation allows I_{hERG}/I_{Kr} to contribute to the repolarisation phase and return the membrane potential back to diastolic levels (Hancox et al. 1998; Vandenberg et al. 2004).The recent resolved structure of hERG shows that there is a

difference in the hERG's selectivity filter. The F627 residue in the hERG GFG sequence is uniquely positioned and is suggested that this conformation is responsible for the rapid inactivation seen in hERG (Wang & MacKinnon 2017).

The hERG channel is unique among the voltage-gated ion channel family due to its unusually long extracellular (~40 residues) linker between the helices of S5 and S6, also known as the S5P linker (Warmke & Ganetzky 1994). Mutations of two outer histidine residues (H578 and H587) located in the hERG S5P linker showed slightly altered inactivation characteristics compared with the WT channel (Jiang et al. 1999). This led to the idea the S5-P linker was another structure that was relevant to the inactivation of hERG channels. Further mutagenesis work by this group revealed that H578 tolerated the substitutions without affecting Kv11.1 gating properties, whereas the H587 residue altered inactivation as well ion selectivity (Dun et al. 1999). A cysteine scan of the full length of the S5P linker region identified a helical region from residues 583-597 where mutations caused a disruption is C-type inactivation, altered K^+ selectivity and a shift in the voltage-dependence of activation (Liu et al. 2002). Indeed, a later study confirmed the presence of an apparent helical region corresponding to W585-I593 as well as a second structure G604-Y611 (Torres et al. 2003). The major helical structure (W585-I593) shows a well-defined hydrophobic face when in the presence of SDS micelles and expected to orientate so that the NH_2-terminal of the helix points towards the central pore (Liu et al. 2002; Torres et al. 2003). Furthermore, this amphipathic α-helix showed voltage-dependent interactions, suggesting that this region of the channel plays an important role in inactivation. To investigate the role of charge of the hERG S5P α-helix on inactivation, a study was completed in which the charged hydrophilic residues were mutated to either a lysine (K) or an aspartate (D) residue. The most high impact changes in the voltage dependence of inactivation was observed with the residues N588 and Q592 (Clarke et al. 2006). These findings are consistent with the discovery of clinical cases of hERG-linked long QT syndrome (N588D (Splawski et al. 1998)) and the short QT syndrome mutation (N588K (Brugada et al. 2004; Cordeiro et al. 2005; Hong, Bjerregaard, et al. 2005; McPate et al. 2005; McPate, H. Zhang, et al. 2009)).

1.2.5 Clinical relevance of the hERG channel

In humans, the normal upper limit of rate-corrected QT interval (QT_c) of the ECG is < 430 ms and < 450 ms for males and females respectively (Garson 1993; Yap & Camm 2003).

QT_c intervals that are larger than 440 ms for males and 460 ms for females are considered to denote prolongation of the QT interval, with QT_c of ~500 ms or more strongly associated with increased likelihood of arrhythmogenesis (Garson 1993; Yap & Camm 2003). Prolongation of the QT interval on the ECG has been documented to be associated with syncope and, in some cases, sudden death. A published case in which prolongation of the QT interval was observed paired with a unique polymorphic ventricular tachycardia named Torsades de Pointes (TdP) (Dessertenne 1990). As the QT interval corresponds to the ventricular action potential, likely candidates for the lengthening the APD at the cellular level are potassium channels involved in normal ventricular repolarisation (Hancox et al. 2008). This prolonged QT interval, also clinically described as 'long QT syndrome', has been strongly associated with channels mediating I_{Kr}/I_{hERG} in two forms: familial/congenital LQTS is related to mutations within the hERG gene (LQT2) whilst acquired LQTS is achieved by drug inhibition of hERG channels (Curran et al. 1995; Sanguinetti et al. 1995).

1.2.5.1 Familial long QT syndrome

To date, mutations in 16 different genes have been identified in clinically diagnosed cases of Long QT syndrome (El-Sherif et al. 2017). LQT2 syndrome is associated with the *KCNH2* gene, and accounts for 30-40% of cases of LQTS (El-Sherif et al. 1997; Vandenberg et al. 2012). Mutations in the hERG gene were first described in 1995 which, in turn, was critical in the understanding between hERG, cardiac repolarisation and LQTS (Curran et al. 1995; Sanguinetti et al. 1995) (see Section 1.2). Since then, over 400 putative mutations in *hERG* have been identified and linked with the disease (Vandenberg et al. 2012). Mutations in the *hERG* can disrupt physiological I_{hERG} in several ways: (1) a reduction or a defect in the protein synthesis. (2) defective trafficking, resulting in lack of functional channels reaching the cell membrane and subsequent reduction in available hERG channels at the surface (Ficker et al. 2000; Kagan et al. 2000; Anderson et al. 2006). (3) abnormal gating which can be divided into two mechanisms; a reduction in activation (Berecki et al. 2005; Chen et al. 1999) or enhanced inactivation (Nakajima et al. 1998). (4) abnormal conduction can be a result of a change in the ion selectivity or in single-channel conductance.

1.2.5.2 Acquired long QT syndrome

Acquired LQTS is strongly associated with pharmacological blockade of hERG/I_{Kr} channels, which can lengthen the QT interval by direct channel block or by an impairment

in hERG channel trafficking (Vandenberg et al. 2012). Drugs with a diverse range of actions and chemical structures have been linked to TdP liability with a common effect being the reduction in I_{Kr}/hERG (Viskin 1999; Vandenberg et al. 2001; Witchel & Hancox 2000; Yap & Camm 2003; Hancox et al. 2008). Because of such a diverse range of structures and pharmacological action of drugs, an *in vitro* assay of the hERG channel is now deemed necessary to evaluate the cardiac safety of novel drugs (International Conference on Harmonisation, ICH, S7B, Step 4 (ICH Expert Working Group 2005) at http://www.ich.org/fileadmin/Public_Web_Site/ICH_Products/Guidelines/Safety/S7B/Step4/S7B_Guideline.pdf).

Many drugs are known to mediate their effects by binding within the inner cavity of hERG channels which subsequently blocks ion conduction. An initial mutagenesis study, based on homology differences observed between hERG and other K_v channels, reported that the residue F656 was important in dofetilide block (Lees-Miller et al. 2000). An alanine scan was completed on the S6 which revealed that polar residues T623 and S624 located at the base of the pore as well as aromatic residues Y652 and F656 are thought to be important for MK-499 binding (Mitcheson, Chen, Lin, et al. 2000). I_{Kr}/hERG is known to show high affinity block (in the nanomolar range) by methansulphonanilides, which includes both dofetilide and MK-499 (Snyders & Chaudhary 1996; Zhou et al. 1998; Lees-Miller et al. 2000; Mitcheson, Chen, Lin, et al. 2000; Kamiya et al. 2008). Depolarisation of the membrane causes a progressive block by methansulphonanilides, suggesting that channel opening is required (Spector & Curran 1996; Snyders & Chaudhary 1996; Zhou et al. 1998). It appears that the drug becomes 'trapped' inside the channel and so recovery from block is slow (Carmeliet 1992; Mitcheson, Chen & Sanguinetti 2000; Mitcheson et al. 2005). It was previously mentioned (Section 1.2.3) that hERG channels are missing the proline motif that causes a 'kink' in the S6 domain that is thought to limit the size of the inner cavity in other K_v channels, and so it is thought this larger inner cavity allows hERG to be blocked a range of drug structures and sizes (del Camino et al. 2000; Mitcheson, Chen & Sanguinetti 2000; Mitcheson et al. 2005; Thouta et al. 2014). The cryo-electron micrscopy (cryo-EM) structure of hERG has shown that hERG channels possess a slightly more narrow region located below the selectivity filter which increases the negative electrostatic potential (Wang & MacKinnon 2017; Vandenberg et al. 2017). An unexpected find from the Wang & MacKinnon structure is that hERG channels contain hydrophobic

'pockets' that extend out from the central pore cavity which could account for its pharmacological promiscuity (Wang & MacKinnon 2017; Vandenberg et al. 2017)

1.2.5.3 Delayed repolarisation of the action potential and arrhythmogenesis

It should be pointed out that there are drugs available, such as the Class III antiarrhythmics, which act to delay repolarisation by blocking potassium channels and so refractoriness is prolonged and re-entrant circuits are disrupted (Singh 1999). However, arrhythmogenesis is connected to an excessively prolonged QT interval in two ways: (1) the prolongation in repolarisation phase is susceptible to the rise of early after-depolarisation (EAD) events (January & Riddle 1989; Fozzard 1992; Volders et al. 2000). (2) delayed repolarisation may become pro-arrhythmic via enhancement of transmural dispersion of repolarisation (TDR). TDR occurs physiologically due to the heterogenous expression of the ion channels, particularly I_{Ks}, across the cardiac walls and can influence the morphology of the ECG (Yan et al. 2003; Antzelevitch 2005; Antzelevitch 2007). I_{Kr} inhibition can augment the effects of TDR, particularly in the mid-myocardium where there is lower expression of I_{Ks} (Antzelevitch 2005) and greater I_{Kr} expression (Akar et al. 2002; Chen et al. 2006). An increased heterogeneity as a result of enhanced TDR can provide a substrate for re-entrant arrhythmia (Lankipalli et al. 2005; Antzelevitch & Sicouri 2012). The idea of increased heterogeneity of repolarisation across the cardiac wall in situations where I_{Kr}/I_{hERG} is reduced (such as cardiac ischaemia) may be of some relevance to the work completed in this thesis.

1.2.5.4 hERG and short QT syndrome

Short QT syndrome (SQTS) is clinically diagnosed with an average QT_C of ~302 ms in females and ~308 ms in males (Gollob et al. 2011). Since the clinical discovery of mutations that cause SQTS in the KCNH2 gene (SQTS1 (Brugada et al. 2004)), a further four gene loci have been linked to SQTS (Patel et al. 2010). The SQTS variant that is connected to hERG, SQTS1, leads to a N588K mutation in the hERG channel that result in an increase in I_{Kr} (Brugada et al. 2004; Hong, Piper, et al. 2005; Hong, Bjerregaard, et al. 2005; McPate et al. 2005; McPate, H. Zhang, et al. 2009). The N588 residue, as mentioned previously, lays in the amphipathic helix of the S5P linker and appears to play a role in hERG channel inactivation. Recent studies have discovered novel SQTS1 mutants E50D, T618I and E1135H which also resulted in loss of inactivation but with a less severe

phenotype than the N588K mutation (Itoh et al. 2009; Redpath et al. 2009; Sun et al. 2011).

1.3 Acidosis

Acidosis is clinically confirmed when arterial pH < 7.35 (Moyle et al. 2002) and can be caused by an increase in pCO_2 (respiratory acidosis) or by a reduction in bicarbonate ions (HCO_3^-, metabolic acidosis) (Steenbergen et al, 1977; Williamson et al, 1976).

1.3.1 Acidosis in the heart

The heart can be subjected to acidosis in a number of pathologies such as myocardial ischaemia. During ischaemic events, anaerobic glycolysis occurs which leads to accumulation of lactate, protons and nicotinamide adenine dinucleotide (NAD^+), and results in a decrease in cell pH (Kalogeris et al. 2012). The cell removes the protons in exchange for Na^+ via the Na^+/H^+ exchanger and the Na^+ are exchanged for Ca^{2+} by the Na^+/Ca^{2+} exchanger. The increase in cytosolic Ca^{2+} can have detrimental effects on the cell, including cell death, whilst the accumulation of protons in the surrrounding ischaemic tissue can cause further damage. The extent of damage caused by protons in the extracellular environment is determined by the buffering capacity of the extracellular milieu; ischaemic events caused by an obstruction in blood flow will reduce the diffusion of CO_2 which increases the partial pressure of carbon dioxide (pCO_2) (Yan & Kléber, 1992). An increase in pCO_2 causes an imbalance in the bicarbonate buffer system; CO_2 reacts with water to form carbonic acid which subsequently dissociates to form bicarbonate and hydrogen ions.

Acute ischaemia is associated with metabolic changes that would result in altered electrical activity and, as a result, increased risk of arrhythmia. Such effects include disruptions in the excitation-contraction coupling mechanism (Fry and Poole-Wilson, 1981; Orchard and Kentish, 1990; Orchard & Cingolani, 1994) as well as the alteration of cardiac ion channels. Such alterations could include suppression of channel current and changes in gating kinetics which could make the heart susceptible to the generation of arrhythmias (Orchard & CIngolani, 1994; Komukai et al, 2002). Previous work studying acidosis in pig myocardium showed that the $[H^+]_e$ peaked at around pH_e 6.3 (Fleet et al. 1985).

Cardiac ion channel and transporter function can be adversely affected in a range of pathologies including acidosis, which occurs in the heart under several pathological conditions. It is one of the most deleterious changes during myocardial ischemia and reperfusion and is well recognised to be responsible for changes in the function of ion channels that can cause arrhythmias.

1.3.2 Modulation of hERG channels by acidosis

HERG channels and native I_{Kr} channels have been shown to be modulated by extracellular acidosis (Anumonwo et al. 1999; Bérubé et al. 1999; Jiang et al. 1999; Jo et al. 1999; Terai et al. 2000; Vereecke & Carmeliet 2000; Bett & Rasmusson 2003; Zhou & Bett 2010; Van Slyke et al. 2012; Du et al. 2010; Shi et al. 2014). Observations show agreement in the effects of protons with a decrease in hERG current amplitude and acceleration in deactivation. However, differences have been seen in the effects of extracellular acidosis on the voltage dependence of hERG channel activation, with some seeing a depolarised shift (Jo et al. 1999; Terai et al. 2000; Vereecke & Carmeliet 2000; Bett & Rasmusson 2003; Du et al. 2010; Van Slyke et al. 2012; Shi et al. 2014) and others showing no shift (Anumonwo et al. 1999; Bérubé et al. 1999; Jiang et al. 1999). Discrepancies could arise from the expression system used or the pH range studied or the idea that the different processes involved in hERG channel gating/conductance have different pH sensitivities (Anumonwo et al. 1999; Bett & Rasmusson 2003; Van Slyke et al. 2012; Shi et al. 2014). The notion of potential multiple binding sites on hERG for extracellular protons will be discussed in a later chapter (Chapter 6).

As the most significant observations seen in hERG channels exposed to extracellular acidosis are the acceleration of deactivation and reduction in I_{hERG}/I_{Kr} amplitude, the contribution of I_{hERG}/I_{Kr} to the repolarisation of the action potential is reduced (Du et al. 2010). As a result, the ability of hERG channels to protect the heart from premature stimuli due to its unique gating kinetics is impaired in extracellular acidosis (Smith et al. 1996; Lu et al. 2001; Vandenberg et al. 2001; Bérubé et al. 1999; Du et al. 2010).

1.4 Aims of my PhD

Based on the background review, it can be concluded that:

- The gating kinetics of channels underpinning I_{Kr}/I_{hERG} make the channels to be physiologically important in the repolarisation of action potentials: rapid, voltage dependent inactivation allows hERG channels to enter a non-conducting state during the depolarised plateau phase of the AP. Rapid recovery from inactivation with slow gating kinetics from the open to closed state allow a robust repolarisation that confers protection from premature stimuli.
- Growing evidence suggests that native I_{Kr} is a teterameric channel composed of hERG1a and 1b subunits
- Acidosis has been shown to modulate macroscopic I_{Kr}/I_{hERG} amplitude and kinetics with discrepencies in the literature suggesting that different I_{hERG} features show different pH sensitivities. However, there are no published data on the effects of extracellular acidosis on the single-channel currents of wild-type hERG.

The aims of the work presented in this thesis are:

- To characterise the effects of extracellular acidosis at the macroscopic and single channel level of homomeric hERG1a and hERG1b channels expressed in mammalian cells (Chapters 3 and 4)
- To investigate the mechanism(s) by which protons modulate the hERG1a channel by carrying out covalent modification experiments (Chapter 5)
- To characterise the concentration dependence of effects of protons on distinct features of I_{hERG} and to make and investigate point mutations to the hERG1a channel, to probe the molecular basis of pH sensitivity (Chapter 6)

2. General Methods and Materials

2.1 hERG plasmid and molecular biology

Experiments carried out in this PhD thesis used channel expression in either the Human Embryonic Kidney (HEK-293; ECACC 85120602) or the Chinese Hamster Ovary (CHO; ECACC 85050302) cells. The HEK-293 cell line either stably expressed wild-type (WT) hERG1a (Zhou et al. 1998) or were transiently transfected with WT hERG1a or mutant hERG 1a constructs. The CHO cell line was transiently transfected with the hERG1b construct (Du et al. 2011).

2.1.1 Plasmid DNA and vector

The hERG 1b plasmid that was used in transient transfections was donated by Dr Gail Robertson (University of Wisconsin;(Jones et al. 2004; Phartiyal et al. 2008; Robertson et al. 2005)). The hERG1a plasmids, containing point mutations, were prepared in the laboratory from a WT hERG1a template using Quikchange® mutagenesis.

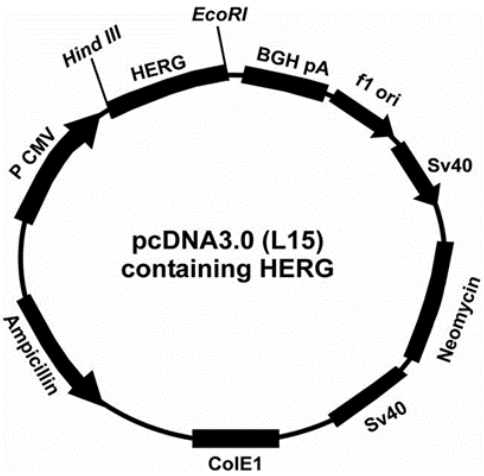

Figure 2-1 L-15 Vector.

Diagram illustrating the modified pcDNA3.0 (L15) vector in which the hERG cDNA has been inserted in between the HindII and EcoRI restriction enzyme site

The vector used to carry the full hERG cDNA sequence (Genbank Accession number U04270) is the 'L15' vector (see Figure 2-1). The L15 construct is a modified pcDNA3.0 vector in which the endogenous BglII and SalI restriction enzyme sites were removed and the hERG cDNA has been inserted in between the HindIII and EcoRI restriction enzymes sites (McPate et al. 2005; Zhang et al. 2011; El Harchi et al. 2012).

2.1.1.1 Site directed mutagenesis

Mutant		Primers
H562N	Forward	5’-CGCTCATCGCGAACTGGCTAGCC-3’
	Reverse	3’-GCGAGTAGCGCTTGACCGATCGG-5’
E575Q	Forward	5’-CGGCAACATGCAGCAGCCACAC-3’
	Reverse	3’-GCCGTTGTACGTCGTCGGTGTG-5’
H578N	Forward	5’-CAACATGGAGCAGCCAAACATGGACTCAC-3’
	Reverse	3’-GTTGTACCTCGTCGGTTTGTACCTGAGTG-5’
D580N	Forward	5’-GCCACACATGAACTCACGCATC-3’
	Reverse	3’-CGGTGTGTACTTGAGTGCGTAG-5’
H587N	Forward	5’-CATCGGCTGGCTGAACAACCTGGGCGA-3’
	Reverse	3’-GTAGCCGACCGACTTGTTGGACCCGCT-5’
N588K	Forward	5’-GCTGGCTGCACAAGCTGGGCGACCA-3’
	Reverse	3’-CGACCGACGTGTTCGACCCGCTGGT-5’
D609N	Forward	5’-GGCCCCTCCATCAAGAACAAGTATGTGACGG-3’
	Reverse	3’-CCGGGGAGGTAGTTCTTGTTCATACACTGCC-5’
E637Q	Forward	5’-CCCAACACCAACTCACAGAAGATCTTCTC-3’
	Reverse	3’-GGGTTGTGGTTGAGTGTCTTCTAGAAGAG-5’
H674N	Forward	5’-GCAACATGCAGCAGCCAAACATGGACTCACG-3’
	Reverse	3’-CGTTGTACGTCGTCGCTTTGTACCTGAGTGC-5’
E575Q/H578N	Forward	5’-GCACAGCCCGCTACAACACACAGATGC-3’
	Reverse	3’-CGTGTCGGGCGATGTTGTGTGTCTACG-5’

Table 2-1 Primers used in thesis.

Each mutant created required a forward and reverse primer to carry out the PCR reaction. The N588K mutation was previously made by a former member of the Hancox laboratory group.

Desired point mutations were introduced into the hERG cDNA sequence using Polymerase Chain Reaction (PCR) primers that were designed using the Quikchange Design program (Agilent Technologies, USA): (http://www.genomics.agilent.com/primerDesignProgram.jsp).

The primers were designed and checked for secondary/hairpin structures before being synthesised by Sigma. For each mutant created, forward and reverse primers were used at a stock concentration of 100 µM when dissolved into water (water for injections, Hameln Pharmaceuticals ltd, UK). Primers that were used for each mutation are shown in Table 2-2.

The sample reactions were set up as: 5 µl 10x reaction buffer, 25-50 ng of template cDNA WT or mutant), 125 ng forward primer, 125 ng reverse primer, 1 µl of dNTP mix, 2.5 µl DMSO, 1 µl PfuTurbo DNA Polymerase (2.5 U/µl), with the remainder made up to 50 µl using sterile water.

Stage	Temperature (°C)	Time duration	Cycles
1	94	45 seconds	1
	94	45 seconds	
2	50/65	45 seconds	16
	68	14 minutes	
3	6	∞	1

Table 2-2 PCR cycle.

A table to show the duration and temperature required for each stage of the PCR reaction.

The PCR cycle is described in Table 2-2 and starts with a 45 second segment (stage 1) in which the polymerase was activated. This was followed by stage 2 which involves the separation of the double-stranded cDNA into single strands, allowing the primers to anneal to the single strands and primer extension. The samples were held at 6 ˚C (stage 3) to finish the reaction. The addition of 1 µl Dpn I restriction enzyme (10 U/µl) to each of the amplification reactions was followed by incubation at 37 ˚C for 3-4 hours to digest any parental/template cDNA. An Overview of this process can be seen in Figure 2-2.

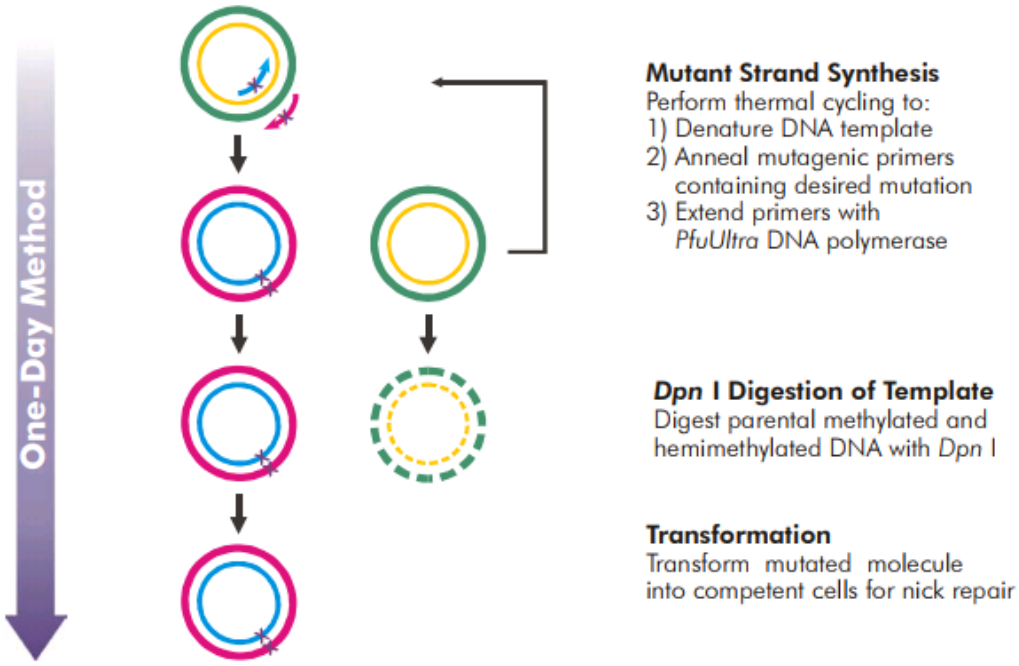

Figure 2-2 Overview of Quikchange® site-directed mutagenesis.

The use of thermal cycling and DNA polymerase allows the production and amplification of the mutant. Parental cDNA is removed by treatment with Dpn1 and the mutant was transformed into competent cells. Image taken from the Quikchange® site-directed mutagenesis manual (http://www.agilent.com/cs/library/usermanuals/Public/200523.pdf)

2.1.1.2 Purification of PCR product

Following the digestion of parental cDNA, the amplification mixture was then purified using the QIAquik PCR Purification Kit (Qiagen, UK). The process was completed using the manufacturer instructions. For completeness, the procedure begins by adding 200 µl PB Buffer to the PCR sample. The sample is placed in a QIAquick column that has been placed in a 2 ml collection tube. To bind the DNA, the QIAquick column is centrifuged at 13,000 rpm for 60 seconds, which the flow-through discarded. To wash the DNA and to remove impurities, 750 µl PE Buffer is added to the QIAquick column and centrifuged at 13,000 rpm for 60 seconds.

The flow-through is discarded and the centrifuge process is repeated. The QIAquick column is then placed in a clean 1.5 ml Eppendorf for DNA collection. To elute the DNA,

50 µl sterile water is added to the centre of the QIAquick membrane and centrifuged at 13,000 rpm for 60 seconds. The DNA collected is now purified to be transformed and sequenced to ensure the correct mutant has been created.

2.1.2 Plasmid cDNA preparation

2.1.2.1 Bacterial transformation

The cDNA that was to be amplified to create plasmid stocks was transformed into bacterial cells. Agar plates were prepared for the growth of the bacteria. A bottle containing 200 ml 1.6% Lysogeny Broth (LB) agar was heated in a microwave (600 W) for 8 minutes. The lids were left loose and swirled every 2 minutes so that bubbles did not form. The agar was left to cool until it was at a temperature in which the bottle could be held, after which the antibiotic of choice was added: 100 µl/100 ml ampicillin for hERG-1a/b (WT or mutant) constructs and 100 µl/100 ml kanamycin for the eGFP construct and swirled gently. The solution was then poured into 100 mm petri-dishes and left on a flat surface to cool down to room temperature, after which the lids were placed back on.

To begin the transformation procedure, a bench-top box containing ice was prepared and a water bath was set to 42 ˚C. A vial of One Shot Top10 chemically competent E. coli was placed on ice to thaw. Once thawed, 1 µl of the plasmid construct (stock: 0.1 µg/µl) was added to the bacteria and left to incubate on ice for 30 minutes. The solution was then heat-shocked for exactly 30 seconds in the water bath before being placed back on ice for 2 minutes. The addition of 250 µl of super optimal broth with catabolite repression (SOC) to each vial was flicked to mix. The vials were then placed in individually labelled 30 ml universal tubes (Greiner Bio-One, UK) and then incubated at 37 ˚C in a shaking incubator for 1 hour at 225 revolutions per minute (rpm). After the incubation, various volumes (50 µl or 100 µl) of the transformation solution were transferred, under aseptic conditions, to the agar dishes and streak-spread using a sterile plastic inoculation loop. The lid was placed back on and the dishes were turned up side-down to prevent the build-up of condensation and placed in a 37 ˚C incubator overnight. The plates were removed from incubation at approximately 09:30 the following morning. The presence of bacterial colonies on the agar plate indicated that the transformation of the cDNA was successful. An individual colony was chosen by prodding a sterile Gilson tip and placed into a fresh 30 ml universal tube containing 2.5 ml LB medium supplemented with the selected antibiotic (100 µl/100 ml). The Universal was then left in the shaking incubator for 7 hours at 37 ˚C. After the

incubation period, the contents of the universal were transferred to a 250 ml conical flask which contained 150 ml LB medium supplemented with 150 µl antibiotic (stock: 100 µg/1ml). The conical flask was then incubated overnight in the shaker incubator, 200-225 rpm at 37 ˚C.

At approximately 10:00 the following morning, the contents of the overnight culture were transferred into a centrifuge bottle and, with a counterbalance, spun in a JA 14 rotor at 6000 g for 15 minutes at 4 ˚C. The supernatant was removed by pouring and the pellet was frozen at approximately -20 ˚C overnight.

2.1.2.2 Qiagen maxi-prep

The plasmid DNA was extracted from the bacteria and purified using a Hi Speed™ plasmid Maxi Kit (Qiagen). The pellet obtained from bacterial transformation was thawed out at room temperature before the addition of 10 ml of buffer P1 (contains 100 µg/ml of RNaseA and the optional LyseBlue at a final dilution of 1:1000). The solution was completely resuspended by pipetting up and down before 10 ml of buffer P2 was added and vigorously mixed by inverting the bottle 5 times, followed by incubation at room temperature for 5 minutes. Due to the addition of LyseBlue to buffer P1, a homogenously blue coloured suspension would form after sufficient mixing. After that, 10 ml of chilled buffer P3 was added followed by vigorous mixing by inversion of the bottle 5 times. This causes the mixture to return to a homogenously colourless solution with the formation of a white ‘fluffy’ precipitate. The contents of the bottle were transferred to a QIAfilter cartridge and then incubated on ice for 20 minutes. During the incubation period a QIAGEN-tip 500 column was equilibrated by the addition of 10 ml QBT buffer and allowing to empty by gravity flow. After incubation, the plunger was inserted in to the cartridge and the contents were filtered into the equilibrated tip and allowed to flow through by gravity. The tip was then washed twice with 30 ml QC buffer after which the DNA was eluted into a 50 ml falcon tube by adding 15 ml QF buffer to the tip. The DNA was then precipitated by adding 10.5 ml isopropanol to the falcon tube and left to incubate at room temperature for 30 minutes. The elute/isopropanol mix was then transferred to a 30 ml syringe with a QIAprecipitator™ Maxi Module attached and then filtered before 2 ml of 70% ethanol was added to the 30 ml syringe and filtered through. The membrane was then air dried by leaving on a clean tissue for 5-10 minutes before attaching to a 5 ml syringe. A 1.5 ml Eppendorf was placed under the syringe and 1 ml of TE buffer was added to the 5 ml

syringe and filtered through to elute DNA. The contents of the Eppendorf were then passed through the syringe and filtered and collected in the same Eppendorf.

2.1.2.3 Determining cDNA yield

The concentration of the plasmid cDNA was determined using a NanoDrop spectrophotometer. A blank measurement was made using 1 µl TE buffer before the construct was measured. Both sides of the sample holder were cleaned with pure water between each measurement. The construct concentration was measured three times to gain an average before diluting in pure water to make a final concentration of 100 ng/µl. This was then aliquoted and frozen down to -20 ˚C and used for subsequent cell line transfection.

2.2 Cell culture

2.2.1 Maintenance of mammalian cell lines

2.2.1.1 HEK-293 cell culture

HEK-293 cells (ECACC, European collection of cell cultures) were kept in CELLSTAR 25 cm^2 cell culture flasks (Greiner Bio-One, UK) in a 5% CO_2 incubator at 37 ˚C. The cells were supplied with ~8 ml Dulbecco's Minimum Essential Medium with Glutamax-1 (DMEM; Gibco, UK), supplemented with 10% Foetal Bovine Serum (FBS; UK), 1% Penicillin/Streptomycin (P/S: Gibco, UK). Cells were passaged at 80-90% confluence which took approximately 3-4 days. The DMEM, phosphate buffered solution (PBS) and the enzyme-dissociation buffer were preheated to ~37 ˚C. Old medium was removed and the cells were washed twice in 5 ml of PBS, then 2 ml dissociation buffer was added for ~3 minutes incubation. The cells were dislodged by gently agitating the flask and then viewed under a microscope to ensure that the cells were displaced from the bottom of the flask. 6 ml of fresh media was added to the cells and thoroughly but gently mixed. The cell suspension was subsequently split into flasks, usually a 1:8 (1 ml cell mixture with 7 ml fresh media) dilution, for continuing cell line maintenance. Additionally, when required, the cell suspension was seeded into 35 mm cell culture dishes (Corning, UK) in a drop-wise manner with ~2 ml fresh DMEM for transfection and electrophysiology. Cells were incubated at 37 ˚C for a minimum of 24 hours before any recordings or transient transfections.

HEK-293 cells stably expressing WT hERG-1a (a kind gift from Dr Craig January, University of Wisconsin (Zhou et al. 1998)) were treated in the same manner as HEK-293 cells. The only difference was that the medium was also supplemented with 400 $\mu g.ml^{-1}$ geneticin in addition to the 10% FBS and the 1% P/S.

2.2.1.2 CHO cell culture

The manner in which CHO cells were maintained and passed was the same as HEK-293 cell culture with the only difference being the medium used to supplement the cells. The Ham's F-12K (Kaighn's Medium) (Life Technologies) medium was used instead of DMEM.

2.2.2 Transfection of HEK-293 cells

HEK cells were passed onto 35 mm petri-dishes and incubated for a minimum of 24 hours before transfection. Transient transfections were carried out by combining the channel plasmid DNA with green fluorescent protein (eGFP) DNA and incubating with 0.2 µg/µl Polyethylenimine (PEI; Alfa Aesar). Transfection tubes were prepared so that the contents would transfect four 35 mm petri-dishes with 500 ng of desired construct and 500 ng eGFP. The transfection tubes consisted of 80 µl PEI (4 times the amount of total DNA concentration in weight), 20 µl WT or mutant hERG1a, and 20 µl eGFP. For mutant constructs that required co-transfection with WT-hERG1a, the ratio used was 1:1 using 250 ng of each construct. The contents were mixed well by tapping the tube in the cell culture hood. The tube was left to incubate for ~10 minutes before adding 680 µl pure DMEM so that there was 200 µl per 35mm petri-dish of the transfection mixture. The solution was added to the cells in a drop-wise manner before being returned to incubation for a minimum of 18 hours before any electrophysiology experiments. The co-transfection of the desired plasmid with eGFP allowed identification of cells expressing the DNA by fluorescence under ultraviolet excitation.

2.2.3 Transfection of CHO cells

The CHO cell line was used for the transfection of the hERG1b isoform due to the poor expression of the channel in HEK-293 cells; the hERG1b isoform contains an endoplasmic reticulum (ER) retention signal, which makes it difficult to express on its own (Phartiyal et al. 2008). Prior work in Hancox laboratory has shown that CHO cells are a suitable alternative for hERG1b expression experiments (Du et al. 2011). CHO cells appear to grow at a faster rate compare to HEK-293 cells which makes it difficult to transfect in a

similar matter to that of HEK-293 cells. As a result, 25 cm^2 flasks of CHO cells were transfected using Lipofectamine LTX with PLUS reagent (Invitrogen). Transfection tubes were set up as; 800 µl Optimem-1 medium (GIBCO), 2.5 µg eGFP, 2.5 µg hERG1b and 5 µl of PLUS reagent (Invitrogen). The contents were mixed and incubated at room temperature for 5 minutes before the addition of 13 µl Lipofectamine LTX (Invitrogen). The tube was then mixed and incubated for 25 minutes at room temperature to allow the cDNA to complex with the Lipofectamine LTX. During the incubation period, the medium from the flask containing cells was removed and replaced with 5 ml of fresh F-12K medium with serum but no antibiotics. The transfection mixture was then added to the flask and the cells were incubated for approximately 24 hours before plating. The cells were plated onto 35 mm dishes in a drop-wise manner in F-12K medium (10% FBS, 1% P/S) and then a further 18-24 hour incubation period was needed before patch clamp recording to allow for sufficient expression of the channel at the cell membrane.

2.2.4 Freezing mammalian cells

To ensure a continuous supply of cells was available, it was essential to freeze down samples into liquid nitrogen regularly. To prevent any damage to the cells, cells were frozen down slowly using a “Mr. Frosty” freezing container (Nalgene 5100-0001) filled with 100% isopropyl alcohol. For both CHO and HEK cell lines, the medium was appropriately replaced at least 6 hours before freezing down. Apart from the freezing solution used, the process was the same for both the HEK and CHO cell lines. At approximately 80-90% confluence, the medium was aspirated, and the cells were washed twice with 5 ml PBS. The cells were then incubated for ~3 minutes in 2 ml dissociation buffer. The cells were viewed under a microscope and dislodged from the flask by gentle agitation. Approximately 8 ml of DMEM or F-12K (10%, 1%) was added to the cells to then be transferred to a 15 ml falcon tube. Using a counterweight, the cells were centrifuged for 10 minutes at 500 rpm to create a pellet. The supernatant was removed and 3 ml of the freezing solution (for HEK; DMEM, 20% FBS, 10% DMSO, and for CHO; F-12K, 20% FBS with 10% DMSO) was slowly added to the pellet. The freezing mixture was pulled up and down in the pipette several times to fully mix the pellet. 1 ml of the freezing solution was then added to a labelled plastic 1.2 ml cryogenic vial (Starlab, UK), which was then placed in the “Mr Frosty” freezing box. The “Mr Frosty” container is designed to achieve a cooling rate of ~ 1 ˚C per minute, and so minimise damage to the cell. The cooling process was

completed at -80 ˚C for at least 24 hours before being transferred to gaseous phase liquid nitrogen.

2.2.5 Thawing mammalian cells

In preparation for thawing out frozen cells, a new 25 cm^2 flask was labelled appropriately and the appropriate pre-warmed medium (supplemented with 20% FBS but no antibiotic) was added. For the HEK cells stably expressing hERG, medium without the selection antibiotic was also used for the first step. The vial containing the cells was removed from liquid nitrogen and immediately placed in warm water for 1-2 minutes. Working in a cell culture hood, the cells were transferred to the flask and then placed in the incubator for ~6 hours before changing the medium with appropriate fresh medium (DMEM or F-12K; 10%, 1%). At this stage, for the stable cell line, medium containing the selection antibiotic (geneticin) was used. Close inspection of the cells was conducted on a daily basis to check cells were growing correctly without any infection. This was carried out until the cells were ready to be passed as described in the Section 2.2.1.

2.3 Electrophysiological recording

2.3.1 Solutions

Cells that were being studied in the whole-cell configuration were continuously superfused with normal Tyrode's solution with a similar composition to that used by other studies in the Hancox laboratory (McPate et al. 2005; McPate, H. Zhang, et al. 2009; Du et al. 2010; Du et al. 2011; El Harchi et al. 2012). The solution contained (in mM): 140 NaCl, 4 KCl, 2 $CaCl_2$, 1 $MgCl_2$, 10 Glucose, 5 HEPES, and 5 MES (titrated to pH7.4 with NaOH). MES was used as well as HEPES as MES acts as a buffer in the pH range 5.5-6.7 with a pK_a 6.1 (Sigma-Aldrich). The acidic external solution had the same composition as the above Tyrode solution, but titrated to the desired pH with HCl. Osmolarity of the external solution was approximately between 285-300 mOsm.

The pipette (internal) solution for whole-cell recordings contained (in mM): 130 KCl, 5 EGTA, 1 $MgCl_2$, 10 HEPES, and 5 MgATP (titrated to pH7.2 with KOH). The osmolarity of the internal solution was ~270 mOsm. The solutions for whole-cell experiments were designed to minimise liquid junction potentials (LJPs) by balancing the ionic concentrations that are most mobile (Cl^-, K^+ and Na^+) (Barry 1994). LJPs were calculated using the

JPCalc software (Axon Instruments). The LJP for solutions used in whole-cell experiments was -4.4 mV which is small and was not corrected for.

Single-channel experiments utilised the same composition for both external and pipette solution due to the pipette solution acting as the external for the patch of cell undergoing experiments. The solution contained (in mM): 140 KCl, 2 $CaCl_2$, 1 $MgCl_2$, 5 HEPES, and 5 MES and titrated to either pH 7.4 or 6.3 with KOH

2.3.2 Recording system set-up

35 mm dishes in which cells plated for electrophysiology experiments were placed into an experimental platform mounted onto an inverted microscope (Zeiss Axiovert 100, Germany). The dishes were perfused by gravity with bathing solution of interest at a rate of 20 ml/min to allow quick exchange of solution. The bath level was controlled using continuous suction (Watson Marlow 505s, Cornwall England). A Ag/AgCl pellet was placed in the bath solution to act as a ground electrode (see Figure 2-3).

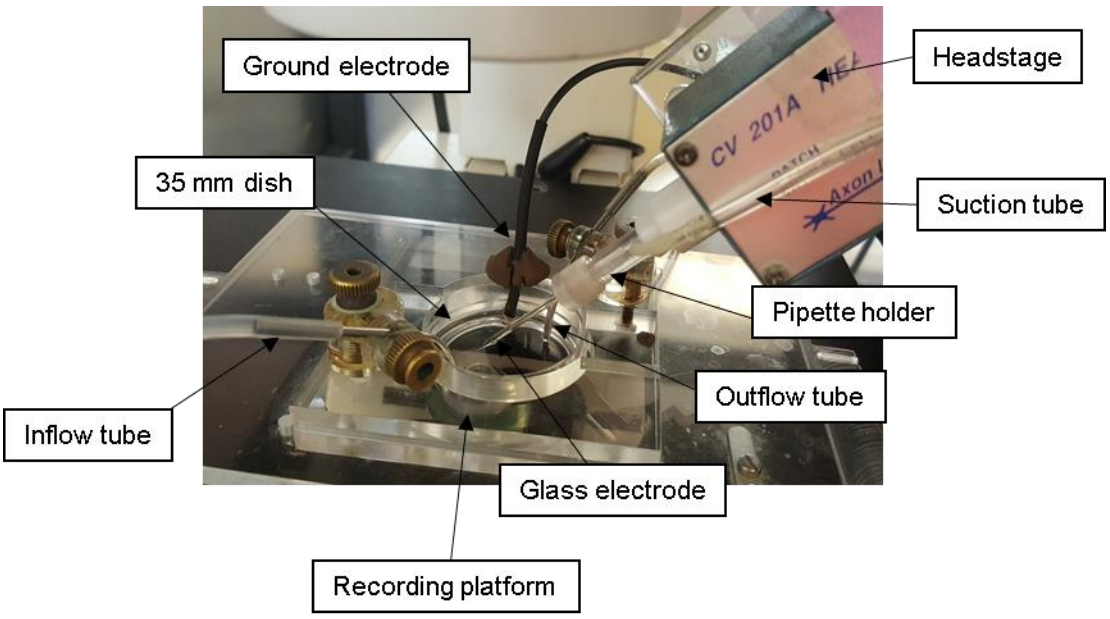

Figure 2-3 Recording chamber set-up.

The recording chamber (35 mm dish containing cells ready for electrophysiological experiments) were placed into the recording platform. External solution was perfused by gravity from the bottom-left. The level of the bath was controlled by an outflow tube which suctioned solution out from the top-right of the chamber.

During recording, solutions of different pH or drug application were applied using different 50 ml tubes set up on a patch-stand. The tubes were connected to a 4-channel tap that allows one solution at a time to be perfused on to the cells (Figure 2-4). At the end of the experimental day, all tubing used were washed with Milli-Q water after drug tubing was washed through with 70% ethanol and subsequently with Milli-Q water.

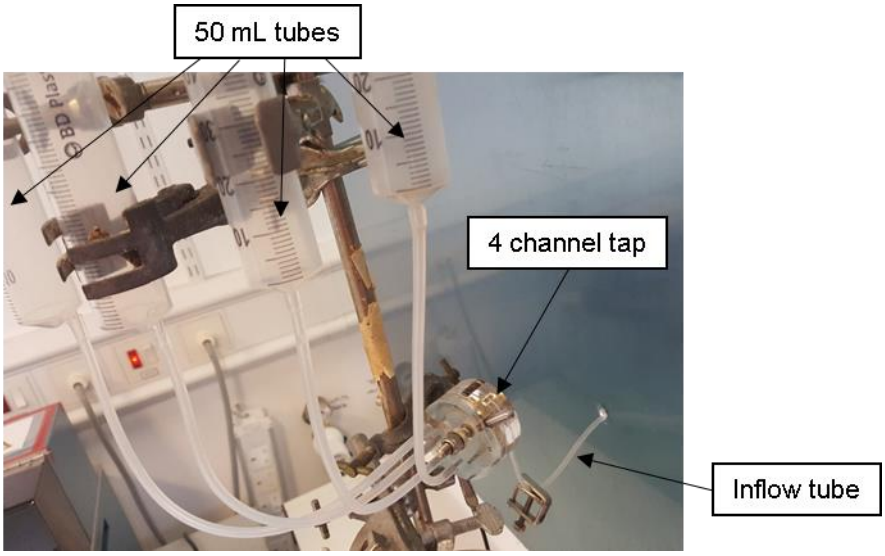

Figure 2-4 Perfusion system.

Solutions used in experiments were placed in 50 mL tubes that were connected to a 4-way channel tap. The tube containing the solution of interest was aligned with the tap to allow perfusion into the recording chamber by the inflow tube.

2.3.3 Data Acquisition

Voltage clamp protocols were designed and applied using Pulse (HEKA). Currents were recorded using an Axopatch 200A amplifier (Axon Instruments) and a CV-201 head-stage (Axon Instruments). Currents were low-pass filtered at 1 kHz (8-pole Bessel, Frequency Devices) and data were acquired at 5-10 kHz using Pulse (HEKA). All recordings were made at room temperature (~22 °C).

The voltage-clamp technique allows a defined voltage to be imposed on the patch, with the purpose to measure the resulting current. This is achieved by the set-up constantly measuring the membrane potential and then changing the voltage to the desired value by effectively injecting current into the circuit. As a result, the membrane is ‘clamped’ and any changes in the membrane current indicates how the cell (or the ion channels under

investigation) react to these changes. Two configurations of the voltage-clamp technique were used in this thesis: whole-cell and cell-attached.

2.3.4 Whole-cell patch clamp

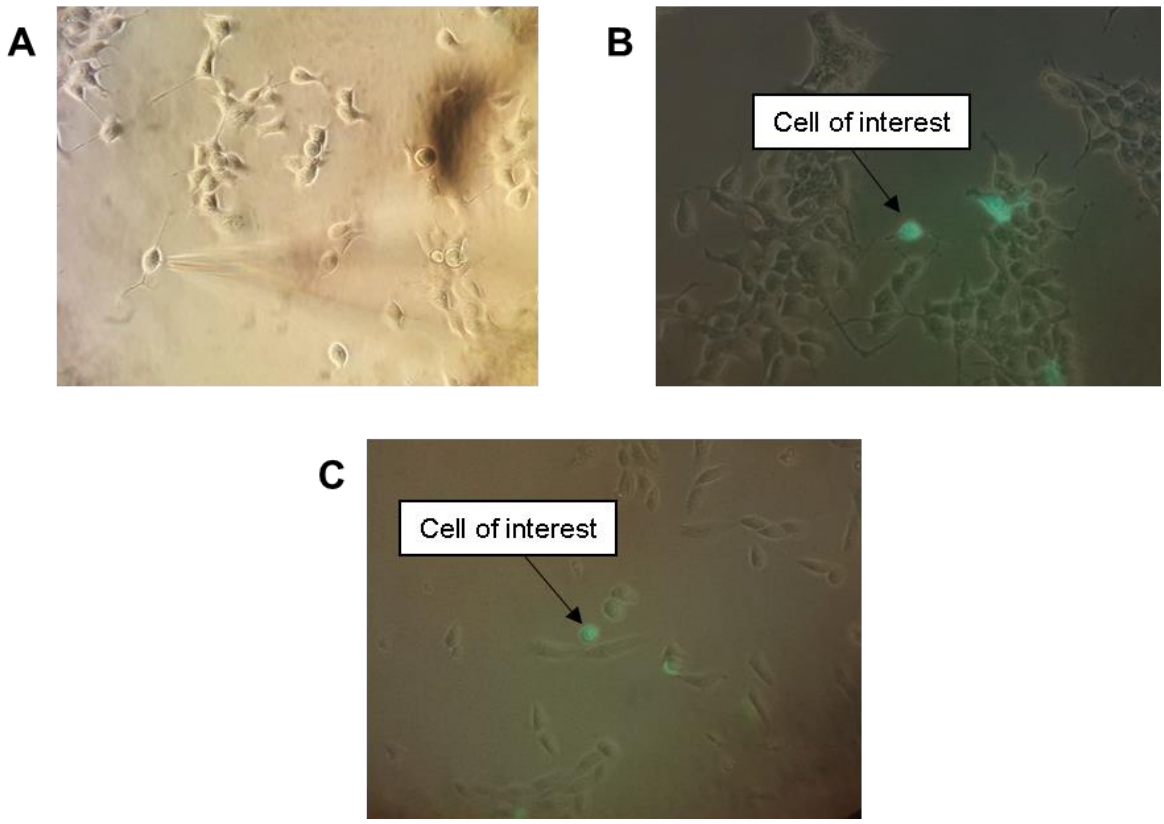

Figure 2-5 Cells used in electrophysiological experiments.

A. HEK-293 cells stably expressing WT hERG1a. A glass pipette containing whole-cell pipette solution positioned just to the right of the cell.
B. HEK-293 cells transiently transfected with channel of interest as well as eGFP. Transfected cells were identified through eGFP expression.
C. CHO cell transiently transfected with WT hERG1b and eGFP. Successfully transfected cells appeared green due to co-expression of eGFP.

All images were taken under a x40 objective.

The whole-cell configuration is achieved by rupturing the membrane patch that is between the pipette solution and the cytoplasm, whilst maintaining a high-quality seal. Whole-cell patch clamp recordings used electrodes fabricated from borosilicate glass that were pulled

using a Narishige (PP-830) puller and fire polished (Narishige MF830) before use. After polishing, electrodes had a resistance of between 2.5 and 4.5 MΩ when filled with whole-cell pipette solution. The pipette electrode was created by coating a silver (Ag) wire with Ag/AgCl by electrolysis in a 0.1% NaCl solution. The pipette was filled with solution as described in 2.3.1 and connected to a pipette holder of a CV 201 Head-stage (Axon Instruments). The head-stage was mounted onto a platform and connected to a PatchStar micromanipulator (Scientifica).

Cells plated onto 35 mm dishes were placed in the recording platform superfused with normal Tyrode solution at room temperature. Cells were observed under the microscope and cells chosen for patching were isolated from other cells and had a smooth appearance (Figure 2-5A-C). HEK or CHO cells that were transfected with channel (mutant or WT) of interest, were co-transfected with eGFP. Using a 490 nm light source with a 510 nm emission filter, the cells transfected with eGFP and presumably the channel looked green when observed through the inverted microscope (Figure 2-5B and C).

The polished pipette tip that was filled with the whole-cell pipette solution (see Section 2.3.1) was lowered close to the cell under study (see Figure 2-5A). A 10 mV 'seal test' voltage step was applied to the pipette using an Axopatch 200A amplifier through a CV-201 headstage. The current produced by applying the 'seal test' allowed close monitoring of the pipette resistance. Contact with the pipette tip and cell membrane caused an increase in pipette resistance and a reduction in the current step amplitude. A giga-Ohm (GΩ) seal was then achieved by applying negative pressure to the patch pipette and clamping the membrane potential at -80 mV. At this point, the current is at 0 nA and the fast capacitance was compensated using the amplifier. The whole-cell configuration was then achieved by suction, causing the cell membrane to rupture and allowing the pipette solution to dialyse with the intracellular compartment of the cell. Series resistance and cell capacitance compensation was then performed: series resistance values were in the range of 2-10 MΩ with ~80% of the series resistance compensated. The series resistance is a sum of the resistances in the circuit (predominantly the pipette and access resistance), which add errors to the clamp; steady state errors and dynamic errors. Steady state errors are due to the amplifier clamping the pipette voltage instead of the membrane potential. Dynamic errors occur when the command voltage produces a chage in the membrane potential with a lag whose time constant is determined by the series resistance and

membrane capacitance. As a result, there is a delay in the rise and fall times in changes of the membrane potential. Membrane cell capacitance compensation values were in the range of 15-23 pF for HEK-293 cells and 11-18 pF for CHO cells. Compensation of the cell capacitance and series resistance is important as it minimises the voltage error that is observed.

2.3.5 Cell-attached patch clamp

The cell-attached patch clamp configuration allows observation of single-channel openings. Quartz pipettes were used because of the electrical characteristics of a low dissipation factor and dielectric constant, which minimised the noise of the patch and thus improving the quality of the data obtained. The quartz pipettes (1.5 mm OD, 0.5 mm ID; Garner Glass Company, Claremont, USA) were pulled using a Sutter P-2000 laser puller to give a pipette resistance of between 8 and 12 MΩ.

Analysis of single-channel activity used TAC (Bruxton, Seattle, USA) software in which channel openings were studied using an event detection process. The process used the 50% threshold technique which involved the program searching the current trace until the threshold is crossed (Figure 2-6). The user sets the threshold limit and then has the option to accept or skip the detected transition. This method meant that all transitions were manually examined so that noise artefacts could be rejected. Accepted transitions were logged in an event table and analysed using TACfit (Bruxton) software to generate amplitude, open- and closed-time duration and burst duration histograms. Both amplitude and duration histograms display the *y* axis as square root transformation of the number of events. It should be noted that detection of events was completed on 'raw' recordings before transients are removed, as seen in Figure 2-6A.

For the generation of amplitude histograms, events with a duration shorter than 1 ms were excluded so that openings that did not reach full amplitude were not analysed. Using a 1 kHz 8-pole Bessel filter and sampling at 10 kHz gives a rise time T_r of 332 µs. All events detected were included in duration histograms. A burst of openings was defined as a group of channel openings separated by closed times that were shorter than a critical time (τ_{crit}) value. τ_{crit} was described as the value where the slowest two closed-time distributions overlap.

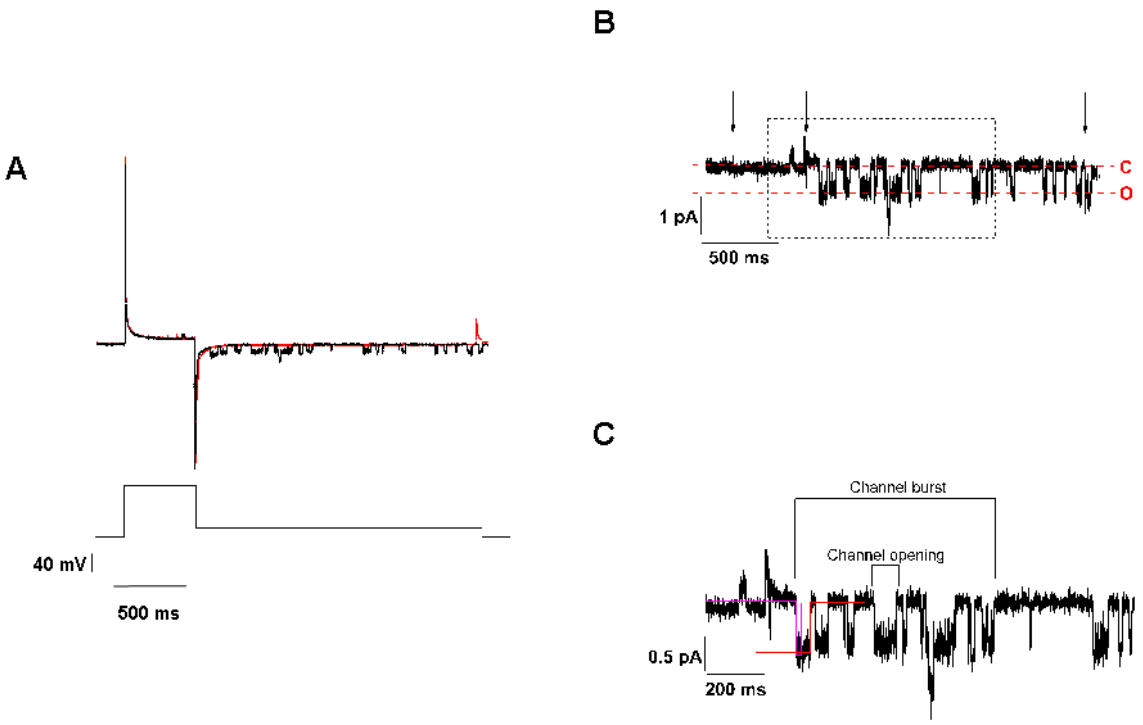

Figure 2-6 Representative hERG single-channel recording.

A. Representative single-channel I_{hERG} at -80 mV (protocol in lower panel) with a pipette solution pH of 7.4. Channel openings are observed as downward deflections. Traces were created by subtracting a 'dummy' sweep (seen as a red sweep with no channel openings) to remove transient current.

B. Trace shown in **A** once transients have been removed. Channel openings are observed as downward deflections shown with red dashed lines; line labelled 'C' represents the closed state and 'O' represents the open state. Downward arrows represent time points at which the current was changed in response to the voltage protocol shown in **A** (lower panel).

C. Enlarged section of **B** (area represented by black dashed box). TAC software (Bruxton, Seattle, USA) was used to analyse single-channel data. A detection process (seen as a red 'arm') scans the data using the threshold set by the user. Detected events that would be used in analysis are shown

2.4 Statistics and equations

Data acquired were analysed using PulseFit (HEKA), Excel 2013, Prism 7.0 (Graphpad Inc.), Origin 9.1 (OriginLab), TAC and TACfit (Bruxton) software. Data in this thesis are presented as mean ± standard error of the mean (SEM). Statistical tests performed were chosen appropriately and two-tailed Student's *t* test (paired or un-paired) or one/two-way

analysis of variance (ANOVA) with a Bonferroni post-test were used. Statistical significance was assumed with *P* values of less than 0.05.

To determine the voltage-dependence of I_{hERG} activation, whole-cell tail currents from the standard current-voltage protocol were normalised to the peak hERG I_{Tail} and plotted against voltage. The plot was then fitted with a Boltzmann function:

Equation 1

$$I = \frac{I_{Max}}{1 + exp\left(\frac{V_{0.5} - V_m}{k}\right)}$$

Where *I* is the peak I_{hERG} tail amplitude at test potential V_m; I_{max} is the maximum I_{hERG} tail observed; $V_{0.5}$ is the half-maximal voltage of I_{hERG} activation, and *k* is the slope of the fitted relationship.

Deactivation of hERG was determined by fitting I_{Tail} with a bi-exponential equation:

Equation 2

$$y = A_s . exp\left(\frac{-x}{\tau_s}\right) + A_f . \left(\frac{-x}{\tau_f}\right) + C$$

Where *y* is the I_{hERG} amplitude at time x, τ_s and τ_f are the slow and the fast time constant of the two components of hERG I_{Tail} deactivation, A_s and A_f represent the total current fitted by the fast and the slow time-constants respectively, and C is any unfitted residual current.

Fractional reduction of hERG I_{Tail} by lowering the extracellular pH to either pH 6.3 or 5.5 was calculated using the following equation:

Equation 3

$$Fractional\ Block = 1 - \frac{I_{hERG\ (pH6.3\ or\ pH5.5)}}{I_{hERG\ (pH7.4)}}$$

Where $I_{hERG\ (pH7.4)}$ is the amplitude of the tail current in control and $I_{hERG\ (ph6.3\ or\ pH5.5)}$ is the amplitude of I_{Tail} in the respective extracellular pH. Fractional block was plotted against the respective membrane potential

The pK_a of these processes were measured using a dose-response curve with a variable Hill slope:

Equation 4

$$y = y_{min} + \frac{y_{max} - y_{min}}{1 + 10^{(LOGx0 - x)p}}$$

Where y_{min} and y_{max} are the minimum and maximum points of the curve respectively, Log*x*0 is the mid-point of the curve and *p* is the Hill slope of the curve.

To determine the pK_a of different processes, the percentage decrease of I_{hERG} was measured across the range of tested pH_e values (Chapter 6). Percentage decrease was measured as:

Equation 5

$$\%\ Decrease = \left(1 - \frac{I_{hERG\ (pH)}}{I_{hERG\ (control)}}\right).100$$

Where $I_{hERG\ (control)}$ is the process being measured ($I_{End\ pulse}$, I_{Tail}, τ_{fast} or τ_{slow}) in control pH7.4 and $I_{hERG\ (pH)}$ is the process measured in a selected pH_e.

3. The effects of extracellular acidosis on the hERG1a isoform

3.1 Introduction

As discussed in Chapter 1, the hERG channel possesses unique gating kinetics that determine its contribution to the repolarisation phase of the cardiac action potential (Vandenberg et al. 2001; Sanguinetti & Tristani-Firouzi 2006). The slow activation of the channel coupled with rapid inactivation allows hERG/I_{Kr} channels to pass limited current during the plateau phase of the action potential (Zhou et al. 1998; Hancox et al. 1998) . In contrast, upon repolarisation, hERG recovers from inactivation rapidly and enters the open state where it will slowly deactivate to the closed state (Smith et al. 1996; Sanguinetti & Jurkiewicz 1990; Vandenberg et al. 2001).

Single-channel recordings, either as native I_{Kr} (Veldkamp et al. 1993; Horie et al. 1990; Shibasaki 1987; Veldkamp et al. 1995; Liu et al. 2004) or from heterologously expressed I_{hERG} channels (Kiehn et al. 1996; McDonald et al. 1997; Zou et al. 1997; Kiehn et al. 1999; Liu et al. 2004), show channel openings during repolarisation to negative potentials (ranging from -120 mV to -20 mV) with a single channel conductance of 9.7-13.4 pS when in isotonic potassium conditions ($[K^+]_o$ between 100 and 150 mM in either cell-attached or inside-out patches). The hERG/I_{Kr} channel has a small unitary conductance in physiological extracellular $[K^+]$ of ~2 pS (Shibasaki 1987; Kiehn et al. 1996).

Cardiac acidosis occurs in several pathological situations such as myocardial ischaemia and is known to modulate several cardiac ion channels (see Section 1.3 (Orchard & Kentish 1990; Carmeliet et al. 1999)). Experiments testing the effects of acidosis on native I_{Kr} or I_{hERG} have consistently shown that extracellular protons reduce peak amplitude of I_{Kr}/I_{hERG} and that deactivation is accelerated (Anumonwo et al. 1999; Bérubé et al. 1999; Jiang et al. 1999; Jo et al. 1999; Terai et al. 2000; Vereecke & Carmeliet 2000; Bett & Rasmusson 2003; Zhou & Bett 2010; Van Slyke et al. 2012; Du et al. 2010; Shi et al. 2014). Inconsistencies arise when concerning the effects of protons on the voltage dependence of activation of I_{hERG}, with some reporting a positive shift (Jo et al. 1999; Terai et al. 2000; Vereecke & Carmeliet 2000; Bett & Rasmusson 2003; Du et al. 2010; Van Slyke et al. 2012; Shi et al. 2014) whilst others see no change (Anumonwo et al. 1999; Bérubé et al. 1999; Jiang et al. 1999). Disparities between results from different studies

may be due to several factors such as the expression system used and the temperature in which recordings were completed. The use of *Xenopus* oocytes allows for stable large currents which is advantageous in mutagenesis studies (Witchel et al. 2003). However, for pharmacological studies, *Xenopus* oocytes reduce drug potency, likely due to the vitelline membrane which can influence drug access and large amounts of yolk present which can absorb the drug (Witchel et al. 2003; Po et al. 1999). Even using mammalian cell lines such as CHO or HEK, which hold greater physiological relevance to native I_{Kr} compared with oocytes, it has been reported that I_{hERG} kinetics/gating is influenced by temperature; an increase in temperature from 22 ºC to 35 ºC can cause a negative shift in the $V_{0.5}$ for activation with a positive shift in $V_{0.5}$ in inactivation as well as accelerated rates in gating kinetics (Zhou et al. 1998; Weerapura et al. 2002; Witchel et al. 2003; Vandenberg et al. 2006). Table 3-1 compares previous studies that looked at the effects of extracellular acidosis using different recording conditions which included; the expression system used, the temperature at which the study was conducted and, the pH of the solutions used in control and in acidic conditions.

Author	Expression System	Temperature (ºC)	pH range	$V_{0.5}$ (mV) control	$V_{0.5}$ (mV) pH
(Anumonwo et al. 1999)	*Xenopus* oocytes	22	7.4 (control) 5.8 (pH)	-8.4	+10.6
(Bérubé et al. 1999)	CHO cells	30	7.4 (control) 6.0 (pH)	-8.5	-4.9
(Jiang et al. 1999)	*Xenopus* oocytes	23-25	7.5 (control) 6.5 (pH)	-12.3	-10
(Jo et al. 1999)	*Xenopus* oocytes	21-23	8.0 (control) 7.0, 6.6, 6.2 (pH)	-41.8	-38.0 (pH 7.0) -33.7 (pH 6.6) -26.7 (pH 6.2)
(Terai et al. 2000)	*Xenopus* oocytes	Room Temperature	7.6 (control) 6.6, 6.0 (pH)	-32.7	-24.5 (pH 6.6) -10.6 (pH 6.0)
(Vereecke & Carmeliet 2000)	Rabbit/guinea pig ventricular myocytes	37	7.4 (control) 6.5 (pH)	-20.2	-11.3

Author	Expression System	Temperature (ºC)	pH range	$V_{0.5}$ (mV) control	$V_{0.5}$ (mV) pH
(Bett & Rasmusson 2003)	*Xenopus* oocytes	Room Temperature	7.4 (control) 5.5 (pH)	-16.4	-0.04
(Du et al. 2010)	CHO cells	37	7.4 (control) 6.3 (pH)	-25.3	-19.7
(Van Slyke et al. 2012)	*Xenopus* oocytes	20-22	7.4 (control) 6.5, 5.5, 4.5 (pH)	-25.8	-23.0 (pH 6.5) +5.0 (pH 5.5) 17.0 (pH 4.5
(Shi et al. 2014)	*Xenopus* oocytes	22-24	7.4 (control) 6.5, 6.0, 5.5	-27.1	-24.7 (pH 6.5) -14.8 (pH 6.0) +5.1 (pH 5.5)

Table 3-1 Effects of extracellular acidosis in previous studies.

Tabulated results to compare the effects of extracellular acidosis on the voltage-dependence on hERG/I_{Kr} channel activation.

The effects of acidosis on hERG have been studied in mammalian cells at physiological (Du et al. 2010), near physiological (Bérubé et al. 1999), and room temperature (Anumonwo et al. 1999) (see Table 3-1). Now, there is very little information on single-channel hERG and even less so on the effects of external protons on single-channel I_{hERG}. Although experiments performed at 37 ºC provide physiological relevance (Zhou et al. 1998; Vandenberg et al. 2006), single-channel recordings are completed at room temperature. This is due to the acceleration in gating kinetics seen at physiological temperature (Zhou et al. 1998; Vandenberg et al. 2006), which may decrease the number of events observed in single-channel recordings.

With this background information, the experiments performed in this chapter aimed to: (1) characterise the effect of acidosis on I_{hERG} using a stably transfected mammalian cell line (HEK-293) and; (2) test and characterise these effects, for the first time, at the single-channel level on WT-hERG channels. To enable a direct comparison of single-channel

and macroscopic I_{hERG}, these characterisations were undertaken at a common (room) temperature.

3.2 Methods

Both macroscopic and single-channel experiments carried out in this chapter were completed in the HEK-293 cell line stably expressing hERG1a. Maintenance of the cell line and solutions used in the experiments are described in Sections 2.2.1.1 and 2.3.1. External solution (pH_e) was 7.4 in control and titrated to pH_e 6.3 or 5.5 using HCl fresh on each experimental day. The external superfusate was continuously supplied to the bath containing cells using gravity at a rate of 20 ml/min (volume of bath ~ 2.9 cm^3) so that rapid exchange of solution was achieved when switching to pH_e 6.3 or 5.5. Cell-attached recordings were completed during continuous external superfusate of pH_e 7.4 with the pipette solution titrated to either pH 7.4 of pH 6.3. Thus, comparison of single-channel measurements at different pH_e was unpaired. In cell-attached experiments, $[K^+]$ of the bathing and pipette solution was at 140 mM so that, assuming that cytosolic $[K^+]$ is similar, the reversal potential would be 0 mV.

All recordings were completed at room temperature and low-pass filtered at 1 kHz and acquired at 10 kHz, except for the fully activated I-V protocol (see Section 3.3.3), where recordings were acquired at 5 kHz.

3.3 Results

3.3.1 Effects of extracellular acidosis on macroscopic I_{hERG} elicited under conventional voltage clamp

Initial experiments to test the effects of lowering the pH_e on $I_{hERG\ 1a}$ was completed using a standard 'square' pulse protocol (as seen in Figure 3-1, lower panel) (Du et al. 2010; Du et al. 2011). A holding potential of -80 mV was applied to the membrane before a 2 second depolarisation to +20 mV. This step allows for I_{hERG} activation and inactivation. The I_{hERG} tail current (I_{Tail}) was observed upon repolarising to -40 mV for 6 seconds. Before the depolarising step, a brief 50 ms step to -40 mV was applied to measure instantaneous leak in the absence of I_{hERG} activation. The amplitude of I_{Tail} was measured by the difference between the peak outward current upon repolarisation to -40 mV and the instantaneous leak current (Du et al. 2011; Zhang et al. 2011; El Harchi et al. 2012). The protocol was continuously repeated prior and during extracellular solution acidification with an interpulse interval of 12 seconds.

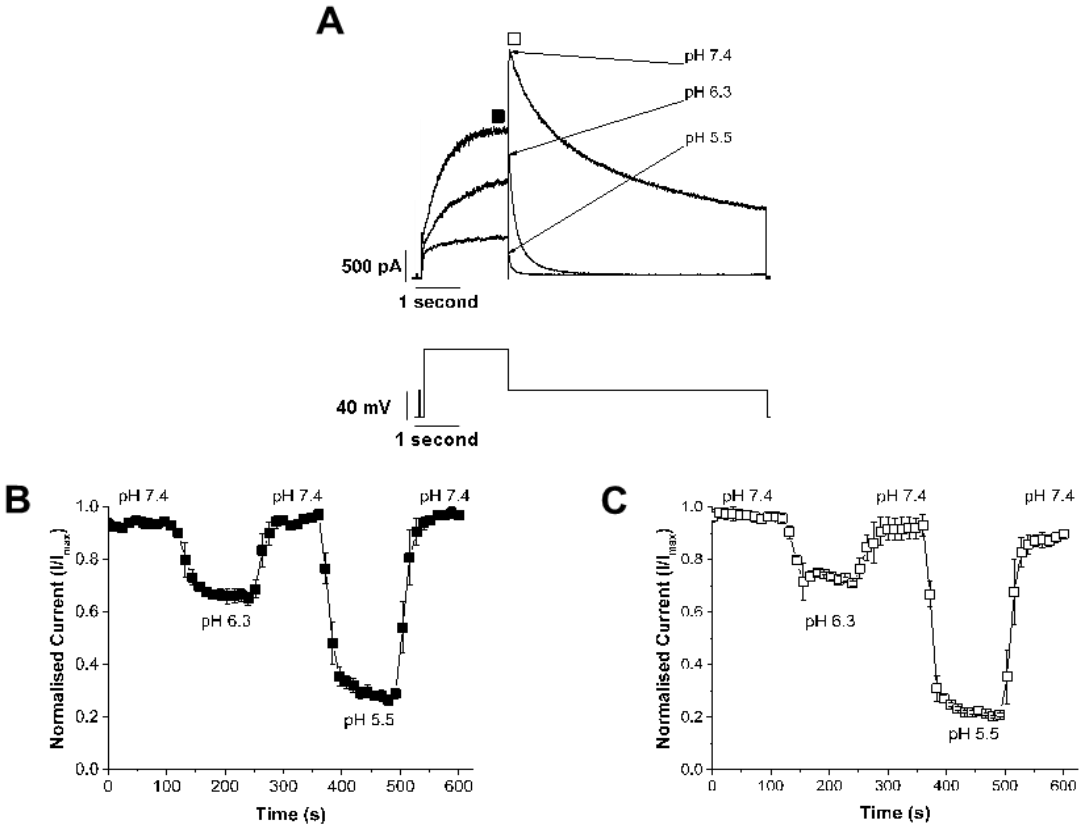

Figure 3-1 The effects of extracellular acidosis on WT-hERG1a channels.

A. Representative traces of I_{hERG} at pH_e 7.4, 6.3 and 5.5 elicited by the protocol shown in lower panel.
B. Mean data (±SEM, n = 5 cells) showing the reduction in end-pulse current ($I_{End\ Pulse}$, point of analysis shown by filled square ■ in **A**) when subjected to varying levels of acidification.
C. Mean data (±SEM, n = 5 cells) showing the effect of extracellular acidosis on the I_{Tail} (point of analysis as shown by an empty square □ in **A**).

Figure 3-1A shows representative recordings of $I_{hERG\ 1a}$ at pH_e 7.4, 6.3 and 5.5. It can be seen at all pH values, depolarisation to +20 mV evoked an outward I_{hERG}, whilst repolarisation to -40 mV induced a tail current that is characteristic of I_{hERG} (Sanguinetti et al. 1995; Trudeau et al. 1995). Upon acidification to pH_e 6.3, a reduction in both depolarising and repolarising currents with a faster decline in I_{Tail} is observed which agrees with previously reported acceleration of I_{hERG} deactivation (Anumonwo et al. 1999; Bérubé et al. 1999; Jiang et al. 1999; Jo et al. 1999; Terai et al. 2000; Vereecke & Carmeliet 2000; Bett & Rasmusson 2003; Zhou & Bett 2010; Van Slyke et al. 2012; Du et al. 2010; Shi et al. 2014). The results here show that extracellular acidosis shows a marked effect on the acceleration of deactivation, which was studied in more detail in Section 3.3.3. Upon acidification to pH_e 5.5, a further reduction in I_{hERG} amplitude and acceleration of I_{hERG} deactivation is observed. Figure 3-1B, C show the time-course of effect of extracellular acidosis on amplitude of end-pulse current ($I_{End\ Pulse}$) and I_{Tail} respectively. The time-course shows that the effect of extracellular acidification was rapid in onset and was reversible. The mean reduction in $I_{End\ Pulse}$ amplitude at pH_e 6.3 was 32.4±1.0% and at pH_e 5.5 was 71.1±1.8%. Mean reduction in I_{Tail} amplitude was 25.3±0.9% at pH_e 6.3 and 76.5±1.0% at pH_e 5.5.

3.3.2 Effects of external protons on I_{hERG} current voltage relationship and the voltage dependence of channel activation

The effects of extracellular acidosis on macroscopic I_{hERG} was further investigated by applying a voltage protocol shown in Figure 3-2C (lower panel). The protocol was comprised of a series of depolarising commands to voltages ranging from -40 mV to +70 mV (stepping in 10 mV increments, with a 12 second interpulse interval). The protocol was applied in control solution and acidic solution once steady state was reached.

Figure 3-2A-C shows representative I_{hERG} traces recorded at pH_e 7.4, 6.3 and 5.5 respectively. The amplitude of both $I_{End\ Pulse}$ and I_{Tail} was analysed as described in Chapter 2.4. To construct I-V relationships, $I_{End\ Pulse}$ was normalised to the maximal $I_{End\ Pulse}$ in pH_e 7.4 and plotted against membrane potential. As seen in Figure 3-2D for control conditions, the $I_{End\ Pulse}$ increased as the test pulse became more depolarised, reaching a maximum at approximately +10 mV (n = 15 cells). As the depolarising command becomes more positive, the amplitude of $I_{End\ Pulse}$ decreased, which created a negative slope in the I-V relation. The region of negative slope is caused by voltage-dependent inactivation and is characteristic of I_{hERG} and is a result of the voltage-dependent inactivation (Sanguinetti et al. 1995; Trudeau et al. 1995; Spector et al. 1996; Smith et al. 1996). At pH_e 6.3, a similar relationship is seen with $I_{End\ Pulse}$ increasing with depolarisation up to 10 - 20 mV (n = 8 cells) before declining at more positive potentials. Acidification to pH_e 5.5 appeared to impair the ability for I_{hERG} to inwardly rectify (and thus inactivate) with an increasing amplitude of $I_{End\ Pulse}$ across the whole range of depolarisation potentials tested (n = 7 cells).

The voltage-dependence of I_{hERG} activation was determined by plotting the I-V relation for hERG I_{Tail}. The I_{Tail} was measured at each depolarising step and normalised to the maximal I_{Tail} observed in each condition before being plotted against membrane potential.

To quantify the voltage-dependence of I_{hERG} activation, the relationship was fitted with a Boltzmann function (Equation 1) to give a half-maximal activation voltage ($V_{0.5}$) value of -9.98±1.20 mV (k = 6.79±0.19 mV) in pH_e 7.4, a $V_{0.5}$ value of -6.99±2.84 mV (k = 8.33±1.09 mV) for pH_e 6.3 and a $V_{0.5}$ of 11.79±2.39 mV (k = 11.88±0.51 mV) for pH_e 5.5.

The positive shift of the half-activation in acidic condition was significantly different from control with pH_e 6.3 (P = 0.0013; paired *t*-test) and pH_e 5.5 (P = 0.0002; paired *t*-test). Maximal conductance (G_{Max}) was derived from the I_{Tail} measurements. Values for G_{Max} were 0.35 nS/pF in pH_e 7.4, 0.25 nS/pF in pH_e 6.3 and 0.10 nS/pF in pH_e 5.5, resulting in a significant decrease in conductance in acidic conditions (P = 0.0003 for pH_e 6.3; paired *t*-test and P < 0.0001 for pH_e 5.5; paired *t*-test).

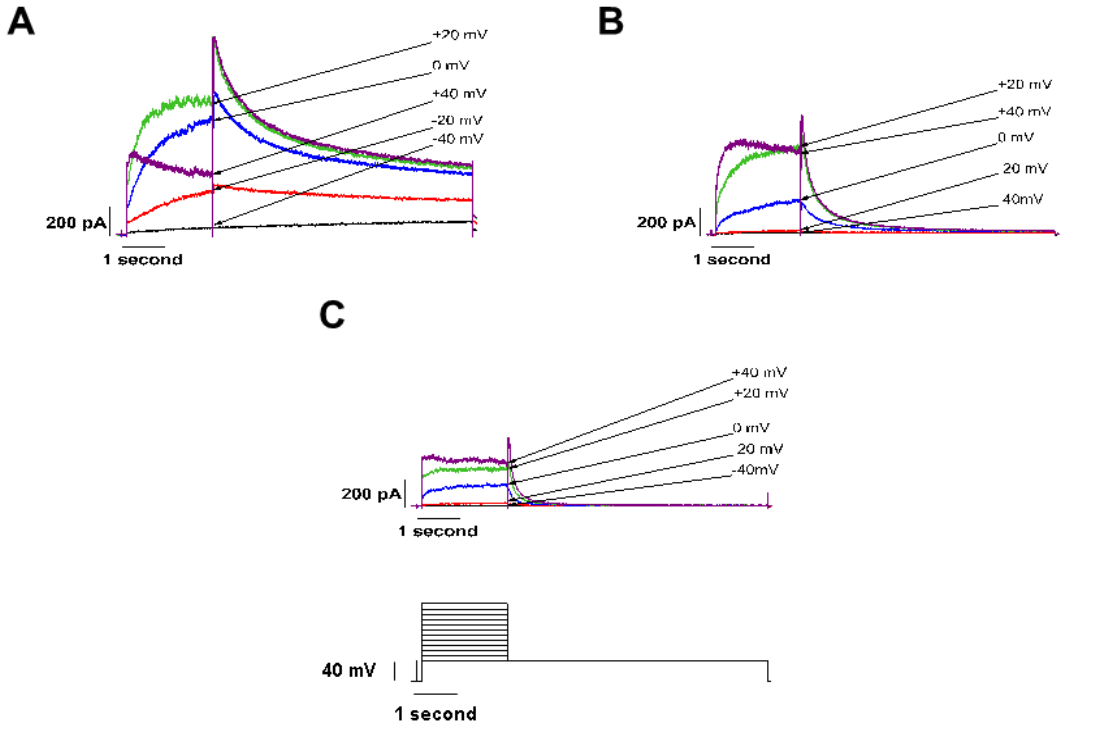
A
+20 mV
0 mV
+40 mV
-20 mV
-40 mV
200 pA
1 second
B
+20 mV
+40 mV
0 mV
20 mV
40mV
200 pA
1 second
C
+40 mV
+20 mV
0 mV
20 mV
-40mV
200 pA
1 second
40 mV
1 second

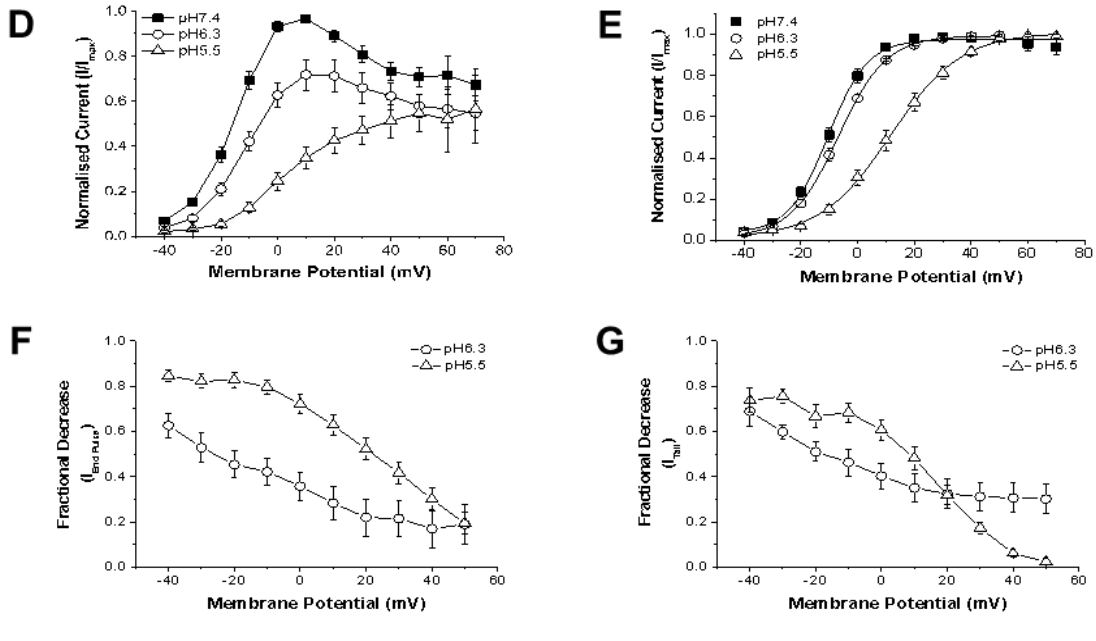
D
pH7.4
pH6.3
pH5.5
Normalised Current (I/I max)
Membrane Potential (mV)
E
pH7.4
pH6.3
pH5.5
Normalised Current (I/I max)
Membrane Potential (mV)

F
pH6.3
pH5.5
Fractional Decrease
(I End Pulse)
Membrane Potential (mV)
G
pH6.3
pH5.5
Fractional Decrease
(I tail)
Membrane Potential (mV)

Figure 3-2 The effect of extracellular acidification on the I_{hERG} current-voltage relationship.

A, B, C. Representative families of I_{hERG} at pH_e values of 7.4 (**A**), 6.3 (**B**) and 5.5 (**C**) when the voltage protocol in lower panel of **C** is applied. Select currents were chosen for clarity of display. **D.** Mean (±SEM) I-V relations for pulse currents at pH_e 7.4 (n = 15 cells), 6.3 (n = 8 cells) and 5.5 (n = 7 cells). Data were normalised to the maximal I_{hERG} current in control and were then plotted against membrane potential.

E. Mean (±SEM) steady-state activation plots for I_{hERG} derived from hERG I_{Tail} measurements on repolarisation to -40 mV. At each pH_e, the data were normalised to the maximal I_{Tail} recorded during the protocol and plotted against corresponding test pulse membrane potentials at pH_e 7.4, 6.3 and 5.5. The relations were fitted with a Boltzmann equation to give $V_{0.5}$ of −10.0±1.2 mV (k = 6.8±0.2 mV) at pH 7.4 (n = 15 cells) a $V_{0.5}$ of −7.0±2.8 mV (k = 8.3±1.1 mV) at pH 6.3 (n = 8 cells) and a $V_{0.5}$ of 11.8±2.4 mV (k = 11.9±0.5 mV) for pH 5.5 (n = 7 cells).

F. Plot of mean (±SEM) fractional decrease of I_{hERG} against test voltages for end-pulse current at pH_e 6.3 (n = 8 cells) and pH_e 5.5 (n = 7 cells).

G. Plot of mean (±SEM) fractional decrease of I_{hERG} against test voltages for tail current at pH_e 6.3 (n = 8 cells) and pH_e 5.5 (n = 7 cells).

Note that data were not necessarily matched with recordings at each pH in the same cell: e.g. two of the cells were subject to all three pH conditions.

3.3.3 Effects of extracellular acidosis on the fully activated I-V relationship and deactivation of I_{hERG}

To investigate the effect of acidosis on the I_{hERG} fully activated I-V relation and deactivation time-course of I_{hERG}, the protocol shown in Figure 3-3 (inset to panel C) was applied; from a holding potential of -80 mV, a 2 second depolarising step to +20 mV. Depolarisation was applied; this was followed by a series of 6 second repolarising commands to various potentials ranging from -120 mV to +20 mV. The protocol was applied during both control and acidic pH_e conditions with an interpulse interval between successive sweeps of 12 seconds.

Figure 3-3A shows a representative trace at selected voltages in control solution. The peak I_{Tail} increased as the membrane potential becomes more depolarised until a maximum is reached at approximately -40 mV. Membrane potentials more positive than -40 mV show a decrease in I_{Tail}.

In acidic external solution, for both pH_e values of 6.3 (Figure 3-3B) and 5.5 (Figure 3-3C), a similar relationship was found to that in control, but with a reduction in amplitude. The hERG I_{Tail} was measured across the membrane potentials and normalised against maximum I_{Tail} in control and plotted against membrane potential (Figure 3-3D). In acidic solution, a positive shift is seen in peak I_{Tail} compared with that in control. The reversal potential (E_{Rev}) was measured from the fully activated I-V relationship from individual cells as the point of intersection with the voltage axis; E_{Rev} values obtained were -88.56±1.06 mV in pH_e 7.4, -88.01±0.91 mV in pH_e 6.3 and -87.99±1.67 mV in pH_e 5.5. As a result, there was no significant difference in the E_{Rev} between the three pH_e values (P = 0.72 for pH_e 6.3; paired *t*-test and P = 0.79 for pH_e 5.5; paired *t*-test).

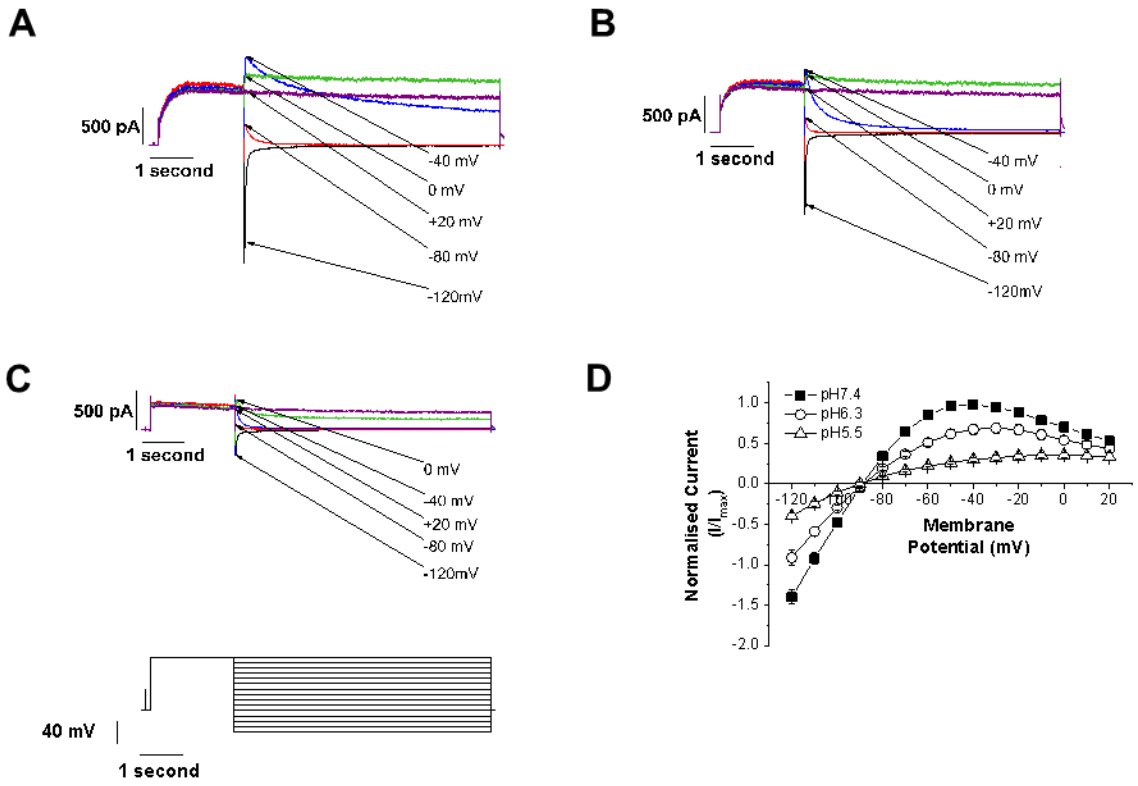

Figure 3-3 Fully activated I_{hERG} and the effects of acidosis.

A, B, C. Families of representative currents for pH_e 7.4 (**A**) 6.3 (**B**) and 5.5 (**C**) when the fully activated protocol shown in lower panel of **C** is elicited. Select potentials were chosen for clarity. **D.** Mean (±SEM) I-V relationship of fully activated I_{hERG} at pH_e 7.4 (n = 15 cells), 6.3 (n = 8 cells) and 5.5 (n = 7 cells).

Note that data are not necessarily matched with recordings at each pH in the same cell: two cells were subject to all three pH conditions.

To evaluate the time-course of I_{hERG} deactivation, the I_{Tail} was fit with a bi-exponential equation across a range of potentials tested (Equation 2). From the fits, a fast (τ_{Fast}) and slow (τ_{Slow}) time constant values were derived and plotted as a logarithmic scale against corresponding membrane potential (Figure 3-4A and B respectively). It should be noted that extrapolation back to the start of the repolarising pulse was not made. As a result, the relative proportions of the fast and slow components represent estimated values. For both time constants, the values become slower as the membrane potential becomes more depolarised. Upon extracellular acidification, the time constants become significantly faster (two-way ANOVA with Bonferroni post-test) compared with corresponding control values (black asterisks for significance in pH_e 6.3 and grey asterisks for significance in pH_e 5.5).

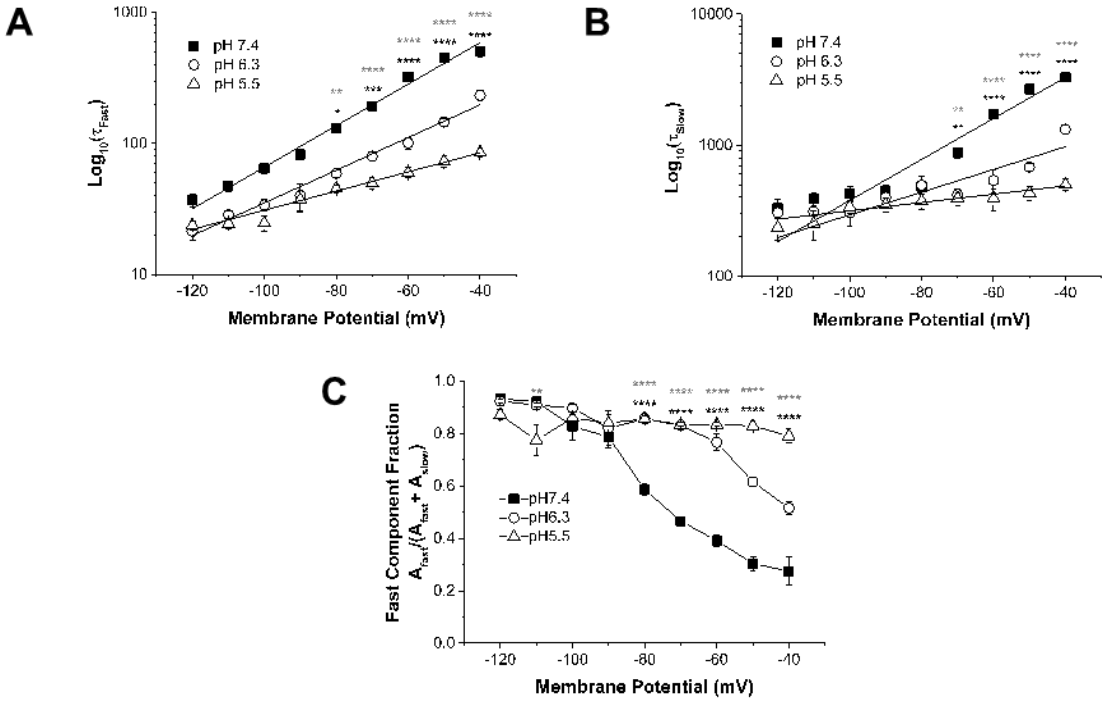

Figure 3-4 The effects of extracellular acidosis on I_{hERG} deactivation.

A. Mean (±SEM) fast time constants (τ_{Fast}) plotted against respective membrane potential at pH_e 7.4 (n = 15 cells), 6.3 (n = 8 cells) and 5.5 (n = 7 cells).

B. Mean (±SEM) plots against voltage of the slow time constant (τ_{Slow}) of deactivation at pH_e 7.4 (n = 15 cells), 6.3 (n = 8 cells) and 5.5 (n = 7 cells).

C. The fraction of deactivation that is described by the τ_{Fast} of deactivation plotted against membrane potentials at pH_e 7.4 (n = 15 cells), 6.3 (n = 8 cells) and 5.5 (n = 7 cells). '*', '**', '***', and '****' denotes statistical significance of $P < 0.05$, $P < 0.01$, $P < 0.001$ and $P < 0.0001$ respectively (2-way ANOVA with Bonferroni post-test).

The proportion of deactivating current described by τ_{Fast} was also evaluated and mean values plotted against membrane potential (Figure 3-4C). Statistical analysis (two-way ANOVA with Bonferroni post-test) showed that the proportion of deactivation described by τ_{Fast} was significantly greater in acidic pH_e; thus, extracellular acidosis both accelerated deactivation time-constants and increased the contribution of the fast deactivation.

3.3.4 The effects of external acidosis on single-channel I_{hERG} conductance

To investigate the effects of protons on the conductance of I_{hERG} at the single-channel level, the protocol shown in Figure 3-5 (lower centre panel) was applied in the cell-attached configuration. From a holding potential of -80 mV, a 500 ms depolarising pulse to +40 mV was applied before repolarisation to a range of voltages, (from -120 mV to -40 mV in 20 mV increments) for 2 seconds. The start-to-start interval between successive sweeps was 6 seconds. The protocol was applied with isotonic potassium (140 K^+) and a pipette pH of either 7.4 or 6.3. The cell-attached configuration means that the pipette solution acts as the external solution for the channel(s) undergoing study.

Figure 3-5 shows representative records of I_{hERG} elicited by the protocol shown in the lower centre panel at both pH_e 7.4 (Figure 3-5A) and pH_e 6.3 (Figure 3-5B). In control pH_e as the membrane potential became more depolarised, the amplitude of channel openings (as seen as downward deflections) in control pH_e decreased but the number of openings increased. A similar pattern is seen for the distinct recording at pH_e 6.3, but with fewer events detected and with decreased amplitude across all potentials tested compared to control conditions.

Patches were analysed with methods described in Chapter 2.3.5 and events from each potential were gathered to create amplitude histograms. Figure 3-6 shows example amplitude histograms from -80 mV at pH_e 7.4 (Figure 3-6A) and the corresponding histogram at pH_e 6.3 (Figure 3-6B). An average of amplitudes was taken for each potential and plotted against membrane potential (Figure 3-6C). Across all potentials, extracellular acidosis caused a significant decrease in the current amplitude (two-way ANOVA with Bonferroni posttest) which is consistent with whole-cell data (Figure 3-2). Plots were fitted with a linear regression equation with the intercept fixed to go through the *x* and *y* axis at 0. The slope value derived from the fit represents the conductance of the channel with values of 12.2±0.1 pS in pH_e 7.4 (n = 10 patches) and a conductance of 9.3±0.1 pS in pH_e 6.3 (n

= 9 patches). Thus, an increase in extracellular proton concentration resulted in a significant decrease in single-channel conductance ($P < 0.0001$; unpaired *t*-test).

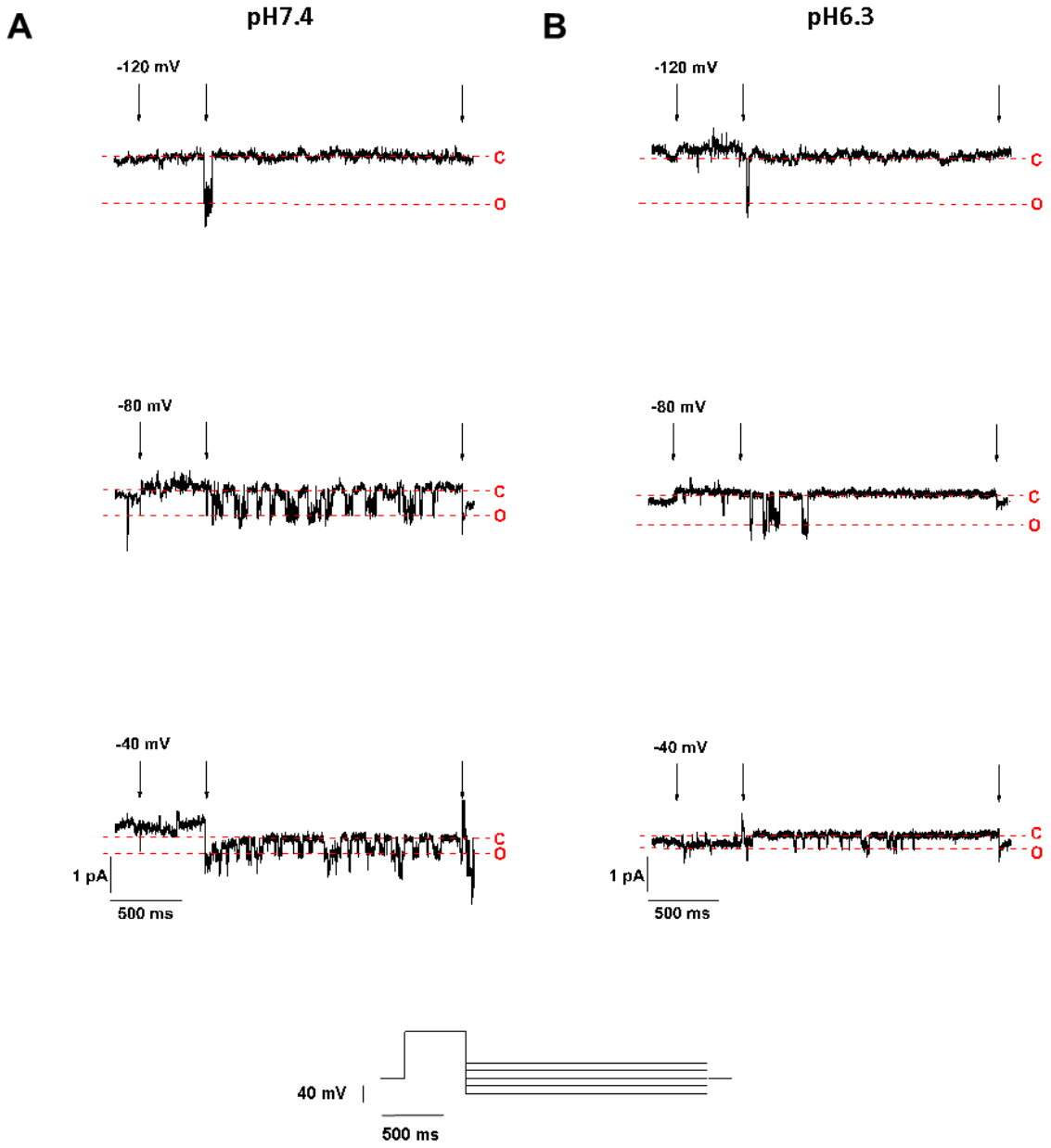

Figure 3-5 Single hERG channels recorded in cell-attached patch.

A, B. Representative traces at selected potentials with a pipette solution pH of 7.4 (**A**) and pH 6.3 (**B**) when protocol in bottom centre was applied. Channel openings are observed as downward deflections and shown with red dashed lines; line labelled 'C' represents the closed state and 'O' represents the open state Traces were created by subtracting a 'dummy' sweep to remove transient current. Downward arrows represent time points at which the current was changed in response to the voltage protocol shown in **A** (lower panel).

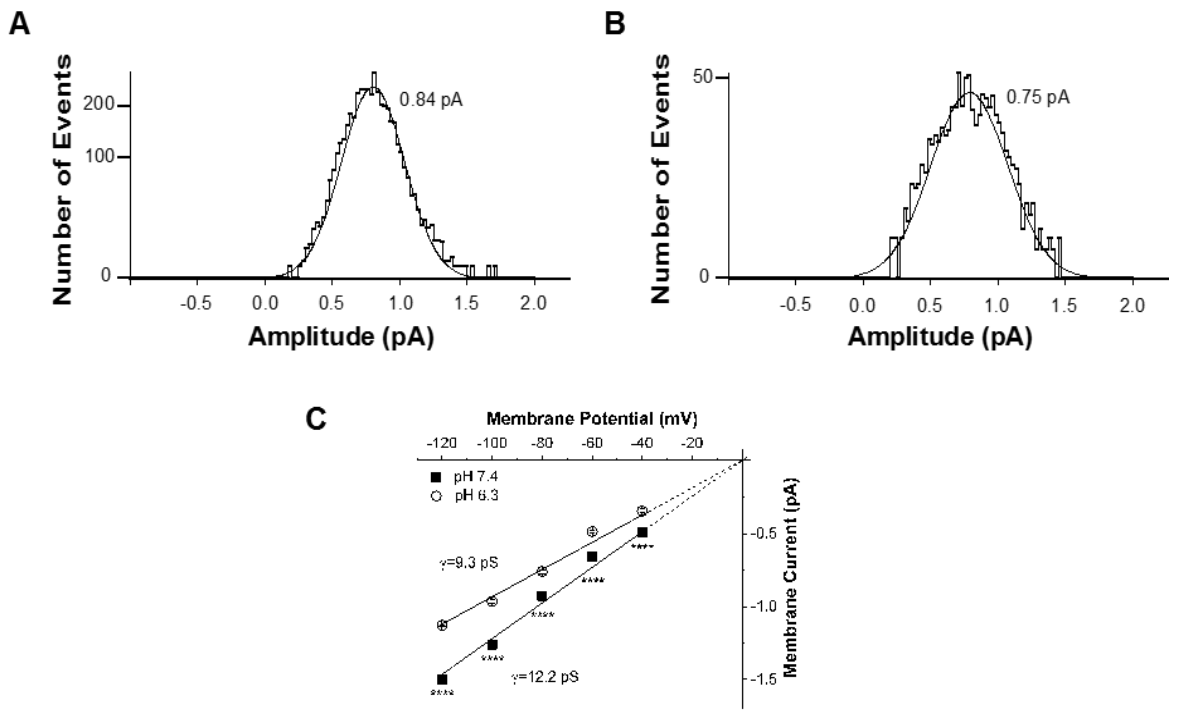

Figure 3-6 The effect of extracellular protons on single-channel I_{hERG}.

A. Amplitude histogram at -80 mV for pH_e 7.4. A Gaussian distribution was fit to reveal an amplitude of 0.84 pA.

B. Amplitude histogram for pH_e 6.3 at -80 mV. When fit with a Gaussian distribution, an amplitude of 0.75 pA was yielded.

C. Amplitude values were obtained for the potentials tested in both pH conditions. Single-channel current-voltage (I-V) relationships were constructed by plotting membrane potential against the respective amplitude. Mean (±SEM) plots were fitted with a linear relationship (solid line) and was constrained to pass through the origin (dashed line) to achieve slope conductance of 12.3±0.2 pS for pH 7.4 (n = 10 cells) and 9.3±0.1 pS for pH 6.3 (n = 9 cells; $P < 0.0001$, unpaired students t-test). '****' denotes significance of $P < 0.0001$ (2-way ANOVA). SEM bars are small and obscured by the symbols for some points.

3.3.5 External protons and the effect on single-channel I_{hERG} kinetics

Currents elicited by the protocol in Figure 3-5 (lower centre panel) were also analysed to determine effects of extracellular acidosis on hERG single-channel current kinetics. As with amplitude analysis, patches were analysed and a duration histogram plotted on a logarithmic scale was configured. Open-time histograms (Figure 3-7A and B) were fit with

a single exponential function to obtain open-time durations of 5.04 ms in pH_e 7.4 and 3.09 ms in 6.3. The same patches used for open-time analysis were used to determine closed-time durations of I_{hERG}. Closed-time durations were best described as a sum of four exponentials for both pH_e 7.4 (Figure 3-7C) and 6.3 (Figure 3-7D). In both conditions, a closure of ~ 0.50 ms was seen within a channel opening which would indicate a brief 'flicker' of channel activity to the closed state. The point in which the third and fourth exponential fit overlapped was used to determine the τ_{Crit} used in burst duration analysis (Figure 3-7E and F) which is indicated by the downwards arrows seen in Figure 3-7C and D. The τ_{Crit} value at -80 mV for pH_e 7.4 was 64 ms and 70 ms for 6.3. The τ_{Crit} value was then used to achieve burst durations of 71.3 ms in pH_e 7.4 and 54.3 ms in pH_e 6.3. Open-time durations obtained across the range of potentials tested were plotted against membrane potential and fit with and exponential function (Figure 3-7G). As the patch potential became more depolarised the open-time duration decreased. A similar, yet slightly more linear relationship was seen with extracellular acidosis.

Statistical analysis (2-way ANOVA with Bonferonni post-test) highlighted that a significant decrease in open-time duration occurred at the most hyperpolarised potentials. Combined patches were used to analyse burst duration for pH_e 7.4 (n = 10 patches) and 6.3 (n = 9 patches). Burst durations were achieved for each potential tested and plotted against membrane potential (Figure 3-7H). Plots were best fit with an exponential function and showed that burst duration increased with depolarisation in both pH conditions (agreeing with whole-cell data, Figure 3-4A and B).

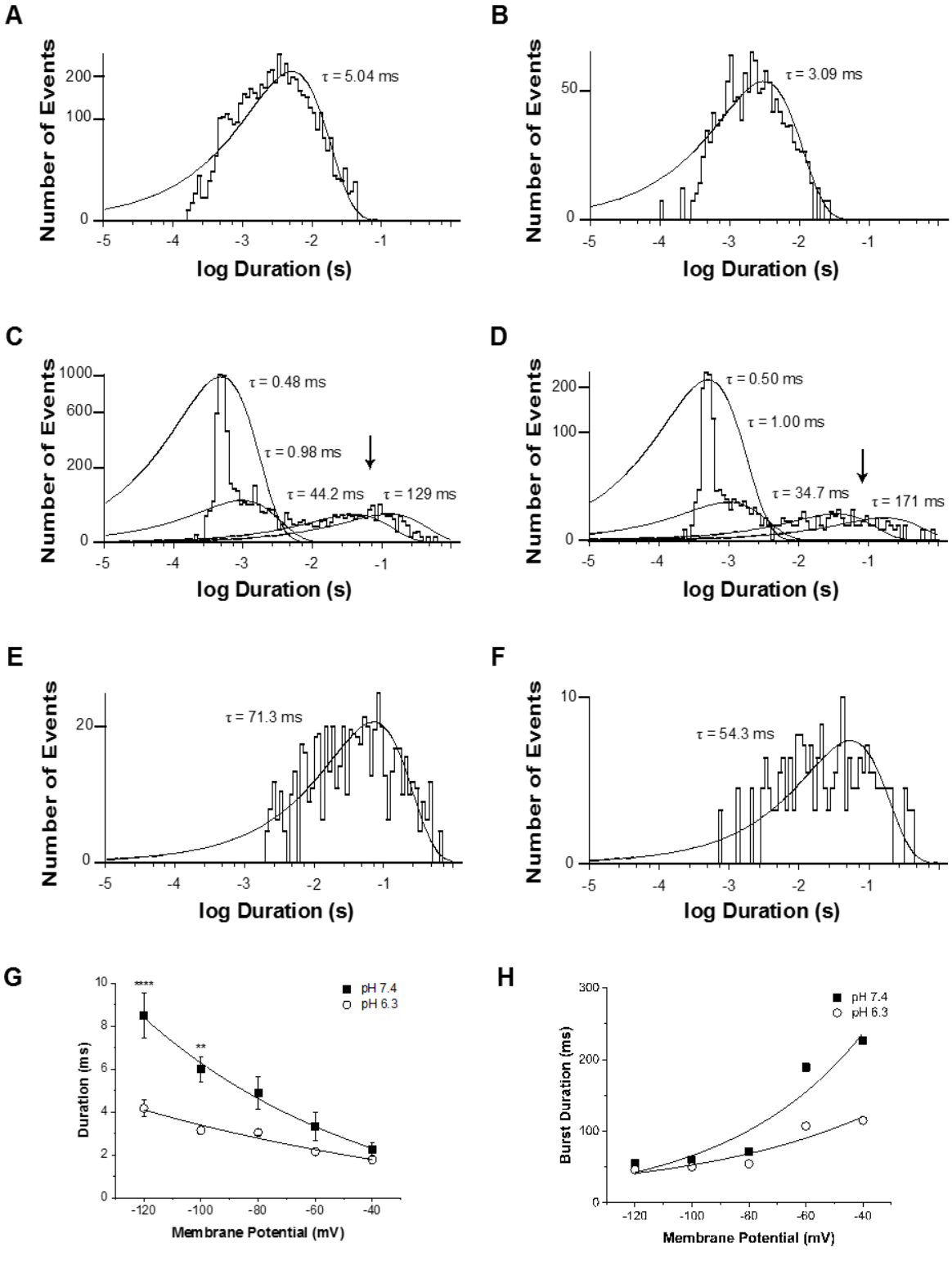
A
Number of Events
200
100
0
τ = 5.04 ms
-5
-4
-3
-2
-1
log Duration (s)
B
Number of Events
50
0
τ = 3.09 ms
log Duration (s)
C
Number of Events
1000
600
200
0
τ = 0.48 ms
τ = 0.98 ms
τ = 44.2 ms
τ = 129 ms
log Duration (s)
D
Number of Events
200
100
0
τ = 0.50 ms
τ = 1.00 ms
τ = 34.7 ms
τ = 171 ms
log Duration (s)
E
Number of Events
20
0
τ = 71.3 ms
log Duration (s)
F
Number of Events
10
0
τ = 54.3 ms
log Duration (s)
G
Duration (ms)
10
8
6
4
2
0
****
**
pH 7.4
pH 6.3
-120
-100
-80
-60
-40
Membrane Potential (mV)
H
Burst Duration (ms)
300
200
100
0
pH 7.4
pH 6.3
-120
-100
-80
-60
-40
Membrane Potential (mV)

Figure 3-7 Kinetics of hERG1a gating upon repolarisation.

A, B. Open-time duration histograms of several patches at -80 mV for pH 7.4 (**A**, n = 10 patches) and pH 6.3 (**B**, n = 9 patches). Histograms were fit with a single exponential function to reveal an open-time duration of 5.04 ms in control and 3.09 ms in pH 6.3.
C, D. Closed-time distributions for hERG in pH 7.4 (**C**) and pH 6.3 (**D**). Distributions in pH 7.4 were best described with four exponentials with time constants (and areas) of 0.48 ms (89.2%), 0.98 ms (5.7%), 44.2 ms (2.5%) and 129 ms (2.6%). Distributions in pH 6.3 were also best described with four exponentials and time constants of 0.50 ms (90.6%), 1.00 ms (5.1%), 54.7 ms (2.5%) and 171 ms (1.8%) were obtained. τ_{crit} values were calculated between the third and fourth component of closed-time distributions as indicated by an arrow.
D, E. Burst duration histograms of hERG at -80 mV for pH 7.4 (**E**) and pH 6.3 (**F**). Histograms use the patches used in **A-D** and were described with a single exponential. Burst durations obtained were 71.3 ms in pH 7.4 and 54.3 ms in pH 6.3.
G. Open-time durations were obtained for each potential tested and plotted against membrane potential. The plots were fitted with an exponential function for 7.4 (n = 10 cells) pH 6.3 (n = 9 cells). '****' and '**' denotes significance of P < 0 .0001 and P < 0.01 respectively (2-way ANOVA).
H. Burst durations were obtained from pooled histograms of 10 patches for pH 7.4 and 9 patches for pH 6.3 and plotted against the respective membrane potential. The plots were fitted with an exponential function.

3.4 Discussion

3.4.1 Results in context

External protons have been shown to modulate cardiac ion channels and, as a result, alter cardiac excitability. The effects of extracellular acidosis have been studied on the native I_{Kr} (Vereecke & Carmeliet 2000), heterologously expressed I_{hERG} in mammalian cell lines (Bérubé et al. 1999; Du et al. 2010), and in *Xenopus* oocytes (Anumonwo et al. 1999; Jiang et al. 1999; Jo et al. 1999; Terai et al. 2000; Bett & Rasmusson 2003; Van Slyke et al. 2012; Shi et al. 2014). Table 3-1 compares the effects of extracellular acidosis in different whole-cell recording conditons. Whilst there is some disagreement in the literature with the effects of protons on the voltage-dependence of activation, Table 3-1 shows that the temperature of the experiments do not account for this discrepancy. Vereecke and Carmeliet reported an approximate +9 mV shift in voltage dependence of activation when exposing I_{Kr} to pH_e of 7.4 to 6.3 (Vereecke & Carmeliet 2000), whilst Du et al noted a ~6 mV depolarising shift when changing pH_e from 7.4 to 6.3 (Du et al. 2010). These values are like what was achieved under recording conditions in these experiments, in which a shift in $V_{0.5}$ of approximately +3 mV was observed. Although the shift is smaller, the effect of protons on voltage dependence of activation was significant. A shift of approximately +22 mV was seen when lowering pH_e from 7.4 to 5.5, which is similar to previous studies: a ~+19 mV shift when lowering pH_e from 7.4 to 5.8 (Anumonwo et al. 1999) and; an approximate +16 mV shift was seen when lowering pH_e from 8.2 to 5.5 (Bett & Rasmusson 2003). In addition, I have shown that the effects of protons on I_{hERG} are rapid and reversible (Figure 3-1) in agreement with I_{Kr} (Vereecke & Carmeliet 2000) and I_{hERG} (Du et al. 2010). The data obtained regarding the deactivation of I_{hERG} (Figure 3-4) showed that upon acidification, both the fast and slow time constant of deactivation became faster with the fraction of the fast time component increasing. This is consistent with what is seen in native I_{Kr} (Vereecke & Carmeliet 2000) and I_{hERG} (Du et al. 2010) at 37 ºC.

Comparatively little information has been published on single-channel I_{Kr}/I_{hERG}. With a single-channel conductance in physiological $[K^+]_e$ of approximately 2 pS (Kiehn et al. 1996; Shibasaki 1987), obtaining data on I_{Kr}/I_{hERG} under “physiological” conditions has proven to be problematic. Several studies have shown that the single-channel conductance of I_{Kr}/I_{hERG} is dependent on extracellular potassium levels (Shibasaki 1987; Horie et al. 1990; Veldkamp et al. 1993; Kiehn et al. 1996). Table 3-2 collates the data from previous studies which have characterised hERG/I_{Kr} channels in different expression systems and

extracellular potassium concentrations. With this taken into consideration, the experiments completed in this chapter used isotonic potassium concentration of 140 mM. The single-channel conductance achieved in my recording conditions were 12.1±0.1 pS at pH7.4, like that of 12.9±0.8 pS found in human ventricular myocytes at near physiological temperatures of 34±2 ºC (Veldkamp et al. 1995) and 11.1 pS at 37 ºC in rabbit nodal cells (Shibasaki 1987).

Author	Expression system	$[K^+]_o$	Conductance (pS)	Open-time (ms)	Closed-time (ms)
(Shibasaki 1987)	Rabbit nodal cells	100 150 200 300	8.4 (100) 11.1 (150) 13.1 (200) 14.7 (300)	2.5 (at -60 mV)	τ_{fast} = 0.7 τ_{slow} = 17.6
(Minoru Horie et al. 1990)	Guinea pig atrial cells	150 300	10 (150) 17 (300)	9 (at -100 mV)	τ_{fast} = 0.4 τ_{slow} = 37
(Veldkamp et al. 1993)	Rabbit ventricular myocytes	150	13.1 (150)		
(Veldkamp et al. 1995)	Human ventricular myocytes	140	12.9		
(Kiehn et al. 1996)	*Xenopus* oocytes	100	10	3.2 (at -100 mV)	τ_{fast} = 1.0 τ_{slow} = 26
(Zou et al. 1997)	*Xenopus* oocytes	120	12.1	τ_{O1} = 2.9 τ_{O2} = 11.8 (at -90 mV)	τ_{fast} = 0.54 τ_{slow} = 14.5
(Kiehn et al. 1999)	*Xenopus* oocytes	100	9.7	3.2 (at -40 mV)	τ_{C1} = 0.95 τ_{C2} = 3.7 τ_{C3} = 45
(Liu et al. 2004)	Mouse ventricular myocytes	150	12.2	3.5 (at -40 mV)	τ_{fast} = 1.7 τ_{slow} = 175

Table 3-2 Comparison of previous hERG/I_{Kr} single-channel studies.

Tabulated results to compare the single-channel data (conductance and open- closed-time kinetics) for hERG/I_{Kr} channels in different recording conditions.

This similarity suggests that using a mammalian cell line can reproduce native I_{Kr} conductance values. There are some discrepancies within the available literature regarding kinetics of single-channel I_{hERG}: for example, whether open-time duration histograms are best fit with a single exponential function (Shibasaki 1987; Horie et al. 1990; Kiehn et al. 1996; Liu et al. 2004) or a double exponential function (Zou et al. 1997), with some agreement that the closed-time histograms are fit with at least two exponential functions (see Table 3-2).

Experimental data regarding single-channel I_{hERG} open-time durations was best fit with a single exponential with values of 2.2±0.3 ms at -40 mV which is close to 3.2 ms (Kiehn et al. 1999) and 3.5 ms (Liu et al. 2004). Previous studies have shown open-time duration to be/nearly be voltage-independent (Shibasaki 1987; Zou et al. 1997; Kiehn et al. 1999). The relation of voltage against open-time duration in this chapter show near voltage independence with -120 mV showing a significant difference to voltages positive to -80 mV (Figure 3-7G). There is a consensus across the literature that the fastest constant of closed-time durations ($\tau_{Closed\ 1}$), which ranges from 0.4 to 1.7 ms, is due to a short-lived transition to the closed state within a channel opening (Shibasaki 1987; Horie et al. 1990; Kiehn et al. 1996; Zou et al. 1997; Kiehn et al. 1999; Liu et al. 2004). The results obtained in this chapter agree with this with the $\tau_{Closed\ 1}$ being ~0.5 ms. This was seen across all membrane potentials tested. There is variability in the literature concerning the second and any further time constants measured, ranging from 14-175 ms. As mentioned by Kiehn et al (1999), the values achieved for the remaining time constants depend on the number of channels present in the patch and so the true values are underestimated (Kiehn et al. 1999). Closed-time histograms of my data were best fit with four exponentials with the overlap of $\tau_{Closed\ 3}$ and $\tau_{Closed\ 4}$ used to determine τ_{Crit} for burst duration analysis (Colquhoun & Hawkes 1995). Burst duration analysis showed strong voltage dependence, with an increase in duration with depolarisation which Kiehn et al also observed (Kiehn et al. 1999).

To my knowledge, this is the first study to have determined the effects of acidic pH_e on wild-type hERG single-channel properties, therefore there are no published data for direct comparison with my results. The only comparative data come from a study by Van Slyke et al (2012) which showed that extracellular acidosis (pH_e 7.4 reduced to 5.5) reduced single-channel current amplitude at a repolarisation voltage of -100 mV from 1.21 pA to 0.94 pA

for the inactivation-deficient S620T mutant (Van Slyke et al. 2012). The effects of acidosis on single-channel I_{hERG} in this thesis was completed with the acidic solution at pH_e 6.3 due to ischemic conditions seen in cardiac acidosis (Fleet et al. 1985). Recordings obtained in WT channels with acidic conditions showed a similar reduction with the amplitude at -100 mV in control at 1.26 pA (pH_e 7.4) reduced to 0.97 pA (pH_e 6.3). No further potentials were tested at the single-channel level by Van Slyke et al, meaning that the effects of acidosis on single-channel conductance was not calculated.

3.4.2 The basis of I_{hERG} modulation by extracellular protons

3.4.2.1 Is I_{hERG} reduced by extracellular acidosis because of the 'surface-potential' theory?

It has been reported that there are several mechanisms in which a channel can be modulated by protons, with one being the surface-potential theory (Hille 2001). As described by Green and Anderson, any charge that is on or near the channel surface will create an electrostatic potential and changes in the local environment e.g. a decrease in extracellular pH will alter the single-channel conductance (Green & Andersen 1991). By lowering the pH, protons will titrate negative charges that contribute to surface-potential, leading to a decrease in K^+ around the channel pore and subsequent reduction in conductance (Green & Andersen 1991; Hille 2001). Bérubé et al noted a negative shift in the voltage dependence of activation when increasing pH_e to 8.0 and suggested that this was due to the effects of surface charge screening (Bérubé et al. 1999). However, on decreasing pH_e to 6.0, no shift in voltage sensitivity was seen, suggesting a different mechanism of proton action (Bérubé et al. 1999). This was not seen in experiments in this chapter, as a reduction in pH_e to 6.3 produced a significant positive shift in activation (see Figure 3-2) with fully activated channels still modulated by protons (see Figure 3-3). Several reports on I_{Kr}/I_{hERG} have rejected the surface-potential theory as a mechanism of proton modulation due to the marked differences in the effects on hERG activation and deactivation kinetics (Ho et al. 1999; Jiang et al. 1999; Vereecke & Carmeliet 2000; Du et al. 2010; Van Slyke et al. 2012).

3.4.2.2 Is the effect pH_e due to secondary intracellular acidosis?

It was seen in studies by Vereecke and Carmeliet and Du et al that the effects of protons on I_{Kr}/I_{hERG} amplitude was almost immediate as well as reversible (Vereecke & Carmeliet 2000; Du et al. 2010). The introduction of NH_4Cl in the bathing solution, which is known to

cause intracellular acidosis, did not affect the native I_{Kr} current amplitude and the deactivation was not accelerated (Vereecke & Carmeliet 2000) confirming the effect of acidosis on the extracellular side of the cell. The rapid onset of reduction in I_{hERG} amplitude was also seen in experiments in this chapter (Figure 3-1) with the effects of protons reversible upon returning to pH_e 7.4. Anumonwo et al showed, using fluorescence, that even after ~50 minutes of exposure to extracellular acidosis, this did not affect the intracellular pH under their conditions, yet I_{hERG} was altered, consistent with an extracellular site of proton action (Anumonwo et al. 1999). This was later shown by Bérubé et al in which intracellular pH was monitored with varying levels of HEPES buffer (Bérubé et al. 1999). With HEPES concentrations of 20 mM and 5 mM, a reduction of pH_e from 7.4 to 6.0 produced similar results, suggesting that the effects seen on I_{hERG} were not secondary to a reduction in intracellular pH (Bérubé et al. 1999). Single-channel data in this chapter also confirms that protons modulate the hERG/I_{Kr} channel from the extracellular side as only the pH of the pipette solution was lowered.

3.4.2.3 Do protons directly interact with the permeation pathway?

A recent study has suggested that extracellular protons block the hERG channel pore thus reducing maximal conductance (Van Slyke et al. 2012). This mechanism was supported by several experimental results including: (1) a reduction in pH_e decreased peak tail current in a voltage dependent manner; (2) inhibition by protons is sensitive to external cations; (3) single-channel current amplitude was reduced in acidosis and; (4) introducing a negative charge to the extracellular mouth of the pore changes the amount of block observed (Van Slyke et al. 2012). There has been general consensus that external cations such as calcium ions compete with protons for a shared binding site (Jo et al. 1999; Kazmierczak et al. 2013; Shi et al. 2014). Van Slyke et al are suggesting that at least one of the sites for proton binding is within the pore and potassium dependent (Van Slyke et al. 2012).

Analysis of their single-channel recordings of the S620T mutant revealed a reduction in amplitude of approximately 25% which is like the ~24% seen in WT recordings from data obtained in this thesis (Figure 3-6C). Van Slyke also noted an ~35% reduction in the whole-cell data of the S620T mutant (Van Slyke et al. 2012) and an approximate 29% reduction was observed in whole-cell recordings in this work. Work in this chapter agrees with the possible interaction of protons with the permeation pathway, however further mutagenesis work may confirm this (see Chapter 6).

3.4.2.4 Do protons titrate residues responsible for hERG pH sensitivity?

Another mechanism by which protons could modulate I_{hERG} amplitude and kinetics is to bind to titratable residues that are accessible from the extracellular side of the channel. Previous studies have shown that hERG has at least two proton binding sites due to distinct pK_a values. Bett and Rasmusson concluded that the site that modulates deactivation (pK_a ~ 6.8) has little or no interaction with the S4 and pore domain which has a pK_a of ~5.5 for I_{hERG} attenuation (Bett & Rasmusson 2003). Other experiments that have investigated the effect of protons on maximal conductance suppression also achieve pK_a values of 5.8 (Anumonwo et al. 1999) and 5.1(Van Slyke et al. 2012). The sensitivity of deactivation of protons also share similar pK_a values across the literature with values of 6.7 (Shi et al. 2014), 6.9 (Van Slyke et al. 2012) and ~7.0 for the fast and slow time constant of I_{hERG} deactivation (Anumonwo et al. 1999). As already mentioned, it is clear from the results obtained in whole-cell experiments that there is more than one site of protonation and further experiments addressing mechanism of action of protons are covered in Chapter 6.

Prior work has also looked into covalently modifying amino acid side chains by using diethylpyrocarbonate (DEPC), which primarily modifies histidine residues but is known to modify others at high DEPC concentrations (Jiang et al. 1999). Results showed that application of DEPC to hERG caused current attenuation, a shift in the voltage dependence of activation and acceleration in deactivation. Jiang et al noted that upon extracellular acidification, further acceleration of deactivation was due to the marked shift in activation but still observed a reduction in I_{hERG} (Jiang et al. 1999). These data support the idea of multiple protonation sites. Experiments in which the effects of DEPC on I_{hERG} expressed in a mammalian cell line are shown in a later Chapter 5.

3.4.3 The physiological consequences of extracellular acidosis on hERG

Extracellular protons have been shown, in this study and several others, to reduce I_{hERG}/I_{Kr} amplitude and accelerate channel kinetics. The result of these effects will cause pathophysiological events, such as arrhythmias, due to the lengthening of the action potential. Previous work testing the effects of acidosis on I_{hERG} using the ventricular AP voltage command observed a more positive potential in which I_{hERG} peaked and a reduction in peak current (Du et al. 2010). The faster I_{hERG} deactivation seen in acidosis

will cause faster closure of channels at the end of the action potential and prevent the ability of I_{hERG} to protect against premature stimuli (Bérubé et al. 1999). This idea was confirmed by Du et al when testing effects of acidosis on I_{hERG} in physiological conditions. It was shown that the acceleration of deactivation reduced the proportion of hERG channels that could conduct a large transient outward current in response to premature depolarisation (Du et al. 2010). The effects of protons on single-channel I_{hERG} can support the whole-cell data. In the set of experiments performed, extracellular acidosis caused a reduction in of a ~24% in single-channel conductance (see Figure 3-6C) which is comparable to the whole-cell reduction seen (~29%). Protons also caused a shortening of open-time (see Figure 3-7G) and burst-time durations (Figure 3-7H) of single-channel $I_{hERG.}$ Upon acidification the open probability appears to be reduced and, when paired with shorter open- and burst-duration kinetics results in the acceleration of whole-cell deactivation. Thus, it is reasonable to assume that results found in whole-cell I_{hERG} recordings can be explained by proton modulation at the single-channel level.

4. Extracellular acidification of the hERG1b isoform

4.1 Introduction

As homomeric channels, ERG1a homomers have robust currents with markedly slow deactivation kinetics (Sanguinetti et al. 1995; Trudeau et al. 1995). On the other hand, ERG1b homomeric channels exhibit small currents and, due to the lack of the eag domain in ERG1b, extremely fast deactivation kinetics compared to ERG1a (London et al. 1997; Lees-Miller et al. 1997; Sale et al. 2008; Larsen et al. 2008). There is recent evidence to suggest that native I_{Kr} channels are heteromeric, composed of ERG1a and ERG1b isoforms (Lees-Miller et al. 1997; London et al. 1997; Larsen et al. 2008; Jones et al. 2004; Sale et al. 2008; Phartiyal et al. 2008; McPate, H Zhang, et al. 2009; Larsen & Olesen 2010; Du et al. 2011; Jones et al. 2014; Liu et al. 2016; McNally et al. 2017). Co-expression of the ERG1a and ERG1b isoforms gives rise to currents with kinetics that are like native I_{Kr} in adult mammalian cardiomyocytes and cardiomyocytes derived from human induced pluripotent stem cells (hiPSC-CMs) (Guasti et al. 2005; Larsen et al. 2008; Jones et al. 2014; Liu et al. 2016).

Co-expression of ERG1a and ERG1b isoforms appear to be critical in the formation of native I_{Kr} with previous studies providing evidence that the isoforms co-immunoprecipitate in cardiomyocytes, brain tissue and in tumour cells (Crociani et al. 2003; Jones et al. 2004; Guasti et al. 2005; Liu et al. 2016). The ERG1b isoform also holds pathophysiological relevance due to the discovery of hERG1b specific mutations that are linked to LQT2 (Sale et al. 2008; Jones et al. 2016). A previous study has also shown that the heteromeric hERG1a/1b current are inhibited by drugs differently compared to hERG1a alone, suggesting that the composition of native I_{Kr} is critical in acquired LQT syndrome (Abi-Gerges et al. 2011).

The effect of acidosis on the hERG1a channel has been extensively examined in this thesis (Chapter 3) and by others (Anumonwo et al. 1999; Bérubé et al. 1999; Jiang et al. 1999; Jo et al. 1999; Terai et al. 2000; Vereecke & Carmeliet 2000; Bett & Rasmusson 2003; Du et al. 2010; Van Slyke et al. 2012; Shi et al. 2014) Recent findings have shown that macroscopic hERG1a/1b heteromeric currents show an enhanced inhibitory effect when exposed to extracellular acidosis compared with hERG1a alone (Du et al. 2011).

The experimental data in this chapter characterises single-channel hERG1b for the first time with the effects of acidosis studies at both macroscopic and single-channel level. Although the study of heteromeric hERG1a/1b would have been more physiologically relevant, the study at the single-channel level would have been difficult to prove if a heteromeric channel was present and consequently was tested as hERG1b homomers.

4.2 Method

A study has shown that hERG1b homomers produce very small or undetectable currents when expressed in *Xenopus* oocytes (London et al. 1997) which is due to a RXR retention motif located in the N-terminus of hERG1b (Phartiyal et al. 2008). Previous work in the Hancox laboratory using the CHO cell line has shown adequate hERG1b expression (Du et al. 2011) and so experiments in this chapter were completed on the CHO cell line with the hERG1b transiently transfected. For the transient transfections, 500 ng hERG1b cDNA plasmid was co-transfected with 500 ng eGFP plasmid. Refer to Chapter 2.2.1.2, 2.2.3, 2.3.1 for detailed methods of maintenance, transient transfections and making of electrophysiological recording solutions respectively. During whole-cell recordings, the pH of the external solution (pH_e) was 7.4 in control and titrated to pH_e 6.3 using HCl fresh on each experimental day (as with experiments in Chapter 3). The external superfusate was continuously supplied to the bath containing cells using gravity at a rate of 20 ml/min so that rapid exchange of solution was achieved when switching. Cell-attached recordings were completed with a continuous external superfusate of pH_e 7.4 with the pipette (extracellular) solution titrated to either pH 7.4 of pH 6.3.

All recordings were completed at room temperature and currents were low-pass filtered at 1 kHz and acquired at 10 kHz.

4.3 Results

4.3.1 Initial recordings of extracellular acidosis on hERG1b

As with the hERG1a isoform (see Section 3.3.1), initial experiments examined the effects of external pH and the extent of these effects on hERG1b current. A pulse protocol (shown in Figure 4-1A, lower panel) was applied; a holding potential of -80 mV was used before a 2 second depolarising pulse to +20 mV to cause channel activation and subsequent inactivation. This was followed by a 6 second pulse to -40 mV to observe peak hERG tail current and channel deactivation. The start-to-start interval was 12 seconds and the protocol were continuously repeated throughout the experiment.

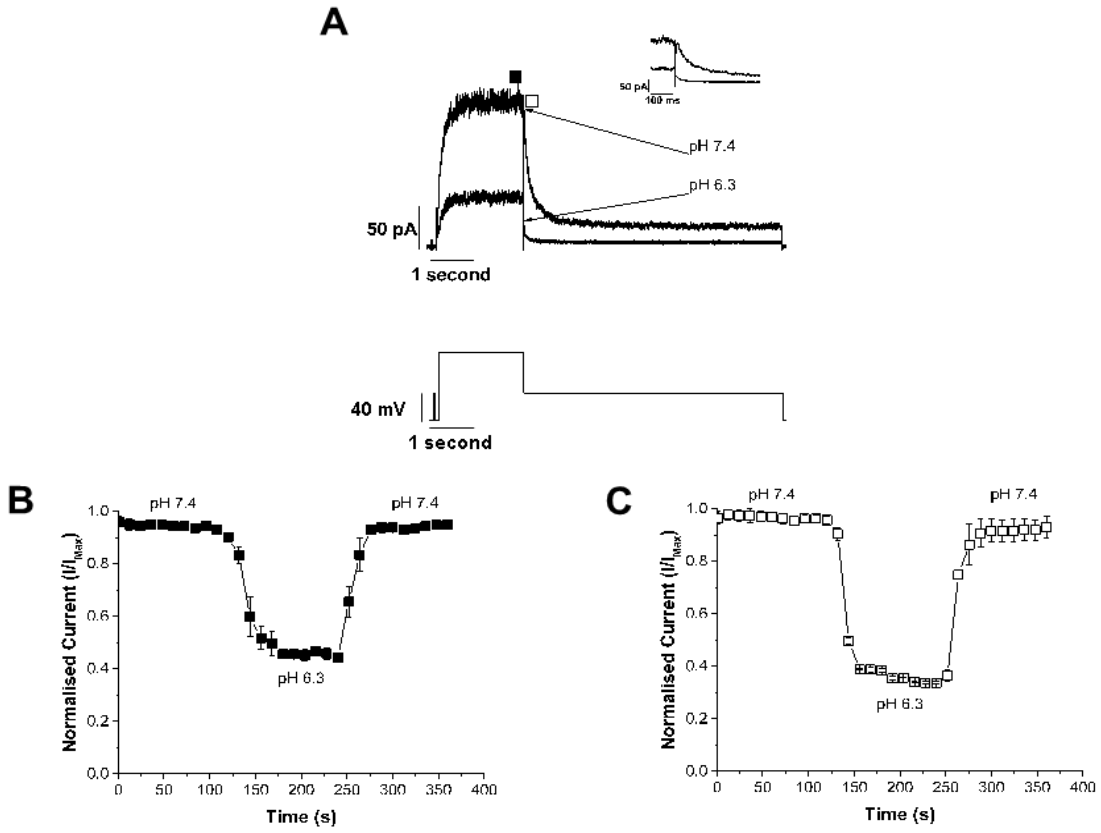

Figure 4-1 The effects of acidosis on hERG1b.

A. Representative current traces from hERG1b at pH_e 7.4 and 6.3 when the protocol in lower panel is elicited. Inset in top right shows expanded time-course upon repolarisation to show extent of rapid acceleration upon deactivation.

B. Mean data (±SEM, n = 4 cells) showing the reduction in $I_{End\ Pulse}$ (point of analysis shown by filled square ■ in A).

C. Mean data (±SEM, n = 4 cells) showing the reduction in I_{Tail} (point of analysis shown by empty square □ in A).

Figure 4-1A show representative current recordings of hERG1b from one voltage with external pH of 7.4 and 6.3. The hERG1b isoform shows characteristic features associated with hERG; an outward current upon depolarisation to +20 mV and a tail current induced upon repolarisation to -40 mV. It is noticeable that the hERG1b isoform has much faster deactivation kinetics compared with that of hERG1a, even in control conditions. Upon acidification to pH_e 6.3, a reduction in the current elicited on depolarisation and upon repolarisation is seen coupled with acceleration of deactivation. The rapid deactivation kinetics of hERG1b is shown in the inset of Figure 4-1A. The time-course showing the effects of protons on the $I_{End\ Pulse}$ and I_{Tail} are shown in Figure 4-1B and Figure 4-1C respectively. The onset of acidosis is rapid and reversible in hERG1b, as was seen in hERG1a (Figure 3-1). The mean reduction in $I_{End\ Pulse}$ and I_{Tail} amplitude was 49.9±1.2% and 62.5±0.1% respectively upon acidification to pH_e 6.3 (n = 4 cells). This is a greater reduction in $I_{End\ Pulse}$ and I_{Tail} compared to hERG1a channels, where a 32.4±1.0% and 25.3±0.9% was respectively seen upon extracellular acidification (see Chapter 3.3.1)

4.3.2 Effects of extracellular protons on hERG1b activation and deactivation

The protocol described in Section 3.3.2 was used to determine the effects of protons on I_{hERG1b} when the membrane potential was depolarised to various voltages. The protocol was applied in control solution and then in acidic solution once steady state was reached with a 12 second start-to-start interval between successive sweeps.

Figure 4-2A and B show representative current traces of hERG1b at pH_e of 7.4 (A) and 6.3 (B) respectively. As with I_{hERG1a}, (Section 3.3.2), hERG1b $I_{End\ Pulse}$ was measured at different command potentials and normalised to maximal $I_{End\ Pulse}$ found in control. Current-voltage (I-V) relationships were constructed by plotting normalised values of $I_{End\ Pulse}$ against the respective voltage as seen in Figure 4-2C.

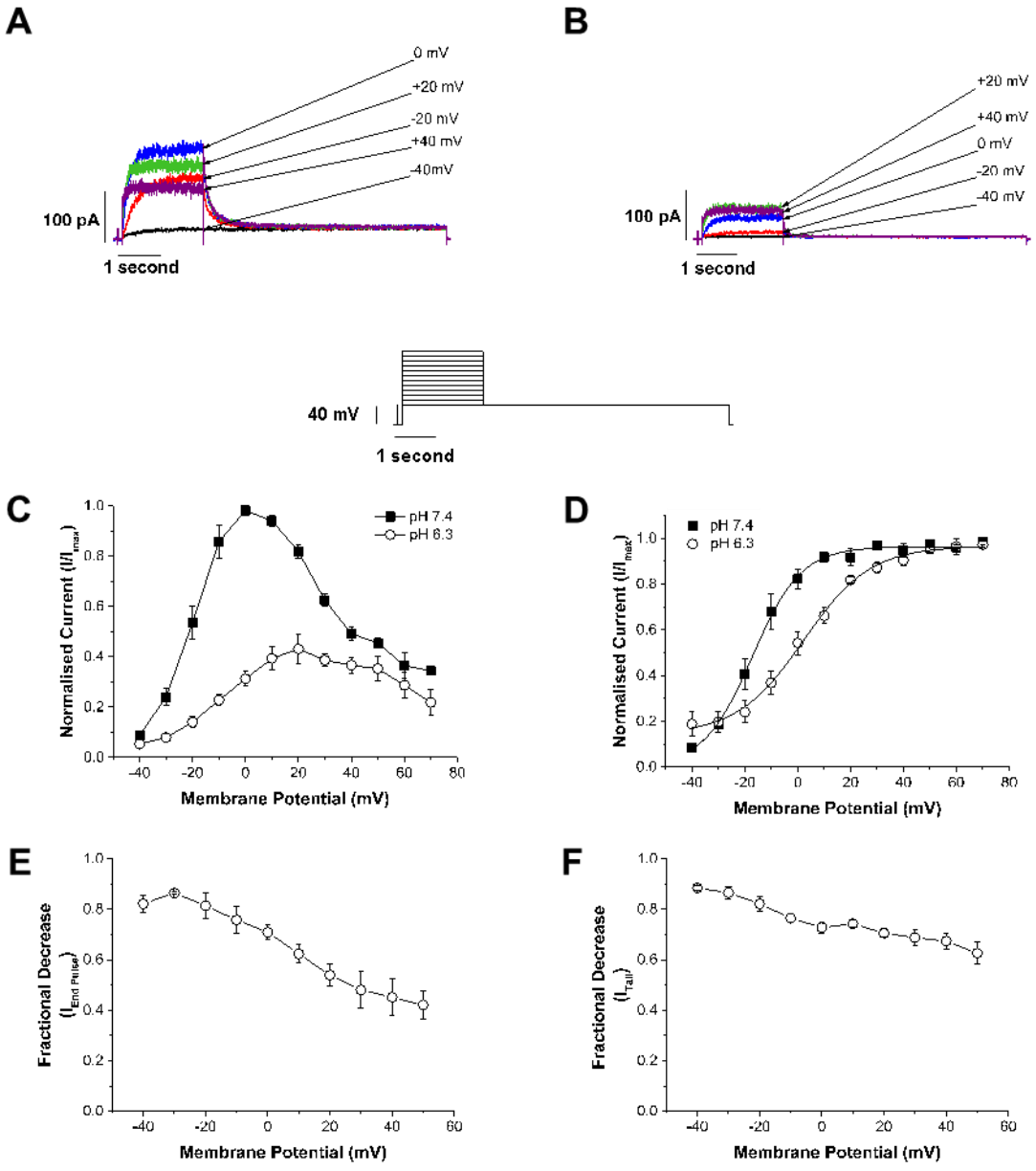
A
0 mV
+20 mV
-20 mV
+40 mV
-40mV
100 pA
1 second
B
+20 mV
+40 mV
0 mV
-20 mV
-40 mV
100 pA
1 second
40 mV
1 second
C
pH 7.4
pH 6.3
Normalised Current (I/I max)
Membrane Potential (mV)
D
pH 7.4
pH 6.3
Normalised Current (I/I max)
Membrane Potential (mV)
E
Fractional Decrease (I End Pulse)
Membrane Potential (mV)
F
Fractional Decrease (I Tail)
Membrane Potential (mV)

Figure 4-2 The current voltage relationship for I_{hERG1b}.

A, B. Representative families of I_{hERG} at pH_e values of 7.4 (**A**), 6.3 (**B**) when the voltage protocol in lower panel is applied. Select currents were chosen for clarity.
C. I-V relations for pulse currents at pH_e 7.4 (n = 7 cells) and 6.3 (n = 7 cells). Data were normalised to the maximal I_{hERG} current in control and were then plotted against membrane potentials.
D. Steady-state activation plots for I_{hERG} derived from hERG I_{Tail} measurements on repolarisation to -40 mV. At each pH_e, the data were normalised to the maximal I_{Tail} and plotted against corresponding test pulse membrane potentials at pH_e 7.4 and 6.3. The relations were fitted with a Boltzmann equation to give $V_{0.5}$ of −16.2±2.8 mV (k = 7.6±0.6 mV) at pH 7.4 (n = 7 cells) and a $V_{0.5}$ of +2.2±1.1 mV (k = 12.6±1.0 mV) at pH 6.3 (n = 7 cells).
E. Plot of mean (±SEM) fractional decrease of I_{hERG} against test voltages for end-pulse current at pH_e 6.3 (n = 7 cells).
F. Plot of mean (± SEM) fractional decrease of I_{hERG} against test voltages for tail current at pH_e 6.3 (n = 7 cells)

In control conditions, $I_{End\ Pulse}$ amplitude increased as potentials became more depolarised, peaking at ~0 mV (n = 7 cells) before decreasing at potentials more positive to this. As was seen with hERG1a (Figure 3-2D), hERG1b channels also exhibit a negative slope corresponding to channel inactivation at more positive potentials (Sanguinetti et al. 1995; Trudeau et al. 1995; Spector et al. 1996; Smith et al. 1996). During acidification to pH_e 6.3 (n = 7 cells), $I_{End\ Pulse}$ was reduced across all potentials tested but still shows a 'bell-shaped' I-V relation which has positively shifted to peak at ~10-20 mV.

The voltage dependence of hERG1b activation was also determined by plotting an I-V relation for I_{Tail} (as seen in 3.3.2). Values obtained at each pH_e were normalised to maximum value for each set of data, plotted as a relationship of membrane potential against normalised current and fitted with a Boltzmann function (Equation 1). The fit gave rise to $V_{0.5}$ values of -16.24±2.83 mV (k = 7.57±0.60 mV) at pH 7.4 (n = 7 cells) and +2.22±1.07 mV (k = 12.61±1.00 mV) at pH 6.3 (n = 7 cells). The positively shifted $V_{0.5}$ seen in pH_e 6.3 was significantly different to that in control ($P < 0.0001$; paired *t*-test). Maximal conductance was calculated from I_{Tail} measurements resulting in G_{Max} values of 0.15 nS/pF in pH_e 7.4 and 0.05 nS/pF in pH_e 6.3. This results in a significant decrease of ~69% in whole-cell conductance, comparable to the effects on I_{Tail} seen in Figure 4-1C ($P < 0.0001$; paired *t*-test). This is a significantly greater reduction compared to the reduction in whole-

cell hERG1a channel conductance (see Chapter 3.3.2), where an approximate 28% reduction was seen in extracellular acidification (P > 0.0001; unpaired *t*-test).

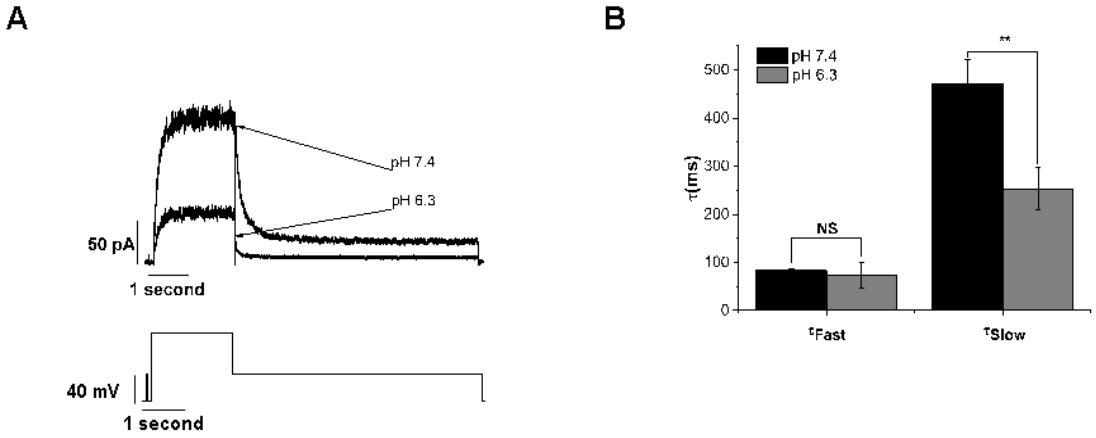

Figure 4-3 The effect of protons on hERG1b deactivation.

A. Representative I_{hERG1b} traces in control pH_e 7.4 (black trace) and in acidic conditions, pH_e 6.3 (grey trace). Inset in top right shows the current upon repolarisation on an enlarged scale to highlight the extent of acidification on I_{hERG1b}.

B. Mean (± SEM) data showing the extent of inhibition of I_{hERG} tail deactivation upon repolarization to -40 mV. Deactivation currents of hERG1b were fit with a bi-exponential function to obtain the fast and slow time constants, τ_{Fast} and τ_{Slow}. Upon acidification, the fast time-constant showed no significant difference (P = 0.7469; paired t-test) whilst the slow time constant was significantly accelerated (P = 0.0074; paired *t*-test).

The effects of extracellular acidosis on the kinetics of I_{hERG1b}, the deactivation of I_{Tail} upon repolarisation to +20 mV were also assessed (Figure 4-3). The protocol, shown in lower panel of Figure 4-3A, was applied before and during exposure to acidic solution. The deactivation of hERG1b I_{Tail} was fit with a bi-exponential equation (Equation 2) to obtain the fast and slow time constants of deactivation.

Figure 4-3B shows the mean fast and slow time constant in both control and acidic conditions. As anticipated for hERG1b channels, both the fast and slow time constant was smaller than hERG1a channels (London et al. 1997; Lees-Miller et al. 1997; Sale et al. 2008; Larsen et al. 2008). Time constant values in control conditions of hERG1b (Figure 4-3B) show an ~6- and ~8-fold increase in the fast and slow time constant respectively

compared with the time constants obtained from hERG1a channels (Figure 3-3A and B; at +20 mV). Upon acidification, acceleration of hERG1b current deactivation was seen with a significant decrease in the slow time constant (P = 0.0074; paired *t*-test).

4.3.3 The effects of protons on the hERG1b single-channel conductance

The effects of extracellular acidosis on single-channel I_{hERG1b} conductance were then investigated. The same protocol as used to characterise single-channel I_{hERG1a} (Figure 3-5) was used (Figure 4-4); from a holding potential of -80 mV, a 500 ms depolarising pulse to +40 mV was applied followed by repolarisation to a range of voltages, (from -120 mV to -40 mV in 20 mV increments) for 2 seconds. The start-to-start interval between successive sweeps was 6 seconds. As with hERG1a, application of the protocol on hERG1b used symmetrical potassium and a pipette solution pH of either 7.4 or 6.3.

Representative I_{hERG1b} records are shown in Figure 4-4 for pH_e 7.4 (A) and pH_e 6.3 (B), in which the protocol in lower centre panel was used. In control, as the membrane potential of the patch became more depolarised, the number of openings increased but with a decrease in current amplitude. Upon extracellular acidification, a reduction in amplitude and number of openings was seen across all potentials tested compared with that in control.

Patches were analysed in the same manner as hERG1a channels were in Section 3.3.4; events from each potential were gathered to create amplitude histograms for both pH conditions. Example amplitude histograms from -80 mV are shown at pH_e 7.4 (Figure 4-4C) and the corresponding histogram at pH_e 6.3 (Figure 4-4D). Histogram data from all potentials tested were used to obtain single-channel amplitudes that were then plotted against respective membrane potential (Figure 4-4E). As was seen for hERG1a channels, extracellular acidification caused a significant decrease in the current amplitude across potentials ranging from -120 mV to -60 mV (two-way ANOVA with Bonferroni posttest).

As with the hERG1a conductance relationship, plots were fitted with a linear regression equation with the intercept fixed to go through the *x* and *y* axis at 0. The slope value derived from the fit represents the conductance of the channel with values of 11.3±0.2 pS in pH_e 7.4 (n = 7 patches) and a conductance of 7.7±0.4 pS in pH_e 6.3 (n = 6 patches).

Thus, an increase in extracellular proton concentration resulted in a significant decrease in single-channel conductance ($P < 0.0001$; unpaired *t*-test).

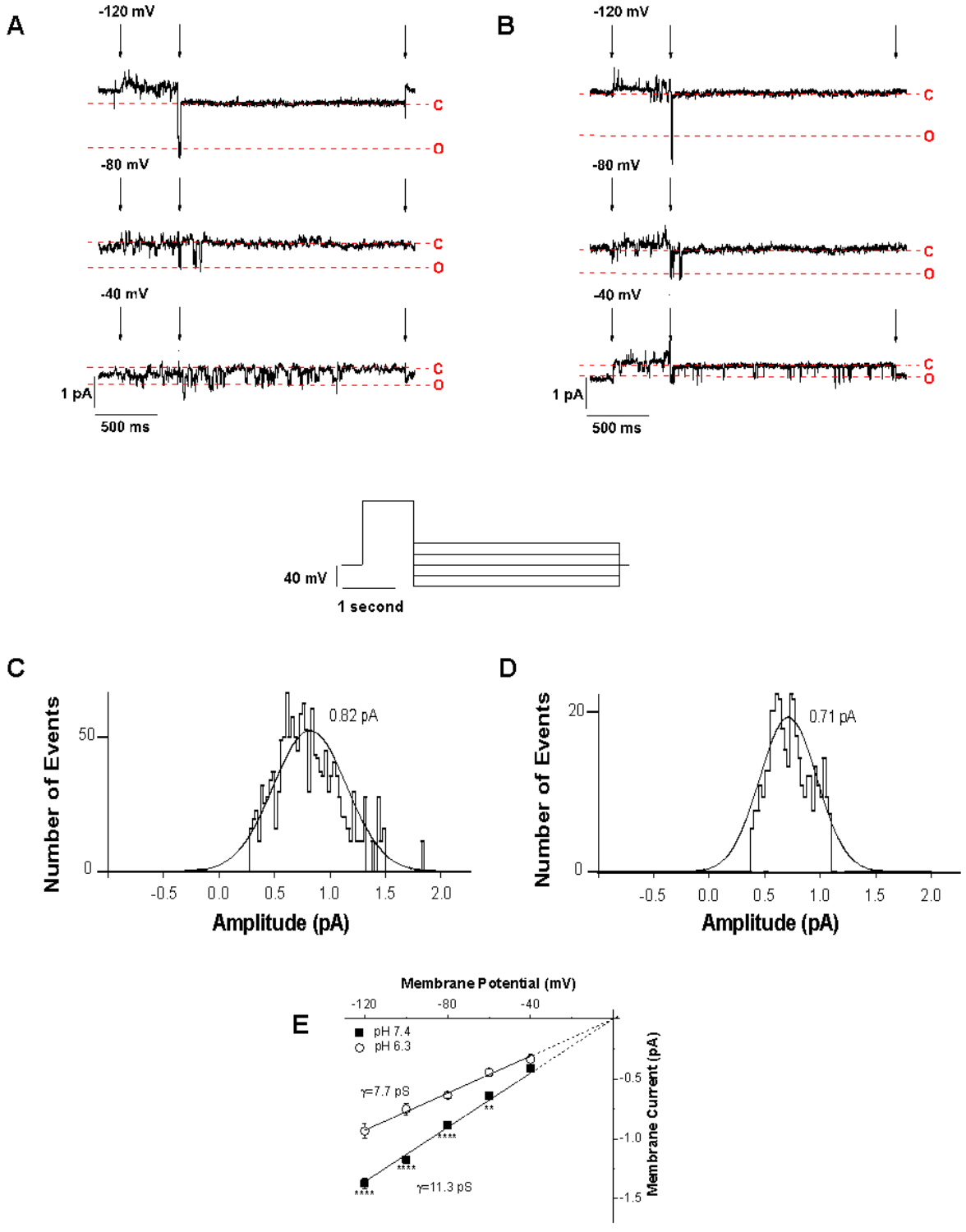

Figure 4-4 Single hERG1b channels recorded in cell-attached patch.

A,B. hERG1b currents were achieved by eliciting the protocol in lower centre panel whilst recording with a pipette pH of 7.4 (**A**) or 6.3 (**B**). Downward arrows represent time points at which the current was changed in response to the voltage protocol shown in **A** and **B** (lower centre panel).
C. Amplitude histogram at -80 mV for pH_e 7.4. A Gaussian distribution was fit to reveal an amplitude of 0.82 pA.
D. Amplitude histogram for pH_e 6.3 at -80 mV. A Gaussian distribution fit yielded an amplitude of 0.71 pA.
E. Single-channel current-voltage (I-V) relationships were constructed by plotting membrane potential against the respective amplitude in the two pH conditions. Plots were fitted with a linear relationship (solid line) and was constrained to pass through the origin (dashed line) to achieve slope conductance of 11.3 ± 0.2 pS for pH 7.4 (n = 7 cells) and 7.7 ± 0.4 pS for pH 6.3 (n = 6 cells; $P < 0.0001$, unpaired students t-test). '****' and '**' denotes significance of $P < 0$ .0001 and $P < 0.01$ respectively (2-way ANOVA).

4.3.4 Extracellular acidosis and its effect on hERG1b single-channel kinetics

As with hERG1a, the effects of extracellular acidosis on single-channel hERG1b current kinetics were also studied. This was examined by analysing patches that were produced by the protocol in Figure 4-5A and B (lower, centre panel) and creating open-time duration histograms for each membrane potential tested. Figure 4-5A and B show open-time durations for -80 mV plotted on a logarithmic scale for pH_e 7.4 and 6.3 respectively. Histograms for open-time duration were fit with a single exponential to obtain open-time durations of 4.66 ms in pH_e 7.4 and 2.86 ms in pH_e 6.3.

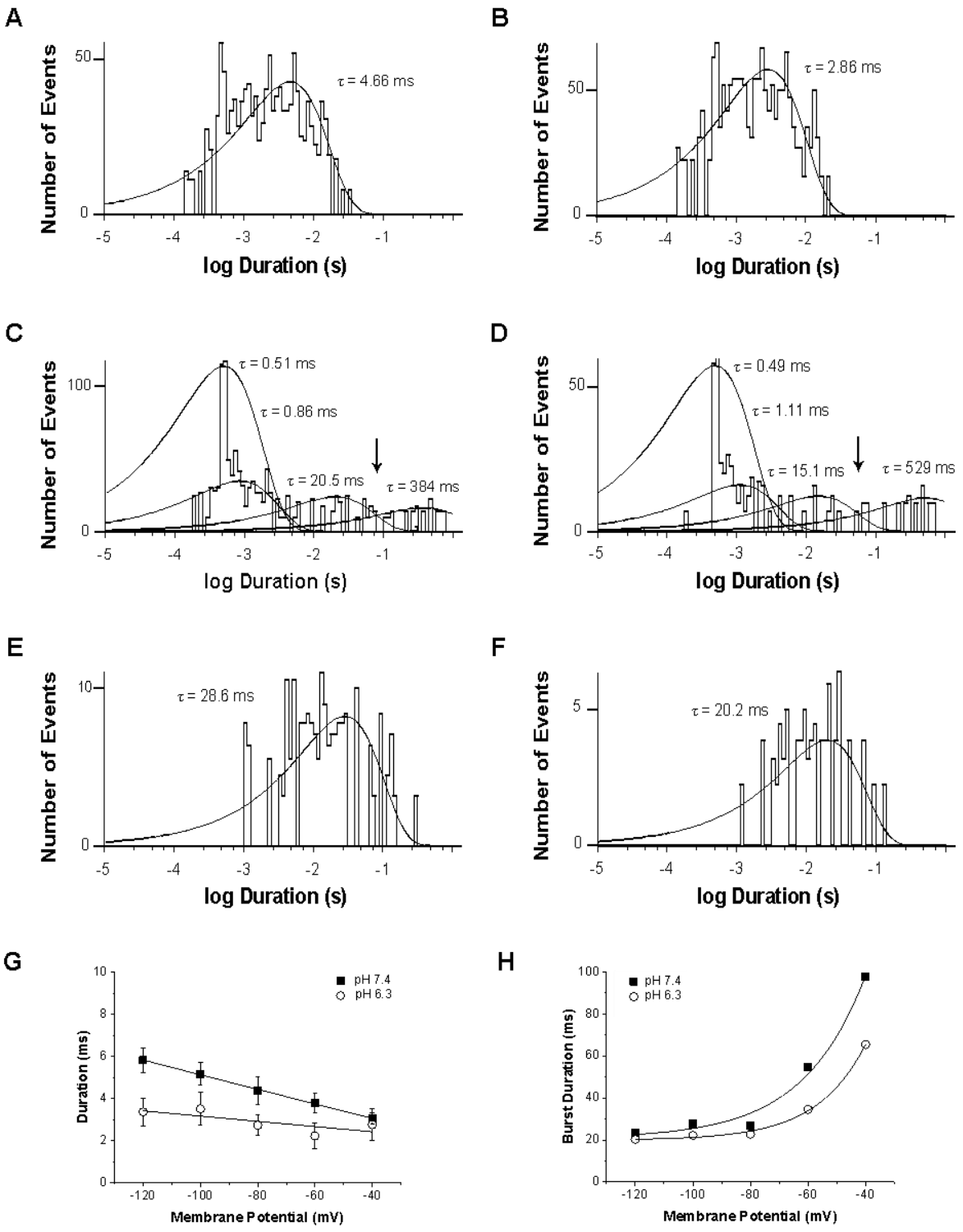
A
Number of Events
50
0
τ = 4.66 ms
-5
-4
-3
-2
-1
log Duration (s)
B
Number of Events
50
0
τ = 2.86 ms
-5
-4
-3
-2
-1
log Duration (s)
C
Number of Events
100
0
τ = 0.51 ms
τ = 0.86 ms
τ = 20.5 ms
τ = 384 ms
-5
-4
-3
-2
-1
log Duration (s)
D
Number of Events
50
0
τ = 0.49 ms
τ = 1.11 ms
τ = 15.1 ms
τ = 529 ms
-5
-4
-3
-2
-1
log Duration (s)
E
Number of Events
10
0
τ = 28.6 ms
-5
-4
-3
-2
-1
log Duration (s)
F
Number of Events
5
0
τ = 20.2 ms
-5
-4
-3
-2
-1
log Duration (s)
G
Duration (ms)
10
8
6
4
2
0
pH 7.4
pH 6.3
-120
-100
-80
-60
-40
Membrane Potential (mV)
H
Burst Duration (ms)
100
80
60
40
20
0
pH 7.4
pH 6.3
-120
-100
-80
-60
-40
Membrane Potential (mV)

Figure 4-5 Kinetics of hERG1b gating upon repolarisation.

A, B. Open-time duration histograms of several patches at -80 mV for pH 7.4 (**A**, n = 7 patches) and pH 6.3 (**B**, n = 6 patches). Histograms were fit with a single exponential function to reveal an open-time duration of 4.66 ms in control and 2.86 ms in pH 6.3.
C, D. Closed-time distributions for hERG in pH 7.4 (**C**) and pH 6.3 (**D**). Distributions in both pH 7.4 and pH 6.3 were best described with four exponentials with time constants (and areas) of 0.51 ms (86.3%), 0.86 ms (8.1%), 20.5 ms (3.8%) and 384 ms (1.8%). Distributions in pH 6.3 obtained time constants of 0.49 ms (85.9%), 1.11 ms (6.8%), 15.1 ms (3.9%) and 529 ms (3.5%). τ_{crit} values were calculated between the third and fourth component of closed-time distributions as indicated by an arrow.
E, F. Burst duration histograms of hERG at -80 mV for pH 7.4 (**E**) and pH6.3 (**F**). Histograms use the patches used in **A-D** and were described with a single exponential. Burst durations obtained were 28.6 ms in pH 7.4 and 20.2 ms in pH 6.3.
G. Open-time durations were obtained for each potential tested and plotted against membrane potential. The plots were fitted with an exponential function for 7.4 (n = 7 cells) pH 6.3 (n = 6 cells).
H. Burst durations were obtained from an average histogram of pooled data and fit with an exponential function (pH 7.4 = 7 patches and pH 6.3 = 6 patches).

Single-channel patches used in open-time duration analysis were also used to determine closed-time durations of I_{hERG1b}. As was the case for hERG1a, analysis of hERG1b closed time durations were best described by fitting four exponentials for both pH_e 7.4 (Figure 4-5C) and pH_e 6.3 (Figure 4-5D). In both conditions, a closure of ~0.50 ms was observed which would suggest a very brief 'flicker' to the closed state within an opening. Comparable with single-channel hERG1a closed-time durations, the τ_{Crit} value is defined by the point in which the third and fourth exponential overlap, which in the case of hERG1b is 79 ms and 57 ms for pH_e 7.4 and 6.3 respectively. The τ_{Crit} values were used to filter open-time durations to obtain burst durations of 28.6 ms in pH_e 7.4 (Figure 4-5E) and 20.2 ms in pH_e 6.3 (Figure 4-5F).

Figure 4-5G shows the relationship of membrane potential and open-time duration in both pH conditions tested. In both pH_e 7.4 and 6.3, a similar relationship was seen in which open-time duration decreased with depolarisation but showed no apparent voltage-dependence (2-way ANOVA with Bonferonni post-test).

Several patches were used to analyse burst duration for pH_e 7.4 (n = 7 patches) and 6.3 (n = 6 patches) in all potentials tested. Membrane potential was plotted against burst duration (Figure 4-5H) for both pH conditions and fit with an exponential function. Burst duration increased with depolarisation, as was observed in hERG1a single-channel currents (Figure 3-7H).

4.4 Discussion

4.4.1 The role of hERG1b in native I_{Kr}

As discussed in the introduction, there is increasing evidence that native I_{Kr} is comprised of heteromers of hERG1a and hERG1b subunits (Lees-Miller et al. 1997; London et al. 1997; Larsen et al. 2008; Jones et al. 2004; Sale et al. 2008; Phartiyal et al. 2008; McPate, H Zhang, et al. 2009; Larsen & Olesen 2010; Du et al. 2011; Jones et al. 2014; Liu et al. 2016; McNally et al. 2017). Recent studies have shown that both hERG1a and hERG1b are expressed in native tissue and appear to co-localise in t-tubules of ventricular myocytes in humans and canine (Jones et al. 2004). Characterisation of I_{Kr} in isolated canine ventricular myocytes (as well as atrial and Purkinje fibre cells) showed variation in the potential in which I_{Kr} transients peaked (Gintant 2000). These findings were reproduced in heterologous expression systems in which the relative abundance of the hERG1a and hERG1b isoform determined the 'peak potential' and kinetics (Larsen & Olesen 2010; McNally et al. 2017). It is suggested that the relative abundance of hERG1a and hERG1b in different regions are responsible for transmural APD heterogeneity with epicardial cells reported to have the shortest APD as well as the fastest I_{Kr} deactivation kinetics (Szabó et al. 2005). The data obtained in this thesis on hERG1a homomers (Chapter3) and hERG1b homomers show different activation and deactivation kinetic properties (see Table 4-1), consistent with previous reports of the two homomers (Lees-Miller et al. 1997; London et al. 1997; Larsen et al. 2008; Sale et al. 2008; Larsen & Olesen 2010).

	Peak Potential (mV)	$V_{0.5}$ (mV)	Conductance (nS/pF)	τ_{Fast} (ms)	τ_{Slow} (ms)
hERG1a	+10	-9.98	0.35	533.75	3790
hERG1b	0	-16.2	0.15	82.725	472

Table 4-1 Comparison of hERG1a and hERG1b channel properties under control conditions. Peak potential were obtained by plotting I-V relationships of $I_{End\ Pulse}$ for hERG1a (Figure 3-2D) and hERG1b (Figure 4-2C). The τ_{Fast} and τ_{Slow} time constants are derived from deactivating I_{Tail} upon repolarisation to -40 mV from a depolarising step to +20 mV.

4.4.2 Extracellular acidosis is enhanced in the hERG1b isoform

Previous studies alongside the work presented in Chapter 3 show that external protons modulate the hERG1a channel by reducing current amplitude and acceleration of deactivation kinetics (Anumonwo et al. 1999; Bérubé et al. 1999; Jiang et al. 1999; Jo et al. 1999; Terai et al. 2000; Van Slyke et al. 2012; Du et al. 2010; Shi et al. 2014; Vereecke & Carmeliet 2000; Bett & Rasmusson 2003). The growing evidence of the hERG1b isoform and its role in native I_{Kr} is now widely accepted (Lees-Miller et al. 1997; London et al. 1997; Larsen et al. 2008; Jones et al. 2014; Larsen & Olesen 2010; McNally et al. 2017), with a recent study demonstrating the effects of acidosis when the hERG1b isoform is co-expressed with the hERG1a isoform in a mammalian cell line (Du et al. 2011). In agreement with this, both the hERG1a homomer and hERG1b homomer were sensitive to protons (see Table 4-2). These findings are physiologically relevant as the N-terminal of hERG1a is involved in deactivation kinetics (Ng et al. 2011; Wang et al. 1998; Wang et al. 2000; Schönherr & Heinemann 1996) and suggests that the site of modulation of I_{hERG} deactivation kinetics is not within the N-terminus.

		Peak Potential (mV)	$V_{0.5}$ (mV)	Conductance (nS/pF)	τ_{Fast} (ms)	τ_{Slow} (ms)
hERG1a	pH 7.4	+10	-9.98	0.35	533.75	3790
	pH 6.3	+10-20	-6.99	0.25	217.75	1276
hERG1b	pH 7.4	0	-16.2	0.15	82.73	472
	pH 6.3	+10-20	+2.2	0.05	73.43	335

Table 4-2 Comparison of hERG1a and hERG1b and the effects of extracellular acidosis.
Peak potential was obtained by plotting I-V relationships of $I_{End\ Pulse}$ for hERG1a (Figure 3-2D) and hERG1b (Figure 4-2C). The τ_{Fast} and τ_{Slow} time constants are derived from deactivating I_{Tail} upon repolarisation to -40 mV from a depolarising step to +20 mV.

As shown in Figure 4-1 the effects of extracellular acidosis on hERG1b channels show a reduction in both $I_{End\ Pulse}$ and I_{Tail} (Figure 4-1) that is greater than the effects observed on hERG1a channel currents (Figure 3-1). The experiments performed in this chapter are the first to characterise the effects of extracellular acidosis on the voltage-dependence of activation on the hERG1b isoform (Figure 4-2). A significant depolarising shift of ~18 mV

was seen in the $V_{0.5}$ values in I_{hERG1b} from -16.2±2.8 mV at pH_e 7.4 and +2.2±1.1 mV at pH_e 6.3 (n = 7 cells). This shift is different from the shift seen in hERG1a homomeric channels (an approximate +3 mV shift was observed, see Table 4-2) and it could be suggested that the differences in voltage-dependence of activation could account for the increase in I_{hERG} inhibition. However, it should be noted that two different cell lines were used: a HEK-293 cell line stably expressing hERG1a and the CHO cell line transiently transfected for hERG1b and could account for some of the difference seen between the two hERG1 isoforms. Previous work using CHO cells shows that an approximate +6 mV shift in homomeric 1a channels and a similar shift in heteromeric 1a/1b channels (Du et al. 2010; Du et al. 2011) and so the difference in expression system cannot account for the large shift seen in hERG1b. Further experiments will need to be conducted to account for the large depolarising shift in the voltage-dependence of activation upon extracellular acidification. In addition, I_{hERG1b} deactivation kinetics were obtained (Figure 4-3) and show that upon acidification of external solution, with a significant decrease in the slow time constant (see Table 4-2).

As mentioned in the introduction of this Chapter, results related to single-channel I_{hERG1b} are the first to be published and therefore comparisons will be made against what is published for I_{hERG1a}. The same recording conditions were made for hERG1b and hERG1a with isotonic potassium (140 mM K^+) and extracellular solution (pipette solution) at either pH 7.4 or 6.3. Single-channel conductance of hERG1b in my recording conditions were 11.3±0.2 pS in pH_e 7.4 (Figure 4-4) which is significantly different, to the hERG1a single-channel conductance of 12.1±0.1 pS (P = 0.0025, unpaired *t*-test) in the same pH condition (Figure 3-6). Previous studies using isotonic potassium (100 -150 mM K^+) on hERG1a show single-channel conductance values between 9.7-13.4 pS upon repolarisation to negative potentials (see Table 4-3 (Zou et al. 1997; Kiehn et al. 1999; Kiehn et al. 1996; Liu et al. 2004; Veldkamp et al. 1995; Veldkamp et al. 1993)). Upon acidification of single-channel I_{hERG1b} from pH_e 7.4 to 6.3, conductance was reduced from 11.3±0.2 pS in pH_e 7.4 (n = 7 patches) to 7.7±0.4 pS in pH_e 6.3 (n = 6 patches) (Figure 4-4). This equates to ~32% reduction in single I_{hERG1b} conductance, which is greater than the reduction seen in single-channel hERG1a conductance (~24%) (P = 0.0491; unpaired *t*-test). This was to be expected due to the augmented effects extracellular protons have on whole-cell hERG1b conductance compared with hERG1a (~67% reduction in I_{hERG1b} conductance versus ~29% reduction for I_{hERG1a} conductance).

Author	Expression system	$[K^+]_o$	Conductance (pS)	Open-time (ms)	Closed-time (ms)
(Shibasaki 1987)	Rabbit nodal cells	100 150 200 300	8.4 (100) 11.1 (150) 13.1 (200) 14.7 (300)	2.5 (at -60 mV)	τ_{fast} = 0.7 τ_{slow} = 17.6
(Minoru Horie et al. 1990)	Guinea pig atrial cells	150 300	10 (150) 17 (300)	9 (at -100 mV)	τ_{fast} = 0.4 τ_{slow} = 37
(Veldkamp et al. 1993)	Rabbit ventricular myocytes	150	13.1 (150)		
(Veldkamp et al. 1995)	Human ventricular myocytes	140	12.9		
(Kiehn et al. 1996)	*Xenopus* oocytes	100	10	3.2 (at -100 mV)	τ_{fast} = 1.0 τ_{slow} = 26
(Zou et al. 1997)	*Xenopus* oocytes	120	12.1	τ_{O1} = 2.9 τ_{O2} = 11.8 (at -90 mV)	τ_{fast} = 0.54 τ_{slow} = 14.5
(Kiehn et al. 1999)	*Xenopus* oocytes	100	9.7	3.2 (at -40 mV)	τ_{C1} = 0.95 τ_{C2} = 3.7 τ_{C3} = 45
(Liu et al. 2004)	Mouse ventricular myocytes	150	12.2	3.5 (at -40 mV)	τ_{fast} = 1.7 τ_{slow} = 175
hERG1a (Chapter 3)	**HEK-293**	**140**	**12.1**	**5.0 (at -80 mV)**	**τ_{C1} = 0.48** **τ_{C2} = 0.98** **τ_{C3} = 44.2** **τ_{C4} = 129**
hERG1b (Chapter 4)	**CHO**	**140**	**11.3**	**4.7 (at -80 mV)**	**τ_{C1} = 0.51** **τ_{C2} = 0.86** **τ_{C3} = 20.5** **τ_{C4} = 384**

Table 4-3 Comparison of single-channel hERG1 data

Tabulated results to compare the single-channel data (conductance and open- closed-time kinetics) for hERG/I_{Kr} channels in different recording conditions. Results from single-channel experiments completed in this thesis are shown in bold.

My experimental data on single-channel hERG1b open-time kinetics (Figure 4-5A and B) were best fit with a single exponential (as was seen in hERG1, Figure 3-7A and B). Open-time duration at -80 mV was 4.66 ms for hERG1b and 5.04 ms for hERG1a. Faster open-time and shorter burst durations are expected to be seen in hERG1b compared with hERG1a due to the quicker deactivation kinetics seen in whole-cell experiments (Figure 4-3). Open-time durations across the voltage range tested showed little voltage-dependence (Figure 4-5G). Upon acidification, a reduction in open-time durations were seen across all potentials in comparison to control conditions (Figure 4-5G). As with single channel I_{hERG1a}, closed-time duration histograms for I_{hERG1b} were best described with four exponentials with the fastest closed time constant ($\tau_{Closed\ 1}$) of ~0.50 ms. This was seen across all membrane potentials tested and is what was seen in hERG1a single-channel recordings, suggesting that it is a short-lived transition to the closed state within a channel opening (Kiehn et al. 1996). Similar to hERG1a, closed time histograms of hERG1b were best fit with four exponentials with the overlap of $\tau_{Closed\ 3}$ and $\tau_{Closed\ 4}$ used to determine τ_{Crit} for burst duration analysis (Colquhoun & Hawkes 1995). Burst duration analysis showed strong voltage-dependence, with an increase in duration with depolarisation which was seen in hERG1a channels (Figure 3-7H) and Kiehn et al also observed (Kiehn et al. 1999).

4.4.3 Physiological consequences of external protons for hERG

The hERG1b isoform is poorly expressed as homomeric channels in *Xenopus* oocytes (London et al. 1997) due to its RXR retention motif located in the unique N-terminus (Phartiyal et al. 2008), but previous work in CHO cells show adequate hERG1b expression making it a suitable expression system (Du et al. 2010; Du et al. 2011). With initial whole-cell experiments, the effects of extracellular acidosis on I_{hERG1b} can be attributed by the reduction in whole-cell conductance, a large and significant depolarising shift in voltage dependence of activation, and the acceleration of deactivation kinetics. Similar observations were made with the hERG1a isoform (Chapter 3) but to a lesser extent (see Table 4-2). A recent study showed a reduction in hERG1a (~25%) and hERG1b (~64%) I_{Tail} similar to that observed here (experiments in this thesis showed a reduction of 29% and 67% for hERG1a and hERG1b respectively) (Du et al. 2011). The same group also

looked at the effect of acidosis on the hERG1a/1b heteromer and achieved an intermediate reduction of ~45% in I_{Tail} (Du et al. 2011). It is unclear as to why the hERG1b isoform is so much more sensitive to extracellular protons compared to the hERG1a isoform. Du et al suggested that differences in the occupancy of gated channel states could have an effect on the availability of the site that protons modulate and bind to the channel (Du et al. 2011).

As with hERG1a, the effects of extracellular acidosis on single hERG1b channels support the whole-cell data obtained; a decrease in amplitude across all membrane potentials tested and a significant decrease in channel conductance was seen, alongside shortening of channel open-time duration coincides with the effects seen in macroscopic recordings. During pathophysiological events, such as cardiac ischemia, the enhanced effects of extracellular protons seen in the hERG1b isoform could prove to have detrimental consequences. Although not physiologically relevant as a homomeric channel (London et al. 1997), it has been shown that heteromeric expression of hERG1a/1b channels or I_{Kr} show heterogeneity in cardiac tissue (Gintant 2000; Jones et al. 2004; Larsen et al. 2008). However, the stoichiometry of native I_{Kr} is yet to be established but a study in which co-expression of known ratios of hERG1a and hERG1b isoform recreated the 'peak potential' range that was observed in canine myocytes (Gintant 2000; Larsen & Olesen 2010). With this background, it can be presumed that single-channel hERG1a/1b heteromers will provide conductance values, and the subsequent effect of extracellular acidosis to be intermediate to what was observed in homomeric hERG1a and hERG1b channels. Du et al also showed that heteromeric hERG1a/1b currents was showed greater inhibition in ventricular and atrial AP voltage-clamp experiments compared to hERG1a alone (Du et al. 2011). As a result, the inhibitory effects of extracellular acidosis can expected to be greater when the hERG1b isoform is present (Du et al. 2011).The extent in which extracellular protons will affect native I_{Kr}, will depend on the relative abundance of hERG1a and hERG1b expression. In respect to this, the regional variation in hERG1 isoform abundances could facilitate heterogeneity of repolarisation during acidosis. This, subsequently, can result in the development of arrhythmias.

5. The modification of hERG1a channels by diethylpyrocarbonate

5.1 Introduction

Chemical modification of proteins has been used for decades for many reasons including structure-function relationship studies and drug development (Feeney et al. 1982; Mendoza & Vachet 2014; Boutureira & Bernardes 2015). Chemical modification involves targeting functional groups in the protein to give insight into the function (Hille 2001). The reaction itself, depends on the amino acid side chain properties (Feeney et al. 1982).

Diethylpyrocarbonate (DEPC) has been used particularly in the study of histidine residues in enzyme catalysis (Miles 1977). Covalent modification of histidine residues in proteins by DEPC results in the formation of an N-carbethoxyhistidyl derivative, as seen in Figure 5-1, which removes the histidine residue's ability to act as a nucleophile.

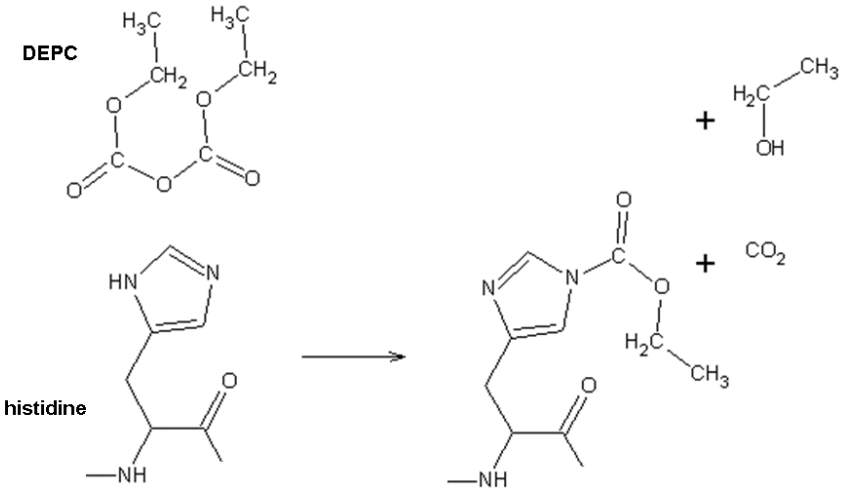

Figure 5-1 The reaction of histidine with diethylpyrocarbonate.

Modification of the side chain of histidine residues: DEPC covalently reacts with imidazole ring located on histidine residues. Image taken and modified from:
http://www.proteinchemist.com/modify/modify.html

With the side-chain of histidine residues possessing an average pK_a value of 6.1, it is reasonable to suggest that histidine residues are most likely to be responsible for proton modulation. DEPC modification of histidine residues have been applied to ion channel function (Holmgren et al. 1998; Wang & Wu 1997; Zhou et al. 2004; Sasaki et al. 2015).

Histidine modification by DEPC has previously been used to study hERG channels with differing results on the effects of DEPC on deactivation kinetics (Jiang et al. 1999; Meves 2001). In this section, the effects of DEPC on the hERG1a current was investigated to determine whether histidine residues within the channel are responsible for proton sensitivity.

5.2 Methods

DEPC hydrolyses in aqueous solution with a half-life of 9-24 minutes (Sigma Aldrich). As a result, 2 mM DEPC was prepared for immediate use. This was achieved by diluting 15 µl DEPC (6.9 M) in 50 µl water before adding to 50 ml external bathing solution. The concentration used is a supra-maximal concentration and has been used in other studies of ERG currents (Jiang et al. 1999; Meves 2001).

All experiments carried out in this chapter were completed in the HEK-293 cell line stably expressing hERG1a. Maintenance of the cell line and solutions used in the experiments are described in Chapter 2.2.1 and 2.3.1. During recordings, the external solution was pH_e was 7.4 in control and in DEPC application (see above for making of 2 mM DEPC solution) and titrated to pH_e 6.3 using HCl. The external superfusate was continuously supplied to the bath containing cells using gravity at a rate of 20 ml/min so that rapid exchange of solution was achieved when switching to 2 mM DEPC or pH_e 6.3. All recordings were completed at room temperature and data were low-pass filtered at 1 kHz and acquired at 10 kHz.

5.3 Results

5.3.1 hERG1a modulation by DEPC

The effects of DEPC on I_{hERG} were measured using the protocol in Figure 5-2A (lower panel): a depolarising pulse to +20 mV for 2 seconds was followed by a 6 second pulse to -40 mV before returning to the holding potential (-80 mV). A 50 ms pulse to -40 mV at the beginning of the pulse was elicited to measure leak current and I_{hERG} tail amplitude was measured relative to the current elicited during this pulse. An inter-pulse interval of 12 seconds was used. Current-voltage (I-V) relationships were also determined pre- and post-DEPC application: the protocol used was like that described above, but with commands to a range of depolarising potentials was tested from -40 mV to +70 mV.

Figure 5-2A shows a representative hERG1a current before (black trace), after 10 minutes exposure to 2 mM DEPC (blue trace) and with subsequent exposure to external protons (pH 6.3, red trace). Current-voltage (I-V) relationships were plotted by normalising data to the maximum $I_{End\ Pulse}$ observed in control and plotted against membrane potential (Figure 5-2B). In control conditions, the relationship showed the same 'bell-shaped' curve seen in previous experiments (Figure 3-2C). However, with 2 mM DEPC treatment, there is a decrease in amplitude from all potentials, other than at +70 mV as well as the loss of negative slope that is associated with inward rectification of the channel. Acidification to pH_e 6.3 post-DEPC application saw a further decrease in current with the similar, more linear relation as seen in DEPC. The voltage-dependence of activation was determined in control conditions and after DEPC exposure by normalising I_{Tail} to maximum I_{Tail} in each condition and plotting against membrane potential. Relationship was not determined for pH_e 6.3 as reduction of current made it difficult to measure currents (Figure 5-2A, red trace). The voltage-dependent activation relationships were fit with a Boltzmann function (Equation 1) and the half-maximal voltage ($V_{0.5}$) was determined. In control conditions, the $V_{0.5}$ was −9.07±3.2 mV (n = 7 cells) and the $V_{0.5}$ after 10-minute treatment of 2 mM DEPC was and a $V_{0.5}$ of -4.24±4.2 mV (n = 7 cells). DEPC treatment caused a non-significant ~5 mV depolarising shift in $V_{0.5}$ of hERG1a channels (P = 0.3776; paired *t*-test). The k value in control was not significantly different to the k value of DEPC treated cells (P = 0.6928; paired *t*-test).

Figure 5-2D shows the time course of hERG $I_{End\ Pulse}$ and I_{Tail} block by 2 mM DEPC. followed by washout and external acidification to pH 6.3. As shown, steady-state block of $I_{End\ Pulse}$ and I_{Tail} by DEPC was reached by the end of the 10 minute perfusion. Wash-out of DEPC was completed for 3 minutes before the bathing solution was switched to pH_e 6.3 to determine if protons were still able to modulate I_{hERG1a}.

Coinciding with the decrease in I_{hERG} amplitude, DEPC also accelerated the rate of hERG I_{Tail} deactivation. Figure 5-2E shows mean ± SEM values for the fast and slow time

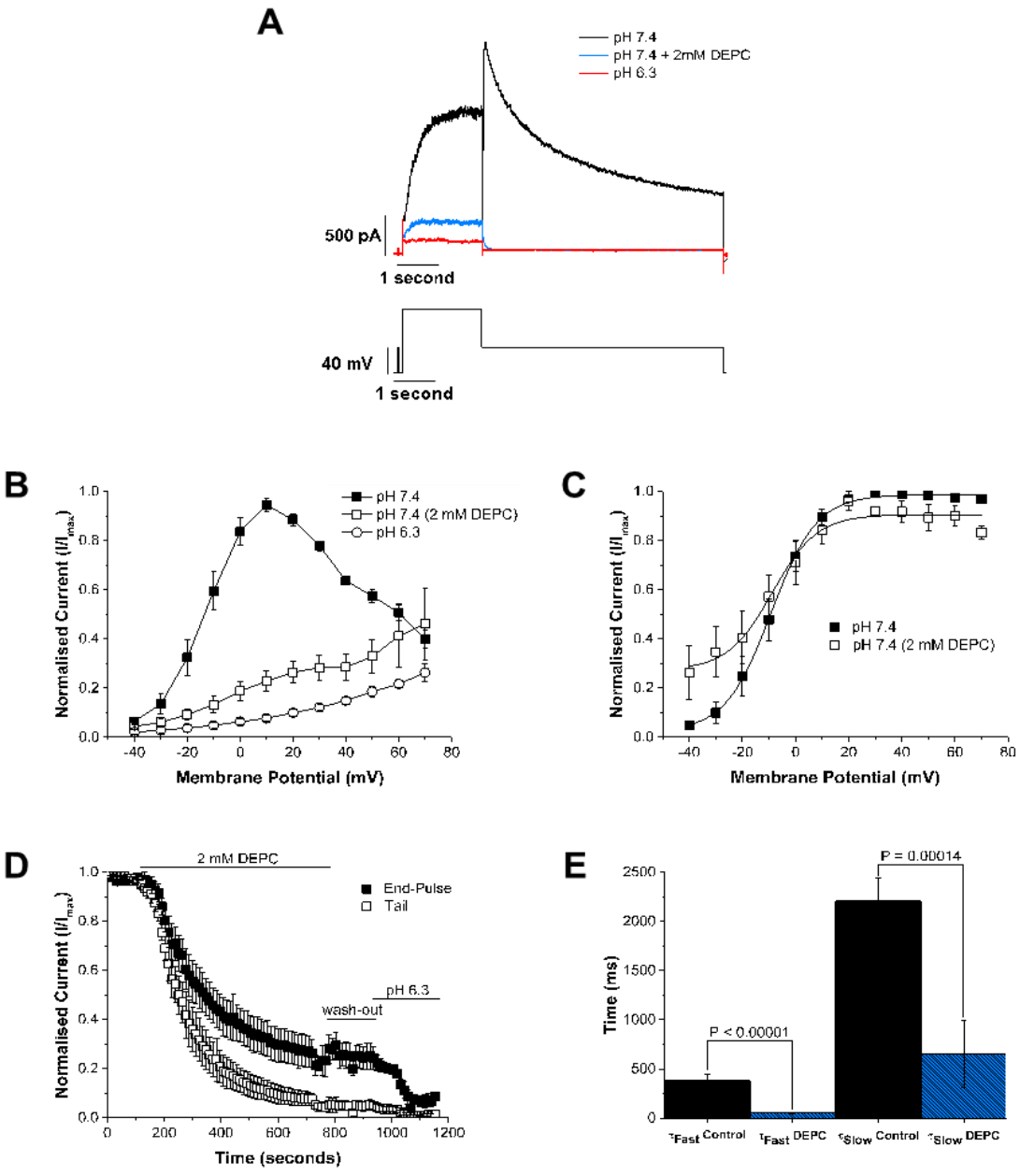

Figure 5-2 The effect of DEPC on hERG1a channels.

A. Representative hERG1a currents in control (black trace), after 10 minutes of 2 mM DEPC application (blue trace) and acidification to pH_e 6.3 (red trace).
B. Current voltage relationships of hERG $I_{End\ Pulse}$ in pH_e 7.4 (n = 7 cells), 2 mM DEPC (n = 7 cells) and pH_e 6.3 (n = 3 cells). Data were normalised to the maximal I_{hERG} current in control and were then plotted against membrane potentials.
C. Steady-state activation plots from hERG I_{Tail} upon repolarisation to -40 mV. For control and 2 mM DEPC, values were normalised to maximal I_{Tail} in each condition and plotted against membrane potential. Relations were fit with a Boltzmann function to give $V_{0.5}$ values of −9.1±3.2 mV (k = 7.1±0.4 mV) in control (n = 7 cells) and a $V_{0.5}$ of -4.2±4.2 mV (k = 8.0±1.9 mV) with 2 mM DEPC treatment (n = 7 cells).
D. Time-course of DEPC treatment. Graph shows 10 minutes of DEPC application followed by a 5-minute wash-out period before completing the experiment with acidification of external solution to pH 6.3.
E. Mean ± SEM of the fast and slow constant before (black bars) and after 10 minutes application of 2 mM DEPC (blue bars). DEPC treatment significantly decreased the both time constants ($P < 0.00001$ for the fast time constant and $P = 0.00014$ for the slow time constant; paired t-test with bonferonni post-test).

constants. After achieving steady-state block by DEPC, the fast time constant decreased from 378±67 ms to 51±19 ms ($P < 0.00001$; paired t-test) and the slow time constant decreased from 2206±229 ms to 657±340 ms ($P = 0.00014$; paired t-test). As already mentioned, the deactivation of I_{Tail} after extracellular acidosis could not be analysed due to insignificantly sized currents (Figure 5-2A, red trace).

5.4 Discussion

5.4.1 The role of diethylpyrocarbonate in chemical modification of protein residues

DEPC covalently reacts with histidine residues by substitution of one of the nitrogen positions on the imidazole ring (Lundblad 2014) as shown in Figure 5-1. For the reaction to occur, the imidazole/histidine residue must be unprotonated (Miles 1977) and so this is expected to be the case in control pH_e 7.4. However, it should also be mentioned that pK_a values of ionisable side chains such as histidine can vary depending on the environment and so can differ from the intrinsic value (Miles 1977; Pace et al. 2010).

Previous studies have also observed that DEPC does not always specifically modify histidine side chains in proteins but also with arginine, tyrosine, methionine and cysteine side chains (Glazer 1970; Miles 1977).

5.4.2 Block of I_{hERG} by DEPC

With this background information, it is reasonable to suggest that, if histidine residues were involved in proton modulation of hERG channel amplitude and kinetics, modification of these residues by DEPC would render the channel insensitive. Figure 5-2 shows that the application of DEPC led to block of I_{hERG}, with further block by protons. Little prior information is available on the effects of DEPC on ERG. Results obtained in these experiments are in agreement with Jiang et al, in which 2 mM DEPC perfusion resulted in a reduction in hERG current amplitude with a dramatic acceleration of hERG deactivation (Jiang et al. 1999). Their results also showed a small depolarising shift of ~4 mV in $V_{0.5}$ values, which was like the shift (approximately +5 mV) seen in the experiments completed in this chapter (pH_e 7.4 $V_{0.5}$ value of −9.1±3.2 mV and a $V_{0.5}$ of -4.2±4.2 mV in 2 mM DEPC; Figure 5-2B). The effects of 2.1 mM DEPC on ERG channels present in mouse neuroblastoma x rat glioma hybrid cells showed minimal reduction on the current amplitude with a slowing of the ERG current deactivation (Meves 2001). Such discrepancy in results is difficult to explain, but cell line and recording conditions may be responsible for some of these differences: Jiang et al recorded outward currents from oocytes with $[K^+]_e$ of 2 mM whereas Meves recorded inward ERG currents from hybrid cells with a $[K^+]_e$ of 40 mM (Jiang et al. 1999; Meves 2001). My recording conditions were more similar to those of Jiang et al (experiments in this chapter looked at outward currents in $[K^+]_e$ of 4 mM), than those of Meves and this might contribute to some of the similarities in results.

5.4.3 DEPC treatment and extracellular acidosis

A previous study that lowered external pH from 7.5 to 6.5 after treatment with 2 mM DEPC showed a decrease in current amplitude and a marked depolarising shift (~18 mV) in the activation curve (Jiang et al. 1999). They also noted that although there was an apparent acceleration in deactivation upon acidification, this could be fully accounted for by the shift in $V_{0.5}$. In experiments completed in this chapter (Figure 5-2A), extracellular acidosis after DEPC treatment showed a reduction in $I_{End\ Pulse}$ and block of I_{Tail} to the extent that the effects on hERG deactivation and the voltage-dependence of activation could not be analysed.

5.4.4 Functional implications of DEPC on hERG1a

With the inhibition of I_{hERG} by DEPC observed in this chapter and in a previous study (Jiang et al. 1999) it is possible to suggest that histidine residues may not be the sole candidate for proton sensitivity. However, involvement of histidine residues should not be precluded, and it should be considered that the pH sensitivity must involve other residues. As previously mentioned, DEPC primarily targets histidine residues but can also covalently modify other residues including arginine and lysine (Glazer 1970; Miles 1977). This could open several possibilities into what residues are responsible for DEPC modification. The results obtained in this chapter are not specific enough to guide targeted mutagenesis studies and so DEPC intervention has limited value for interrogating the underlying basis of hERG modification by protons.

6. The effect of extracellular acidosis on titratable residues within the hERG1a channel

6.1 Introduction

As previously mentioned in Chapter 3 and previously published studies, the hERG channel is modulated by extracellular protons in which whole-cell conductance is reduced and deactivation of hERG I_{Tail} is accelerated (Anumonwo et al. 1999; Bérubé et al. 1999; Jiang et al. 1999; Jo et al. 1999; Terai et al. 2000; Vereecke & Carmeliet 2000; Bett & Rasmusson 2003; Zhou & Bett 2010; Van Slyke et al. 2012; Du et al. 2010; Shi et al. 2014). Earlier studies have shown that these processes have different sensitivities to protons giving different pK_a values, suggesting that there is more than one site of proton modulation (Anumonwo et al. 1999; Bett & Rasmusson 2003; Van Slyke et al. 2012; Shi et al. 2014).

A previous investigation showed that extracellular cations and protons compete for the same binding site within the hERG channel; an increase in calcium concentration inhibited the effects of the shift observed in $V_{0.5}$ upon extracellular acidification but the reduction in channel conductance was unaffected (Jo et al. 1999). This notion supports the idea of >1 proton binding site on the hERG channel. Mutagenesis studies confirmed the site of cation binding to be in the S2 (D456 and D460) and S3 (D509) transmembrane domains of the hERG channel with the D460 and D509 residues being conserved across EAG superfamily (Fernandez et al. 2005; Kazmierczak et al. 2013; Shi et al. 2014). Moreover, neutralising all three residues (to alanine) completely abolished the shift in activation observed in extracellular acidosis (Shi et al. 2014). However, the reduction in whole-cell conductance and acceleration of deactivation is still observed (Shi et al. 2014).

The mechanism by which extracellular protons accelerate the rate of hERG channel deactivation is unknown. There are several factors which contribute to the rate of deactivation in the hERG channel including the NH_2-terminal 'PAS' domain (Cabral et al. 1998; Wang et al. 2000) as well as conformational changes in S4-S5 linker and cytoplasmic half of the S6 (Tristani-Firouzi et al. 2002). A recent study proposed that tyrosine residues in the S4-S5 linker are critical for the slow deactivation of the hERG channel (Ng et al. 2016).

The flow of ions, and therefore channel conductance, is regulated by the reversible collapse of the intervening pore loop between the S5 and S6 transmembrane domain (Ju et al. 2009). The intervening loop in hERG channels is known to include the selectivity filter and an amphiphatic α-helix that contains residues critical for normal channel function (Doyle et al. 1998; Torres et al. 2003; Clarke et al. 2006).

The structure and function of proteins depend on the net charge and the subsequent ionisation state of individual residues within the protein (Pace et al. 2010). As a result, these ionisable residues will possess pK_a values which can be influenced by several factors including the local environment. Recent studies have shown that lysine and glutamic acid residues, with a pK_a of approximately 10.6 and 4.2 respectively, can possess a pK_a of as low as 5.3 for lysine or as high as 7.2 for glutamic acid residues due to environmental factors (Isom et al. 2011; Harms et al. 2009).

Against this background, the experiments performed in this chapter aimed to: (1) determine the concentration-dependent effects of extracellular protons on the hERG channel processes and (2) target, using site-directed mutagenesis, titratable residues that could be accessed from the extracellular side with whole-cell characterisation of the mutant channels to determine proton sensitivity. *In silico* hERG homology modelling was used to support what residues will be targeted.

6.2 Methods

Experiments carried out in this chapter were completed in the HEK-293 cell line which was either stably transfected with WT hERG1a or transiently transfected with hERG1a channel mutants. Detailed coverage of the mutagenesis method and primer sets for mutants created is given in (Chapter 2.1.1.1, Table 2-1). Briefly; "QuikChange" PCR (Agilent Technologies) was used to introduce point mutations into hERG cDNA using specifically designed primers before purification of the PCR product and subsequent transformation of the cDNA. Mutant hERG cDNA was sequenced (Eurofin Genomics, Germany) to determine if the correct mutation had been created, prior to transfection of HEK-293 cells by mutant constructs. For the transient transfections, 500 ng hERG1a mutant cDNA plasmid was co-transfected with 500 ng eGFP plasmid. Where transfection with mutant cDNA alone did not result in expression of functional channels, co-transfection with WT-hERG1a cDNA (250 ng of mutant cDNA with 250 ng WT-hERG1a) was performed. Chapter 2.2.1, 2.2.2 and 2.3.1 contains detailed methods of maintenance, transient transfections and making of electrophysiological recording solutions.

During whole cell I_{hERG} recordings, the pH of the external solution (pH_e) was 7.4 in control and was titrated to a range of pH_e values (8.0, 7.7, 7.0, 6.5, 6.0, 5.5, 5.0 and 4.5) using NaOH or HCl fresh on each experimental day. Characterisation of mutant channels using a standard I-V protocol was conducted with the pH of bathing solution at either 7.4 (control), 6.3 or 5.5. The external superfusate was continuously supplied to the bath containing cells using gravity at a rate of 20 ml/min so that rapid exchange of solution was achieved when switching to a different pH_e. Cell-attached recordings were completed with a continuous external superfusate of pH_e 7.4 and isotonic potassium (140 mM K^+) with the pipette solution titrated to either pH 7.4 or pH 6.3. All recordings were conducted at room temperature and low-pass Bessel filtered at 1 kHz and acquired at 10 kHz.

6.3 Results – Part I

6.3.1 Initial experiments to determine the concentration-dependence of effects of protons on I_{hERG1a}

Effects of a range of external pH values were tested on hERG using the standard 'square' pulse protocol. In Figure 6-1A, as the external perfusate became more acidic, the negative effects on the characteristics of I_{hERG1a} (end-pulse current, tail current and deactivation kinetics) became more apparent. The characteristics were then analysed at each pH_e value tested by comparing the value in test pH_e with control pH_e of 7.4 and expressed as % decrease (Equation 5). Values obtained at pH_e values of 8.0 and 7.7 were larger than that in control and so these pH_e values shown in Figure 6-1B-E are a negative decrease i.e. a % increase compared with control. The mean ± SEM of each analysed characteristic were plotted against the respective pH_e value and fit with a concentration-response equation with a variable Hill slope (Equation 4) with the mid-point of the fit corresponding to the pK_a (acid dissociation constant) of that I_{hERG} characteristic. Figure 6-1B-E show each I_{hERG} characteristic fit with Equation 4 to give four separate pK_a values. For the $I_{End\ Pulse}$ (Figure 6-1B) a pK_a value of 6.9±0.2 (n = 7 cells) was obtained; a pK_a of 5.5±0.2 (n = 7 cells) was seen for hERG I_{Tail} (Figure 6-1C). The deactivation of I_{Tail} was best described with a bi-exponential function (Equation 2) to obtain the fast and slow time constants named τ_{Fast} and τ_{Slow} respectively. The pK_a value obtained for τ_{Fast} (Figure 6-1D) is 6.8±0.1 and the τ_{Slow} (Figure 6-1E) pK_a value was 7.3±0.2 (n = 7 cells). Statistical analysis (one-way ANOVA with Bonferonni post-test) showed a significant difference between the pK_a for the I_{Tail} and the three individual characteristics ($P < 0.0001$). A small significance was observed between $I_{End\ Pulse}$ and τ_{Slow} ($P = 0.0445$), whilst no statistical significance was seen between $I_{End\ Pulse}$ and τ_{Fast} or between τ_{Fast} and τ_{Slow}.

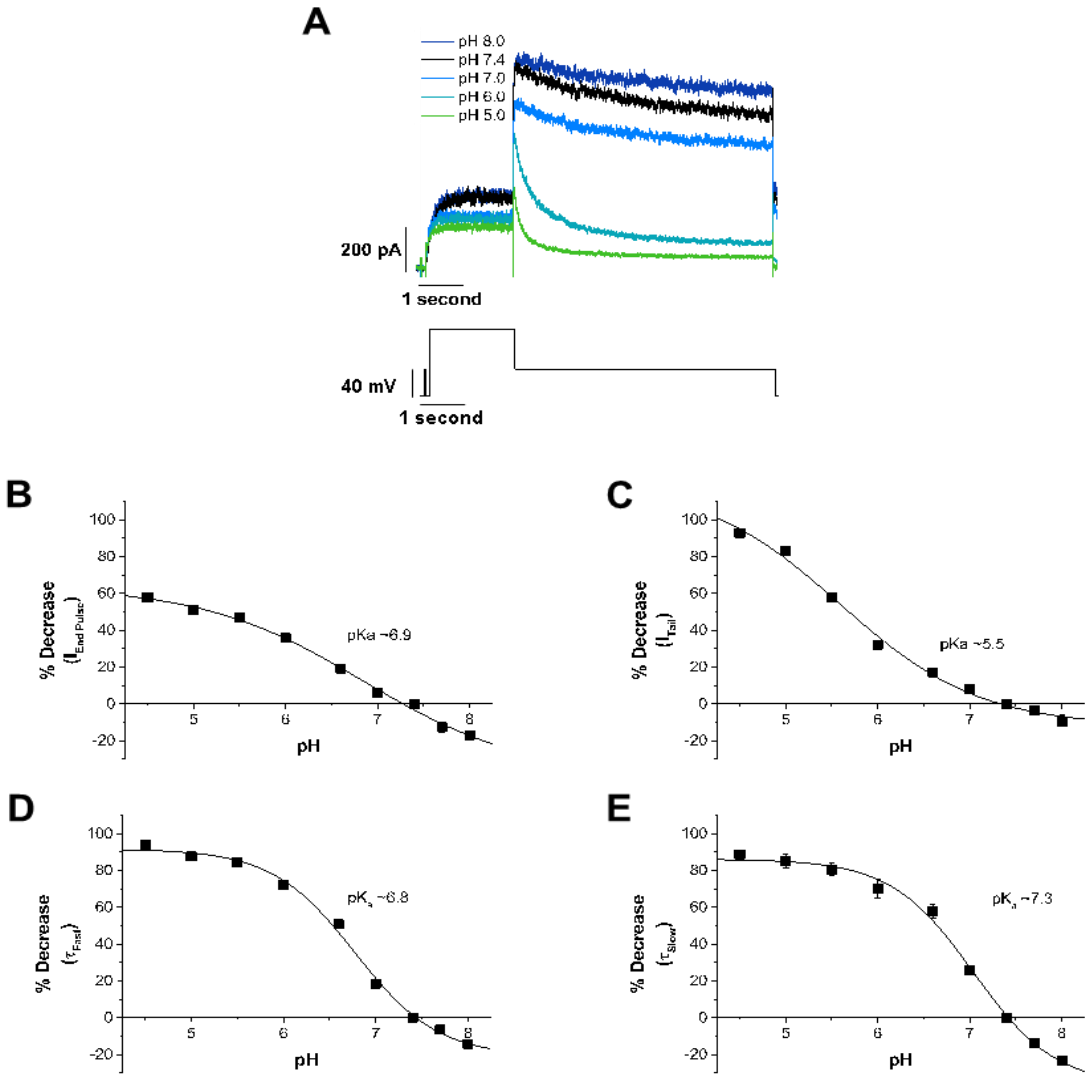

Figure 6-1 The effects of protons on hERG channel characteristics.

A. Representative current traces of I_{hERG} when subjected to various pH_e values ranging from pH 8.0 to 4.5. Select pH_e values are chosen for clarity.

B. Mean ± SEM values of the % decrease in end pulse current of I_{hERG}. % values were compared to that seen in control conditions (pH_e 7.4) and plotted against the respective pH. Plot were fit with a dose-response equation with a variable Hill slope to achieve a pK_a value of 6.9±0.2 (k = -0.5±0.1).

C. hERG I_{Tail} % decrease compared to control I_{Tail} (mean ± SEM). A dose response fit achieved a pK_a value of 5.5±0.2 (k = -0.6±0.1).

D, E. hERG tail current deactivation fit with a bi-exponential function to achieve τ_{Fast} (**D**) and τ_{Slow} (**E**). Plots show mean ± SEM values of % decrease in τ_{Fast} (**D**) and τ_{Slow} (**E**) against respective pH_e value. pK_a values derived from fitting the plots with dose-response equation with a variable Hill slope were 6.8±0.1 (k = -1.0±0.1) for τ_{Fast} and 7.3±0.2 (k = -1.0±0.2) for τ_{Slow}.

6.3.2 Determining target titratable residues in the hERG1a channel

The pK_a values obtained from these initial experiments give an indication as to what amino acid residues may play a role in proton sensitivity. When these results are considered together with the data obtained in Chapter 3 and published previously, the residues responsible for the effects of protons on I_{hERG} must be titratable at between pH_e 5.5 and 6.5 (Anumonwo et al. 1999; Bérubé et al. 1999; Jiang et al. 1999; Jo et al. 1999; Terai et al. 2000; Vereecke & Carmeliet 2000; Bett & Rasmusson 2003; Zhou & Bett 2010; Van Slyke et al. 2012; Du et al. 2010).

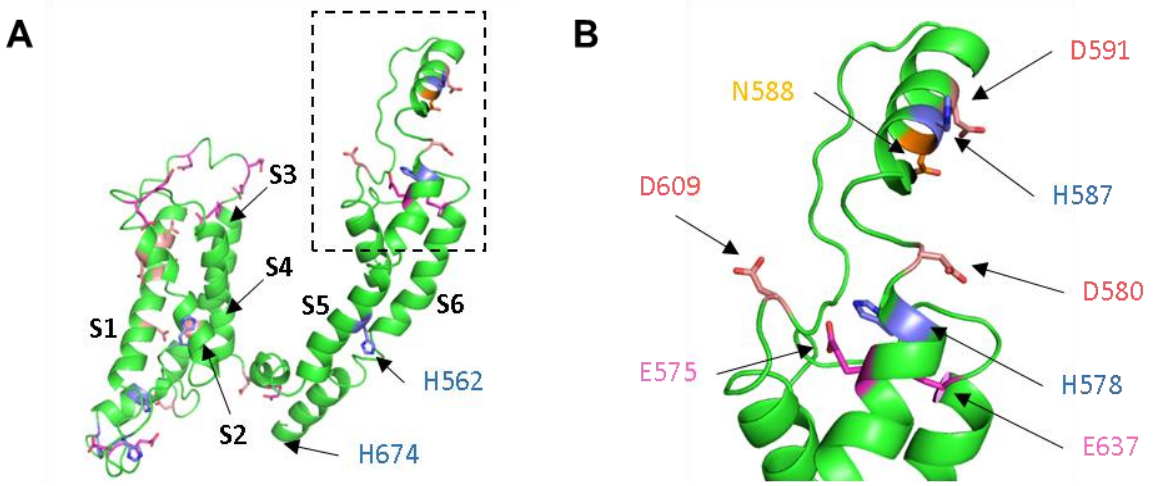

Figure 6-2 hERG homology model with target titratable residues.

A, B. A single hERG1a subunit based on the K_v1.2/2.1 chimera homology model with each region labelled accordingly (**A**). The target residues based at the top of the S5, S5-P linker and S6 are enclosed in the dashed box and shown at a larger scale in **B**. Two histidine residues, H562 and H674, are located on the middle of S5 and bottom of S6 respectively.

Homology modelling was carried out by Dr Chris Dempsey.

A homology model of the open-state hERG channel constructed based on the crystal structure of the Kv1.2/2.1 chimera (Colenso et al. 2013) was used to consider titratable residues accessible from the extracellular surface of the channel. Figure 6-2A shows an individual hERG1a subunit based on this model with the histidine (blue), glutamic acid (pink) and aspartic acid (red) residues highlighted.

As shown in Figure 6-2A there is a small cluster of titratable residues located at the top of the S5 and S6 region including the S5-P linker and the pore helix. This region is highlighted by a dashed box and Figure 6-2B shows the individual residues on a larger scale. Residues highlighted in Figure 6-2A possess negative or acidic side chains and were chosen for mutagenesis as they would be more likely to be involved in sensing protons.The individual residues were mutated so that the charged side chain was removed and replaced with an amino acid residue that possesses a polar, uncharged side chain that would minimise the structural implications inherent in changing amino acid identity. The only exception being the inactivation-impairing mutation N588K (Figure 6-2B, orange residue) (Brugada et al. 2004; Cordeiro et al. 2005; Hong, Bjerregaard, et al. 2005; McPate et al. 2005; McPate, H. Zhang, et al. 2009).

6.3.3 Characterising the effects of extracellular acidosis on mutant hERG1a channels

Characterisation of the mutants (H562N, E575Q, H578N, D580N, H587N, N588K, D609N, E637Q, H674N and E575Q/H578N) was completed by applying a voltage protocol which involved a series of depolarising commands (ranging from -40 mV to +70 mV in 10 mV increments) before repolarisation to -40 mV. The protocol was applied in control solution and in acidic solution once steady state was reached with a 12 second start-to-start interval between successive sweeps.

6.3.4 Extracellular acidosis and the hERG H562N mutant

The H562N mutation, located mid-way on the S5 helices, appeared to create a trafficking deficiency, as no current was observed when the H562N construct was transfected into HEK-293 cells alone. As a result, cells were transfected at a 1:1 ratio of WT hERG and hERG H562N cDNA. The effects of extracellular acidosis are shown in Figure 6-3, in which representative traces (Figure 6-3A-C) show characteristics similar to that of WT hERG1a (Figure 3-2A-C).

Current-voltage relationships for end-pulse currents were constructed by normalising $I_{End\ Pulse}$ to maximal $I_{End\ Pulse}$ seen in control and plotted against membrane potential. As for WT I_{hERG}, the $I_{End\ Pulse}$ of hERG H562N increased with depolarisation reaching a peak at 0 mV (n = 4 cells), with a decrease in $I_{End\ Pulse}$ at more positive potentials (Figure 6-3D).

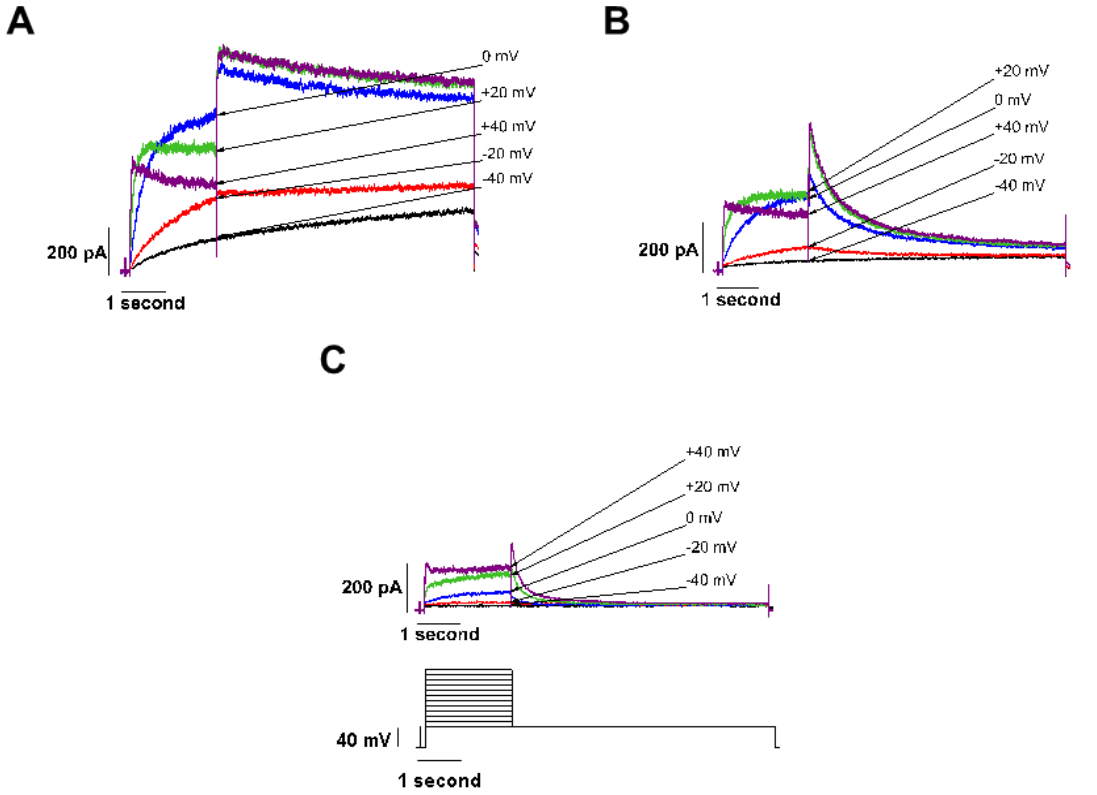
A
0 mV
+20 mV
+40 mV
-20 mV
-40 mV
200 pA
1 second
B
+20 mV
0 mV
+40 mV
-20 mV
-40 mV
200 pA
1 second
C
+40 mV
+20 mV
0 mV
-20 mV
-40 mV
200 pA
1 second
40 mV
1 second
D
pH 7.4
pH 6.3
pH 5.5
WT pH 7.4
WT pH 6.3
WT pH 5.5
Normalised Current (I/I_max)
Membrane Potential (mV)
E
pH 7.4
pH 6.3
pH 5.5
WT pH 7.4
WT pH 6.3
WT pH 5.5
Normalised Current (I/I_max)
Membrane Potential (mV)
F
pH 6.3
pH 5.5
WT pH 6.3
WT pH 5.5
Fractional Decrease
(I_End Pulse)
Membrane Potential (mV)
G
pH 6.3
pH 5.5
WT pH 6.3
WT pH 5.5
Fractional Decrease
(I_Tail)
Membrane Potential (mV)

Figure 6-3 The current voltage relationship for the hERG H562N mutant.

A, B, C. Representative families of I_{hERG} at pH_e values of 7.4 (**A**), 6.3 (**B**) and 5.5 (**C**) when the voltage protocol in lower panel of **C** was applied. Select currents were chosen for clarity. **D.** I-V relations for end-pulse currents at pH_e 7.4 (n = 4 cells), 6.3 (n = 4 cells) and 5.5 (n = 4 cells). Data were normalised to the maximal I_{hERG} current in control and were then plotted against membrane potentials.
E. Steady-state activation plots for I_{hERG} derived from hERG I_{Tail} measurements on repolarisation to -40 mV. The data were normalised to the maximal I_{Tail} in each pH_e and plotted against corresponding test pulse membrane potentials. The relations were fitted with a Boltzmann equation to give $V_{0.5}$ of −21.3±3.2 mV (k = 6.8±1.4 mV) at pH 7.4 (n = 4 cells) a $V_{0.5}$ of −12.1±3.9 mV (k = 8.8±0.6 mV) at pH 6.3 (n = 4 cells) and a $V_{0.5}$ of 14.4±1.2 mV (k = 14.7±2.3 mV) for pH 5.5 (n = 4 cells).
F. Plot of mean (±SEM) fractional decrease of I_{hERG} against test voltage for end-pulse current at pH_e 6.3 (n = 4 cells) and pH_e 5.5 (n = 4 cells).
G. Plot of mean (± SEM) fractional decrease of I_{hERG} against test voltages for tail current at pH_e 6.3 (n = 4 cells) and pH_e 5.5 (n = 4 cells).
WT data (grey) is shown in D-G for comparison.

Acidification to pH_e 6.3 resulted in a similar I-V relationship to that in control WT/H562N but with a decrease across all potentials tested and a peak in maximal $I_{End\ Pulse}$ shifted to +10 mV (n = 4 cells). At pH_e 5.5, $I_{End\ Pulse}$ was further decreased but no negative slope region was evident in the I-V relation. Instead a plateau was reached at potentials positive to +30 mV (n = 4 cells).

The voltage-dependence of I_{hERG} activation was determined by plotting I-V relation for hERG I_{Tail}. The I_{Tail} was measured at each depolarising step and normalised to the maximal I_{Tail} observed during the protocol in each condition before being plotted against membrane potential. To quantify the voltage-dependence of I_{hERG} activation, the relationship was fitted with a Boltzmann function (Equation 1) to give a half-maximal activation voltage ($V_{0.5}$) value of −21.31±3.19 mV (k = 6.76±1.38 mV) at pH 7.4 (n = 4 cells) a $V_{0.5}$ of −12.12±3.85 mV (k = 8.77±0.58 mV) at pH 6.3 (n = 4 cells) and a $V_{0.5}$ of 14.38±1.21 mV (k = 14.69±2.28 mV) for pH 5.5 (n = 4 cells). The positive shift of the activation, $V_{0.5}$, in acidic condition was significantly different to control for pH_e 6.3 (P = 0.0430; paired *t*-test) and pH_e 5.5 (P = 0.0014; paired *t*-test). Maximal conductance (G_{Max})

was derived from the I_{Tail} measurements. Values for G_{Max} were 0.37 nS/pF in pH_e 7.4, 0.21 nS/pF in pH_e 6.3 and 0.10 nS/pF in pH_e 5.5, resulting in a significant decrease in conductance in acidic conditions (P = 0.0299 for pH_e 6.3; paired *t*-test and P = 0.0099 for pH_e 5.5; paired *t*-test).

6.3.4.1 The hERG D580N mutant and the effects of extracellular acidosis

Figure 6-4A-C shows representative current traces for the hERG D580N mutant in control conditions (Figure 6-4A) and under acidic conditions (Figure 6-4B and C). The hERG D580N mutant showed WT hERG characteristics.

I-V relationships were constructed by normalising $I_{End\ Pulse}$ to the maximal $I_{End\ Pulse}$ seen in control (pH_e 7.4) conditions and plotted against membrane potential (Figure 6-4D). With pH_e 7.4, $I_{End\ Pulse}$ amplitude increased with depolarising voltage commands with a peak at 0 mV. Potentials more positive to this showed a negative slope on the I-V relationship, indicating a decrease in $I_{End\ Pulse}$ amplitude. Acidification of the extracellular solution to pH 6.3 caused a reduction in $I_{End\ Pulse}$ amplitude across all membrane potentials tested. The I-V relationship was similar in pH_e 6.3, with depolarisation causing an increase in $I_{End\ Pulse}$ up to +10 mV before a decline in $I_{End\ Pulse}$. Further acidification to pH_e 5.5 caused further attenuation of the end pulse current over the potentials tested. An increase in current was seen with depolarisation up until approximately +20 mV before a plateau in $I_{End\ Pulse}$ current amplitude was reached.

The voltage-dependence of I_{hERG} activation was determined by plotting I-V relations for hERG I_{Tail}, as described above for H562N, at each pH_e (Figure 6-4E). The I-V relationship for I_{Tail} was fitted with a Boltzmann function (Equation 1) to derive $V_{0.5}$ values. In control conditions, the half-maximal voltage for activation for the D580N mutant was −13.44±2.33 mV (k = 7.49±0.42 mV, n = 6 cells). Upon acidification, a shift in $V_{0.5}$ was observed: a $V_{0.5}$ of −7.42±2.26 mV (k = 8.65±0.58 mV) was seen at pH 6.3 (n = 6 cells) and a $V_{0.5}$ of 11.29±2.08 mV (k = 13.92±2.12 mV) was seen for pH 5.5 (n = 4 cells). The positive shift of $V_{0.5}$ in acidic condition was significantly different to control with pH_e 6.3 (P = 0.0060; paired *t*-test) and pH_e 5.5 (P = 0.0048; paired *t*-test). Maximal conductance (G_{Max}) was derived from the I_{Tail} measurements. Values for G_{Max} were 1.03 nS/pF in pH_e 7.4, 0.57 nS/pF in pH_e 6.3 and 0.21 nS/pF in pH_e 5.5, resulting in a significant decrease in conductance in acidic conditions (P = 0.0073 for pH_e 6.3; paired *t*-test and P = 0.0084 for pH_e 5.5; paired *t*-test).

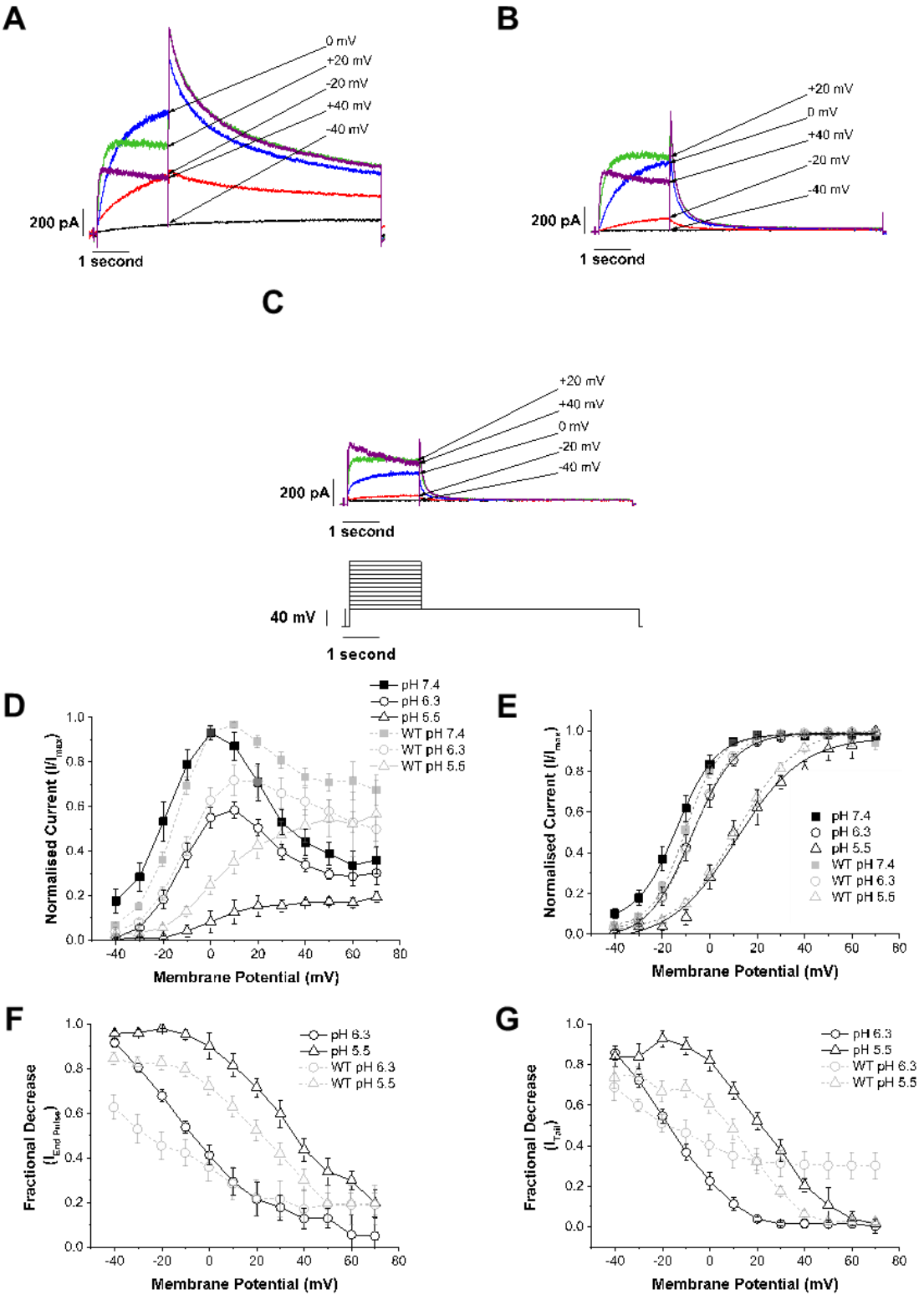
A
0 mV
+20 mV
-20 mV
+40 mV
-40 mV
200 pA
1 second
B
+20 mV
0 mV
+40 mV
-20 mV
-40 mV
200 pA
1 second
C
+20 mV
+40 mV
0 mV
-20 mV
-40 mV
200 pA
1 second
40 mV
1 second
D
pH 7.4
pH 6.3
pH 5.5
WT pH 7.4
WT pH 6.3
WT pH 5.5
Normalised Current (I/I_max)
Membrane Potential (mV)
E
pH 7.4
pH 6.3
pH 5.5
WT pH 7.4
WT pH 6.3
WT pH 5.5
Normalised Current (I/I_max)
Membrane Potential (mV)
F
pH 6.3
pH 5.5
WT pH 6.3
WT pH 5.5
Fractional Decrease (I_End Pulse)
Membrane Potential (mV)
G
pH 6.3
pH 5.5
WT pH 6.3
WT pH 5.5
Fractional Decrease (I_Tail)
Membrane Potential (mV)

Figure 6-4 Current-voltage relationship for the hERG D580N mutant.

A, B, C. Representative traces of I_{hERG} at pH_e values of 7.4 (**A**), 6.3 (**B**) and 5.5 (**C**) when the voltage protocol in lower panel of **C** was applied. Selected. Select currents were chosen for clarity.
D. I-V relations for end-pulse currents at pH_e 7.4 (n = 6 cells), 6.3 (n = 6 cells) and 5.5 (n = 4 cells). Data were normalised to the maximal I_{hERG} current in control and were then plotted against membrane potentials.
E. Steady-state activation plots for I_{hERG} derived from hERG I_{Tail} measurements on repolarisation to -40 mV. The data were normalised to the maximal I_{Tail} in each pH_e and plotted against corresponding test pulse membrane potentials. The relations were fitted with a Boltzmann equation to give $V_{0.5}$ of −13.4±2.3 mV (k = 7.5±0.4 mV) at pH 7.4 (n = 6 cells) a $V_{0.5}$ of −7.4±2.3 mV (k = 8.7±0.6 mV) at pH 6.3 (n = 6 cells) and a $V_{0.5}$ of 11.3±2.1 mV (k = 13.9±2.1 mV) for pH 5.5 (n = 4 cells).
F. Plot of mean (±SEM) fractional decrease of I_{hERG} against test voltages for end-pulse current at pH_e 6.3 (n = 6 cells) and pH_e 5.5 (n = 4 cells).
G. Plot of mean (± SEM) fractional decrease of I_{hERG} against test voltages for tail current at pH_e 6.3 (n = 6 cells) and pH_e 5.5 (n = 4 cells).
WT data (grey) is shown in D-G for comparison.

6.3.4.2 The hERG1a mutant H587N and extracellular acidosis

The hERG H587N mutant produced a channel with WT hERG1a features when in pH_e 7.4 as seen in Figure 6-5A with attenuation of I_{hERG} amplitude under acidic conditions (Figure 6-5B and C). The current-voltage relationship of hERG H587N end-pulse current was plotted in D. Control (pH_e 7.4) conditions showed the typical 'bell-shaped' I-V relationship seen in WT (Figure 3-2D) with the peak end pulse current at +10 mV (n = 6 cells) and a negative slope at more positive potentials. Decreasing the pH_e to 6.3 caused a reduction in $I_{End\ Pulse}$ amplitude, with the gradient of the negative region less pronounced compared with control after the maximum value at +10-20 mV (n = 6 cells). A reduction to pH_e 5.5 caused a further reduction in the amplitude of $I_{End\ Pulse}$: an increase in $I_{End\ Pulse}$ was observed from -40 to +20 mV, where a plateau was reached from +20 to +50 mV, before a small increase at the most positive potentials.

The hERG H587N tail current upon repolarisation to -40 mV was also analysed to determine the voltage-dependence of activation. The I_{Tail} was measured and normalised to the maximal I_{Tail} observed in each pH_e condition and plotted against membrane potential. The voltage-dependence of $I_{hERG\ H587N}$ activation was determined by fitting the I-V

relationship of I_{Tail} with a Boltzmann function (Equation 1) to give $V_{0.5}$ values. The $V_{0.5}$ value in pH_e 7.4 was -10.78±1.78 mV (k = 8.92±0.67 mV, n = 6 cells), -3.37±3.13 mV (k = 10.89±1.69 mV, n = 6 cells) for pH_e 6.3 and 19.31±3.83 mV (k= 11.55±0.41 mV; n = 4 cells) for pH_e 5.5. The positive shift of the half-activation in acidic condition was significantly different from control for pH_e 6.3 (P = 0.0104; paired *t*-test) and pH_e 5.5 (P = 0.0009; paired *t*-test). Maximal conductance (G_{Max}) was derived from the I_{Tail} measurements. Values for G_{Max} were 1.16 nS/pF in pH_e 7.4 (n = 6 cells), 0.75 nS/pF in pH_e 6.3 (n = 6 cellls) and 0.48 nS/pF in pH_e 5.5 (n = 4 cells), resulting in a significant decrease in conductance in acidic conditions (P = 0.0441 for pH_e 6.3; paired *t*-test and P = 0.0222 for pH_e 5.5; paired *t*-test).

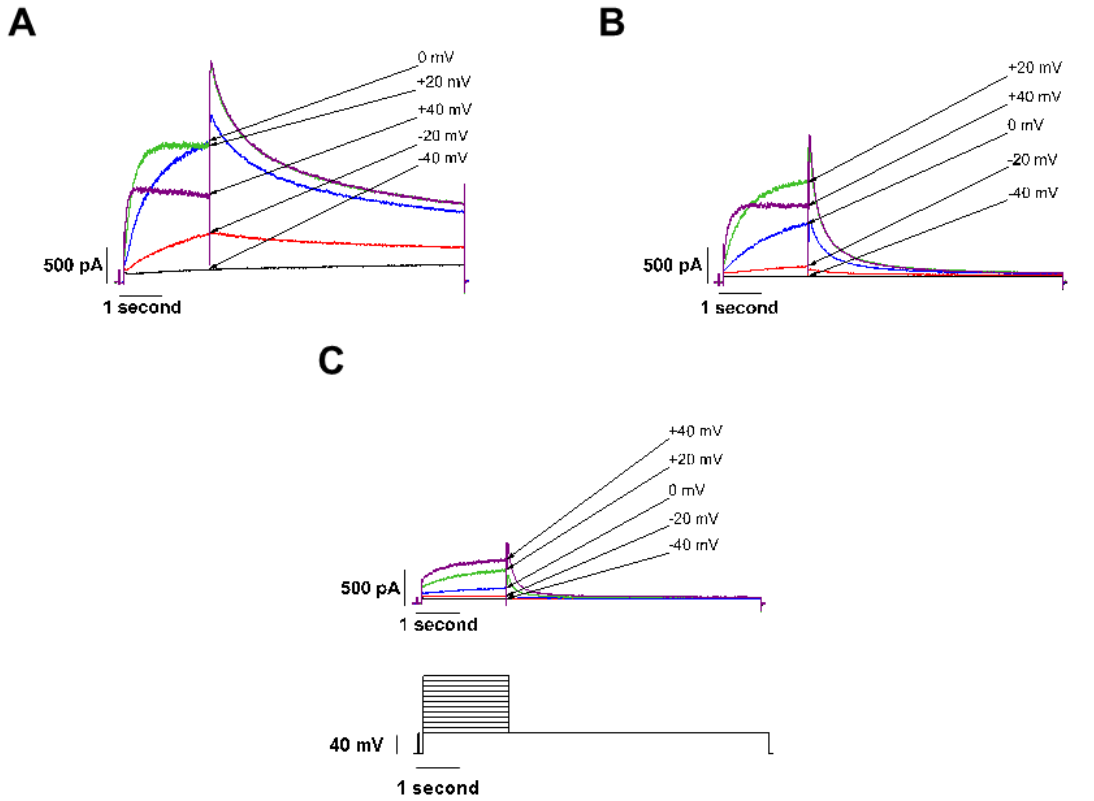
A
0 mV
+20 mV
+40 mV
-20 mV
-40 mV
500 pA
1 second
B
+20 mV
+40 mV
0 mV
-20 mV
-40 mV
500 pA
1 second
C
+40 mV
+20 mV
0 mV
-20 mV
-40 mV
500 pA
1 second
40 mV
1 second
D
pH 7.4
pH 6.3
pH 5.5
WT pH 7.4
WT pH 6.3
WT pH 5.5
Normalised Current (I/I_max)
Membrane Potential (mV)
E
pH 7.4
pH 6.3
pH 5.5
WT pH 7.4
WT pH 6.3
WT pH 5.5
Normalised Current (I/I_max)
Membrane Potential (mV)
F
pH 6.3
pH 5.5
WT pH 6.3
WT pH 5.5
Fractional Decrease (I_End Pulse)
Membrane Potential (mV)
G
pH 6.3
pH 5.5
WT pH 6.3
WT pH 5.5
Fractional Decrease (I_Tail)
Membrane Potential (mV)

Figure 6-5 The effect of external protons on the hERG H587N mutant.

A, B, C. Representative current traces of hERG H587N in control (**A**), pH_e 6.3 (**B**) and pH_e 5.5 (**C**) when the protocol shown in **C** (lower panel) was applied. Select potentials are shown for clarity.
D. I-V relationship of hERG H587N $I_{End\ Pulse}$. Data from each potential tested were normalised to maximal $I_{End\ Pulse}$ observed in pH_e 7.4 and plotted against membrane potential.
E. hERG H587N I_{Tail} I-V relationship: I_{Tail} were normalised to maximal I_{Tail} in each pH condition and plotted against membrane potential. The relationship was fitted with a Boltzmann function to determine the half-maximal activation voltage ($V_{0.5}$) value of $I_{hERG\ H587N}$. At pH_e 7.4 (n = 6 cells), the $V_{0.5}$ was -10.8±1.8 mV (k = 8.9±0.7 mV), -3.4±3.1 mV (k = 10.9±1.7 mV) for pH_e 6.3 (n = 6 cells) and 19.3±3.8 mV (k= 11.6±0.4 mV) for pH_e 5.5 (n = 4 cells).
F. Plot of mean (±SEM) fractional decrease of I_{hERG} against test voltages for end-pulse current at pH_e 6.3 (n = 6 cells) and pH_e 5.5 (n = 4 cells).
G. Plot of mean (± SEM) fractional decrease of I_{hERG} against test voltages for tail current at pH_e 6.3 (n = 6 cells) and pH_e 5.5 (n = 4 cells).
WT data (grey) is shown in D-G for comparison.

6.3.4.3 Extracellular acidosis and the hERG N588K mutant

The N588K mutation in hERG was identified in clinical cases of hereditary short-QT syndrome (Brugada et al. 2004; Hong, Bjerregaard, et al. 2005), showing a lack of inward rectification in the physiological range of potentials (Brugada et al. 2004; Cordeiro et al. 2005; McPate et al. 2005). Figure 6-6A shows representative $I_{hERG\ N588K}$ in control conditions when the protocol shown in Figure 6-6C (lower panel) was utilised. Current-voltage relationships of end-pulse currents were constructed by normalising $I_{End\ Pulse}$ to maximal $I_{End\ Pulse}$ seen in control and plotted against membrane potential (Figure 6-6D). Upon depolarisation, an increase in $I_{End\ Pulse}$ amplitude was observed in pH_e 7.4 up until approximately +50 mV before a slight decline at the more positive potentials (n = 7 cells). Upon acidification to pH_e 6.3, the I-V relation of $I_{End\ Pulse}$ showed a similar pattern to that in control with a reduction in $I_{End\ Pulse}$ amplitude across all potentials tested (n = 7 cells). In pH_e 5.5, the I-V relation showed lack of a region of negative slope for end-pulse $I_{hERG\ N588K}$, with a slight increase in $I_{End\ Pulse}$ observed as the test potential becomes more depolarised (n = 4 cells).

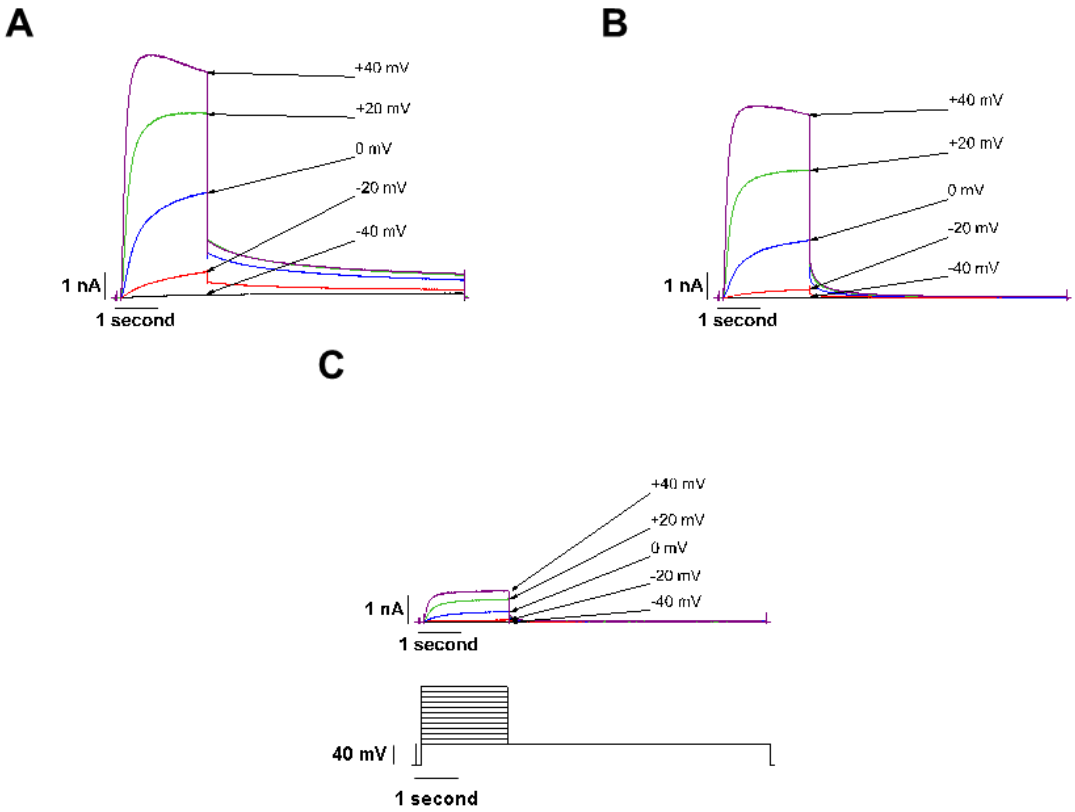
A
+40 mV
+20 mV
0 mV
-20 mV
-40 mV
1 nA
1 second
B
+40 mV
+20 mV
0 mV
-20 mV
-40 mV
1 nA
1 second
C
+40 mV
+20 mV
0 mV
-20 mV
-40 mV
1 nA
1 second
40 mV
1 second
D
pH 7.4
pH 6.3
pH 5.5
WT pH 7.4
WT pH 6.3
WT pH 5.5
Normalised Current (I/I_max)
Membrane Potential (mV)
E
pH 7.4
pH 6.3
pH 5.5
WT pH 7.4
WT pH 6.3
WT pH 5.5
Normalised Current (I/I_max)
Membrane Potential (mV)
F
pH 6.3
pH 5.5
WT pH 6.3
WT pH 5.5
Fractional Decrease
(I_End Pulse)
Membrane Potential (mV)
G
pH 6.3
pH 5.5
WT pH 6.3
WT pH 5.5
Fractional Decrease
(I_Tail)
Membrane Potential (mV)

Figure 6-6 The effects of extracellular acidification on the hERG N588K mutant.

A, B, C. Representative families of I_{hERG} at pH_e values of 7.4 (**A**), 6.3 (**B**) and 5.5 (**C**) when the voltage protocol in lower panel of **C** was applied. Select currents were chosen for clarity. **D.** I-V relations for end-pulse currents at pH_e 7.4 (n = 7 cells), 6.3 (n = 7 cells) and 5.5 (n = 4 cells). Data were normalised to the maximal I_{hERG} current in control and were then plotted against membrane potentials.

E. Steady-state activation plots for I_{hERG} derived from hERG I_{Tail} measurements on repolarisation to -40 mV. The data were normalised to the maximal I_{Tail} in each pH_e and plotted against corresponding test pulse membrane potentials. The relations were fitted with a Boltzmann equation to give $V_{0.5}$ of -17.6±2.5 mV (k = 7.2±2.5 mV) at pH 7.4 (n = 7 cells) a $V_{0.5}$ of -9.0±2.3 mV (k = 8.8±0.7 mV) at pH 6.3 (n = 7 cells) and a $V_{0.5}$ of -2.0±3.4 mV (k = 15.8±3.6 mV) for pH 5.5 (n = 4 cells).

F. Plot of mean (±SEM) fractional decrease of I_{hERG} against test voltages for end-pulse current at pH_e 6.3 (n = 7 cells) and pH_e 5.5 (n = 4 cells).

G. Plot of mean (± SEM) fractional decrease of I_{hERG} against test voltages for tail current at pH_e 6.3 (n = 7 cells) and pH_e 5.5 (n = 4 cells).

WT data (grey) is shown in D-G for comparison.

The hERG N588K tail current upon repolarisation to -40 mV was analysed to determine the voltage-dependence of activation. The I_{Tail} was measured and normalised to the maximal I_{Tail} observed in each pH_e condition and plotted against membrane potential. The voltage-dependence of $I_{hERG\ N588K}$ activation was determined by fitting the I-V relationship of I_{Tail} with a Boltzmann function (Equation 1) to give $V_{0.5}$ values. The $V_{0.5}$ value in pH_e 7.4 was -17.59±2.52 mV (k = 7.19±0.19 mV, n = 7 cells), -9.03±2.33 mV (k = 8.77±0.66 mV, n = 7 cells) for pH_e 6.3 and -1.96±3.42 mV (k= 15.83±3.63 mV, n = 4 cells) for pH_e 5.5. The positive shift of the half-activation in acidic condition was significantly different to control with pH_e 6.3 (P = 0.0018; paired *t*-test) and pH_e 5.5 (P = 0.0003; paired *t*-test). Maximal conductance (G_{Max}) was derived from the I_{Tail} measurements. Values for G_{Max} were 0.82 nS/pF in pH_e 7.4 (n = 7 cells), 0.50 nS/pF in pH_e 6.3 (n = 7 cells) and 0.12 nS/pF in pH_e 5.5 (n = 4 cells), resulting in a significant decrease in conductance in acidic conditions (P = 0.0097 for pH_e 6.3; paired *t*-test and P = 0.0036 for pH_e 5.5; paired *t*-test).

6.3.4.4 The hERG D609N mutant and extracellular acidosis

Figure 6-7A-C shows representative $I_{hERG\ D609N}$ traces recorded at pH_e 7.4 (A), 6.3 (B) and 5.5 (C) respectively when the voltage protocol shown in Figure 6-7C (lower panel) was

applied. To construct I-V relationships, $I_{End\ Pulse}$ was normalised to the maximal $I_{End\ Pulse}$ in pH_e 7.4 and plotted against membrane potential. As seen in Figure 6-7D for control (pH_e 7.4) conditions, the $I_{End\ Pulse}$ increased as the test pulse became more depolarised, reaching a maximum at approximately 0 mV (n = 6 cells). As the depolarising command became more positive, the amplitude of $I_{End\ Pulse}$ decreased, creating a negative slope in the I-V relation. At pH_e 6.3, a similar relationship was seen, with $I_{End\ Pulse}$ increasing with depolarisation up to +20 mV (n = 6 cells) before declining at more positive potentials. Acidification to pH_e 5.5 appeared to remove the ability for $I_{hERG\ D609N}$ to inwardly rectify with an increasing $I_{End\ Pulse}$ across the whole range of depolarisation potentials tested (n = 4 cells).

The voltage-dependence of I_{hERG} activation was determined by plotting normalised I-V relations for hERG I_{Tail}. To quantify the voltage-dependence of I_{hERG} activation, the relationship was fitted with a Boltzmann function (Equation 1) to give a half-maximal activation voltage ($V_{0.5}$) value of -11.69±2.42 mV (k = 7.79±0.34 mV, n = 6 cells) in pH_e 7.4, -1.24±4.39 mV (k = 9.06±0.58 mV, n = 6 cells) for pH_e 6.3 and 27.99±0.64 mV (k= 12.77±0.82 mV, n = 4 cells) for pH_e 5.5. The positive shift of the half-activation in acidic condition was significantly different to control for pH_e 6.3 (P = 0.0152; paired *t*-test) and pH_e 5.5 (P < 0.0001; paired *t*-test). Maximal conductance (G_{Max}) was derived from the I_{Tail} measurements. Values for G_{Max} were 1.03 nS/pF in pH_e 7.4 (n = 6 cells), 0.57 nS/pF in pH_e 6.3 (n = 6 cells) and 0.21 nS/pF in pH_e 5.5 (n = 4 cells), resulting in a significant decrease in conductance in acidic conditions (P = 0.0023 for pH_e 6.3; paired *t*-test and P = 0.0034 for pH_e 5.5; paired *t*-test).

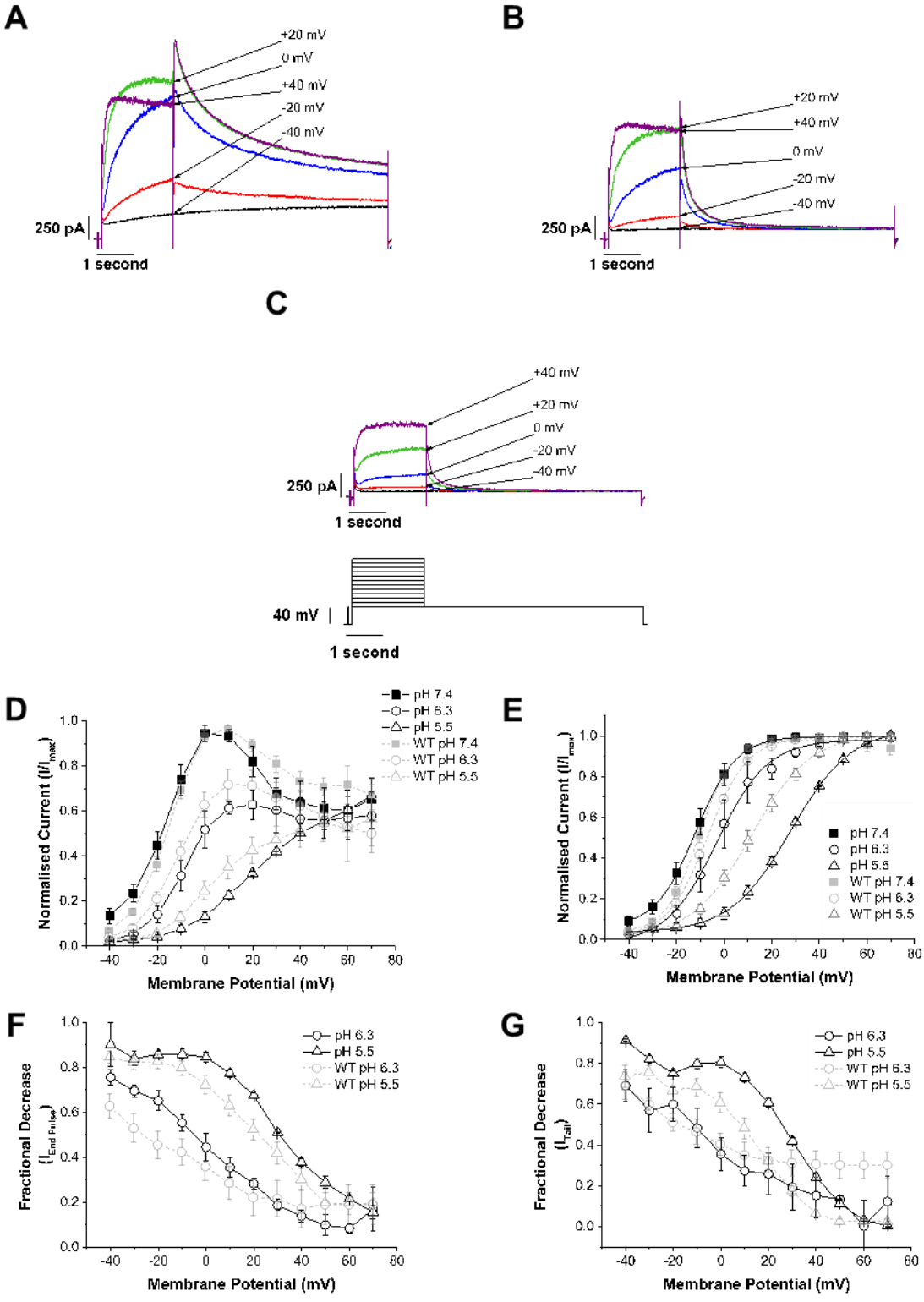
A
+20 mV
0 mV
+40 mV
-20 mV
-40 mV
250 pA
1 second
B
+20 mV
+40 mV
0 mV
-20 mV
-40 mV
250 pA
1 second
C
+40 mV
+20 mV
0 mV
-20 mV
-40 mV
250 pA
1 second
40 mV
1 second
D
pH 7.4
pH 6.3
pH 5.5
WT pH 7.4
WT pH 6.3
WT pH 5.5
Normalised Current (I/I_max)
Membrane Potential (mV)
E
pH 7.4
pH 6.3
pH 5.5
WT pH 7.4
WT pH 6.3
WT pH 5.5
Normalised Current (I/I_max)
Membrane Potential (mV)
F
pH 6.3
pH 5.5
WT pH 6.3
WT pH 5.5
Fractional Decrease
(I_End Pulse)
Membrane Potential (mV)
G
pH 6.3
pH 5.5
WT pH 6.3
WT pH 5.5
Fractional Decrease
(I_tail)
Membrane Potential (mV)

Figure 6-7 The effect of extracellular acidosis on the hERG D609N mutant.

A, B, C. Representative traces of $I_{hERG\ D609N}$ at pH_e values of 7.4 (**A**), 6.3 (**B**) and 5.5 (**C**) when the voltage protocol in lower panel of **C** was applied. Select currents were chosen for clarity. **D.** I-V relations for end-pulse currents at pH_e 7.4 (n = 6 cells), 6.3 (n = 6 cells) and 5.5 (n = 4 cells). Data were normalised to the maximal I_{hERG} current in control and were then plotted against membrane potentials.

E. Steady-state activation plots for I_{hERG} derived from hERG I_{Tail} measurements on repolarisation to -40 mV. The data were normalised to the maximal I_{Tail} in each pH_e and plotted against corresponding test pulse membrane potentials. The relations were fitted with a Boltzmann equation to give $V_{0.5}$ of -11.7±2.4 mV (k = 7.8±0.3 mV) in pH_e 7.4, -1.2±4.4 mV (k = 9.1±0.6 mV) for pH_e 6.3 and 28.0±0.6 mV (k= 12.8±0.8 mV) for pH_e 5.5.

F. Plot of mean (±SEM) fractional decrease of $I_{hERG\ D609N}$ against test voltages for end-pulse current at pH_e 6.3 (n = 6 cells) and pH_e 5.5 (n = 4 cells).

G. Plot of mean (± SEM) fractional decrease of $I_{hERG\ D609N}$ against test voltages for tail current at pH_e 6.3 (n = 6 cells) and pH_e 5.5 (n = 4 cells).

WT data (grey) is shown in D-G for comparison.

6.3.4.5 Extracellular protons and the effects on the hERG E637Q mutant

The E637Q hERG mutant created a channel that did not express macroscopic current. Like the H562N channel (see Section 6.3.3.1), co-expression of hERG E637Q with WT hERG1a cDNA at a 1:1 ratio was required to characterise the effects of extracellular protons on the E637Q/WT heteromer. Figure 6-8A shows the E637Q mutant in control pH_e 7.4, showing WT like characteristics, upon depolarisation to various voltages evokes an outward $I_{hERG\ E637Q/WT}$, whilst repolarisation to -40 mV. Like the WT hERG1a current, upon acidification, E637Q causes a reduction in both depolarising and repolarising currents with a faster decline in I_{Tail} is observed (Figure 6-8B). Unlike WT hERG1a, the end-pulse I-V of the mutant E637Q showed a lack inward rectification over the potential range tested (Figure 6-8C). Acidification to pH_e 6.3 showed a similar I-V relationship to that seen in control (pH_e 7.4) conditions but with a reduction in $I_{End\ Pulse}$ amplitude across the potentials.

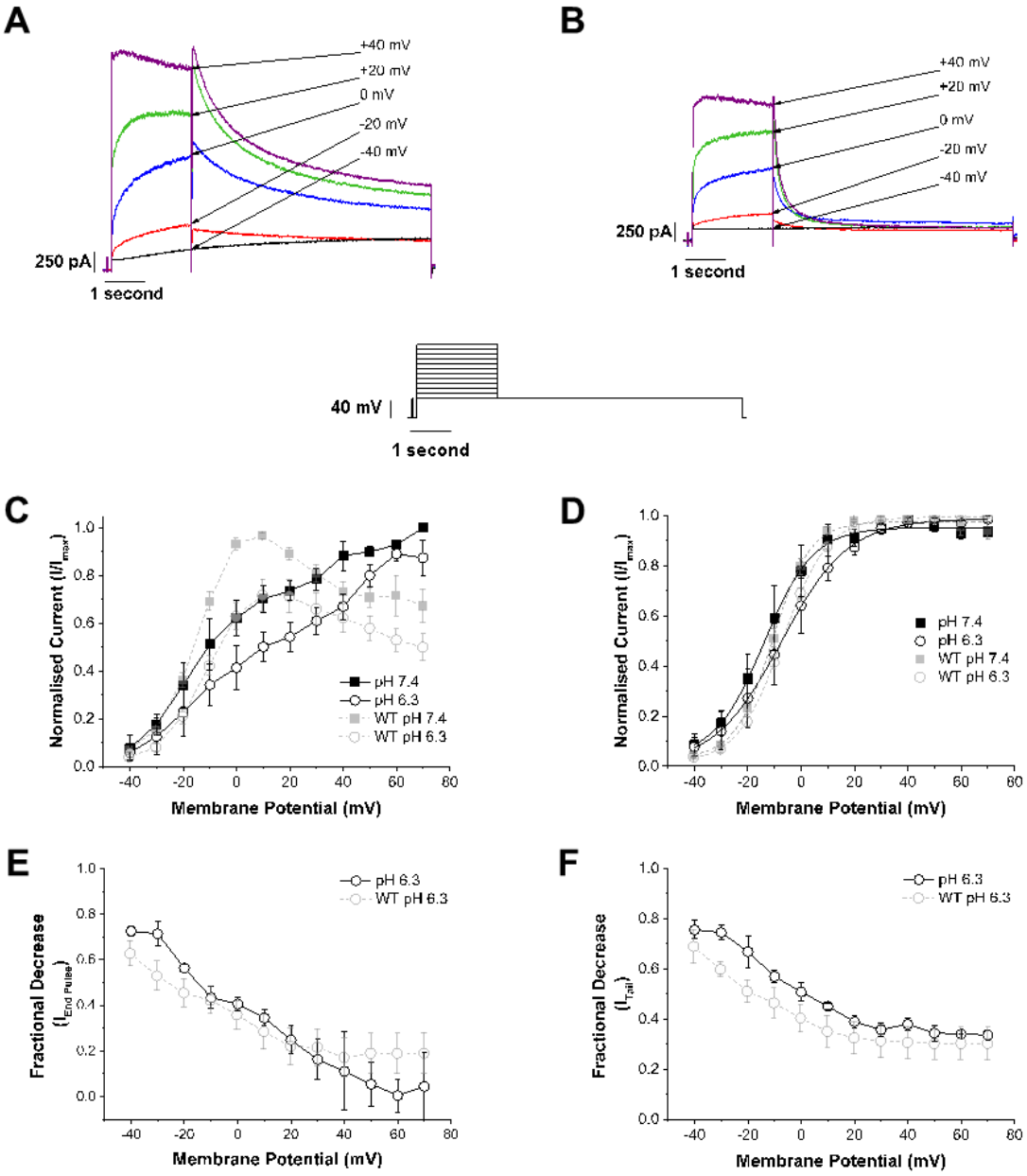
A
+40 mV
+20 mV
0 mV
-20 mV
-40 mV
250 pA
1 second
B
+40 mV
+20 mV
0 mV
-20 mV
-40 mV
250 pA
1 second
40 mV
1 second
C
Normalised Current (I/I$_{max}$)
Membrane Potential (mV)
pH 7.4
pH 6.3
WT pH 7.4
WT pH 6.3
D
Normalised Current (I/I$_{max}$)
Membrane Potential (mV)
pH 7.4
pH 6.3
WT pH 7.4
WT pH 6.3
E
Fractional Decrease (I$_{End Pulse}$)
Membrane Potential (mV)
pH 6.3
WT pH 6.3
F
Fractional Decrease (I$_{Tail}$)
Membrane Potential (mV)
pH 6.3
WT pH 6.3

Figure 6-8 Characterisation of the hERG E637Q mutant and the effects of external protons.

A, B. Representative current traces of $I_{hERG\ E637Q/WT}$ in control pH_e 7.4 (**A**) and pH_e 6.3 (**B**) when the protocol shown below **A** and **B** was applied. Selected currents are shown for clarity.
C. I-V relationship of $I_{End\ Pulse}$ at pH_e 7.4 (n = 4 cells) and 6.3 (n = 4 cells). Data were normalised to the maximal current in control and then plotted against test potential.
D. Steady-state activation plots for I_{hERG} derived from hERG I_{Tail} measurements. The data were normalised to the maximal I_{Tail} in each pH_e and plotted against membrane potential. The relations were fitted with a Boltzmann equation to give $V_{0.5}$ of -12.8±5.1 mV (k = 7.5±0.9 mV) in pH_e 7.4 and-7.5±4.9 mV (k = 12.1±2.6 mV) for pH_e 6.3.
E, F. Plot of mean (±SEM) fractional decrease of $I_{hERG\ E637Q/WT}$ against test voltages for end-pulse current (**E**) and tail current (**F**) at pH_e 6.3 (n = 4 cells).
WT data (grey) is shown in C-F for comparison.

The hERG E637Q/WT tail current upon repolarisation to -40 mV was analysed to determine the voltage-dependence of activation. The I_{Tail} was measured and normalised to the maximal I_{Tail} observed in each pH_e condition and plotted against membrane potential. The voltage-dependence of $I_{hERG\ E637Q/WT}$ activation was determined by fitting the I-V relationship with a Boltzmann function (Equation 1) to give $V_{0.5}$ values; pH_e 7.4 $V_{0.5}$ was -12.79±5.09 mV (k = 7.46±0.86 mV, n = 4 cells) and -7.47±4.93 mV (k = 12.12±2.64 mV, n = 4 cells) for pH_e 6.3. The positive shift of the half-activation in acidic condition was significantly different to control with pH_e 6.3 (P = 0.9494; paired *t*-test). Maximal conductance (G_{Max}) was derived from the I_{Tail} measurements. Values for G_{Max} were 0.65 nS/pF in pH_e 7.4 and 0.40 nS/pF in pH_e 6.3, resulting in a significant decrease in conductance in acidic conditions (P = 0.0023 for pH_e 6.3; paired *t*-test).

6.3.4.6 Extracellular acidosis and the hERG H674N mutant

The H674N mutation produced a channel with currents that shared similar characteristics to those of WT hERG. Initial testing of this mutant showed that a large outward current was seen upon depolarisation to -40 mV. As a result, the voltage protocol was modified so that the range of depolarising potentials started at -70 mV up to +70 mV (as seen in Figure 6-9 panel below A and B).

In control conditions, $I_{End\ Pulse}$ amplitude increased as potentials became more depolarised, peaking at -20 mV (n = 6 cells) before decreasing at potentials more positive to this.

During acidification to pH_e 6.3 (n = 6 cells), $I_{End\ Pulse}$ was reduced across all potentials tested up to +40 mV before showing similar values seen in pH_e 7.4 at potentials between +50 and +70 mV. The acidification of the hERG H674N showed the same 'bell-shaped' I-V relation seen in control (pH_e 7.4) conditions but with the peak of the relation peaking at -10 mV.

Figure 6-9 The hERG H674N mutant and the effects of extracellular acidosis.

A, B. Representative current traces of the hERG H674N mutant in pH_e 7.4 (**A**) and pH_e 6.3 (**B**) when the protocol shown under A and B was applied. Selected traces are shown for clarity. **C.** I-V relationship of $I_{End\ Pulse}$ at pH_e 7.4 (n = 6 cells) and 6.3 (n = 6 cells). Data were normalised to the maximal current in control and then plotted against membrane potentials.

D. Steady-state activation plots for I_{hERG} derived from hERG I_{Tail} measurements. The data were normalised to the maximal I_{Tail} in each pH_e and plotted against membrane potential. The relations were fitted with a Boltzmann equation to give $V_{0.5}$ of -44.9±1.9 mV (k = 9.3±0.8 mV) in pH_e 7.4 and-30.4±2.0 mV (k = 11.6±1.8 mV) for pH_e 6.3.

E, F. Plot of mean (±SEM) fractional decrease of $I_{hERG\ E637Q/WT}$ against test voltages for end-pulse current (**E**) and tail current (**F**) at pH_e 6.3 (n = 6 cells).

WT data (grey) is shown in C-F for comparison.

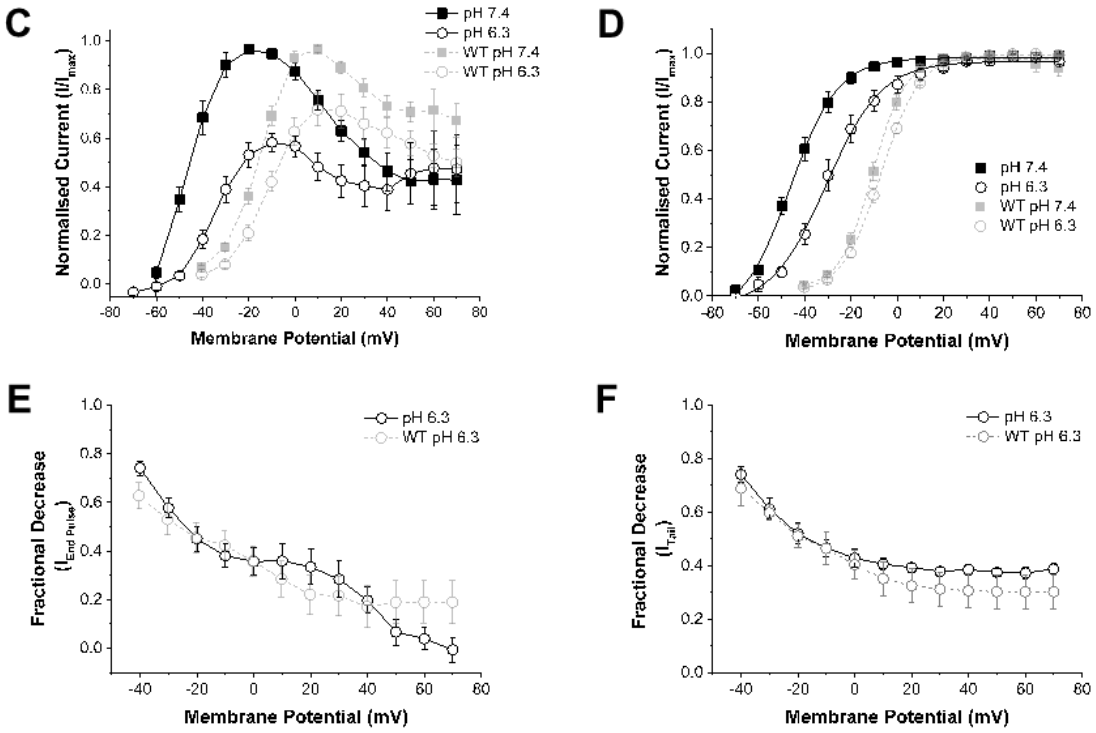

The voltage-dependence of hERG H674N activation was also determined, by plotting an I-V relation of I_{Tail}. Values obtained in each pH_e were normalised to maximum value for each set of data, plotted as a relationship of membrane potential against normalised current and fit with a Boltzmann function (Equation 1). The fit gave rise to $V_{0.5}$ values of -44.89±1.94 mV (k = 9.29±0.80 mV) at pH 7.4 (n = 6 cells) and -30.44±2.04 mV (k = 11.64±1.83 mV) at pH 6.3 (n = 6 cells). The positive shift in $V_{0.5}$ seen in pH_e 6.3 was significantly different to that in control (P < 0.0001; paired *t*-test). Maximal conductance was calculated from I_{Tail}

measurements resulting in G_{Max} values of 1.47 nS/pF in pH_e 7.4 (n = 6 cells) and 0.67 nS/pF in pH_e 6.3 (n = 6 cells) (P = 0.0178; paired *t*-test).

6.3.5 Comparing the effects of acidosis on the hERG mutations and WT hERG1a

The mutations created were characterised with the I-V protocol under control (pH_e 7.4) and acidic conditions. To determine if these hERG mutants were modified by extracellular protons differently from WT hERG1a, comparisons were made at +20 mV in pH_e 6.3 compared with pH_e 7.4. The effects were quantified as a % decrease from control.

Figure 6-10 shows the effects of protons on WT and mutant hERG channel characteristics. The $I_{End\ Pulse}$ (Figure 6-10A) was analysed in WT hERG1a channels and a decrease of 13.5±2.6% was observed. A small insignificant decrease in effect of protons was seen in $I_{End\ Pulse}$ of the D580N mutant (12.3±3.2%; P > 0.9999, one- way ANOVA with Bonferroni post-test). The remaining mutants, except for H674N, saw no effect of protons on $I_{End\ Pulse}$. The H674N mutant exhibited a significant increase in proton block of $I_{End\ Pulse}$ compared with effects observed in WT channels (33.5±7.4%; P = 0.0076, one-way ANOVA with Bonferroni post-test).

The effects of protons on WT and mutant hERG channel I_{Tail} were also analysed upon repolarisation to -40 mV (Figure 6-10B). In WT channels, a decrease of 26.8±3.7% in I_{Tail} upon acidification to pH_e 6.3 was observed. In all the mutants created, the effects of lowering the external pH on I_{Tail} did not reduce the response to extracellular acidosis. Certain hERG mutants appeared to have a greater effect in % decrease of I_{Tail}; the H674N, D609N and the D580N mutant (P = 0.0462, P = 0.0069 and P = 0.0032 respectively; one-way ANOVA with Bonferroni post-test).

To determine the effects of protons on hERG activation, $V_{0.5}$ values obtained from characterisation of the WT (Section 3.3.2) and mutant channels (Section 6.3.3) were used and plotted as absolute values (Figure 6-10C) and as the shift observed in acidification (Figure 6-10D). The H674N channel was the only mutant to show a significantly different absolute $V_{0.5}$ value in both pH_e 7.4 and pH_e 6.3 compared with WT (P < 0.0001 for both pH conditions; one-way ANOVA with Bonferroni post-test) as well as the shift observed upon acidification (P < 0.0001; one-way ANOVA with Bonferroni post-test).

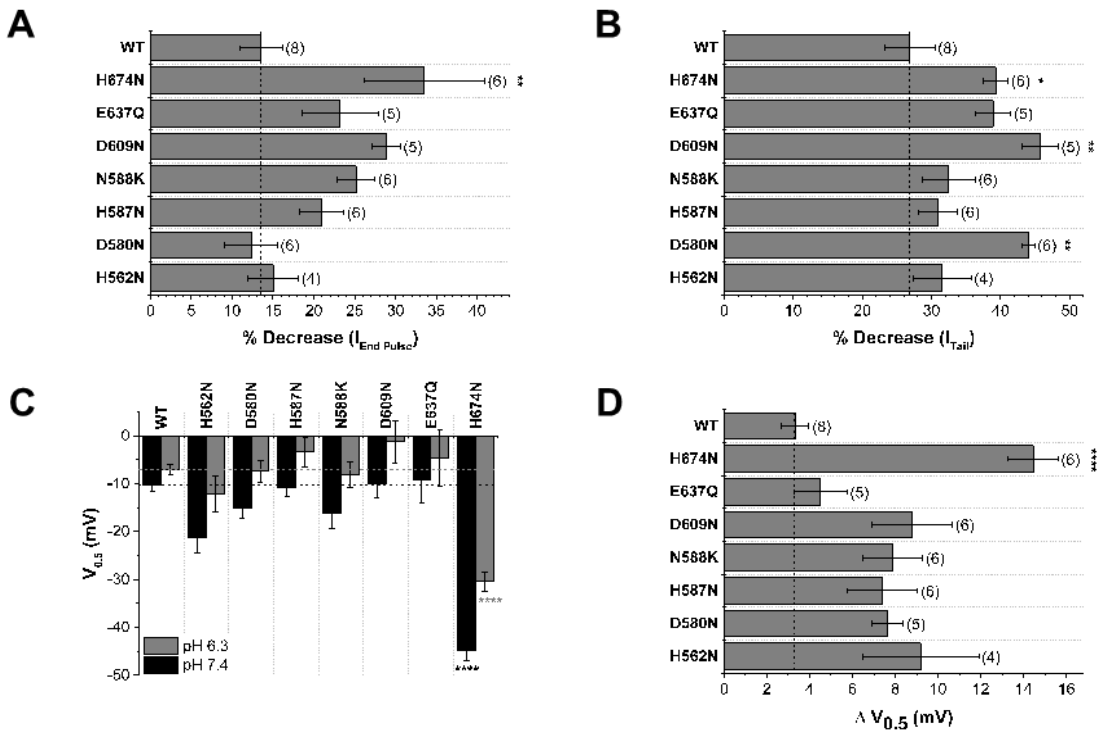

Figure 6-10 The effects of extracellular acidosis on characteristics of hERG mutants.

A. The effects of extracellular acidosis on the $I_{End\ Pulse}$ on hERG WT and mutant channels. The vertical dashed line represents the block seen in WT channels. Statistical significance was observed for in the H674N mutant compared to WT. Comparisons were made when the cell membrane was depolarised to +20 mV in pH_e 7.4 and 6.3.

B. hERG WT and mutant channels and the effects of extracellular protons on the decrease in tail current. The vertical dashed line represents the % decrease in I_{Tail} seen in WT. Tail current was elicited upon repolarisation to -40 mV after membrane depolarisation to +20 mV.

C. Mean ± SEM of raw $V_{0.5}$ values for WT and mutant channels in pH_e 7.4 (black bars) and pH_e 6.3 (grey bars). Horizontal dashed lines represent values seen in WT in control (black) and pH_e 6.3 (grey). Statistical tests were completed in each pH condition and compared to WT.

D. The shift in $V_{0.5}$ (in mV) seen when WT and mutant hERG channels are exposed to protons. Raw values observed in **C** were used to calculate the difference in $V_{0.5}$ in control and pH_e 6.3.

Numbers in brackets indicate cell numbers. '*', '**' and '****' denotes statistical significance of $P < 0.01$, $P < 0.001$ and $P < 0.0001$ respectively compared to WT values (one-way ANOVA with Bonferroni post-test).

The deactivation of the I_{Tail} was also analysed to determine the effects of extracellular acidosis by fitting the deactivating current with a bi-exponential function (Equation 2) to obtain the fast and slow time constants. Figure 6-11A and B show raw values for τ_{Fast} (A) and τ_{Slow} (B) in control (black bars) and pH_e 6.3 (grey bars). Wild-type channels displayed τ_{Fast} values of 553±36.3 ms in control (pH_e 7.4) and 217.8±18.0 ms in pH_e 6.3. It is shown that the hERG mutations created affected the deactivation kinetics. As seen in Figure 6-11A the raw values in control conditions are faster in the all mutants compared with WT hERG1a, with three mutants (H674N, H587N and D580N) showing significantly faster τ_{Fast} values. Upon acidification, τ_{Fast} raw values of the hERG mutants showed no statistical significance to the τ_{Fast} value observed in WT pH_e 6.3 except for the N588K mutant (P = 0.0179; one-way ANOVA with Bonferroni post-test). Figure 6-11B shows the raw τ_{Slow} values with WT hERG1a channels exhibiting τ_{Slow} of 3790±215 ms in pH_e 7.4 and 1276±74 ms in pH_e 6.3. For the mutant channels, the control τ_{Slow} values are all significantly faster than that of WT. In acidic conditions all mutants showed faster τ_{Slow} values compared to WT with 3 mutant channels (H674N, N588K and D580N) showing a significant acceleration (P = 0.0098, P = 0.0359 and P = 0.0106 respectively; one-way ANOVA with Bonferroni post-test.

The % decrease in τ_{Fast} and τ_{Slow} values are shown in Figure 6-11C and D respectively. A decrease in deactivation time constants signifies an acceleration in deactivation in which no significance was observed for either time constant, suggesting that the extent of acceleration in the mutants did not differ from WT.

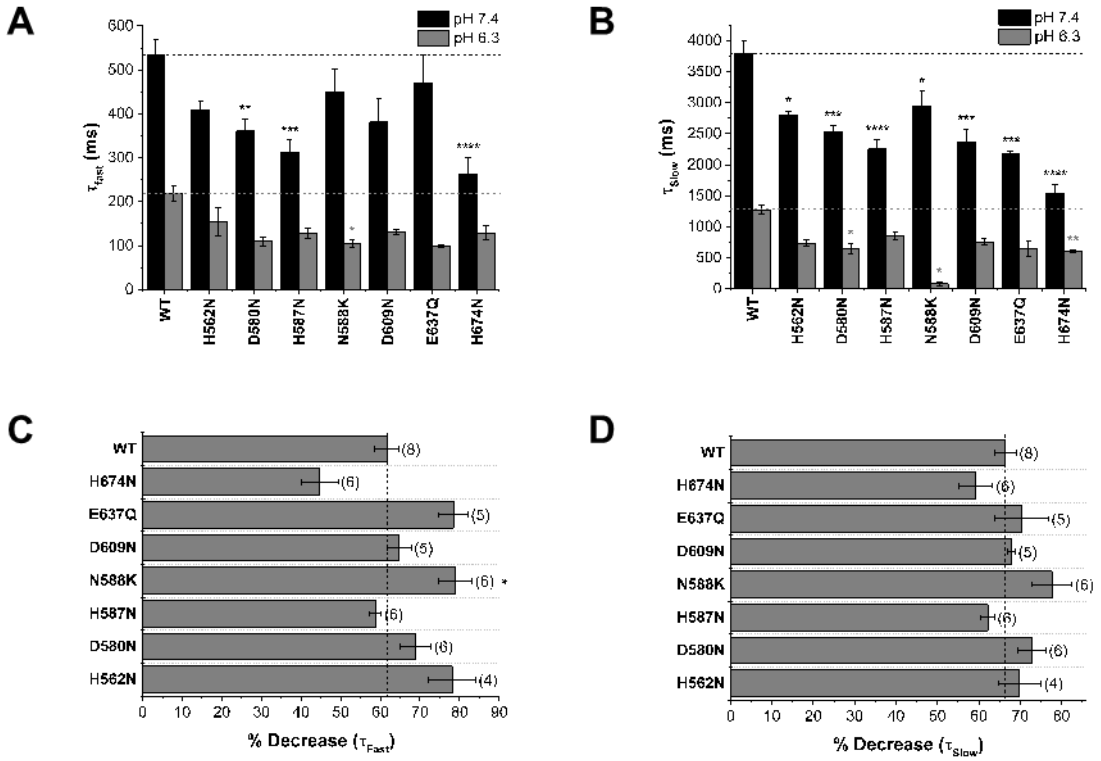

Figure 6-11 The effects of protons on hERG channel deactivation kinetics.

Tail current was elicited upon repolarisation to -40 mV after membrane depolarisation to +20 mV. Deactivating currents were fit with Equation 2 to obtain the fast (**A**) and slow (**B**) time constant.

A. The effects of extracellular acidosis on the fast time constant of deactivation in hERG WT and mutant channels. Horizontal dashed lines represent values seen in WT in control (black) and pH_e 6.3 (grey). Statistical tests were completed in each pH condition and compared to WT.

B. Mean ± SEM of raw τ_{Slow} values for WT and mutant channels in pH_e 7.4 (black bars) and pH_e 6.3 (grey bars). Horizontal dashed lines represent values seen in WT in control (black) and pH_e 6.3 (grey). Statistical tests were completed in each pH condition and compared to WT.

C. The % decrease of the τ_{Fast} when exposed to extracellular protons. The decrease was calculated using raw values that are shown in **A**. The vertical dashed line represents the decrease seen in WT channels.

D. The % decrease of the slow time constant when subjected to extracellular acidosis. The decrease was calculated using raw values that are shown in **B**. The vertical dashed line represents the decrease seen in WT channels.

Numbers in brackets indicate cell numbers. '*', '**', '***' and '****' denotes statistical significance of $P < 0.01$, $P < 0.001$, $P < 0.0005$ and $P < 0.0001$ respectively compared to WT values (one-way ANOVA with Bonferroni post-test).

6.4 Results – Part II

With the hERG mutations characterised in Section 6.3.3 still presenting attenuation in current amplitude and an acceleration in deactivation with an increase in external proton concentration, it could be presumed that those individual residues are not involved in proton sensitivity. As shown in Figure 6-2, there is a glutamic acid residue (E575) and histidine residue (H578) near one another and the role of these was then investigated as single point mutations as well a double mutant channel. The rationale for studying the double mutant was due to their proximity to one another, it can be presumed that some electrostatic interactions are present between the two residues. As a result, the pK_a values of their side chains may be altered and, together, may be responsible for pH modulation.

6.4.1 Characterising the effects of protons on the hERG E575Q and H578N mutant channels.

Characterisation of the E575Q and H578N mutants was conducted using the same voltage protocol as applied in Figure 6-3 to Figure 6-9.

6.4.1.1 Extracellular acidosis and the hERG E575Q mutant

Figure 6-12A-C shows representative current traces for the hERG E575Q mutant in control conditions (Figure 6-12A) and under acidic conditions (Figure 6-12B and C). The hERG E575Q mutant shows WT hERG characteristics.

I-V relationships were constructed by normalising $I_{End\ Pulse}$ to the maximal $I_{End\ Pulse}$ seen in control conditions and plotted against membrane potential (Figure 6-12D). With pH_e 7.4, $I_{End\ Pulse}$ amplitude increases with depolarising potentials with a peak at 0 mV. Potentials more positive to this showed a negative slope on the I-V relationship, indicating a decrease in $I_{End\ Pulse}$ amplitude. Acidification of the extracellular solution to pH 6.3 caused a reduction in $I_{End\ Pulse}$ amplitude in the potential range of -40 mV to +10 mV. Potentials more positive to this showed no reduction in $I_{End\ Pulse}$ amplitude in pH_e 6.3. The profile of the I-V relationship was similar in pH_e 6.3, with depolarisation causing an increase in $I_{End\ Pulse}$ with the peak potential at +10-20 mV before a decline in $I_{End\ Pulse}$. Further acidification to pH_e 5.5 caused further attenuation of the end pulse current over all the potentials tested. An increase is seen with depolarisation up until approximately +40 mV before a plateau in $I_{End\ Pulse}$ current amplitude is reached.

The voltage-dependence of I_{hERG} activation was determined by plotting I-V relation for hERG I_{Tail}. In control conditions (pH_e 7.4, n = 6 cells), the half-maximal voltage for activation for the E575Q mutant was −18.34±2.94 mV (k = 7.07±0.75 mV). Upon acidification, a shift in $V_{0.5}$ was observed: a $V_{0.5}$ of −12.56±3.28 mV (k = 8.39±0.53 mV) was seen at pH 6.3 (n = 6 cells) and a $V_{0.5}$ of 28.00±0.72 mV (k = 11.89±0.87 mV) was seen for pH 5.5 (n = 6 cells). The positive shift of $V_{0.5}$ in acidic condition was significantly different from control with pH_e 6.3 (P = 0.0027; paired *t*-test) and pH_e 5.5 (P = 0.0007; paired *t*-test). Maximal conductance (G_{Max}) was derived from the I_{Tail} measurements. Values for G_{Max} were 0.83 nS/pF in pH_e 7.4 (n = 6 cells), 0.58 nS/pF in pH_e 6.3 (n = 6 cells) and 0.17 nS/pF in pH_e 5.5 (n = 6 cells), resulting in a significant decrease in conductance in acidic conditions (P = 0.0266 for pH_e 6.3; paired *t*-test and P = 0.0065 for pH_e 5.5; paired *t*-test).

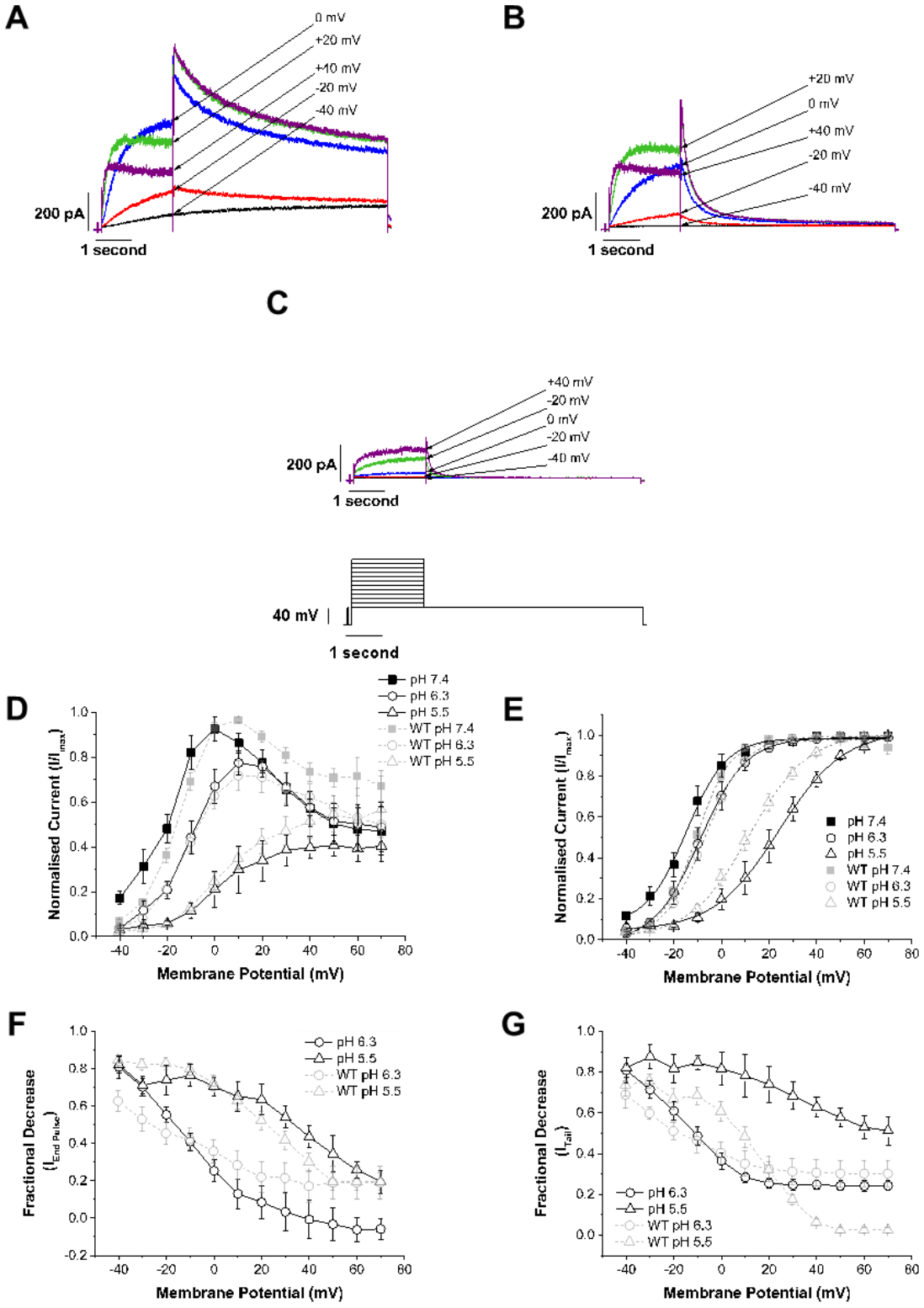
A
0 mV
+20 mV
+10 mV
-20 mV
-40 mV
200 pA
1 second
B
+20 mV
0 mV
+40 mV
-20 mV
-40 mV
200 pA
1 second
C
+40 mV
-20 mV
0 mV
-20 mV
-40 mV
200 pA
1 second
40 mV
1 second
D
pH 7.4
pH 6.3
pH 5.5
WT pH 7.4
WT pH 6.3
WT pH 5.5
Normalised Current (I/I max)
Membrane Potential (mV)
E
pH 7.4
pH 6.3
pH 5.5
WT pH 7.4
WT pH 6.3
WT pH 5.5
Normalised Current (I/I max)
Membrane Potential (mV)
F
pH 6.3
pH 5.5
WT pH 6.3
WT pH 5.5
Fractional Decrease (I End Pulse)
Membrane Potential (mV)
G
pH 6.3
pH 5.5
WT pH 6.3
WT pH 5.5
Fractional Decrease (I tail)
Membrane Potential (mV)

Figure 6-12 the effects of extracellular acidosis on the hERG E575Q mutant.

A, B, C. Representative traces of I_{hERG} at pH_e values of 7.4 (**A**), 6.3 (**B**) and 5.5 (**C**) when the voltage protocol in lower panel of **C** was applied. Selected currents are displayed for clarity. **D.** I-V relations for end-pulse currents at pH_e 7.4 (n = 6 cells), 6.3 (n = 6 cells) and 5.5 (n = 6 cells). Data were normalised to the maximal I_{hERG} current in control and were then plotted against membrane potentials.

E. Steady-state activation plots for $I_{hERG\ E575Q}$ derived from hERG E575Q I_{Tail} measurements on repolarisation to -40 mV. The data were normalised to the maximal I_{Tail} in each pH_e and plotted against corresponding test pulse membrane potentials. The relations were fitted with a Boltzmann equation to give $V_{0.5}$ of −18.3±2.9 mV (k = 7.1±0.8 mV) at pH 7.4 (n = 6 cells) a $V_{0.5}$ of −12.6±3.3 mV (k = 8.4±0.5 mV) at pH 6.3 (n = 6 cells) and a $V_{0.5}$ of 28.0±0.7 mV (k = 11.9±0.9 mV) for pH 5.5 (n = 6 cells).

F. Plot of mean (±SEM) fractional decrease of I_{hERG} against test voltages for end-pulse current at pH_e 6.3 (n = 6 cells) and pH_e 5.5 (n = 6 cells).

G. Plot of mean (± SEM) fractional decrease of I_{hERG} against test voltages for tail current at pH_e 6.3 (n = 6 cells) and pH_e 5.5 (n = 6 cells).

WT data (grey) is shown in D-G for comparison.

6.4.1.2 The effects of external protons on the H578N mutant

The hERG H578N mutant produced a channel with WT hERG1a features as seen in Figure 6-13A with attenuation of I_{hERG} amplitude under acidic conditions (Figure 6-13A B and C). The current-voltage relationship of hERG H578N end-pulse current was plotted in Figure 6-13A: $I_{End\ Pulse}$ was normalised to maximal $I_{End\ Pulse}$ observed in control conditions and plotted against membrane potential. Control conditions (pH_e 7.4) show the typical 'bell-shaped' I-V relationship seen in WT (Figure 3-2D) with the peak membrane potential at +10 mV (n = 11 cells), with a negative slope at more positive potentials. Decreasing the pH_e to 6.3 caused a reduction in $I_{End\ Pulse}$ amplitude across the potentials tested, except for +70 mV, with maximum value at +10-20 mV (n = 7 cells). A reduction to pH_e 5.5 caused a further reduction in the amplitude of $I_{End\ Pulse}$: an increase in $I_{End\ Pulse}$ was observed with depolarisation and no region of negative slope was observed (n = 6 cells).

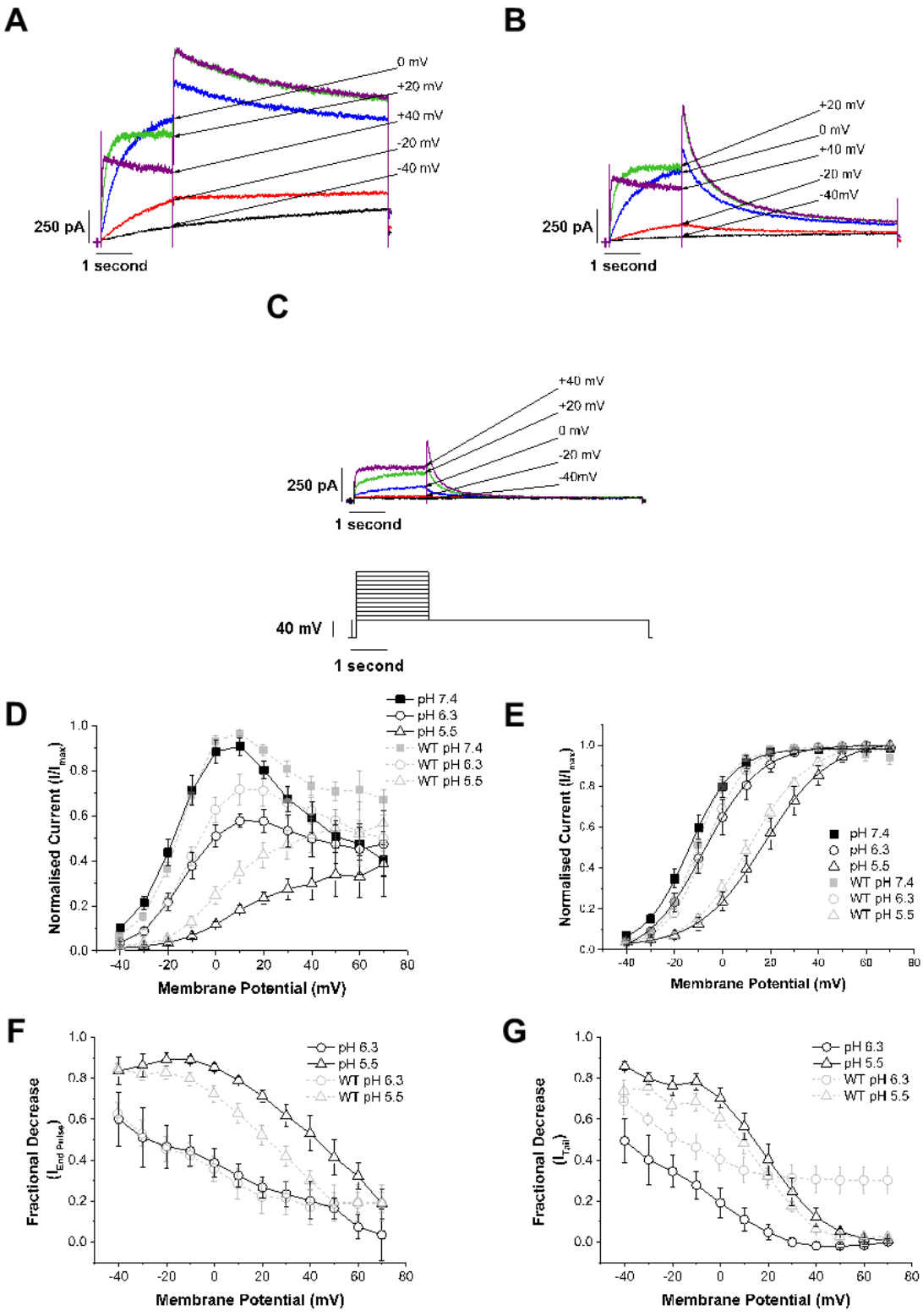
A
0 mV
+20 mV
+40 mV
-20 mV
-40 mV
250 pA
1 second
B
+20 mV
0 mV
+40 mV
-20 mV
-40mV
250 pA
1 second
C
+40 mV
+20 mV
0 mV
-20 mV
-40mV
250 pA
1 second
40 mV
1 second
D
pH 7.4
pH 6.3
pH 5.5
WT pH 7.4
WT pH 6.3
WT pH 5.5
Normalised Current (I/I$_{max}$)
Membrane Potential (mV)
E
pH 7.4
pH 6.3
pH 5.5
WT pH 7.4
WT pH 6.3
WT pH 5.5
Normalised Current (I/I$_{max}$)
Membrane Potential (mV)
F
pH 6.3
pH 5.5
WT pH 6.3
WT pH 5.5
Fractional Decrease
(I$_{End\ Pulse}$)
Membrane Potential (mV)
G
pH 6.3
pH 5.5
WT pH 6.3
WT pH 5.5
Fractional Decrease
(I$_{Tail}$)
Membrane Potential (mV)

Figure 6-13 The hERG H578N mutant and the effects of extracellular acidification.

A, B, C. Representative current traces of hERG H578N in control (**A**), pH_e 6.3 (**B**) and pH_e 5.5 (**C**) when the protocol shown in **C** (lower panel) was applied. Selected potentials are displayed for clarity.
D. I-V relationship of hERG H578N $I_{End\ Pulse}$. Data from each potential tested were normalised to maximal $I_{End\ Pulse}$ observed in pH_e 7.4 and plotted against membrane potential.
E. hERG H578N I_{Tail} I-V relationship: I_{Tail} were normalised to maximal I_{Tail} in each pH condition and plotted against membrane potential. Relationship was fit with a Boltzmann function to determine the half-maximal activation voltage ($V_{0.5}$) value of $I_{hERG\ H587N}$. At pH_e 7.4 (n =11 cells), the $V_{0.5}$ was -17.3±1.2 mV (k = 7.9±0.6 mV), -11.7±1.4 mV (k = 10.4±0.9 mV) for pH_e 6.3 (n = 7 cells) and 15.5±2.4 mV (k= 14.2±0.5 mV) for pH_e 5.5 (n = 6 cells).
F. Plot of mean (±SEM) fractional decrease of I_{hERG} against test voltages for end-pulse current at pH_e 6.3 (n = 7 cells) and pH_e 5.5 (n = 6 cells).
G. Plot of mean (± SEM) fractional decrease of I_{hERG} against test voltages for tail current at pH_e 6.3 (n = 7 cells) and pH_e 5.5 (n = 6 cells).
WT data (grey) is shown in D-G for comparison.

The hERG H578N tail current upon repolarisation to -40 mV was analysed to determine the voltage-dependence of activation. The I_{Tail} was measured and normalised to the maximal I_{Tail} observed in each pH_e condition and plotted against membrane potential. The voltage-dependence of $I_{hERG\ H578N}$ activation was determined by fitting the I-V relationship of I_{Tail} with a Boltzmann function (Equation 1) to give $V_{0.5}$ values. The $V_{0.5}$ value in pH_e 7.4 was -17.31±1.16 mV (k = 7.92±0.57 mV, n = 11 cells), -11.69±1.41 mV (k = 10.44±0.85 mV, n = 7 cells) for pH_e 6.3 and 15.53±2.36 mV (k= 14.19±0.52 mV, n = 6 cells) for pH_e 5.5. The positive shift of the half-activation in acidic condition was significantly different to control with pH_e 6.3 ($P = 0.0001$; paired *t*-test) and pH_e 5.5 ($P < 0.0001$; paired *t*-test). Maximal conductance (G_{Max}) was derived from the I_{Tail} measurements. Values for G_{Max} were 0.79 nS/pF in pH_e 7.4 (n = 11 cells), 0.56 nS/pF in pH_e 6.3 (n = 7 cells) and 0.24 nS/pF in pH_e 5.5 (n = 6 cells), resulting in a significant decrease in conductance in acidic conditions ($P = 0.0486$ for pH_e 6.3; paired *t*-test and $P = 0.0104$ for pH_e 5.5; paired *t*-test).

6.4.2 The characterisation of the hERG E575Q/H578N double mutant

6.4.2.1 The whole-cell effects of extracellular protons on the E575Q/H578N mutant

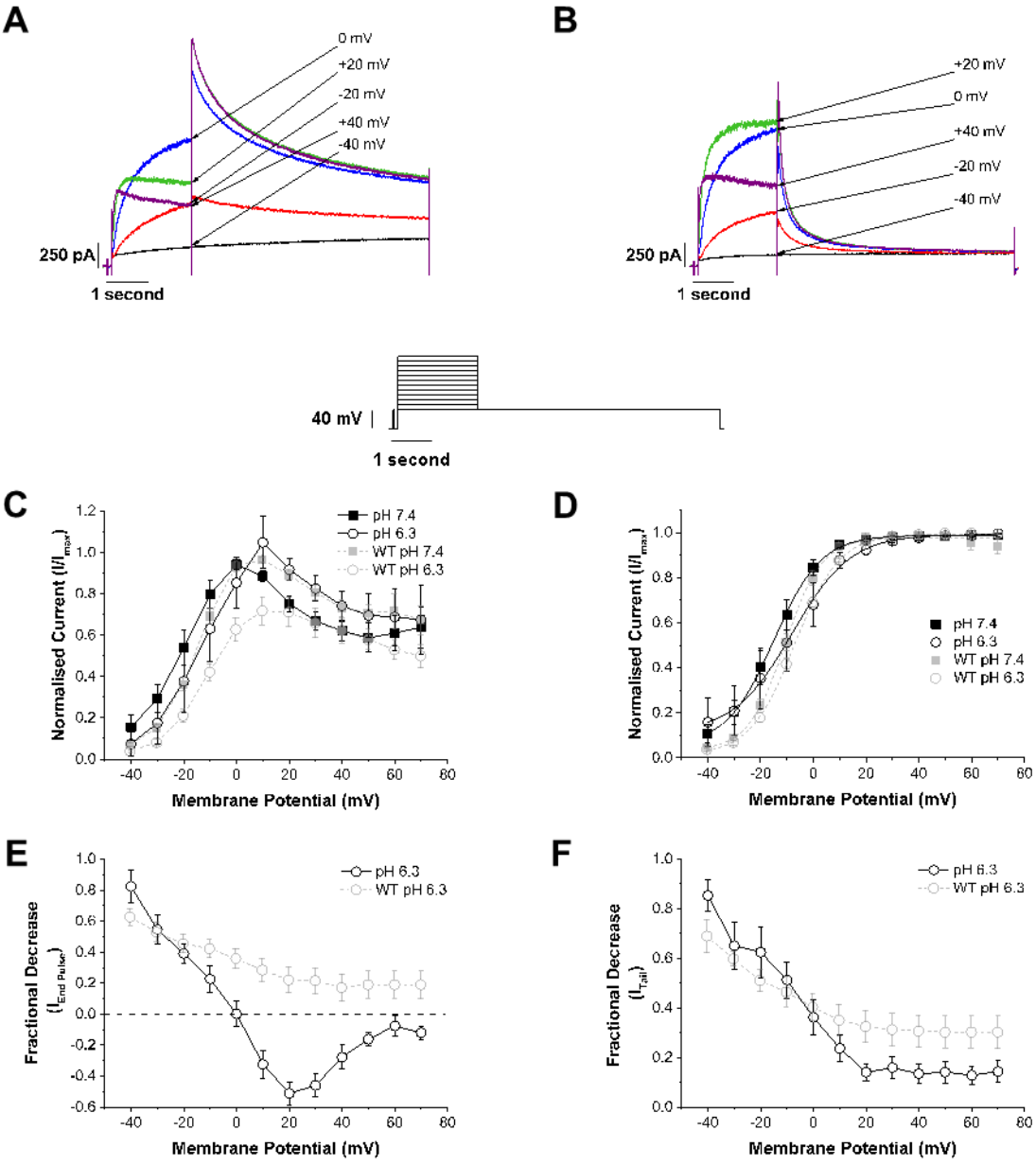

Figure 6-14 The effect of external protons on the E575Q/H578N mutant.

A, B. Representative current traces of the hERG E575Q/H578N mutant in pH_e 7.4 (**A**) and pH_e 6.3 (**B**) when the protocol shown under A and B was applied. Selected traces are shown for clarity. **C.** I-V relationship of $I_{End\ Pulse}$ at pH_e 7.4 (n = 7 cells) and 6.3 (n = 7 cells). Data were normalised to the maximal current in control and then plotted against membrane potentials.
D. Steady-state activation plots for $I_{hERG\ E575Q/H578N}$. The data were normalised to the maximal I_{Tail} in each pH_e and plotted against membrane potential. The relations were fit with a Boltzmann equation to give $V_{0.5}$ of -15.6±2.9 mV (k = 8.2±0.8 mV) in pH_e 7.4 and-12.0±5.5 mV (k = 12.0±1.9 mV) for pH_e 6.3.
E, F. Plot of mean (±SEM) fractional decrease of $I_{hERG\ E575Q/H578N}$ against test voltages for end-pulse current (**E**) and tail current (**F**) at pH_e 6.3 (n = 7 cells). Horizontal dashed line in E represents the point of no block in end-pulse current.
WT data (grey) is shown in C-F for comparison.

Figure 6-14A and B show representative current traces of hERG E575Q/H578N mutant at pH_e of 7.4 (A) and 6.3 (B) respectively. The hERG E575Q/H578N $I_{End\ Pulse}$ amplitudes were measured and normalised to maximal $I_{End\ Pulse}$ found in control (pH_e 7.4). I-V relations were constructed by plotting normalised values against the respective voltage as seen in Figure 6-14C. In control conditions, $I_{End\ Pulse}$ amplitude increased as potentials became more depolarised, peaking at 0 mV (n = 7 cells) before decreasing at potentials more positive to this. During acidification to pH_e 6.3 (n = 7 cells), a 'bell-shaped' I-V relation peaking at +10 mV was seen but with the amplitude of $I_{End\ Pulse}$ in the potential range of +10-70 mV showing no reduction in amplitude compared to pH_e 7.4.

The voltage-dependence of E575Q/H578N activation was also determined by plotting I-V relations for I_{Tail} to determine the voltage dependence of activation. Values obtained at each pH_e were normalised to the maximum value for each set of data, plotted as a relationship of membrane potential against normalised current and fit with a Boltzmann function (Equation 1). The fit gave rise to $V_{0.5}$ values of -16.64±2.87 mV (k = 8.25±0.81 mV) at pH 7.4 (n = 7 cells) and -11.98±5.46 mV (k = 11.98±1.90 mV) at pH 6.3 (n = 7 cells).

The positive shift in $V_{0.5}$ seen in pH_e 6.3 was not significantly different to that in control (P = 0.5334; paired *t*-test). Maximal conductance was calculated from I_{Tail} measurements resulting in G_{Max} values of 0.51 nS/pF in pH_e 7.4 (n = 7 cells) and 0.44 nS/pF in pH_e 6.3 (n

= 7 cells). This resulted in a non-significant decrease in conductance when exposed to extracellular protons (P = 0.3016; paired *t*-test).

6.4.2.2 Comparison between WT and mutant hERG channel characteristics under extracellular acidosis

Comparisons were made at +20 mV in pH_e 6.3 compared with pH_e 7.4 to determine if the mutant channels were affected by extracellular protons differently compared with WT channels. The effects were quantified as a % decrease from control and shown in Figure 6-15.

Figure 6-15A shows the % decrease in $I_{End\ Pulse}$ for the WT and mutant channels. In WT hERG1a channels a decrease of 13.5±2.6% was observed and, most notably, the E575Q/H578N mutant caused an increase of 12.5±5.6 % in $I_{End\ Pulse}$ amplitude in acidic conditions (n = 7 cells) compared to control (n = 7 cells). This increase in $I_{End\ Pulse}$ amplitude was significantly different to the results in WT channels (P = 0.0003; one-way ANOVA with Bonferroni post-test. No significance from WT was observed for either E575Q or H578N single mutants.

A similar pattern was observed in the decrease of I_{Tail} in response to extracellular protons: no significant different from WT hERG was seen for the single point mutations E575Q and H578N but a significant attenuation in proton block of I_{Tail} was seen for the double mutant E575Q/H578N (11.1±4.0%) compared to the 26.8±3.7% seen in WT channel (P = 0.0083; one-way ANOVA with Bonferroni post-test).

To determine the effects of protons on I_{hERG} activation, $V_{0.5}$ values obtained from characterisation of the WT (Section 3.3.2 and 3.3.2) and mutant channels (Section 6.4.1 and 6.4.2) were used and plotted as raw values (Figure 6-15C) and as the shift observed in acidification (Figure 6-15D). No significance in the raw $V_{0.5}$ (pH_e 7.4 and 6.3) values or the shift in $V_{0.5}$ was seen in any of the mutants.

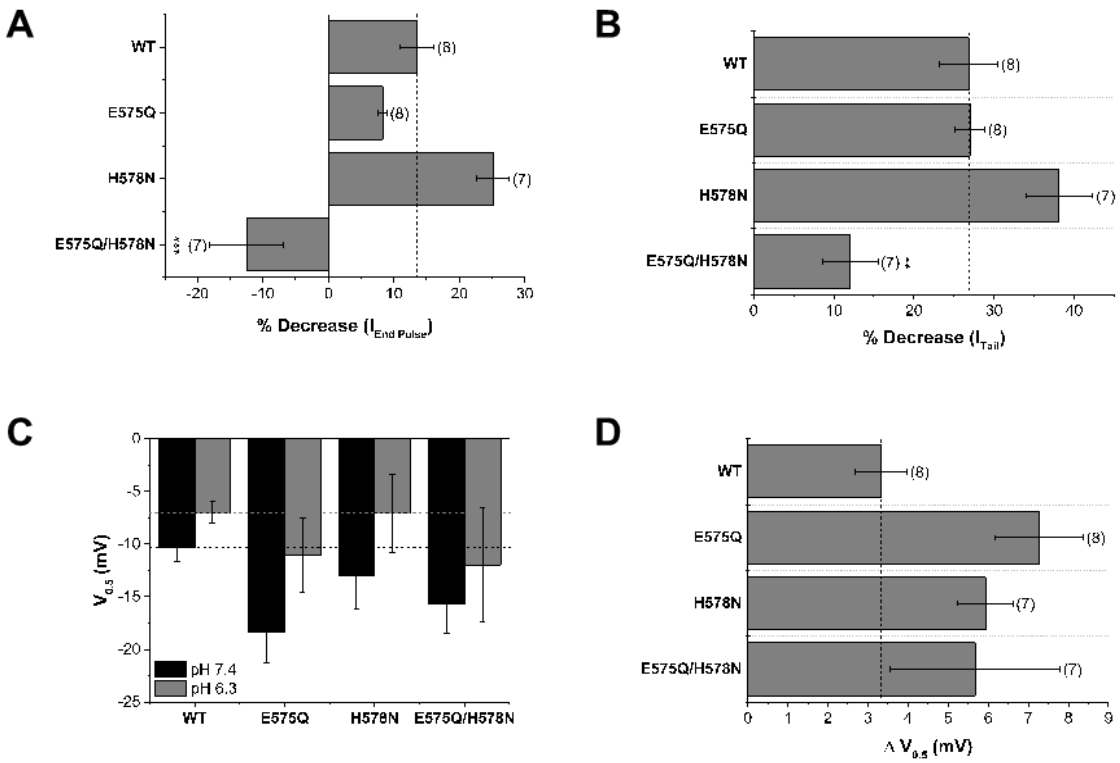

Figure 6-15 The effects of extracellular acidification on the WT and mutant hERG channels.

A. The effects of extracellular acidosis on the $I_{End\ Pulse}$ on hERG WT and mutant channels. The vertical dashed line represents the block seen in WT channels Comparisons were made when the cell membrane was depolarised to +20 mV in pH_e 7.4 and 6.3.

B. hERG WT and mutant channels and the effects of extracellular protons on the decrease in tail current. The vertical dashed line represents the % decrease in I_{Tail} seen in WT. Tail current was elicited upon repolarisation to -40 mV after membrane depolarisation to +20 mV.

C. Mean ± SEM of raw $V_{0.5}$ values for WT and mutant channels in pH_e 7.4 (black bars) and pH_e 6.3 (grey bars). Horizontal dashed lines represent values seen in WT in control (black) and pH_e 6.3 (grey). Statistical tests were completed in each pH condition and compared to WT.

D. The shift in $V_{0.5}$ (in mV) seen when WT and mutant hERG channels are exposed to protons. Raw values observed in **C** were used to calculate the difference in $V_{0.5}$ in control and pH_e 6.3.

Numbers in brackets indicate cell number. '**' and '***' denotes statistical significance of $P < 0.001$ and $P < 0.0001$ respectively compared to WT values (one-way ANOVA with Bonferroni post-test).

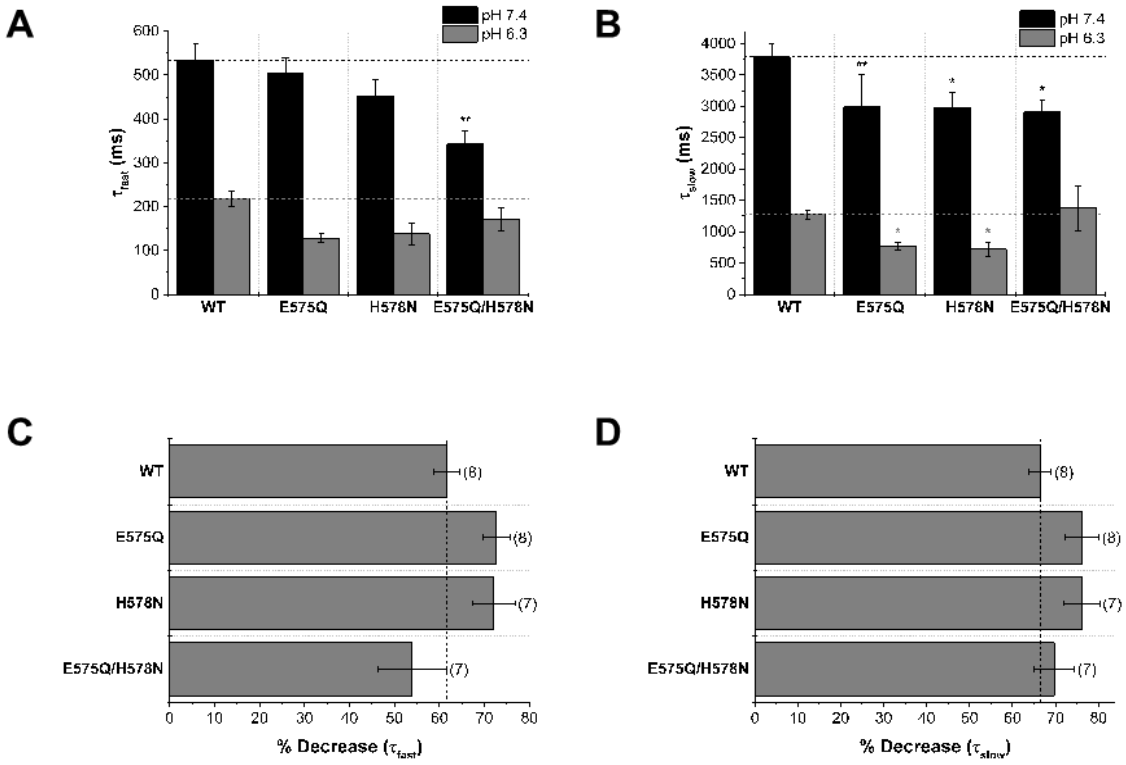

Figure 6-16 The deactivation kinetics of WT and mutant hERG channels during acidification.

Tail current was elicited upon repolarisation to -40 mV after membrane depolarisation to +20 mV. Deactivating currents were fit with Equation 2 to obtain the fast (**A**) and slow (**B**) time constant.

A. Effects of extracellular acidosis on the fast time constant of deactivation in hERG WT and mutant channels. Horizontal dashed lines represent values seen in WT in control (black) and pH_e 6.3 (grey).

B. Raw τ_{Slow} values for WT and mutant channels in pH_e 7.4 (black bars) and pH_e 6.3 (grey bars). Horizontal dashed lines represent values seen in WT in control (black) and pH_e 6.3 (grey).

C. Mean ± SEM of the % decrease of the τ_{Fast} when exposed to extracellular protons. The decrease was calculated using raw values that are shown in **A**. The vertical dashed line represents the decrease seen in WT channels.

D. Mean ± SEM of the % decrease of the slow time constant when subjected to extracellular acidosis. The decrease was calculated using raw values that are shown in **B**. The vertical dashed line represents the decrease seen in WT channels.

Numbers in brackets represent the number of cells. '*' and '**', denotes statistical significance of $P < 0.05$ and $P < 0.005$ respectively compared to WT values (one-way ANOVA with Bonferroni post-

As was completed for the other hERG mutations (Figure 6-11), the deactivation of the I_{Tail} was also analysed to determine the effects of extracellular acidosis by fitting the

deactivating current with a bi-exponential function (Equation 2) giving the values plotted in Figure 6-16A (τ_{Fast}) and Figure 6-16B (τ_{Slow}). The data obtained in control (pH_e 7.4) are presented as black bars and the data in pH_e 6.3 are shown as grey bars. In pH_e 7.4, the τ_{Fast} value of the double mutant E575Q/H578N was the only channel to be significantly different from that in WT, with a value of 342.2±30.6 ms (n = 6 cells) compared to 553±36.3 ms in WT (n = 15 cells) (P = 0.0012; one-way ANOVA with Bonferroni post-test). No significance was observed in the τ_{Fast} value upon extracellular acidosis. Wild-type channels displayed τ_{Slow} values of 3790±215 ms in pH_e 7.4 and 1276±74 ms in pH_e 6.3. It is shown that the hERG mutations created affected the deactivation kinetics. As seen in Figure 6-16B the raw values in control conditions are faster in the all mutants compared with WT hERG1a with significance in all three mutant hERG channels tested. Upon acidification, τ_{Slow} raw values of the hERG E575Q/H578N mutant did not differ significantly to the τ_{Fast} value observed in WT pH_e 6.3 (P > 0.9999; one-way ANOVA with Bonferroni post-test). However, the two single hERG channel mutations E575Q and H578N showed a small but significant acceleration in τ_{Slow} values compared to WT upon extracellular acidification (P = 0.0362 and P = 0.0329 respectively; one-way ANOVA with Bonferroni post-test).

The % decrease in τ_{Fast} and τ_{Slow} values are shown in Figure 6-16C and D respectively. A decrease in deactivation time constants signifies an acceleration in deactivation. No significance was observed between the mutants and WT I_{hERG} in the % decrease in the fast and slow time constants.

6.4.2.3 Single-channel recordings of the hERG E575Q/H578N channel mutant

To investigate the effects of protons on the conductance and open-time kinetics of $I_{hERG\ E575Q/H578N}$ at the single-channel level, the protocol shown in Figure 6-17 (lower centre panel) was applied in the cell-attached configuration. The protocol was applied with isotonic potassium and a pipette pH of either 7.4 or 6.3. Thus, in the cell-attached configuration, the pipette solution is considered the external solution in the experiment.

Figure 6-17 shows representative records of I_{hERG} elicited by the protocol shown in the lower centre panel at both pH_e 7.4 (Figure 6-17A) and pH_e 6.3 (Figure 6-17B). In control pH_e (7.4), as the membrane potential became more depolarised the amplitude of channel openings (seen as downward deflections) decreased. With depolarisation of the

membrane potential in control, the number of openings increased. A similar pattern was seen at pH_e 6.3, with similar amplitudes to that seen in control but with fewer channel openings observed.

Data from these experiments were analysed using the methods described in Chapter 2.3.5 and events from each potential were gathered to create amplitude histograms. Figure 6-18A shows example amplitude histograms from -80 mV at pH_e 7.4 (Figure 6-18A) and at pH_e 6.3 (Figure 6-18B). An average of amplitudes was taken for each potential and plotted against membrane potential (Figure 6-18E). Across all potentials there was no significance in the effect of protons on the current amplitude. In some cases, the amplitude was greater in acidic conditions compared with control which was seen in whole-cell data (Figure 6-14C). Plots were fitted with a linear regression equation with the *x* - *y* intercept fixed at 0 mV. The single-channel conductance values derived from the slope of the fits were 11.7±0.4 pS at pH_e 7.4 (n = 5 patches) and 12.0±0.6 pS at pH_e 6.3 (n = 6 patches; P = 0.7032; unpaired *t*-test).

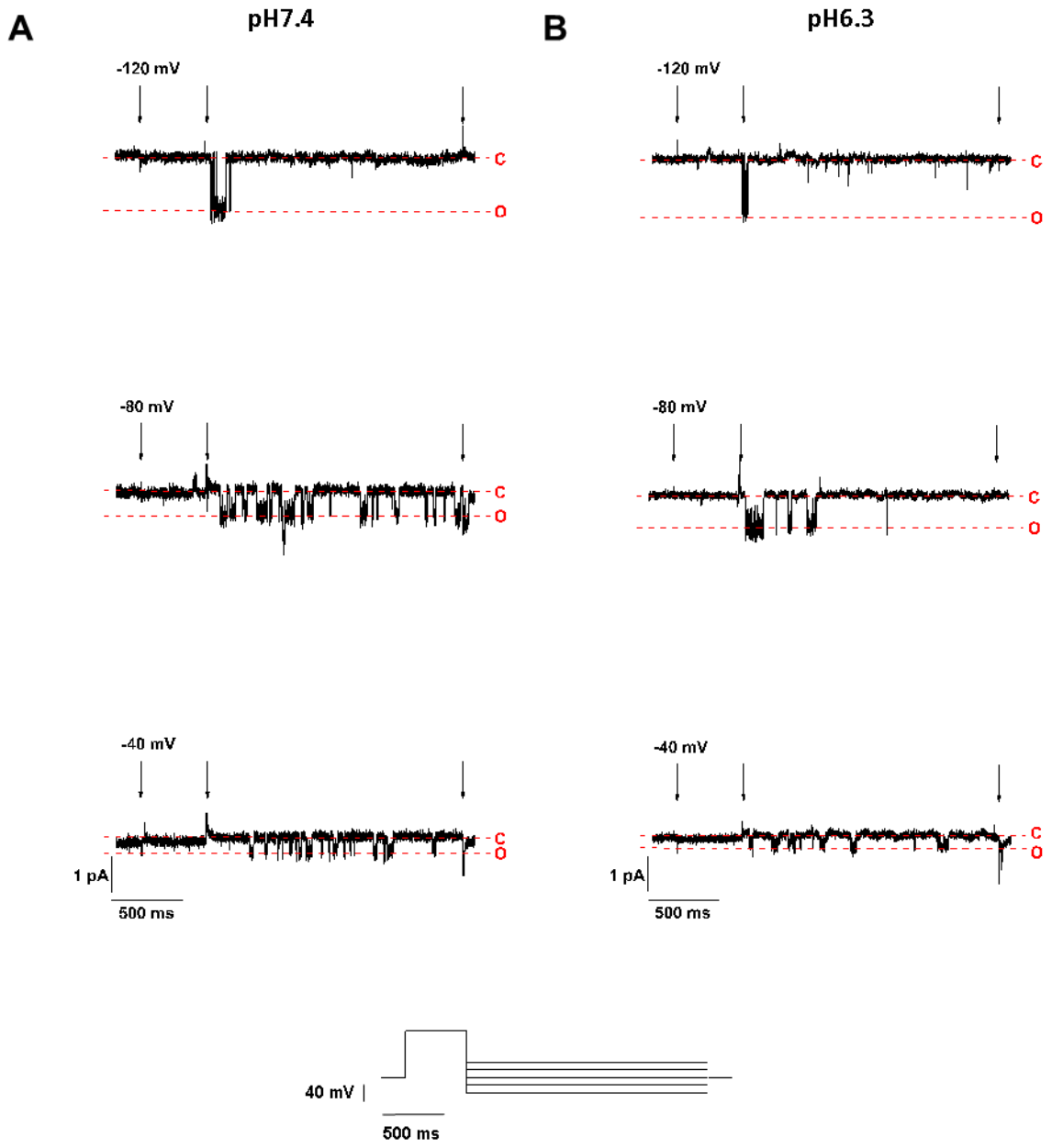

Figure 6-17 Single-channel recordings of the hERG E575Q/H578N channel mutant.

A, B. Representative current records at selected potentials with a pipette solution pH 7.4 (**A**) and pH 6.3 (**B**) when protocol in bottom centre was applied. Channel openings are shown as downward deflections and shown with red dashed lines; line labelled 'C' represents the closed state and 'O' represents the open state. Traces were created by subtracting a 'dummy' sweep to remove transient current. Downward arrows represent time points at which the current was changed in response to the voltage protocol shown in bottom centre.

Currents elicited by the protocol in Figure 6-18 (lower centre panel) were also analysed to determine whether extracellular acidosis affected the single-channel kinetics of $I_{hERGE575Q/H578N}$. Duration histograms on a logarithmic scale were constructed (Figure 6-18C and D) and were fitted with a single exponential function to obtain open-time durations of 5.90 ms in pH_e 7.4 and 5.64 ms in 6.3. An average of open-times was taken for each potential and plotted against membrane potential (Figure 6-18F). Upon extracellular acidification, no significant difference was observed in open-time durations (P = 0.9646; two-way ANOVA with Bonferroni post-test). The reduction in channel openings observed in acidic conditions will likely be due to decreased burst durations or increased closed-time durations.

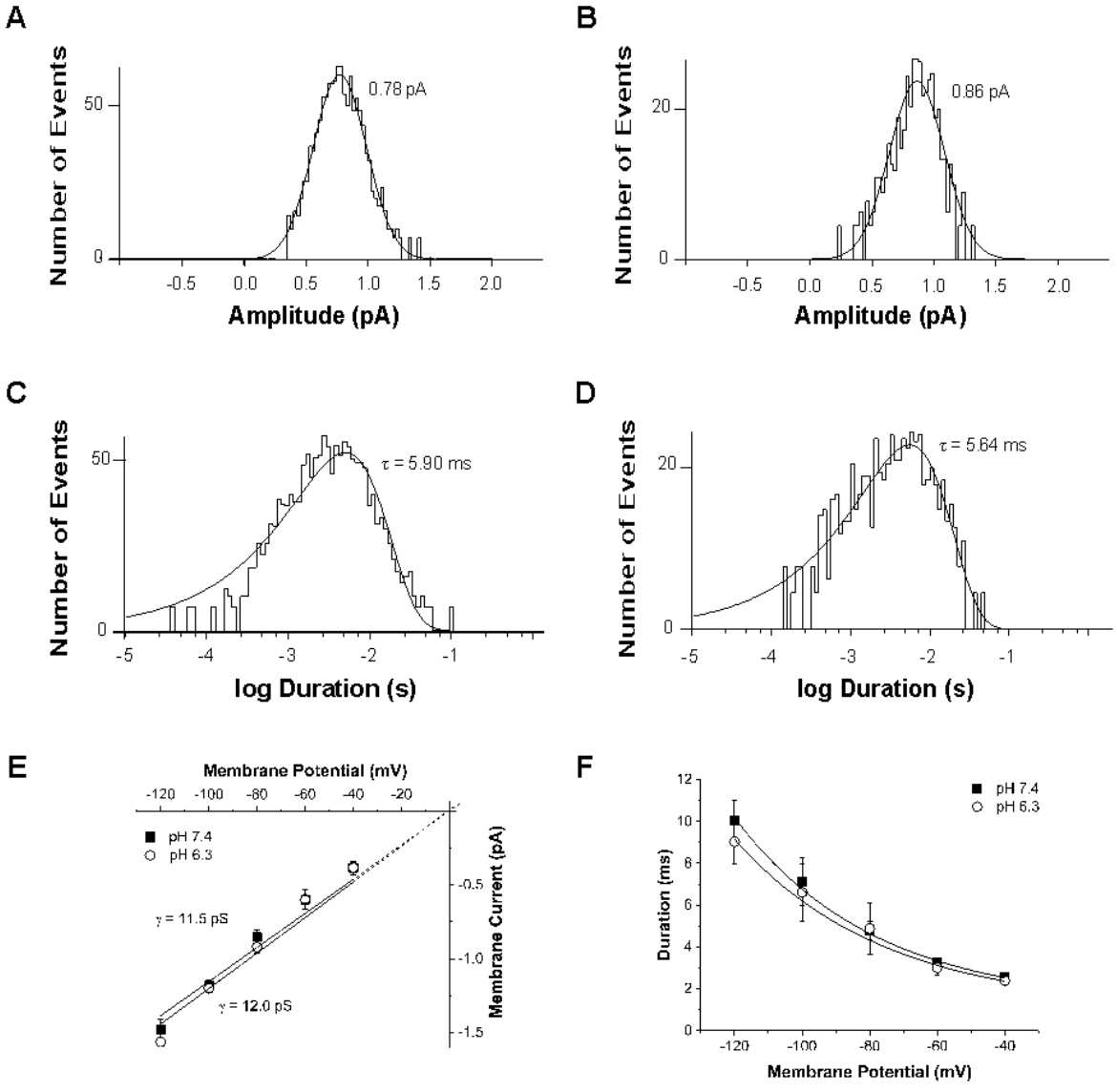

Figure 6-18 The effects of extracellular protons on single-channel conductance and open channel kinetics of the hERG E575Q/H578N mutant.

A. Amplitude histogram from multiple patches at -80 mV for pH_e 7.4. A Gaussian distribution was fit to reveal an amplitude of 0.78 pA.
B. Amplitude histogram from multiple patches pooled together for pH_e 6.3 at -80 mV. When fit with a Gaussian distribution, an amplitude of 0.86 pA was yielded.
C, D. Open-time duration histograms of several patches at -80 mV for pH 7.4 (**C**, n = 5 patches) and pH 6.3 (**D,** n = 6 patches). Histograms were fit with a single exponential function to reveal an open-time duration of 5.90 ms in control and 5.64 ms in pH 6.3.
E. Amplitude values were obtained for the potentials tested in both pH conditions. Single-channel current-voltage (I-V) relationships were constructed by plotting membrane potential against the respective amplitude. Plots were fitted with a linear relationship (solid line) and was constrained to pass through the origin (dashed line) to achieve slope conductance of 11.7±0.4 pS for pH 7.4 (n = 5 cells) and 12.0±0.5 pS for pH 6.3 (n = 6 cells; P = 0.7032, unpaired students t-test).
F. Open-time durations were obtained for each potential tested and plotted against membrane potential. The plots were fitted with an exponential function for 7.4 (n = 5 cells) pH 6.3 (n = 6 cells). No significance was observed between pH and membrane potential (two-way ANOVA with Bonferroni post-test).

Contributions were made by Professor Neil Marrion is acknowledged for his contribution to these experiments (three of six experiments. Three cells were obtained at each pH_e condition and included in the analysis).

6.5 Discussion

6.5.1 Results in context

6.5.1.1 The effects of extracellular acidification and subsequent pK_a values

The experiments in this chapter considered how external protons modulate the hERG channel. Initial experiments confirmed that there are distinct and separate sites of proton modulation. Site-directed mutagenesis of individual titratable residues on the hERG1a channel still showed proton sensitivity. A novel double mutation E575Q/H578N showed that macroscopic and single-channel conductance is not affected by extracellular protons.

External protons have been shown to modify the I_{Kr}/I_{hERG} with a general agreement that acidosis causes a reduction in I_{Kr}/I_{hERG} amplitude and accelerates current deactivation (Anumonwo et al. 1999; Bérubé et al. 1999; Jiang et al. 1999; Ho et al. 1999; Terai et al. 2000; Vereecke & Carmeliet 2000; Bett & Rasmusson 2003; Zhou & Bett 2010; Van Slyke et al. 2012; Du et al. 2010; Shi et al. 2014). A previous study introduced the notion of multiple binding sites for extracellular protons on hERG, as protons were seen to affect activation and deactivation processes in two distinct pH_e ranges (Bett & Rasmusson 2003). The study observed a pK_a of ~5.5 for current suppression and a pK_a of ~6.8 for channel deactivation (Bett & Rasmusson 2003). The results in this section show similar findings with a reduction in I_{Tail} presenting a pK_a of 5.5 (Figure 6-1C). The effect of protons on I_{hERG} deactivation was analysed using a double exponential (rather than the single exponential used for *Xenopus* oocyte data by Bett and Rasmusson, 2003) and so two pK_a values were derived for the two-time constants of deactivation (Figure 6-1D and E). The pK_a values were ~6.8 and ~7.3 for the fast and slow time constant respectively, which is comparable with ~6.8 observed with a single exponential function (Bett & Rasmusson 2003). A separate study in which the deactivation of I_{hERG} was resolved with a bi-exponential function revealed pK_a values of ~7.0 and ~7.1 for the fast and slow time constant respectively (Anumonwo et al. 1999). Other studies of effects of extracellular protons on hERG, have reported pK_a values for current suppression ranging from 5.1-5.8 (Anumonwo et al. 1999; Bett & Rasmusson 2003; Van Slyke et al. 2012) and pK_a values for I_{hERG} deactivation of ~6.8 (Bett & Rasmusson 2003), 6.9 (Van Slyke et al. 2012) and 6.7 (Shi et al. 2014) when analysed with a single exponential. In this study, the effect of protons on the $I_{End\ Pulse}$ of hERG1a was examined for the first time with a pK_a of ~6.9 (Figure 6-1B). Other analyses completed by previous studies shows that the activation of I_{hERG} is also affected by protons. The shift in half-maximal activation ($V_{0.5}$) of I_{hERG} resulted in pK_a

values of 5.5 (Anumonwo et al. 1999) and 5.6 (Shi et al. 2014). Due to only a single pulse protocol used in these experiments, the effect of protons on the shift in $V_{0.5}$ was not observed. However, due to similar pK_a values of other processes (the effects of protons on current suppression and deactivation), it can be assumed that similar values would be achieved if current-voltage experiments were carried out. Thus, it can be concluded that data obtained in this Chapter agree with previous studies and that there are multiple sites of proton action on the hERG channel.

6.5.1.2 Histidine residues as targets for pH sensing

As briefly discussed in (Section 3.4.2.4 and 3.4.2.4), extracellular protons may modulate I_{hERG} by titrating the side chains of amino acids that are important in channel processes. It has been previously thought that, due to the pK_a of histidine being approximately 6.1, the two histidine residues H578 and H587 located on the S5-P linker would play a role in pH sensitivity (Jiang et al. 1999; Van Slyke et al. 2012). In this study, several histidine residues including the H578 and H587 were mutated to asparagine to determine if they were responsible for pH_e sensitivity of I_{hERG}. Histidine residues H562 and H674 (located on the S5 and bottom of S6 respectively) were also mutated as they may be accessible from the extracellular environment (Figure 6-2). Although the H562N mutant required co-expression with WT hERG1a for channel expression, channel properties such as activation parameters (see Table 6-1) were different from that of WT suggesting the formation of heteromeric channels. A previous study highlighted the importance of the H562 residue with evidence that *in silico* hydrogen bonding between H562 amino acids T618 and S621 in the pore helix play a critical role in stabilising the structure and function of the S5-pore helix (Lees-Miller et al. 2009).

Data presented in this chapter and summarised below in (Table 6-1) demonstrate that removal of these individual histidine residues does not abolish pH sensitivity.

	pH 7.4		pH 6.3		pH 5.5	
	$V_{0.5}$	K	$V_{0.5}$	k	$V_{0.5}$	k
WT	-10.0±1.2	6.8±0.2	-7.0±2.8	8.3±1.1	11.8±2.4	11.9±0.5
H562N	-21.3±3.2	6.8±1.2	-12.1±3.9	8.8±0.6	14.4±1.2	14.7±2.3
H578N	-17.3±1.2	7.9±0.6	-11.7±1.4	10.4±0.9	15.5± 2.4	14.2±0.5
H587N	-10.8±1.8	8.9±0.7	-3.4±3.1	10.9±1.7	19.3± 3.8	11.6±0.4
H674N	-44.9±1.9*****	9.3±0.8	-30.4±2.0*****	11.6±1.8	-	-

Table 6-1The activation and slope values of the histidine mutations tested.

Mean ± SEM of $V_{0.5}$ (in mV) and the corresponding slope (in mV) values in control, pH_e 6.3 and pH_e 5.5 (excluding the H674N mutant which was not tested at pH_e 5.5).

'*' represents significance of $P < 0.05$ to corresponding value in WT channels (one-way ANOVA with Bonferroni post-test).

Previous studies have predominantly investigated the effects in removing the two most outer histidine residues H578 and H587. Introduction of a negative charge to these two sites as a double mutant resulted in a channel (H578E/H587E) that was still modulated by extracellular protons (Jiang et al. 1999). Another study examined the two histidine residues individually by mutating to glutamine (Van Slyke et al. 2012). Upon exposure to extracellular acidosis these mutant channels, H578Q and H587Q, showed similar results to WT channels with attenuation in current amplitude and acceleration in the rate of deactivation. The same group also targeted three other histidine residues that may be attainable from the extracellular side; H562, H492 and H485. Mutating these residues still resulted in a channel in which I_{hERG} was attenuated by extracellular protons. In contrast, initial data presented in abstract form suggests that the H562 residue acts as a pH sensor in channel gating (Bett et al. 2011). The data obtained in this section suggests that the individual histidine residues mutated are not responsible for pH sensitivity. This does not rule out the possibility that protons may interact with more than one histidine residue (WT hERG1a contains over 20 histidine residues) or the binding of protons to one or more different titratable residues, such as glutamate or aspartate.

6.5.1.3 The role of aspartic acid residues in hERG channel proton sensitivity

There is consensus, as mentioned in Section 6.1, that hERG is modulated by protons at more than one site. The data in this section also confirms this (Figure 6-1) with a focus on titratable residues with a majority located at the top of the S5 and S6 including the S5-Pore linker and pore helix (Figure 6-2). This area of the channel was the focus of experiments carried out in this Chapter as a study by Van Slyke et al suggested that one site of proton modulation is within the conduction pathway (Van Slyke et al. 2012). Previous studies have shown that aspartic acid residues, with a pKa of ~3.9, were involved in the shift in channel activation upon extracellular acidification (Kazmierczak et al. 2013; Shi et al. 2014). It therefore seemed plausible that aspartic acid residues elsewhere in the channel may act as pH sensors for other channel processes. The aspartic acid residues targeted in this study were the D580 and D609 residues (located at the top of the S5 transmembrane domain and immediately before the pore helix respectively, see Figure 6-2).

Data from this study suggests that the two individual aspartic acid residues are not involved in sensing low pH as substitution of aspartic acid to asparagine resulted in hERG currents that were still modulated by protons (Figure 6-4 and Figure 6-7). Although it appears to not be involved in proton sensitivity, the D609 residue appears to be critical for normal channel function. A recent clinical study observed that the D609G missense mutation causes a loss of function of I_{hERG} in a dominant-negative manner, associated with severe LQT syndrome (Yamaguchi et al. 2005).

6.5.1.4 Inactivation deficient mutants and extracellular acidosis

The N588K mutation has been studied thoroughly in previous studies (Brugada et al. 2004; Cordeiro et al. 2005; Hong, Bjerregaard, et al. 2005; McPate et al. 2005; McPate, H. Zhang, et al. 2009) and manifests itself in clinical cases of SQTS. In this study, the response of the N588K mutant to extracellular acidosis was investigated to determine if the clinically significant mutation is modulated by protons and to probe if the suppressive effects of protons requires inactivation (Figure 6-6). The data presented show that the voltage-dependence of activation is not significantly different from to that of WT channels in pH_e 7.4 and so in agreement with an earlier study (McPate et al. 2005). Upon acidification, the channel behaves in the same manner as WT; a decrease in I_{hERG} amplitude, acceleration of deactivation and a depolarised shift the voltage-dependence of activation (Figure 3-2). Prior work on the effects of extracellular acidosis on the voltage-

dependence on I_{hERG} inactivation showed an approximate 1 mV depolarising shift was observed in the $V_{0.5}$ of inactivation with no significance in the time-course of development of inactivation (Du et al. 2010). This data suggests that the inactivation process of hERG channels is unaffected by external protons. This notion is supported by single-channel work completed on the S620T inactivation deficient mutant, in which single-channel current amplitude at -110 mV was reduced by ~22% in extracellular acidosis (Van Slyke et al. 2012)

Upon testing the E637Q mutation, it appeared to create a non-functional channel. This is in agreement with other studies as substitution of E637 to either a lysine, glutamine or glycine produced non-expressing currents (Hayashi et al. 2002; Amorós et al. 2011; Van Slyke et al. 2012). However, when this mutant was co-expressed with WT hERG1a, channels were formed that showed different gating characteristics from WT alone (Figure 6-8). It appeared that upon depolarisation, the region of negative slope on the I-V relation that is seen in WT channels was not seen in the potentials tested in the E637Q mutant. This relationship was also observed with co-expression of a long QT syndrome mutant E637G with WT channels (Amorós et al. 2011). In contrast , the co-expression of another Long QT syndrome mutation E637K with WT hERG1a channels generated channels that was similar to that of WT channels (Hayashi et al. 2002). The differences between studies in this regard is likely to be attributable to different substitutions made in place of the glutamic acid. As with the other inactivation deficient mutants discussed in this section, the E637Q/WT channel was still influenced by extracellular protons.

6.5.2 The hERG E575 residue senses protons

The glutamic acid residue at position 575 in WT hERG1a channels is located at the top of the S5 transmembrane domain (Figure 6-2) and, as a result, is associated with the 'outer mouth' structure (Tseng et al. 2007). The S5 and 'outer mouth' region (also containing the S5-P linker) has been shown to be critical in hERG activation and inactivation processes (Torres et al. 2003; Clarke et al. 2006; Ju et al. 2009). Extracellular acidosis experiments completed in this section on the hERG E575Q channel mutant showed a slight attenuation in the effects of protons on the $I_{End\ Pulse}$ with no block observed at potentials positive to +20 mV (Figure 6-12). Earlier experiments revealed that the modulation of the end pulse current in hERG had a pK_a of ~6.7 (Figure 6-1A). This pK_a value is much more alkaline than the pK_a of a glutamic acid (~4.2) and so it would suggest that the local environment,

such as nearby titratable residues to E575 would play a role in increasing its pK_a. In theory, at pH 7.4, the unperturbed pK_a of glutamic acid is ~4.2 and so will be negatively charged. In the same conditions, a histidine residue will have a pK_a of ~6.1 and will be uncharged. As mentioned, the local environment will influence these values and in the case of E575 and the closest titratable residue H578, both residues are positioned on the external surface of the hERG channel (see Figure 6-2). Previous work has provided evidence that ionisable groups positioned on the protein surface will most likely display pK_a via charge-charge interactions (Laurents et al. 2003; Pace et al. 2010). If this was indeed the case, other ionisable residues neighbouring the E575 residue would be involved in altering its pK_a. This is due to the electrostatic interactions between a glutamic acid and histidine: in their ionised form, the glutamic acid and histidine are respectively negatively and positively charged. As a result, to form favourable interactions, the histidine will decrease the pK_a of glutamic acid and the glutamic acid will increase the pK_a of the histidine. Therefore, to increase the pK_a of the glutamic acid to a value that would match the data obtained in these experiments, another negatively charged residue will need to be nearby. Figure 6-2 shows that the D580 residue is close to E575 being only 5 amino acid residues apart and, dependent on the actual configuration of the tertiary structure of the protein, the D609 residue could be close enough to perturb the E575 pK_a.

6.5.2.1 Outer pore block by protons: are E575 and H578 involved?

Previous studies have suggested that extracellular protons reduced hERG conductance by pore block (Van Slyke et al. 2012). Using the Woodhull model, they observed that the proton at its binding site sensed ~18% of the electrical field experienced from the external side of the channel. This binding site was altered when a glutamate was introduced at the site of H587 and an approximate 4% of the electrical field was sensed. The H587 residue has been identified to be a part of the helical structure found in the S5-P linker and involved in channel gating (Dun et al. 1999; Torres et al. 2003; Clarke et al. 2006). The Woodhull analysis performed following mutation of H587 to glutamate suggests that the H587 residue is located at a more superficial site than one of the proton modulation sites in WT hERG channels. This could support the idea that E575 and H578 are involved in pH sensing.

Whole-cell (Figure 6-14) and single-channel (Figure 6-18) characterisations of the double hERG mutant E575Q/H578N were carried out in this experimental chapter. Whole-cell

recordings using the I-V protocol shown in Figure 6-14 (below A and B) showed that, at voltages from +10 mV to more positive potentials, the $I_{End\ Pulse}$ was unchanged in extracellular acidification rather than the decrease observed in WT channels (Figure 3-2D). The double mutant channel still showed a depolarised shift in activation of ~3 mV which is comparable to what was seen in WT channels. This shows that E575 and H578 are not involved in the pH sensor of hERG activation even though the apparent pK_a of activation is ~5.5 (Anumonwo et al. 1999; Shi et al. 2014) which is like the pK_a (5.1 – 5.8) for conductance/reduction in I_{Tail} (Anumonwo et al. 1999; Bett & Rasmusson 2003; Van Slyke et al. 2012). This highlights further that there are multiple sites of proton action in the hERG channel and that the aspartates located in the 'metal ion binding pocket' in S2 and S3 involved in the proton-induced shift in channel activation (Shi et al. 2014) are likely not also to be involved in mediating current suppression. The current suppression effect is removed in this double mutant and the idea that E575 and H578 are involved in the reduction of hERG channel conductance is reinforced by the single-channel recording data, showing a lack of reduction of single-channel conductance for the double mutant.

6.5.2.2 The conductance of E575Q/H578N is not reduced in extracellular acidification

In WT channels, the effects of extracellular acidosis on macroscopic hERG current is the reduction in amplitude and an acceleration in the rate of deactivation. Single-channel analysis of I_{hERG} in extracellular acidification confirms this with a reduction in single-channel conductance (Figure 3-6) and a decrease in open-time and burst-duration kinetics paired with an increase in closed-time (Figure 3-7). For the E575Q/H578N double mutant, macroscopic currents showed a decrease in conductance (~14%) with and acceleration in deactivation. Analysis of single-channel patches showed that decreasing the extracellular pH to 6.3 from 7.4 did not affect the single-channel current amplitude, and consequently the conductance, over the range of potentials tested (Figure 6-18E). This provides evidence that, in the double mutant, the decrease observed in whole-cell currents are not due to the occlusion of the open pore but rather it is linked to the channel availability. A similar conclusion was observed in a previous study in which single-channel conductance of $K_v1.5$ was unaffected in extracellular acidosis (Kwan et al. 2006). They reasoned that the main effect of protons was to decrease the open probability (P_O) of the channel as well as a decrease in the average burst duration. This concept could be used to interpret the single channel data obtained in this chapter. Open-time duration seems to be unaffected

by extracellular protons (Figure 6-18F) but as can be seen in the representative recordings in Figure 6-17, extracellular acidosis decreases the channel activity and channel bursts appear to be reduced. Analysis of closed-time and burst-duration analysis was not feasible, however, due to lower event numbers captured than are required. Further experiments with this double mutant are anticipated to advance our knowledge on proton block of hERG. From initial experiments completed in this chapter, there is bias towards E575 and H578 interaction and their involvement in pore block of the hERG channel.

6.5.3 Physiological significance of extracellular acidosis and ionisable residues within the hERG channel

As previously mentioned, extracellular protons have been shown in this study and others to reduce I_{hERG}/I_{Kr} amplitude and accelerate deactivation kinetics. The effect of protons on these processes appear to act at different sites on the hERG channel. Several mutagenesis studies have attempted to elucidate the residues within the channel that act as pH sensors with very little success. It has been determined that a cation binding site within the voltage sensor domain is responsible for producing the depolarising shift in channel activation seen in extracellular acidosis (Jo et al. 1999; Kazmierczak et al. 2013; Shi et al. 2014). However, in these mutations, a reduction in amplitude and acceleration was still observed, emphasising the theory of multiple binding sites.

The residues targeted for mutagenesis in this chapter have shown that single mutations of titratable residues do not remove pH sensitivity. In some cases, the effect of pH was augmented in relation to the reduction in I_{hERG} amplitude (both end-pulse and tail current). Across all the mutants, including the double mutant which removed pH sensitivity to channel conductance, still showed acceleration in the rate of deactivation like what was seen in WT channels. These results would suggest that there at least one more site of proton modulation that affects the deactivation kinetics. In this study, and in others, the pK_a of deactivation is between 6.7 and 7.3 (dependent on analysis) (Anumonwo et al. 1999; Bett & Rasmusson 2003). With a pK_a that is in the pH range observed in pathological events, it suggests that the rate of deactivation will be the process most affected and so revealing the residues would be greatly beneficial into understanding the deactivation process. As discussed in Section 3.4.3 and 3.4.3, the consequence of accelerated deactivation could lead to arrhythmogenesis via reduction in channels available to counteract premature depolarisations.

In this study, a novel mutation E575Q/H578N removed proton block of channel conductance. The discovery that the two ionisable residues, located at the top of the S5 and the beginning the S5-P linker, interact somehow to allow protons to bind is significant in increasing our knowledge of proton modulation sites in the hERG channel. Further work would still be needed to fully characterise the mutant channel (ion permeation, activation and inactivation kinetics as well as single channel kinetics). The initial work completed shows that neutralisation of the two ionisable residues removes pore block via protons.

As mentioned, there is growing evidence that native I_{Kr} is a heteromer of the hERG 1a and 1b isoforms. As shown in Chapter 4, as well as by a previous study, the effects of extracellular acidosis are augmented in the hERG 1b isoform (Du et al. 2011) with a larger attenuation in $I_{hERG\ 1b}$ amplitude and conductance compared with hERG 1a alone. The hERG 1b channel is identical to hERG 1a in the entire channel except the N-terminal region and so the E575 and H578 residues will be in the same position as the 1a isoform. Therefore, electrophysiological studies of the hERG1a/1b heteromer with the E575Q/H578N mutation will shed light on the effects on conductance and relate this to native I_{Kr}.

7. General Discussion

7.1 Overview of experimental data

The work in this thesis has investigated in detail the effects of extracellular acidosis on hERG1a and hERG1b homomeric potassium channels, using whole-cell and cell-attached patch-clamp techniques. Work that focused on the WT hERG1a isoform (Chapter 3) showed that the results obtained at whole-cell were consistent with previous studies (Anumonwo et al. 1999; Bérubé et al. 1999; Jiang et al. 1999; Jo et al. 1999; Terai et al. 2000; Vereecke & Carmeliet 2000; Bett & Rasmusson 2003; Zhou & Bett 2010; Van Slyke et al. 2012; Du et al. 2010; Shi et al. 2014). Moreover, I have provided the first characterisation of the effects of acidosis on WT hERG1a channels at the single-channel level (finding a decrease in single-channel conductance and open-time duration). The work in Chapter 4 shows that the effect of external protons is enhanced in the hERG1b isoform. The modulation of macroscopic hERG1b by acidosis also showed a reduction in I_{hERG} amplitude, a positive shift in the voltage dependence of I_{hERG} activation and accelerated deactivation. Data in this chapter also described, for the first time, the effects of extracellular acidosis on single-channel I_{hERG1b}. The decrease in channel conductance was augmented in the hERG1b isoform compared to hERG1a under external acidification. The effects seen at the single-channel level for both the hERG1a (Chapter 3) and hERG1b (Chapter 4) could explain the modulation observed at the macroscopic level. To determine the molecular basis of proton modulation in the hERG1a channel, two approaches were taken: (1) modification of the channel using DEPC to covalently modify native histidine residues (Chapter 5); (2) site-directed mutagenesis of titratable residues that were accessible from the extracellular side of the channel (Chapter 6). Modification of the hERG1a channel with DEPC still rendered it sensitive to protons, suggesting that histidine residues are not solely responsible. The final set of experiments in this thesis (Chapter 6) has shown that there are distinct proton binding sites that possess different pK_a values (Anumonwo et al. 1999; Bett & Rasmusson 2003; Van Slyke et al. 2012; Shi et al. 2014). For the first time, it has been revealed that two titratable residues (E575 and H578) located at the top of the S5 helix are responsible for the proton sensitivity of single hERG channel conductance. The following sections will look at the implications of each finding and the opportunities that are available for future work.

7.2 hERG1a channels are modulated by external protons (Chapter 3)

The key findings of this chapter are: (1) extracellular acidification modulates the macroscopic I_{hERG} amplitude by causing a reduction in conductance, depolarising the activation potential and acceleration of deactivation kinetics. (2) similar observations were made in single-channel I_{hERG} recordings when exposed to extracellular acidosis with; a reduction in amplitude and subsequent decrease in single-channel conductance, reduced open- and burst- time durations and, increased closed-time durations.

Single-channel recordings reveal information on the unitary conductance and kinetics of the channel and the effects seen in single-channel recordings could account for the modulation of whole-cell I_{hERG} by protons. Single-channel experiments in this thesis were completed in the cell-attached configuration. The cell-attached configuration is ideal in measuring I_{hERG} as the cell membrane stays intact and so the quality of the single-recordings are maintained for longer. However, the exact cytosolic ion concentrations are unknown and subsequently the reversal potential of the patch undergoing study is unknown and requires assumptions to be made regarding intracellular $[K^+]$. I_{hERG} appears to run-down in excised patches (Zou et al. 1997; Bian et al. 2001), limiting viable recording time. Despite potential issues of current run-down (which might be reduced by inclusion of appropriate intracellular messengers (Bian et al. 2001)), excised patches could remove this uncertainty as the ionic composition of both solutions are known. It may be worthwhile studying the effects of acidosis on single I_{hERG} in both the outside-out and inside-out configuration. If stable excised single-channel recordings could be maintained, it opens the possibility to investigate the effects of protons in a concentration dependent manner. Experiments utilising this configuration could determine any pK_a values for single-channel effects, such as conductance and open-time durations.

7.3 The effects of acidosis are enhanced in the hERG1b isoform (Chapter 4)

The findings in this chapter are that the hERG1b isoform augments the effects of extracellular protons. Similar observations were made in hERG1b channels in comparison to the hERG1a isoform; whole-cell I_{hERG1b} amplitude and conductance was decreased with extracellular acidification, a marked positive shift in activation was seen and, deactivation

kinetics was accelerated. Single-channel recordings of hERG1b channels in control and acidic conditions were also comparable to hERG1a; single-channel amplitude and conductance was decreased, open- and burst-time durations decreased, and closed-time durations increased.

The hERG1b isoform is identical to the hERG1a isoform except for a unique truncated N-terminus and so the eag PAS domain that is critical for slow deactivation is absent in hERG1b channels (Schönherr & Heinemann 1996; Lees-Miller et al. 1997; London et al. 1997; Cabral et al. 1998; Wang et al. 1998; Wang et al. 2000). Previous work that co-expressed hERG1a and hERG1b in CHO cells showed that the effects of extracellular acidosis was augmented when the hERG1b isoform was present (Du et al. 2011). These findings agree with work completed in Chapters 3 and 4 to suggest that the N-terminus is not the site of modulation that causes the acceleration in deactivation and that deactivation is sensed by pH in another intracellular domain.

It is unclear as to why the effects of extracellular acidosis are enhanced in the hERG1b isoform. As discussed in Chapter 4, a possible reason for this could be the greater depolarising shift in the voltage dependence of activation seen in the hERG1b isoform (~16 mV) compared to the hERG1a (~3 mV). In contrast, heteromeric hERG1a/1b channels showed a 6.6 mV depolarising shift in activation when subjected to extracellular acidification (Du et al. 2011). Du et al suggested that differences in the occupancy of gated channel states could have an effect on the availability of the site that protons modulate and bind to the channel (Du et al. 2011). As with hERG1a, further characterisation at the single-channel level of hERG1b as well as heteromeric hERG1a/1b channels will help determine the gating kinetics/state transitions and how they are affected during acidosis.

7.4 Histidine residues are not solely responsible for pH sensitivity in hERG1a channels (Chapter 5)

Diethylpyrocarbonate is the most extensively used reagent for the modification of histidine residues. Histidine residues have a pK_a of ~6.1 and so, if they are involved the sensing of pH in the hERG channel, are appropriate targets for modification. Data presented in Chapter 5 showed that DEPC application caused a reduction in I_{hERG} amplitude, an acceleration in deactivation and a modest depolarising shift in the voltage dependence of activation. These findings agree with a separate study completed in *Xenopus* oocytes

(Jiang et al. 1999). Acidification to pH_e 6.3 post-DEPC application caused a further decrease in current amplitude and tail currents that could not be analysed to interpret the effects on deactivation kinetics. A previous study showed that acidification to pH_e 6.5 after treatment of DEPC also saw accelerated deactivation kinetics but that this could due to the marked shift in activation (~ +18 mV) and not the effect of protons (Jiang et al. 1999).

Although DEPC primarily modifies histidine residues, it has also been shown to modify other residues including tyrosine (Glazer 1970; Miles 1977). A recent study has suggested that tyrosine residues on the S4-S5 linker in hERG channels are critical for the slow deactivation kinetics (Ng et al. 2016). This could be a possible explanation to the accelerated deactivation kinetics with DEPC application. To test this, the tyrosine residues could be mutated to a residue that is unlikely to be modified by DEPC such as glycine to determine if deactivation kinetics are affected.

7.5 Titratable residues in the outer pore of hERG1a channels act as pH sensors (Chapter 6)

Previous work and experiments completed in this chapter (Section 6.3.1) have shown that hERG channel processes have more than one site of proton binding due to the distinct pK_a values (Anumonwo et al. 1999; Bett & Rasmusson 2003; Van Slyke et al. 2012; Shi et al. 2014).

Work completed in this chapter looked at residues located on the extracellular side of the channel to see if they were responsible for the proton sensitivity of the channel. As previously mentioned, histidine residues are the most likely candidate with a pK_a of ~6.1. However, studies mutating the two outer most histidine residues H578 and H587 still rendered the channel sensitive to extracellular protons (Jiang et al. 1999; Van Slyke et al. 2012). Tom Claydon and colleagues also mutated other histidine residues that are thought to be accessible from the extracellular side (H485, H492 and H562) and noted that the effects of acidosis are still observed (Van Slyke et al. 2012). In contrast to this, and to results obtained in this chapter, a recent study has shown that the H562 residue is a pH sensor with neutralisation resulting in reduced pH sensitivity to the hERG channel deactivation time constants (Bett et al. 2011). Although the inconsistencies between results is unknown it can be presumed that these results, alongside the DEPC data (see

Section 7.4), suggest that histidine residues are not solely responsible for the modulation of the hERG channel by extracellular protons.

As mentioned in Section 6.5.1.3, three aspartic acid residues (D456, D460 and D509) that form a metal-ion binding pocket are responsible for proton-induced shift in hERG channel activation (Kazmierczak et al. 2013; Shi et al. 2014). With a pK_a of ~3.9, unperturbed aspartic acid residues are unlikely to be involved in proton modulation. However, because of the 'pocket' in which they are located, the pK_a values can be affected due to electrostatic interactions. Although this was not seen with the two aspartic acid residues tested (D580 and D609), this concept can be used for other amino acid residues with titratable side chains. The glutamic acid residue has a side chain pK_a of ~4.2 and as just mentioned, this can be altered dependent on the local environment and any interactions with other residues. The E575 residue appears to play a role in sensing protons. An individual mutation of E575 to glutamine provided small decrease in the effects of protons on the hERG $I_{End\ Pulse}$. Although the effect on proton sensitivity was insignificant, this

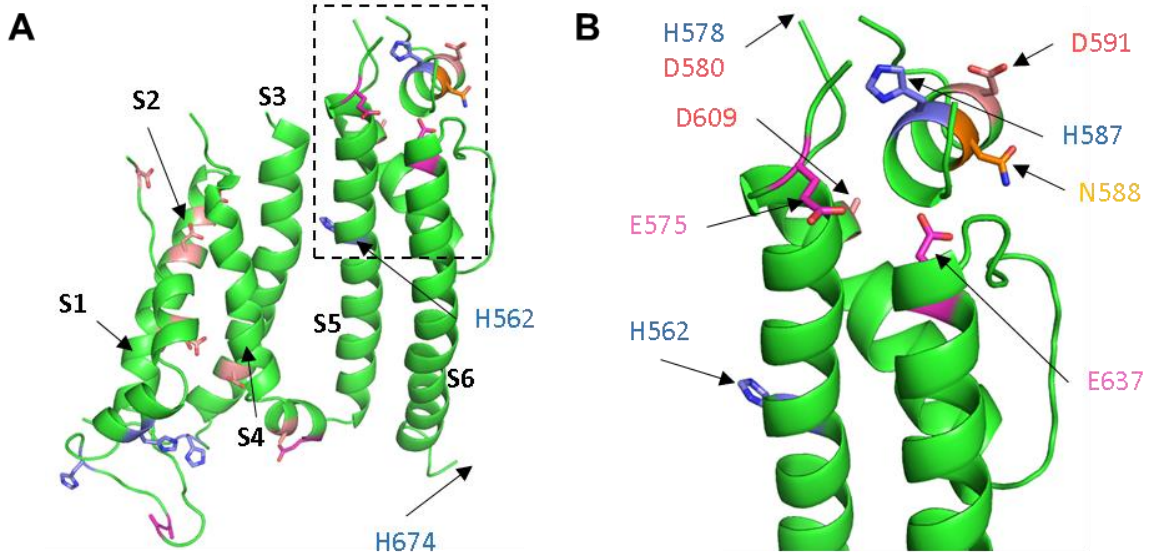

Figure 7-1 Titratable residues on the hERG cryo-EM structure.

A, B. A single hERG1a subunit in the open state (**A**). The target residues based at the top of the S5, S5-P linker and S6 are enclosed in the dashed box and shown at a larger scale in **B.** Residues H578, D580 and H674 are in a region of the channel with little resolution and so are not shown in the model.

Modelling was carried out by Dr Chris Dempsey.

mutation was the only one tested that attenuated protons and so further investigations led to the double mutation of E575 and H578. As the residues are near one another, it was thought that they may influence each other's side chain pK_a values. The hERG E575Q/H578N mutant was shown to remove the effect of protons on the channel conductance at whole-cell and single-channel level.

The work completed in this chapter was based on the Kv1.2/2.1 chimera homology model and while this was a good basis for determining which residues are most likely to be accessible from the extracellular milieu, exact positions of the residues are unknown. Since the completion of these experiments, a hERG structure has been determined using cryo EM (Wang et al. 2017). Figure 7-1 shows the recent structure with the titratable residues targeted in these sets of experiments. Although the positions of the residues are not significantly different to what was shown in the homology model (Figure 6-2) it should be noted that the E575 and H578 residues are now in a region with no organised structure. This may reinforce the idea that they are involved in the removal of proton block of the pore as they are in a more flexible region of the channel and may be able to interact with other residues more readily e.g. D580 residue is nearby E575 being only 5 amino acid residues apart and the D609 residue can be close enough to perturb the E575 pK_a.

This novel double-mutation is significant in increasing our knowledge of proton modulation sites in the hERG channel. Further work is warranted to fully characterise the mutant channel (ion permeation, activation and inactivation kinetics as well as single-channel kinetics). To determine if the two residues do indeed interact with one another, whether by inter- or intra-subunit interactions, further experiments such as cysteine modification could confirm this. Cysteine residues contain a highly reactive thiol group and, under certain conditions, can form disulphide bonds with other cysteine residues that are in close proximity (Jiang 2013)

7.6 Conclusion

In conclusion, the work that has been carried out and presented in this thesis has provided new insights in to the functional and molecular consequences of acidosis on the hERG K^+ channel. Extracellular acidification reduces I_{hERG} amplitude and conductance as well as alters the channel kinetics. Single-channel experiments reinforce this notion with reduced single-channel amplitude and conductance combined with shorter open-time durations. These findings were augmented in the hERG1b isoform, which is now accepted to be

physiologically relevant in the cardiac action potential. As has been discussed, future experimental studies may be beneficial to increase our knowledge and understanding: (1) interactions of protons on the heteromeric hERG1a/1b channel at the single-channel level; (2) full characterisation of the E575Q/H578N mutant at the macroscopic and single-channel level with cysteine mutagenesis to elucidate possible interactions between the two residues; (3) further mutagenesis work to elucidate the site at which protons affect the deactivation kinetics of I_{hERG}. These experiments will improve our understanding of the adverse effects that arise during cardiac acidosis.

.

8. References

Abbott, G.W. et al., 1999. MiRP1 forms I_{Kr} potassium channels with HERG and is associated with cardiac arrhythmia. *Cell*, 97(2), pp.175–187.

Abbott, G.W., Xu, X. & Roepke, T.K., 2007. Impact of ancillary subunits on ventricular repolarization. *Journal of Electrocardiology*, 40(6 SUPPL. 1).

Abi-Gerges, N. et al., 2011. HERG subunit composition determines differential drug sensitivity. *British Journal of Pharmacology*, 164(2 B), pp.419–432.

Akar, F.G. et al., 2002. Unique topographical distribution of M cells underlies reentrant mechanism of torsade de pointes in the long-QT syndrome. *Circulation*, 105(10), pp.1247–1253.

Akhavan, A., Atanasiu, R. & Shrier, A., 2003. Identification of a COOH-terminal segment involved in maturation and stability of human ether-a-go-go-related gene potassium channels. *Journal of Biological Chemistry*, 278(41), pp.40105–40112.

Amorós, I. et al., 2011. Functional effects of a missense mutation in HERG associated with type 2 long QT syndrome. *Heart Rhythm*, 8(3), pp.463–470.

Anantharam, A., & Abbott, G.W., 2005. Does hERG coassemble with a β subunit? Evidence for roles of MinK and MiRP1. *Novartis Foundation Symposium*, 266, pp.100–112.

Anderson, C.L. et al., 2006. Most LQT2 mutations reduce K_v11.1 (hERG) current by a class 2 (trafficking-deficient) mechanism. *Circulation*, 113(3), pp.365–73..

Antzelevitch, C., 2007. Ionic, molecular, and cellular bases of QT-interval prolongation and torsade de pointes. *Europace : European pacing, arrhythmias, and cardiac electrophysiology : journal of the working groups on cardiac pacing, arrhythmias, and cardiac cellular electrophysiology of the European Society of Cardiology*, 9 Suppl 4.

Antzelevitch, C., 2005. Role of transmural dispersion of repolarization in the genesis of drug-induced torsades de pointes. *Heart Rhythm*, 2(11 SUPPL. 2).

Antzelevitch, C. & Sicouri, S., 2012. Mechanisms Underlying Arrhythmogenesis in Long QT Syndrome. *Cardiac Electrophysiology Clinics*, 4(1), pp.17–27.

Anumonwo, J.M. et al., 1999. Proton and zinc effects on HERG currents. *Biophysical journal*, 77(1), pp.282–98.

Barry, P.H., 1994. JPCalc, a software package for calculating liquid junction potential corrections in patch-clamp, intracellular, epithelial and bilayer measurements and for correcting junction potential measurements. *Journal of Neuroscience Methods*, 51(1), pp.107–116.

Berecki, G. et al., 2005. HERG Channel (Dys)function Revealed by Dynamic Action Potential Clamp Technique. *Biophysical Journal*, 88(1), pp.566–578.

Bers, D.M., 2002. Cardiac excitation–contraction coupling. *Nature*, 415(6868), pp.198–205.

Bers, D.M. & Perez-Reyes, E., 1999. Ca channels in cardiac myocytes: Structure and function in Ca influx and intracellular Ca release. *Cardiovascular Research*, 42(2), pp.339–360.

Bérubé, J., Chahine, M. & Daleau, P., 1999. Modulation of HERG potassium channel properties by external pH. *Pflugers Archiv European Journal of Physiology*, 438(3), pp.419–422.

Bett, G.C.L., Liu, M. & Rasmusson, R.L., 2011. Histidine 562 on S5 is a pH Sensor for HERG Gating. *Biophysical Journal*, 100(3), p.426a.

Bett, G.C.L. & Rasmusson, R.L., 2003. Functionally-distinct proton-binding in HERG suggests the presence of two binding sites. *Cell Biochemistry and Biophysics*, 39(3), pp.183–193.

Bett, G.C.L., Zhou, Q. & Rasmusson, R.L., 2011. Models of HERG gating. *Biophysical Journal*, 101(3), pp.631–642.

Bian, J., Cui, J. & McDonald, T. V., 2001. HERG K+ Channel Activity Is Regulated by Changes in Phosphatidyl Inositol 4,5-Bisphosphate. *Circulation Research*, 89(12),

Boutureira, O. & Bernardes, G.J.L., 2015. Advances in Chemical Protein Modification. *Chemical Reviews*, 115(5), pp.2174–2195.

Brelidze, T.I. et al., 2012. Structure of the carboxy-terminal region of a KCNH channel. *Nature*, 481(7382), pp.530–533.

Brelidze, T.I. et al., 2013. Structure of the C-terminal region of an ERG channel and functional implications. *Proceedings of the National Academy of Sciences of the United States of America*, 110(28), pp.11648–53.

Brelidze, T.I., Carlson, A.E. & Zagotta, W.N., 2009. Absence of direct cyclic nucleotide modulation of mEAG1 and hERG1 channels revealed with fluorescence and electrophysiological methods. *Journal of Biological Chemistry*, 284(41), pp.27989–27997.

Brugada, R. et al., 2004. Sudden Death Associated with Short-QT Syndrome Linked to Mutations in HERG. *Circulation*, 109(1), pp.30–35.

Burton, F.L. & Cobbe, S.M., 2001. Dispersion of ventricular repolarization and refractory period. *Cardiovascular Research*, 50(1), pp.10–23.

Cabral, H.M. et al., 1998. Crystal Structure and Functional Analysis of the HERG Potassium Channel N Terminus : *Cell*, 95, pp.649–655.

del Camino, D. et al., 2000. Blocker protection in the pore of a voltage-gated K^+ channel and its structural implications. *Nature*, 403(6767), pp.321–325.

Carmeliet, E. et al., 1999. Cardiac ionic currents and acute ischemia: from channels to arrhythmias. *Physiological reviews*, 79(3), pp.917–1017.

Carmeliet, E., 1992. Voltage- and time-dependent block of the delayed K^+ current in cardiac myocytes by dofetilide. *The Journal of pharmacology and experimental therapeutics*, 262(2), pp.809–817.

Chen, J. et al., 1999. Long QT syndrome-associated mutations in the Per-Arnt-Sim (PAS) domain of HERG potassium channels accelerate channel deactivation. *Journal of Biological Chemistry*, 274(15), pp.10113–10118.

Chen, X. et al., 2006. Use of arterially perfused rabbit ventricular wedge in predicting arrhythmogenic potentials of drugs. *Journal of Pharmacological and Toxicological Methods*, 54(3), pp.261–272.

Cheng, J. & Kodama, I., 2004. Two components of delayed rectifier K^+ current in heart: molecular basis, functional diversity, and contribution to repolarization. *Acta pharmacologica Sinica*, 25(2), pp.137–145.

Chinn, K., 1993. Two delayed rectifiers in guinea pig ventricular myocytes distinguished by tail current kinetics. *The Journal of pharmacology and experimental therapeutics*, 264(2), pp.553–60.

Clarke, C.E. et al., 2006. Effect of S5P alpha-helix charge mutants on inactivation of hERG K^+ channels. *The Journal of physiology*, 573(2006), pp.291–304.

Clay, J.R. et al., 1995. A quantitative description of the E-4031-sensitive repolarization current in rabbit ventricular myocytes. *Biophysical Journal*, 69(5), pp.1830–1837.

Colenso, C.K. et al., 2013. Interactions between Voltage Sensor and Pore Domains in a hERG K + Channel Model from Molecular Simulations and the E ff ects of a Voltage Sensor Mutation. *Chemical Information and modeling*, 53, pp.1358–1370.

Colquhoun, D. & Hawkes, A.G., 1995. The Principles of the Stochastic Interpretation of Ion-Channel Mechanisms. In B. Sakmann & E. Neher, eds. *Single-Channel Recording*. Boston, MA: Springer US, pp. 397–482.

Cordeiro, J.M. et al., 2005. Modulation of IKr inactivation by mutation N588K in KCNH2: A link to arrhythmogenesis in short QT syndrome. *Cardiovascular Research*, 67(3), pp.498–509.

Crociani, O. et al., 2003. Cell cycle-dependent expression of HERG1 and HERG1B isoforms in tumor cells. *Journal of Biological Chemistry*, 278(5), pp.2947–2955.

Cui, J. et al., 2000. Cyclic AMP regulates the HERG K^+ channel by dual pathways. *Current Biology*, 10(11), pp.671–674.

Curran, M.E. et al., 1995. A molecular basis for cardiac arrhythmia: HERG mutations cause long QT syndrome. *Cell*, 80(5), pp.795–803.

Dessertenne, F., 1990. Ventricular tachycardia with two variable foci. *Cardiovascular Drugs and Therapy*, 4(4), pp.1171–1176.

DiFrancesco, D., Noma, A. & Trautwein, W., 1979. Kinetics and magnitude of the time-dependent potassium current in the rabbit sinoatrial node. *Pflügers Arch.*, 381(3), pp.271–279.

Doyle, D.A. et al., 1998. The Structure of the Potassium Channel: Molecular Basis of K^+ Conduction and Selectivity. *Science*, 280(April 3), pp.69–77.

Du, C. et al., 2013. Modification by KCNE1 variants of the hERG potassium channel response to premature stimulation and to pharmacological inhibition. *Physiological Reports*, 1(6), pp.1–15.

Du, C.Y. et al., 2010. Acidosis impairs the protective role of hERG K(+) channels against premature stimulation. *Journal of cardiovascular electrophysiology*, 21(10), pp.1160–9.

Du, C.Y. et al., 2011. Inhibitory effect of acidosis on hERG potassium channels that incorporate the hERG1b isoform. *Biochemical and biophysical research communications*, 405, pp.222–227.

Dun, W., Jiang, M. & Tseng, G.N., 1999. Allosteric effects of mutations in the extracellular S5-P loop on the gating and ion permeation properties of the hERG potassium channel. *Pflugers Archiv European Journal of Physiology*, 439, pp.141–149.

Ehrlich, J.R. et al., 2004. K_vLQT1 modulates the distribution and biophysical properties of HERG: A novel alpha-subunit interaction between delayed rectifier currents. *Journal of Biological Chemistry*, 279(2), pp.1233–1241.

References

El-Sherif, N. et al., 1997. Electrophysiological Mechanism of the Characteristic Electrocardiographic Morphology of Torsade de Pointes Tachyarrhythmias in the Long-QT Syndrome : Detailed Analysis of Ventricular Tridimensional Activation Patterns. *Circulation*, 96(12), pp.4392–4399.

El-Sherif, N., Turitto, G. & Boutjdir, M., 2017. Congenital Long QT syndrome and torsade de pointes. *Annals of Noninvasive Electrocardiology*, (April), pp.1–11.

Feeney, R.E., Yamasaki, R.B. & Geoghegan, K.F., 1982. Chemical Modification of Proteins: An Overview [Food composition research]. *Advances in Chemistry Series (USA)*, 198, pp.3–55.

Fernandez, D. et al., 2005. Molecular mapping of a site for Cd^{2+}-induced modification of human ether-à-go-go-related gene (hERG) channel activation. *The Journal of physiology*, 567(Pt 3), pp.737–55.

Ficker, E. et al., 2000. Novel characteristics of a misprocessed mutant HERG channel linked to hereditary long QT syndrome. *Am.J Physiol Heart Circ.Physiol*, 279(0363-6135 SB - M), pp.H1748–H1756.

Fleet, W.F. et al., 1985. Effect of serial brief ischemic episodes on extracellular K^+, pH, and activation in the pig. *Circulation*, 72(4), pp.922–932.

Foster, M.N. & Coetzee, W.A., 2016. K_{ATP} Channels in the Cardiovascular System. *Physiological Reviews*, 96(1), pp.177–252.

Fozzard, H.A., 1992. Afterdepolarizations and triggered activity. *Basic Res Cardiol*, 87 Suppl 2, pp.105–113.

Garson, A., 1993. How to measure the QT interval-What is normal? *The American Journal of Cardiology*, 72(6).

Gintant, G.A., 2000. Characterization and functional consequences of delayed rectifier current transient in ventricular repolarization. *American journal of physiology. Heart and circulatory physiology*, 278(3), pp.H806–17.

Gintant, G.A., 1996. Two components of delayed rectifier current in canine atrium and ventricle. Does I_{Ks} play a role in the reverse rate dependence of class III agents? *Circ. Res.*, 78(1), pp.26–37.

Glazer, A.N., 1970. Specific Chemical Modification of Proteins 717. *Annu. Rev. Biochem.*, 39(2), pp.101–130.

Gollob, M.H., Redpath, C.J. & Roberts, J.D., 2011. The short QT syndrome: Proposed diagnostic criteria. *Journal of the American College of Cardiology*, 57(7), pp.802–812.

Goodchild, S.J., Macdonald, L.C. & Fedida, D., 2015. Sequence of Gating Charge Movement and Pore Gating in hERG Activation and Deactivation Pathways. *Biophysj*, 108(6), pp.1435–1447.

Grant, A.O., 2009. Cardiac ion channels: Basic science for the clinical electrophysiologist. *Circulation: Arrhythmia and Electrophysiology*, 2(2), pp.185–194.

Green, W.N. & Andersen, O.S., 1991. Surface Charges and ION Channel Function. *Annual Review of Physiology*, 53(1), pp.341–359.

Grover, G.J. & Garlid, K.D., 2000. ATP-Sensitive potassium channels: a review of their cardioprotective pharmacology. *Journal of molecular and cellular cardiology*, 32, pp.677–695.

Guasti, L. et al., 2005. Expression Pattern of the ether-a-go-go-related (ERG) family proteins in the adult mouse central nervous system: Evidence for coassembly of different subunits. *Journal of Comparative Neurology*, 491(2), pp.157–174.

Gustina, A.S. & Trudeau, M.C., 2009. A recombinant N-terminal domain fully restores deactivation gating in N-truncated and long QT syndrome mutant hERG potassium channels. *Proceedings of the National Academy of Sciences of the United States of America*, 106(31), pp.13082–13087.

Gustina, A.S. & Trudeau, M.C., 2011. hERG potassium channel gating is mediated by N- and C-terminal region interactions. *The Journal of General Physiology*, 137(3), pp.315–325.

Gustina, A.S. & Trudeau, M.C., 2012. HERG potassium channel regulation by the N-terminal eag domain. *Cellular signalling*, 24(8), pp.1592–8.

Haitin, Y., Carlson, A.E. & Zagotta, W.N., 2013. The structural mechanism of KCNH-channel regulation by the eag domain. *Nature*, 501(7467), pp.444–448.

Hancox, J.C. et al., 2008. The hERG potassium channel and hERG screening for drug-induced torsades de pointes. *Pharmacology and Therapeutics*, 119(2), pp.118–132.

Hancox, J.C., Levi, a J. & Witchel, H.J., 1998. Time course and voltage dependence of expressed HERG current compared with native “rapid” delayed rectifier K current during the cardiac ventricular action potential. *Pflügers Archiv : European journal of physiology*, 436(6), pp.843–53.

El Harchi, A. et al., 2012. Molecular determinants of hERG potassium channel inhibition by disopyramide. *Journal of Molecular and Cellular Cardiology*, 52(1), pp.185–195.

Harms, M.J. et al., 2009. The pK_a Values of Acidic and Basic Residues Buried at the Same Internal Location in a Protein Are Governed by Different Factors. *Journal of Molecular Biology*, 389(1), pp.34–47.

Hayashi, K. et al., 2002. Characterization of a novel missense mutation E637K in the pore-S6 loop of HERG in a patient with long QT syndrome. *Cardiovascular Research*, 54(1), pp.67–76.

Heginbotham, L. et al., 1994. Mutations in the K^+ channel signature sequence. *Biophysical Journal*, 66(4), pp.1061–1067.

Hibino, H. et al., 2010. Inwardly Rectifying Potassium Channels: Their Structure, Function, and Physiological Roles. *Physiological reviews*, 90(1), pp.291–366.

Hille, B., 2001. Ion Channel Excitable Membranes. *Sunderland Massachusetts USA*, pp.1–37.

Ho, W.K. et al., 1999. Blockade of HERG channels expressed in *Xenopus laevis* oocytes by external divalent cations. *Biophysical Journal*, 76(4), pp.1959–1971.

Holmgren, M., Shin, K.S. & Yellen, G., 1998. The activation gate of a voltage-gated K^+ channel can be trapped in the open state by an intersubunit metal bridge. *Neuron*, 21(3), pp.617–621.

Hong, K., Piper, D.R., et al., 2005. De novo KCNQ1 mutation responsible for atrial fibrillation and short QT syndrome in utero. *Cardiovascular Research*, 68(3), pp.433–440.

Hong, K., Bjerregaard, P., et al., 2005. Short QT syndrome and atrial fibrillation caused by mutation in KCNH2. *Journal of Cardiovascular Electrophysiology*, 16(4), pp.394–396.

Horie, M., Hayashi, S. & Kawai, C., 1990. Two types of delayed rectifying K^+ channels in atrial cells of guinea pig heart. *The Japanese journal of physiology*, 40(4), pp.479–90.

Hoshi, N. et al., 1998. KCR1, a membrane protein that facilitates functional expression of non- inactivating K^+ currents associates with rat EAG voltage-dependent K^+ channels. *Journal of Biological Chemistry*, 273(36), pp.23080–23085.

Hoshi, T. & Armstrong, C.M., 2013. C-type inactivation of voltage-gated K^+ channels: Pore constriction or dilation? *The Journal of General Physiology*, 141(2), pp.151–160.

Hoshi, T., Zagotta, W. & Aldrich, R., 1990. Biophysical and molecular mechanisms of Shaker potassium channel inactivation. *Science*, 250(4980), pp.533–538.

Hoshi, T., Zagotta, W.N. & Aldrich, R.W., 1991. Two types of inactivation in Shaker K^+ channels: Effects of alterations in the carboxy-terminal region. *Neuron*, 7(4), pp.547–556.

Huffaker, S.J. et al., 2009. A primate-specific, brain isoform of KCNH2 affects cortical physiology, cognition, neuronal repolarization and risk of schizophrenia. *Nature Medicine*, 15(5), pp.509–518.

Hurst, J.W., 1998. Naming of the waves in the ECG, with a brief account of their genesis. *Circulation*, 98(18), pp.1937–1942.

ICH Expert Working Group, 2005. S7B Nonclinical Evaluation of the Potential for Delayed Ventricular Repolarization (QT Interval Prolongation) by Human Pharmaceuticals. *International Conference on Harmonisation of Technical Requirements for Registration of Pharmaceuticals for Human Use*, 70(202), pp.61133–61134.

Isom, D.G. et al., 2011. Large shifts in pK_a values of lysine residues buried inside a protein. *Proceedings of the National Academy of Sciences*, 108(13), pp.5260–5265.

Ito, H. & Ono, K., 1995. A rapidly activating delayed rectifier K+ channel in rabbit sinoatrial node cells. *The American journal of physiology*, 269(2 Pt 2), pp.H443–52.

Itoh, H. et al., 2009. A novel KCNH2 mutation as a modifier for short QT interval. *International Journal of Cardiology*, 137(1), pp.83–85.

James, A.F., Choisy, S.C.M. & Hancox, J.C., 2007. Recent advances in understanding sex differences in cardiac repolarization. *Progress in Biophysics and Molecular Biology*, 94(3), pp.265–319.

January, C.T. & Riddle, J.M., 1989. Early afterdepolarizations: mechanism of induction and block. A role for L-type Ca^{2+} current. *Circulation research*, 64(5), pp.977–990.

Jiang, C. et al., 1994. Two long QT syndrome loci map to chromosomes 3 and 7 with evidence for further heterogeneity. *Nat.Genet.*, 8(2), pp.141–147.

Jiang, L., 2013. Cysteine-Based Cross-Linking Approach to Study Inter-domain Interactions in Ion Channels. *Methods in Molecular Biology*, 998, pp.267–276.

Jiang, M., Dun, W. & Tseng, G.N., 1999. Mechanism for the effects of extracellular acidification on HERG-channel function. *The American journal of physiology*, 277(4 Pt 2), pp.H1283–92.

Jiang, Y. et al., 2002. Crystal structure and mechanism of a calcium-gated potassium channel. *Nature*, 417(6888), pp.515–522..

Jo, S.H. et al., 1999. Blockade of HERG channels expressed in Xenopus oocytes by external H+. *Pflügers Archiv : European journal of physiology*, 438(1), pp.23–9.

Jones, D.K. et al., 2016. Dominant Negative Consequences of a hERG 1b-Specific Mutation Associated with Intrauterine Fetal Death. *Progress in Biophysics and Molecular Biology*, 120(1-3), pp.67–76.

Jones, D.K. et al., 2014. hERG 1b is critical for human cardiac repolarization. *Proceedings of the National Academy of Sciences of the United States of America*, 2014, pp.1–5.

Jones, E.M.C. et al., 2004. Cardiac I_{Kr} channels minimally comprise hERG 1a and 1b subunits. *The Journal of biological chemistry*, 279(43), pp.44690–4.

Ju, P. et al., 2009. The Pore Domain Outer Helix Contributes to Both Activation and Inactivation of the hERG K^+ Channel. *Journal of Biological Chemistry*, 284(2), pp.1000–1008.

Kagan, A. et al., 2000. The dominant negative LQT2 mutation A561V reduces wild-type HERG expression. *Journal of Biological Chemistry*, 275(15), pp.11241–11248.

Kalogeris, T. et al., 2012. Cell Biology of Ischemia/Reperfusion Injury. *Int Rev Cell Mol Biol,* 298, pp.229-317.

Kamiya, K. et al., 2008. Molecular determinants of hERG channel block by terfenadine and cisapride. *Journal of pharmacological sciences*, 108(3), pp.301–7.

Katz, A.M., 1993. Cardiac Ion Channels. *New England Journal of Medicine*, 328(17), pp.1244–1251.

Kazmierczak, M. et al., 2013. External pH modulates EAG superfamily K^+ channels through EAG-specific acidic residues in the voltage sensor. *The Journal of general physiology*, 141(6), pp.721–35.

Keating, M. et al., 1991. Linkage of a cardiac arrhythmia, the long QT syndrome, and the Harvey ras-1 gene. *Science (New York, N.Y.)*, 252(5006), pp.704–706.

Kiehn, J. et al., 1996. Molecular Physiology and Pharmacology of HERG; *Circulation*, 94(10), p.2572–2579.

Kiehn, J., Lacerda, a E. & Brown, a M., 1999. Pathways of HERG inactivation. *The American journal of physiology*, 277(1 Pt 2), pp.H199–210.

Kupershmidt, S. et al., 1998. A K^+ channel splice variant common in human heart lacks a C-terminal domain required for expression of rapidly activating delayed rectifier current. *Journal of Biological Chemistry*, 273(42), pp.27231–27235.

Kupershmidt, S. et al., 2003. The I_{Kr} drug response is modulated by KCR1 in transfected cardiac and noncardiac cell lines. *The FASEB journal : official publication of the Federation of American Societies for Experimental Biology*, 17(15), pp.2263–2265.

Kwan, D.C.H., Fedida, D. & Kehl, S.J., 2006. Single Channel Analysis Reveals Different Modes of Kv1 . 5 Gating Behavior Regulated by Changes of External pH Cell preparation. , 90(February), pp.1212–1222.

De La Peña, P. et al., 2011. Demonstration of physical proximity between the n terminus and the S4-S5 linker of the human ether-à-go-go-related gene (hERG) potassium channel. *Journal of Biological Chemistry*, 286(21), pp.19065–19075.

Lankipalli, R.S. et al., 2005. Mechanisms underlying arrhythmogenesis in long QT syndrome. *Journal of Electrocardiology*, 38(4), pp.69–73.

Larsen, A.P. et al., 2008. Characterization of hERG1a and hERG1b potassium channels-a possible role for hERG1b in the I (Kr) current. *Pflügers Arc*

Larsen, A.P. & Olesen, S.P., 2010. Differential expression of hERG1 channel isoforms reproduces properties of native I_{Kr} and modulates cardiac action potential characteristics. *PLoS ONE*, 5(2).

Laurents, D. V. et al., 2003. Charge-charge interactions are key determinants of the pK values of ionizable groups in ribonuclease Sa (pI=3.5) and a basic variant (pI=10.2). *Journal of Molecular Biology*, 325(5), pp.1077–1092.

Lees-Miller, J.P. et al., 1997. Electrophysiological Characterization of an Alternatively Processed ERG K^+ Channel in Mouse and Human Hearts. *Circulation Research*, 81(5), p.719 LP – 726.

Lees-Miller, J.P. et al., 2009. Interactions of H562 in the S5 helix with T618 and S621 in the pore helix are important determinants of hERG1 potassium channel structure and function. *Biophysical journal*, 96(9), pp.3600–10.

Lees-Miller, J.P. et al., 2000. Molecular determinant of high-affinity dofetilide binding to HERG1 expressed in *Xenopus* oocytes: involvement of S6 sites. *Molecular pharmacology*, 57(2), pp.367–374.

Li, G.R. et al., 1996. Evidence for two components of delayed rectifier K^+ current in human ventricular myocytes. *Circulation Research*, 78, pp.689–696.

Liu, F. et al., 2016. Cotranslational association of mRNA encoding subunits of heteromeric ion channels. *Proceedings of the National Academy of Sciences*, 113(17), pp.4859–4864.

Liu, G.X. et al., 2004. Single-channel recordings of a rapid delayed rectifier current in adult mouse ventricular myocytes: basic properties and effects of divalent cations. *The Journal of physiology*, 556(Pt 2), pp.401–13.

Liu, J. et al., 2003. Negative charges in the transmembrane domains of the HERG K channel are involved in the activation- and deactivation-gating processes. *The Journal of general physiology*, 121(6), pp.599–614.

References

Liu, J. et al., 2002. Structural and Functional Role of the Extracellular S5-P Linker in the HERG Potassium Channel. *The Journal of General Physiology*, 120(5), pp.723–737.

Liu, S. et al., 1996. Activation and inactivation kinetics of an E-4031-sensitive current from single ferret atrial myocytes. *Biophysical Journal*, 70(6), pp.2704–2715.

London, B. et al., 1997. Two Isoforms of the Mouse Ether-a-go-go-Related Gene Coassemble to Form Channels With Properties Similar to the Rapidly Activating Component of the Cardiac Delayed Rectifier K^+ Current. *Circulation Research*, 81(5), p.870–878.

Long, S.B., 2005a. Crystal Structure of a Mammalian Voltage-Dependent Shaker Family K^+ Channel. *Science*, 309(5736), pp.897–903.

Long, S.B., 2005b. Voltage Sensor of $K_v1.2$: Structural Basis of Electromechanical Coupling. *Science*, 309(5736), pp.903–908.

Lu, Y. et al., 2001. Effects of premature stimulation on HERG K^+ channels. *The Journal of physiology*, 537(Pt 3), pp.843–51.

Lu, Y. et al., 2003. Mutant MiRP1 subunits modulate HERG K^+ channel gating: a mechanism for pro-arrhythmia in long QT syndrome type 6. *The Journal of physiology*, 551(Pt 1), pp.253–62.

Lundblad, R.L., 2014. *Chemical Reagents for Protein Modification, Fourth Edition*, CRC Press.

Lundquist, A.L. et al., 2005. Expression of multiple KCNE genes in human heart may enable variable modulation of I_{Ks}. *Journal of Molecular and Cellular Cardiology*, 38(2), pp.277–287.

Marques-Carvalho, M.J. et al., 2012. Structural, biochemical, and functional characterization of the cyclic nucleotide binding homology domain from the mouse EAG1 potassium channel. *Journal of Molecular Biology*, 423(1), pp.34–46.

Mazhari, R. et al., 2001. Molecular Interactions Between Two Long-QT Syndrome Gene Products, HERG and KCNE2, Rationalized by In Vitro and In Silico Analysis. *Circulation Research*, 89(1), pp.33–38.

McDonald, T. V et al., 1997. A minK – HERG complex regulates the cardiac potassium current I Kr. *Letters to Nature*, 388, pp.289–292.

McNally, B.A., Pendon, Z. & Trudeau, M.C., 2017. hERG1a and hERG1b potassium channel subunits directly interact and preferentially form heteromeric channels. *The Journal of Biological Chemistry*, (3), 292(52), pp.21548-21557

McPate, M.J., Zhang, H., et al., 2009. Comparative effects of the short QT N588K mutation at 37 °C on herg K^+ channel current during ventricular, Purkinje fibre and atrial action potentials: An action potential clamp study. *Journal of Physiology and Pharmacology*, 60(1), pp.23–41.

McPate, M.J., Zhang, H., et al., 2009. hERG1a/1b heteromeric currents exhibit amplified attenuation of inactivation in variant 1 short QT syndrome. *Biochemical and Biophysical Research Communications*, 386(1), pp.111–117.

McPate, M.J. et al., 2005. The N588K-HERG K^+ channel mutation in the "short QT syndrome": mechanism of gain-in-function determined at 37 °C. *Biochemical and biophysical research communications*, 334(2), pp.441–9.

Mendoza, V.L. & Vachet, R.W., 2014. Improved Protein Surface Mapping Using Diethylpyrocarbonate with Mass Spectrometric Detection. *Analytical Chemistry*, 80(8), pp.2895–2904.

Meves, H., 2001. Slowing of ERG current deactivation in NG108-15 cells by the histidine-specific reagent diethylpyrocarbonate. *Neuropharmacology*, 41, pp.220–228

Miles, E.W., 1977. Modification of Histidyl Residues in Proteins by Diethylpyrocarbonate. *Methods in Enzymology*, 47(C), pp.431–442.

Mitcheson, J. et al., 2005. Structural determinants for high-affinity block of hERG potassium channels. *Novartis Found Symp*, 266, pp.136–138.

Mitcheson, J.S., Chen, J., Lin, M., et al., 2000. A structural basis for drug-induced long QT syndrome. *Proceedings of the National Academy of Sciences of the United States of America*, 97(22), pp.12329–33.

Mitcheson, J.S., Chen, J. & Sanguinetti, M.C., 2000. Trapping of a methanesulfonanilide by closure of the HERG potassium channel activation gate. *The Journal of general physiology*, 115(3), pp.229–240.

Moyle, G.J. et al., 2002. Hyperlactataemia and lactic acidosis during antiretroviral therapy: Relevance, reproducibility and possible risk factors. *Aids*, 16(10), pp.1341–1349.

Muskett, F.W. et al., 2011. Mechanistic insight into human ether-a-go-go-related gene (hERG) K^+ channel deactivation gating from the solution structure of the EAG domain. *Journal of Biological Chemistry*, 286(8), pp.6184–6191.

Nakajima, T. et al., 1998. Novel mechanism of HERG current suppression in LQT2: shift in voltage dependence of HERG inactivation. *Circulation research*, 83(4), pp.415–422.

Nerbonne, J.M., 2016. Molecular Basis of Functional Myocardial Potassium Channel Diversity. *Cardiac Electrophysiology Clinics*, 8(2), pp.257–273.

Nerbonne, J.M. & Kass, R.S., 2005. Molecular physiology of cardiac repolarization. *Physiological reviews*, 85(4), pp.1205–53.

Ng, C.A. et al., 2014. Multiple interactions between cytoplasmic domains regulate slow deactivation of K_v11.1 channels. *The Journal of biological chemistry*, 289(37), pp.25822–32.

Ng, C.A. et al., 2011. The N-terminal tail of hERG contains an amphipathic α-helix that regulates channel deactivation. *PLoS ONE*, 6(1).

Ng, C.A. et al., 2012. The S4-S5 linker acts as a signal integrator for hERG K^+ channel activation and deactivation gating. *PLoS ONE*, 7(2).

Ng, C.A. et al., 2016. Tyrosine residues from the s4-s5 linker of K_v11.1 channels are critical for slow deactivation. *Journal of Biological Chemistry*, 291(33), pp.17293–17302.

Noble, D. & Tsien, R.W., 1969. Outward membrane currents activated in the plateau range of potentials in cardiac Purkinje fibres. *The Journal of Physiology*, 200(1), pp.205–231.

Noma, A. & Irisawa, H., 1976. A time- and voltage-dependent potassium current in the rabbit sinoatrial node cell. *Pflügers Archiv European Journal of Physiology*, 366(2-3), pp.251–258.

Ojeda, C. & Rougier, O., 1974. Kinetic analysis of the delayed outward currents in frog atrium. Existence of two types of preparation. *The Journal of physiology*, 239(1), pp.51–73.

Orchard, C.H. & Kentish, J.C., 1990. Effects of changes of pH on the contractile function of cardiac muscle. *Am J Physiol*, 6(Part 1), pp.C967–C981.

Pace, C.N., Grimsley, G.R. & Scholtz, J.M., 2010. Protein Ionizable Groups : pK Values and Their Contribution., 284(20), pp.13285–13289.

Patel, C., Yan, G.X. & Antzelevitch, C., 2010. Short QT syndrome: From bench to bedside. *Circulation: Arrhythmia and Electrophysiology*, 3(4), pp.401–408.

Perrin, M.J. et al., 2008. Human ether-a-go-go related gene (hERG) K^+ channels: Function and dysfunction. *Progress in Biophysics and Molecular Biology*, 98(2-3), pp.137–148.

Perry, M.D. et al., 2015. Getting to the heart of hERG K^+ channel gating. *The Journal of physiology*, 12(November 2014), pp.2575–2585.

Phan, K. et al., 2017. The S1 helix critically regulates the finely tuned gating of K_v11.1 channels. *Journal of Biological Chemistry*, 292(18), pp.7688–7705.

Phartiyal, P. et al., 2008. Endoplasmic reticulum retention and rescue by heteromeric assembly regulate human ERG 1a/1b surface channel composition. *The Journal of biological chemistry*, 283(7), pp.3702–7.

Piper, D.R. et al., 2003. Gating currents associated with intramembrane charge displacement in HERG potassium channels. *Proceedings of the National Academy of Sciences of the United States of America*, 100(18), pp.10534–9.

Piper, D.R., Sanguinetti, M.C. & Tristani-Firouzi, M., 2005. Voltage sensor movement in the hERG K^+ channel. *Novartis Found Symp*, 266, pp.46,95–99.

Po, S.S. et al., 1999. Modulation of HERG potassium channels by extracellular magnesium and quinidine. *Journal of cardiovascular pharmacology*, 33(2), pp.181–5.

Pourrier, M. et al., 2003. Canine ventricular KCNE2 expression resides predominantly in Purkinje fibers. *Circulation Research*, 93(3), pp.189–191.

Rasmusson, R.L. et al., 1998. Inactivation of voltage-gated cardiac K^+ channels. *Circulation research*, 82(7), pp.739–50.

Redpath, C.J. et al., 2009. Rapid genetic testing facilitating the diagnosis of short QT syndrome. *The Canadian journal of cardiology*, 25(4), pp.133–5.

Robertson, G. a, Jones, E.M.C. & Wang, J., 2005. Gating and assembly of heteromeric hERG1a/1b channels underlying I_{Kr} in the heart. *Novartis Foundation symposium*, 266, pp.4–15; discussion 15–8, 44–5.

Roden, D.M. et al., 2002. Cardiac Ion Channels. *Annual Review of Physiology*, 64, pp.431–475.

Sale, H. et al., 2008. Physiological properties of hERG 1a/1b heteromeric currents and a hERG 1b-specific mutation associated with Long-QT syndrome. *Circulation research*, 103(7), pp.81–95.

Sanguinetti, M. & Keating, M., 1997. Role of delayed rectifier potassium channels in cardiac repolarization and arrhythmias. *News in physiological sciences*, 12(August).

Sanguinetti, M.C. et al., 1995. A Mechanistic Link between an Inherited and an Acquired Cardiac Arrhythmia : HERG Encodes the I_{Kr} Potassium Channel., 81, pp.299–307.

Sanguinetti, M.C. et al., 1996. Coassembly of K_VLQT1 and minK (IsK) proteins to form cardiac I_{Ks} potassium channel. *Nature*, 384(6604), pp.80–83.

Sanguinetti, M.C. & Jurkiewicz, N.K., 1991. Delayed rectifier outward K^+ current is composed of two currents in guinea pig atrial cells. *The American journal of physiology*, 260(2 Pt 2), pp.H393–9.

Sanguinetti, M.C. & Jurkiewicz, N.K., 1990. Two Components of Cardiac Delayed Rectifier K^+ Current Differential Sensitivity to Block by Class III Antiarrhythmic Agents. *J. Gen. Physiol.*, 96(July), pp.195–215.

Sanguinetti, M.C. & Tristani-Firouzi, M., 2006. hERG potassium channels and cardiac arrhythmia. *Nature*, 440(7083), pp.463–9.

Sasaki, S. et al., 2015. Involvement of histidine residue His382 in pH regulation of MCT4 activity. *PLoS ONE*, 10(4), pp.1–12.

Schönherr, R. & Heinemann, S.H., 1996. Molecular determinants for activation and inactivation of HERG, a human inward rectifier potassium channel. *The Journal of physiology*, 493 (Pt 3), pp.635–42.

Sesti, F., Tai, K.K. & Goldstein, S.A.N., 2000. MinK endows the I_{Ks} potassium channel pore with sensitivity to internal tetraethylammonium. *Biophysical Journal*, 79(3), pp.1369–1378.

Shi, Y.P. et al., 2014. External protons destabilize the activated voltage sensor in hERG channels. *European biophysics journal* , 43(2-3), pp.59–69.

Shibasaki, B.Y.T., 1987. Conductance and kinetics of delayed rectifier potassium channels in nodal cells of the rabbit heart. *J. Physiol*, 387, pp.227–250.

Shrier, A. & Clay, J.R., 1986. Repolarization currents in embryonic chick atrial heart cell aggregates. *Biophysical Journal*, 50(5), pp.861–874.

Singh, B.N., 1999. Overview of trends in the control of cardiac arrhythmia: Past and future. In *American Journal of Cardiology*. pp. 3–10.

Van Slyke, A.C. et al., 2010. Mutations within the S4-S5 linker alter voltage sensor constraints in hERG K^+ channels. *Biophysical journal*, 99(9), pp.2841–52.

Van Slyke, A.C. et al., 2012. Proton block of the pore underlies the inhibition of hERG cardiac K^+ channels during acidosis. *American journal of physiology. Cell physiology*, 302(12), pp.C1797–806.

Smith, P.L., Baukrowitz, T. & Yellen, G., 1996. The inward rectification mechanism of the HERG cardiac potassium channel. *Nature*, 379(6568), pp.833–836.

Smith, P.L. & Yellen, G., 2002. Fast and slow voltage sensor movements in HERG potassium channels. *The Journal of general physiology*, 119(3), pp.275–93.

Snyders, D.J. & Chaudhary, a, 1996. High affinity open channel block by dofetilide of HERG expressed in a human cell line. *Mol Pharmacol*, 49(6), pp.949–955.

Spector, P. & Curran, M., 1996. Class III antiarrhythmic drugs block HERG, a human cardiac delayed rectifier K+ channel open-channel block by methanesulfonanilides. *Circulation*, 78(3), pp.499–503.

Spector, P.S. et al., 1996. Fast inactivation causes rectification of the I_{Kr} channel. *The Journal of general physiology*, 107(May), pp.611–619.

Splawski, I. et al., 1998. Genomic structure of three long QT syndrome genes: K_VLQT1, HERG, and KCNE1. *Genomics*, 51(1), pp.86–97.

Subbiah, R.N. et al., 2005. Tryptophan scanning mutagenesis of the HERG K^+ channel: the S4 domain is loosely packed and likely to be lipid exposed. *The Journal of physiology*, 569(Pt 2), pp.367–79.

Sun, Y. et al., 2011. A novel mutation in the KCNH2 gene associated with short QT syndrome. *Journal of molecular and cellular cardiology*, 50(3), pp.433–41.

Szabó, G. et al., 2005. Asymmetrical distribution of ion channels in canine and human left-ventricular wall: Epicardium versus midmyocardium. *Pflugers Archiv European Journal of Physiology*, 450(5), pp.307–316.

Tamargo, J. et al., 2004. Pharmacology of cardiac potassium channels. *Cardiovascular Research*, 62, pp.9–33.

Tao, X. et al., 2010. A Gating Charge Transfer Center in Voltage Sensors. *Science*, 328(5974), pp.67–73.

Terai, T. et al., 2000. Effects of external acidosis on HERG current expressed in *Xenopus* oocytes. *Journal of molecular and cellular cardiology*, 32(1), pp.11–21.

Thouta, S. et al., 2014. Proline scan of the HERG channel S6 helix reveals the location of the intracellular pore gate. *Biophysical journal*, 106(5), pp.1057–69.

Torres, A.M. et al., 2003. Structure of the HERG K^+ channel S5P extracellular linker: Role of an amphipathic α-helix in C-type inactivation. *Journal of Biological Chemistry*, 278(43), pp.42136–42148.

Tristani-Firouzi, M., Chen, J. & Sanguinetti, M.C., 2002. Interactions between S4-S5 linker and S6 transmembrane domain modulate gating of HERG K^+ channels. *The Journal of biological chemistry*, 277(21), pp.18994–9000.

Tristani-Firouzi, M. & Sanguinetti, M.C., 2003. Structural determinants and biophysical properties of HERG and KCNQ1 channel gating. *Journal of Molecular and Cellular Cardiology*, 35(1), pp.27–35.

Trudeau, M. et al., 1995. HERG, a human inward rectifier in the voltage-gated potassium channel family. *Science*, 269(5220), pp.92–95.

Trudeau, M.C. et al., 2011. hERG1a N-terminal eag domain-containing polypeptides regulate homomeric hERG1b and heteromeric hERG1a/hERG1b channels: a possible mechanism for long QT syndrome. *The Journal of general physiology*, 138(6), pp.581–92.

Tseng, G., 2001. I_{Kr}: The hERG Channel. *Journal of Molecular and Cellular Cardiology,* 33(5), pp.835–849.

Tseng, G., et al., 2007. Probing the outer mouth structure of the HERG channel with peptide toxin footprinting and molecular modeling. *Biophysical journal*, 92(10), pp.3524–40.

Vandenberg, J.I. et al., 2012. hERG K^+ Channels: Structure, Function, and Clinical Significance. *Physiological Reviews*, 92(3), pp.1393–1478.

Vandenberg, J.I. et al., 2006. Temperature dependence of human ether-a-go-go-related gene K^+ currents. *American journal of physiology. Cell physiology*, 291(1), pp.C165–75.

Vandenberg, J.I. et al., 2004. The HERG K^+ channel: Progress in understanding the molecular basis of its unusual gating kinetics. *European Biophysics Journal*, 33(2), pp.89–97.

Vandenberg, J.I., Perozo, E. & Allen, T.W., 2017. Towards a Structural View of Drug Binding to hERG K^+ Channels. *Trends in Pharmacological Sciences*, 38(10), pp.899–907.

Vandenberg, J.I., Walker, B.D. & Campbell, T.J., 2001. HERG K^+ channels: friend and foe. , 22(5), pp.240–246.

Veerman, C.C., Wilde, A.A.M. & Lodder, E.M., 2015. The cardiac sodium channel gene SCN5A and its gene product $Na_V1.5$: Role in physiology and pathophysiology. *Gene*, 573(2), pp.177–187.

Veldkamp, M., van Ginneken, A.C.G. & N, B.L., 1993. Single delayed rectifier channels in the membrane of rabbit ventricular myocytes. *Circulation research*, 72, pp.865–878.

Veldkamp, M.W. et al., 1995. Delayed Rectifier Channels in Human Ventricular Myocytes. *Circulation*, 92(12), pp.3497–3504.

Vereecke, J. & Carmeliet, E., 2000. The effect of external pH on the delayed rectifying K^+ current in cardiac ventricular myocytes. *Pflügers Archiv: European journal of physiology*, 439(6), pp.739–51.

Viskin, S., 1999. Long QT syndromes and torsade de pointes. *Lancet*, 354(9190), pp.1625–1633.

Volders, P.G.A. et al., 2000. Progress in the understanding of cardiac early afterdepolarizations and torsades de pointes: Time to revise current concepts. *Cardiovascular Research*, 46(3), pp.376–392.

Wang, D.T. et al., 2011. Mapping the sequence of conformational changes underlying selectivity filter gating in the K_v11.1 potassium channel. *Nature structural & molecular biology*, 18(1), pp.35–41.

Wang, J. et al., 1998. Regulation of deactivation by an amino terminal domain in human ether-à-go-go-related gene potassium channels. *The Journal of general physiology*, 112(5), pp.637–47.

Wang, J., Myers, C.D. & Robertson, G.A., 2000. Dynamic control of deactivation gating by a soluble amino-terminal domain in HERG K^+ channels. *The Journal of general physiology*, 115(6), pp.749–58.

Wang, R. & Wu, L., 1997. The chemical modification of K_{Ca} channels by carbon monoxide in vascular smooth muscle cells. *The Journal of biological chemistry*, 272(13), pp.8222–8226.

Wang, S. et al., 1997. A quantitative analysis of the activation and inactivation kinetics of HERG expressed in *Xenopus* oocytes. *The Journal of Physiology*, 502(1), pp.45–60.

Wang, W. & MacKinnon, R., 2017. Cryo-EM Structure of the Open Human Ether-à-go-go-Related K^+ Channel hERG. *Cell*, 169(3), pp.422–430.e10.

Wang, Z. et al., 2013. Components of gating charge movement and S4 voltage-sensor exposure during activation of hERG channels. *The Journal of general physiology*, 141(4), pp.431–43.

Wang, Z., Fermini, B. & Nattel, S., 1994. Rapid and slow components of delayed rectifier current in human atrial myocytes. *Cardiovascular Research*, 28(10), pp.1540–1546.

Warmke, J.W. & Ganetzky, B., 1994. A family of potassium channel genes related to eag in *Drosophila* and mammals. *Proceedings of the National Academy of Sciences of the United States of America*, 91(8), pp.3438–3442.

Weerapura, M. et al., 2002. A comparison of currents carried by HERG, with and without coexpression of MiRP1, and the native rapid delayed rectifier current. Is MiRP1 the missing link? *The Journal of Physiology*, 540(1), pp.15–27.

Witchel, H.J. et al., 2003. Troubleshooting problems with in vitro screening of drugs for QT interval prolongation using HERG K^+ channels expressed in mammalian cell lines and Xenopus oocytes. *Journal of pharmacological and toxicological methods*, 48(2), pp.65–80.

References

Witchel, H.J. & Hancox, J.C., 2000. Familial and acquired long QT syndrome and the cardiac rapid delayed rectifier potassium current. *Clinical and Experimental Pharmacology and Physiology*, 27(10), pp.753–766.

Yamaguchi, M. et al., 2005. Compound heterozygosity for mutations Asp611-->Tyr in KCNQ1 and Asp609-->Gly in KCNH2 associated with severe long QT syndrome. *Clinical science (London, England : 1979)*, 108(2), pp.143–50.

Yan, G-X & Kléber, A.G., 1992. Changes in Extracellular and Intracellular pH in Ischemic Rabbit Papillary Muscle. *Circulation Research*, 71, pp 460-470

Yan, G.-X. et al., 2003. Ventricular repolarization components on the electrocardiogram: cellular basis and clinical significance. *Journal of the American College of Cardiology*, 42(3), pp.401–409.

Yap, Y.G. & Camm, A.J., 2003. Drug induced QT prolongation and torsades de pointes. *Heart*, 89(11), pp.1363–1372.

Zhang, M. et al., 2005. Interactions between charged residues in the transmembrane segments of the voltage-sensing domain in the hERG channel. *Journal of Membrane Biology*, 207(3), pp.169–181.

Zhang, M., Liu, J. & Tseng, G.-N., 2004. Gating charges in the activation and inactivation processes of the HERG channel. *The Journal of general physiology*, 124(6), pp.703–18.

Zhang, Y.H. et al., 2011. The hERG K^+ channel S4 domain L532P mutation : Characterization at 37 °C. *BBA - Biomembranes*, 1808(10), pp.2477–2487.

Zhou, F. et al., 2004. Mutational analysis of histidine residues in human organic anion transporter 4 (hOAT4). *The Biochemical journal*, 384(Pt 1), pp.87–92.

Zhou, Q. & Bett, G., 2010. Regulation of the voltage-insensitive step of HERG activation by extracellular pH. *AJP- Heart Circ Physiol*, 298, pp.1710–1718.

Zhou, Z. et al., 1998. Properties of HERG channels stably expressed in HEK 293 cells studied at physiological temperature. *Biophysical journal*, 74(1), pp.230–41.

Zou, A. et al., 1997. Single HERG delayed rectifier K^+ channels expressed in Xenopus oocytes. *The American journal of physiology*, 272(3 Pt 2), pp.H1309–14.